Contributions to Gemology

No.7 December 2008 Second Edition

WINZA RUBIES IDENTIFIED

Positive Europium Anomaly in Pargasite

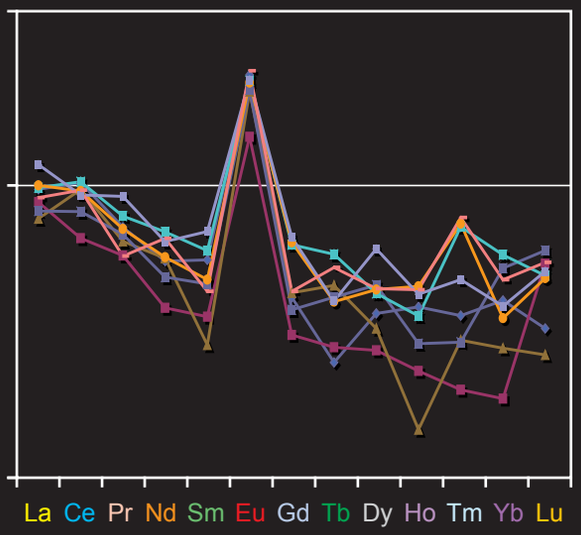

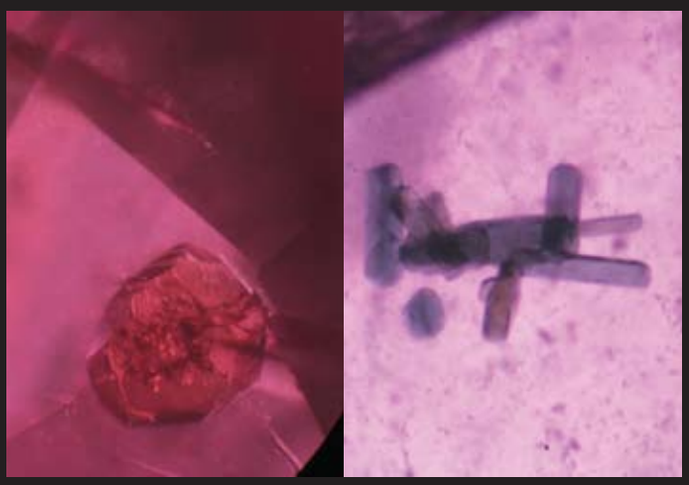

Winza Ruby over 10ct

GRS GEMRESEARCH SWISSLAB

Editor

Dr. A. Peretti, FGG, FGA, EurGeol
GRS Gemresearch Swisslab AG, P.O.Box 4028, 6002 Lucerne, Switzerland

adolf@peretti.ch

Previous Journal

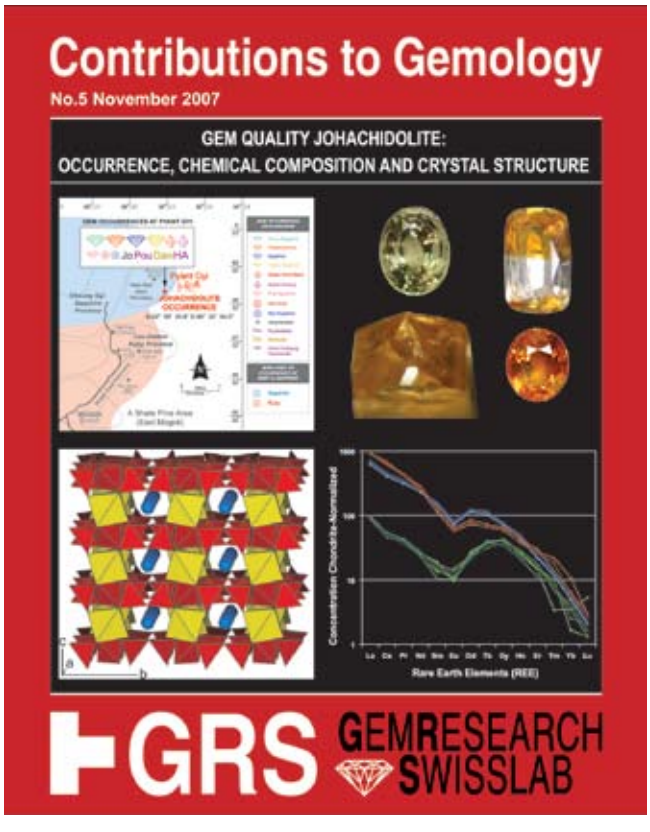

More about our johachidolite research can be found in the Schreyer Memorial Issue of the European Journal of Mineralogy of 2008:
Milen KADIYSKI, Thomas ARMBRUSTER, Detlef GÜNTHER, Eric REUSSER and Adolf PERETTI (2008): Johachidolite, $CaAl[B_3O_7]$, a mineralogical and structural peculiarity. Eur. J. Mineral. 2008, 20, 965–973.

This journal follows the rules of the Commission on New Minerals and Mineral Names of the IMA in all matters concerning mineral names and nomenclature.

Distributor

GRS (Thailand) Co., LTD
257/919 Silom Rd., JTC Building
Bangkok 10500, Thailand.

Journal and Website Copyrighted by GRS (Thailand) Co. LTD, Bangkok, Thailand and GRS Gemresearch Swisslab AG, Lucerne, Switzerland

This report is available online at www.gemresearch.ch

ISBN 978-3-9523359-7-0

Foreword

Gem Research Swisslab is very proud to present you this special edition of Contributions to Gemology. This issue covers our exclusive in-depth research of a newly discovered ruby deposit in Tanzania. In March 2008 we examined some rubies with “vibrant red” colors and extremely fine clarity and brilliancy of over 10cts in size. After careful analysis we discovered the source of these rubies to be from Tanzania that we subsequently reported on in April 2008 in our online news (first edition of Contributions to Gemology No.7, online only at www.gemresearch.ch) and on Youtube in May 2008.

In a small area called Winza, in the district of Dodoma, rubies were found which are comparable to the most prestigious gems found in Mogok (Burma, Myanmar). In keeping our position as a leader in origin identification, we were fortunately granted special permission by the government of Tanzania to undertake geological field studies and collect reference samples. Working together with local Tanzanian geologists, GRS was able to record exact GPS locations of the ruby mining sites.

Our cooperation and detailed fieldwork with the Tanzanian miners allowed GRS to go into the tunnels and investigate the primary mines 15 meters below the surface. For onsite mineral examinations we used our new portable Field-Raman spectrometer. GRS collected samples referenced with exact GPS positions to initiate an extensive in-depth research campaign into these new gemstones. Research included chemical analysis (LA-ICP-MS and ED-XRF), color analysis (UV-VIS-NIR), infrared analysis (FTIR), scanning electron-microscope analysis (SEM-EDX) and structural analysis (XRD, Raman). Gemresearch Swisslab carried out an extensive chemical investigation together with the research laboratories in Switzerland (ETH Zurich) which is well-known for trace element analysis.

From this unique data, and groundbreaking research, we were able to better understand the origin and formation of these Winza rubies. These gems were created by metamorphism within exotic rock suites originating from the lower crust or upper mantle of the earth.

This exciting investigation and our research data is presented in this edition, in order to help with the gemological identification of these new Winza rubies from synthetic and natural counterparts. We hope you will enjoy this adventure into the exciting world of modern gemology and origin determination.

Adolf Peretti

GRS Winza Rubies Identified

New Ruby Source from Tanzania 1-2

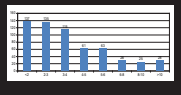

Market Importance of New Tanzanian Rubies 3

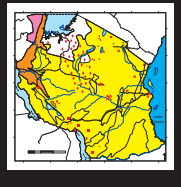

Map on Natural Resources of Tanzania Including the New Rubies from Winza 4

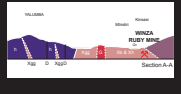

Geology and Petrography of the "Winza" Mining Area 5-6

Geology Map of the "Winza" Mine and Surrounding Area 7-8

Details of Mining Activities at the "Winza Ruby Mine" in Tanzania 9-10

Field Work at "Winza" Ruby Mine 11

Details of Mining Activities at "Winza" (Tanzania) 12

Collecting Reference Samples at the "Winza" Ruby Mine 13

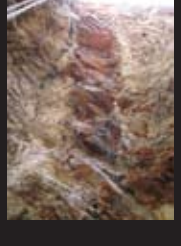

Details of Primary Mining Activities at "Winza" (Tanzania) 14

Detailed Studies in the Primary Ruby Mine Shafts at "Winza" (Tanzania) 15-16

GRS Portable Field Raman Spectrometer 17

Rock Samples from the "Winza" Ruby Mine 18

Garnet-Pargasite Rock Samples Containing Rubies and Sapphires from "Winza" 19

Thin Section Analysis of Rocks from the Ruby Mine at Winza 20

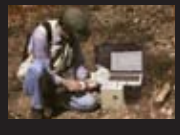

Raman Analysis of Rock-Forming Pargasite and Spinel from "Winza" (Tanzania) 21

Selecting Ruby Samples from the "Winza" Mine 22

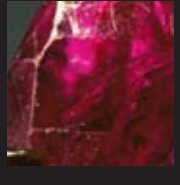

Ruby Samples from "Winza" (Tanzania) 23-24

Reference Sample Collection from "Winza" (Tanzania) 25

Summary Inclusion Identifications 26

Color-zoning in a Ruby from "Winza" (Tanzania) 27

Fluid Inclusions in Rubies from "Winza" (Tanzania) 28-30

Arching and Spiraling needle-like Inclusions in Rubies from "Winza" (Tanzania) 31-32

Pargasite Inclusions in Rubies from "Winza" (Tanzania) 33-35

Garnet Inclusions in Rubies from "Winza" (Tanzania) 36-37

Contents of Contributions to Gemology No.7

Talc Inclusions in Rubies from "Winza" (Tanzania) 38

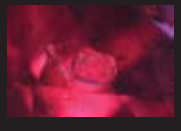

Xenothim, Apatite and Pyrite Inclusions in Rubies from "Winza" (Tanzania) 39

Inclusions in Rubies from "Winza" (Tanzania) 40

Inclusion Research by Chemical (SEM-EDX) and Structural Analysis (XRD) 41

Scanning Electron Microscope (SEM-EDX) Analysis of Inclusions 42-48

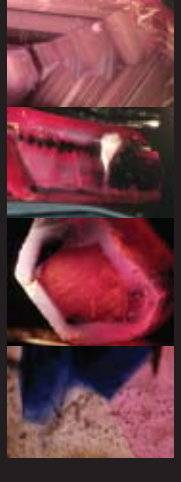

Color-zoning and Growth Features in Rubies from "Winza" (Tanzania) 49-60

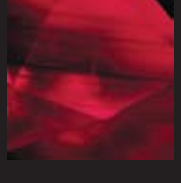

Inclusion Features in Rubies from "Winza" (Tanzania) 61-62

Inclusion Features (Micro-Particles) in Rubies from "Winza" (Tanzania) 63-64

Inclusion Features in Rubies from "Winza" (Tanzania) 65-66

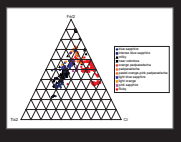

Chemical Analysis of "Winza" Rubies by LA-ICP-MS 67-69

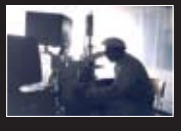

Chemical Analysis by LA-ICP-MS: Methods 70

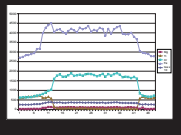

Chemical Analysis Profile of "Winza" Rubies by LA-ICP-MS 71-86

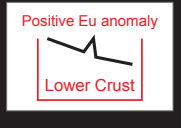

Interpretation of Rare Earth Element (REE) Patterns 87

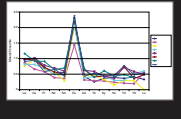

REE Patterns in Pargasite and Garnet 88

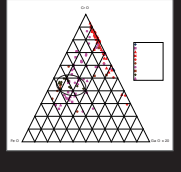

ED-XRF Analysis of Corundum from the "Winza Mine" (Tanzania) and other Origins 89

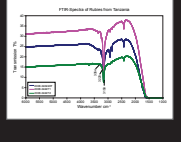

FTIR Analysis of Corundum from the "Winza Mine" (Tanzania) and other Origins 90

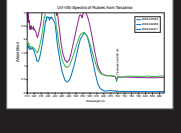

UV-VIS-NIR Spectroscopy Analysis of Corundum from the "Winza Mine" (Tanzania) Unheated/heated 91

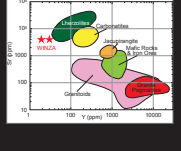

Formation Conditions and Gemmological Conclusions 92, 95

LA-ICP-MS Analysis of Cl-Ferro-Pargasite and Apatite Inclusions 93

LA-ICP-MS Analysis of Garnet Inclusions 94

Acknowledgments 95

About the Authors and Literature 96-97

WINZA RUBIES IDENTIFIED

Adolf Peretti (1,2,3), Francesca Peretti (2), Anong Kanpraphai (3), Willy Peter Bieri (2,3), Kathrin Hametner (4) and Detlef Günther (4) ,

(1) GRS Gemresearch Swisslab Ltd, Sempacherstr. 1, CH-6003 Lucerne, Switzerland
(2) GRS Gemresearch Swisslab Ltd, Rue du Marche 12, CH-1204 Geneva, Switzerland
(3) GRS (Thailand) CO LTD, Bangkok, Silom 919/257, 10500 Bangkok, Thailand
(4) Laboratory of Inorganic Chemistry, ETH Hönggerberg, HCI, G113, CH-8093 Zurich, Switzerland

INTRODUCTION

A completely new type of ruby material has been discovered in Tanzania in the area of "Winza" in the province of Dodoma. The mine is situated SW of the capital (Dodoma) and can be reached by driving to the local town of "Mpwapwa" (pronounced "Papua") and by a further 3 hours of driving (in the dry season) to the mining site, locally known as "Winza Mine".

The rubies are found mostly in primary mines or in the near-surface alteration zone. Miners from many different parts of Tanzania rushed to the mining site when gem quality rubies of excellent colors and exceptional clarity were discovered in spring 2008. Primitive methods were used to mine the sites rather than mechanized large-scale mining. A large number of companies, including gem dealers from Tanzania, Sri Lanka and Thailand positioned themselves in the local town of "Mpwapwa", about 100km from the mining site, where they established local buying offices. As a consequence, significant numbers of rubies were excavated and appeared on the world market in the year 2008. (Fig. Tan01, 04)

Other corundum varieties, such as blue sapphire, pink sapphire, orangy-pink sapphire ("Padparadscha" -color) and color-changing sapphire have also been discovered from the Winza mine. However, only the rubies gained market importance.

We published a first report on the properties and identification of the new ruby material from this mine in Tanzania on our website (Lit. Tan07). The aim was to support the identification of these rubies at a critical time, when synthetic or heated materials could have been mixed with parcels of "Winza" rubies. In the same period of time other laboratories also noticed the importance of the materials (Lit Tan01-Tan11) particularly during the Basel Fair in April 2008. Our initial research was based on a first expedition by one of the directors of GRS (Thailand) to the mine in March 2008. Extensive fieldwork and sampling was only possible after a special permission was granted to GRS by the Tanzanian government on the initiative of a Tanzanian miner and the support of the Thai and Sri Lankan gem community in August 2008 (see acknowledgements). During the onsite investigation took place, the labor at the mine already sharply declined as many miners rushed to a gold finding nearby and when it became clear that the simple methods used for mining did not produce any further valuable ruby findings. A new phase of mining is expected to begin in early 2009 when more advanced methods are eventually introduced at "Winza".

Fig. Tan01 Top: A pair of gem-quality "Winza" rubies over 13 ct and a heart-shape "Winza" ruby over 7ct. Row 2 and 3: The two rough on the left were faceted to the rubies over 10cts that are shown on the right (tested by GRS in Bangkok in March 2008). These rubies were partly responsible for initiating the rush to Winza (Tanzania). These faceted rubies of over 10ct possess excellent color ("vibrant" red), are eye-clean and of high brilliancy, and are spared of thermal enhancement. Because of the magnificent quality of these rubies, the Winza ruby mine became a new landmark among the most important ruby sources (Fig. Tan02). For the total number of gem quality rubies tested by GRS see Fig. Tan04.

Fig. Tan02 Geographic map shows the occurrence of rubies and sapphires with commercial importance. The new ruby mine of Winza appears in addition to the ruby mines of Burma, Vietnam, Madagascar, Thailand and Tajikistan. The localities (black stars) of North-West-Thailand (Kanchanaburi), Sri Lanka, Kashmir and South Madagascar (Illakaka) are mostly sapphire occurrences. The occurrence of Siamese rubies and Kashmir sapphires are nearly exhausted.

Fig. Tan03 The local town of Mpwapwa (left) and a stop at the local gasoline station for a wheel change (right). One of the author's (AP) plans the last expedition details with an important Tanzanian miner and sponsor (see acknowledgments). In the dry season of August 2008, the mine was accessible within 2-3 hours from this point, which is about 60 miles away.

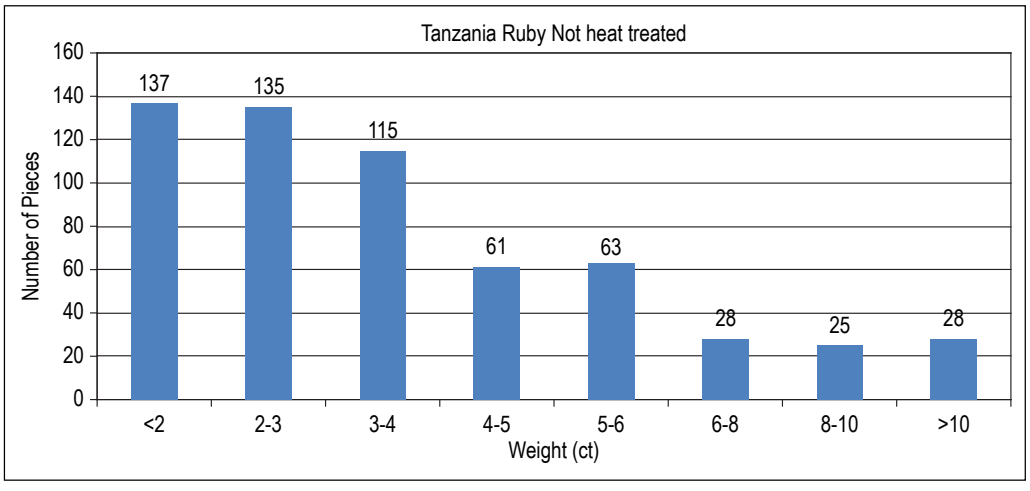

Fig. Tan04 The graph shows the number and sizes of gem quality "Winza" rubies (eye-clean and with "vibrant red" colors) that have been tested by the GRS laboratory in 2008. Note that magnificent rubies over 5 ct are extremely rare. Two dozens gem quality faceted rubies over 10cts have so far been tested. All rubies in this statistic are spared of thermal enhancement. Over 30 stones received a special report of the GRS laboratory confirming that they are considered amongst the World's most beautiful rubies (GRS Platinum Award).

Fig. Tan05 One of the authors (AP) was granted permission to use a portable gemological laboratory operated by the Sri Lankan group in "Mpwapwa", the nearest town to the mine (See acknowledgments). Many gem agent companies in this booming town had to establish gem-testing labs because they were offered synthetics (e.g. synthetic flame-fusion rough ruby fragments) and ruby imitations (e.g. synthetic flux-grown rough spinel resembling some type of rough Winza rubies).

Fig. Tan07 The picture shows the customs office in Dar-es-Salaam. The ruby rough and rock sample parcels collected at the Winza ruby mine by one of the authors (AP) were sealed and the papers were stamped for export permission in August 2008.

Fig. Tan06 Rubies appear in vibrant colors of pure red, slightly orangy-red or orange-red colors. The colors differ from those of Burmese rubies. In general Burmese rubies are more fluorescent and have slightly more purplish secondary colors. Color-changing sapphires, blue sapphires, orangy-pink ("Padparadscha) and pink sapphires were also found in the Winza mine. They have not gained market importance, with the exception of the "Padparadscha" varieties.

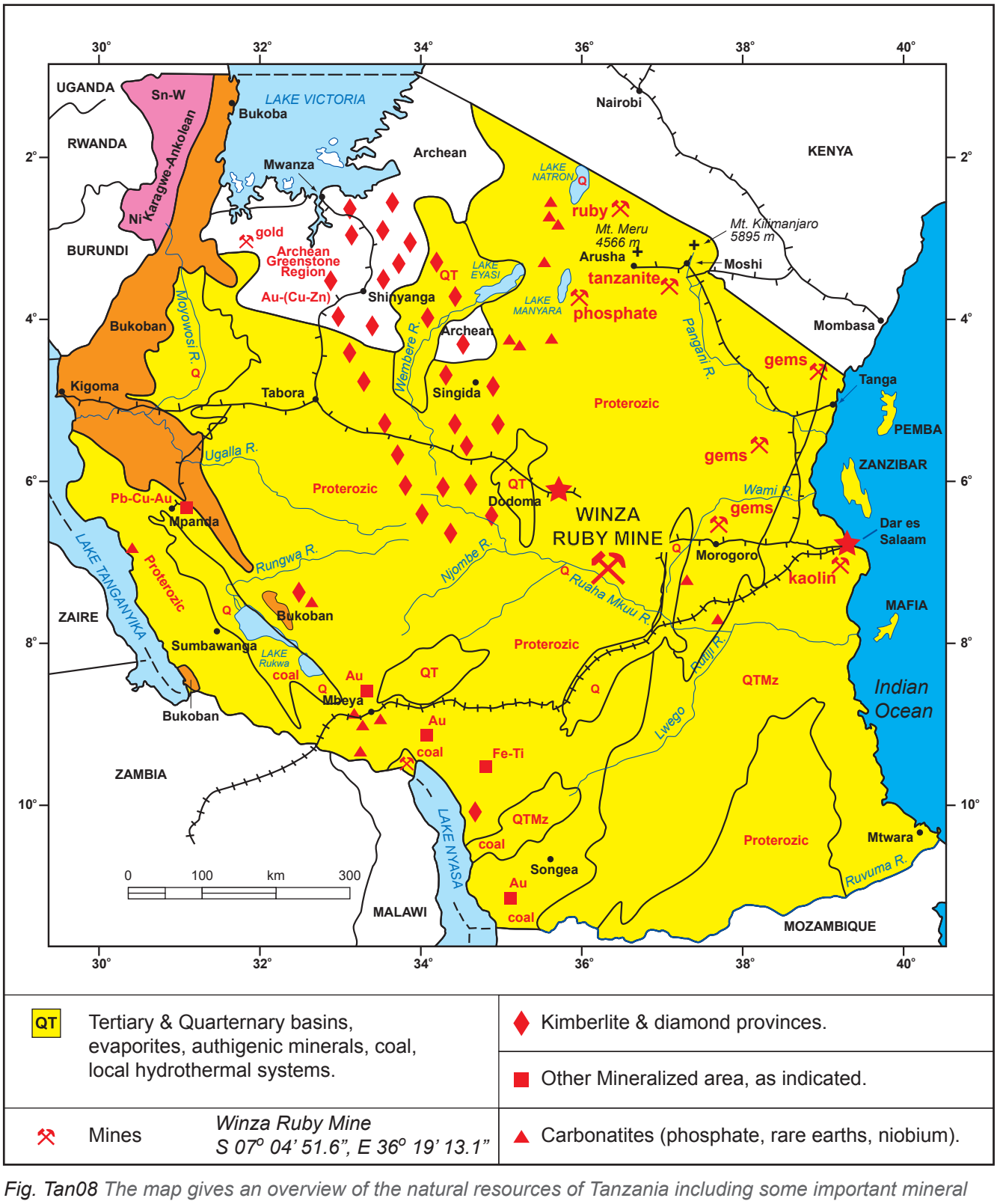

QT	Tertiary & Quarternary basins, evaporites, authigenic minerals, coal, local hydrothermal systems.	♦	Kimberlite & diamond provinces.
		■	Other Mineralized area, as indicated.
⚒	Mines *Winza Ruby Mine* *S 07° 04' 51.6", E 36° 19' 13.1"*	▲	Carbonatites (phosphate, rare earths, niobium).

Fig. Tan08 The map gives an overview of the natural resources of Tanzania including some important mineral occurrences such as gold and diamonds. Other important ruby mines in Tanzania and the famous tanzanite mine are also indicated. The new ruby mine has been added based on our GPS data. Map reproduced with permission from the Government (Source: United Republic of Tanzania (2005): Opportunities for Mineral Resource Development, Ministry of Energy and Minerals, Minerals Department, Fourth Edition, p.1-130).

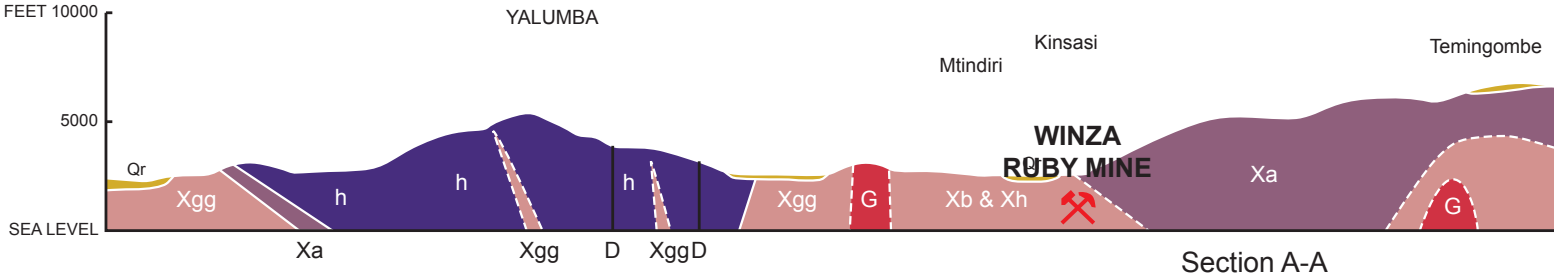

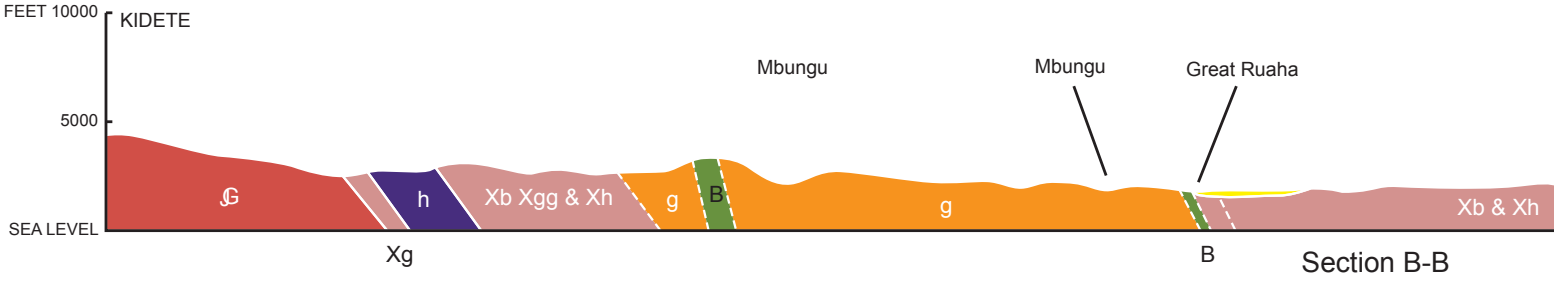

GEOLOGY AND PETROGRAPHY

The geological framework at the Winza mine was studied during two days of fieldwork at the Winza mine in August 2008 (Fig. Tan16-Tan19). The relevant part of the geological framework was obtained from local publications, selected figures and maps have been simplified. The Winza mine locality was added to the map (Fig. Tan10). Two geological profiles were drawn across the rock suites in the mining area (Fig. Tan09). As it can be seen in the geological map and profiles, the variety of rock types in the “Winza” area is enormous. High-grade metamorphic rocks, typical for high-temperature and high-pressure metamorphism are found in the close vicinity of the mine, such as garnet-pyroxene amphibolites, eclogite rocks, kyanite-garnet-biotite gneiss and schists. Isolated granites and so-called migmatite rocks, quartz-feldspar gneisses and amphibolites occur as well. Most of these rocks could be confirmed in and around the “Winza” mine during our field trip (See Fig. Tan16a, Tan17a, Tan17c, Tan19, Tan22, Tan23, Tan24 and Tan25). The rubies are found in association with amphibolites in pure corundum-garnet-pargasite rocks (Fig. Tan17d, Tan19f). Only in one rock sample, ruby was associated to a plagioclase-rich amphibolite (Fig.Tan31a). In localized zones these metamorphosed rocks occasionally form dykes (Fig. Tan17) suggesting their magmatic origin. This observation was confirmed by the results of chemical testing (Fig. Tan133). Thin section analysis of the rocks, however, also confirmed that these rocks are of highly metamorphic origin (Fig. Tan25). The rubies are therefore formed in magmatic rocks that are metamorphically overprinted. Strongly altered ultramafic rocks, such as talc-serpentinites, are present in the rock suite as well (Fig. Tan23d), but they are not the host rocks of the rubies. Pegmatite rocks intruded into the pargasite rocks locally as it was evident by huge 10 kg large mica crystals. No corundum was directly associated to these rocks. The corundum-garnet-pargasite rocks (containing rubies) are penetrated by a network of late fissure systems that are filled with carbonate (mostly magnesite) and agate (Fig. Tan20-22). These veins are indicative of late stage hydrothermal overprint of the rocks in the direct vicinity of the ruby-bearing garnet-pargasite rocks (Fig. Tan19a-d). Large quartz crystals or quartz-nodules are present in the mining area and were used as indicator minerals by the miners. We could not verify a direct relation between the ruby formation and the quartz formation but we found some quartz crystals at the mining site in the cover soil (Fig. Tan16d) and agate veins were present in the rocks containing the rubies (Fig. Tan19a). Marble rocks such as often occurring in other ruby deposits (Lit. Tan14, 24, 26, 30, 35) were largely absent at the mining site. A series of migmatite rocks were present at the marginal part of the main amphibolite rocks. They consisted of mixed layers and nodules of various rock types including white mica schist, layered gneiss, amphibolites and serpentinites (Fig. Tan16a).

ROCK-TESTING IN THE FIELD

Minerals were identified by a portable diode-laser Raman spectrometer. This portable GRS Field-Raman consists of a Two-Color Laser source in two separate boxes (NIR-Laser 785nm and green 532nm Laser). The probe includes a fiber optic bundle and a hand held long distance objective. It enables the measurements in direct contact of the uneven surfaces of rocks and minerals (Fig. Tan 20). The battery-supported instrument was tested for the Winza rocks with the following results. The NIR-Raman identified apatite, agate, magnesite, calcite, garnet and zoisite. The 532-Raman successfully detected rubies in the Winza host

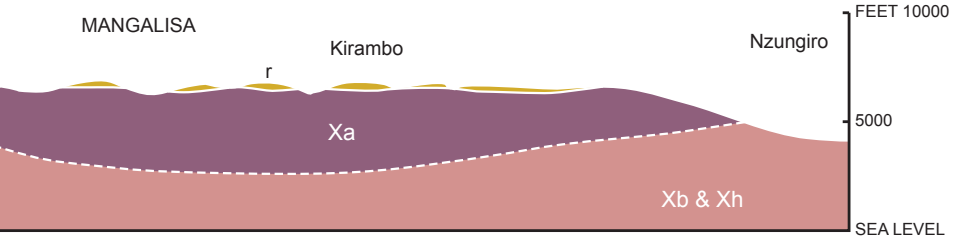

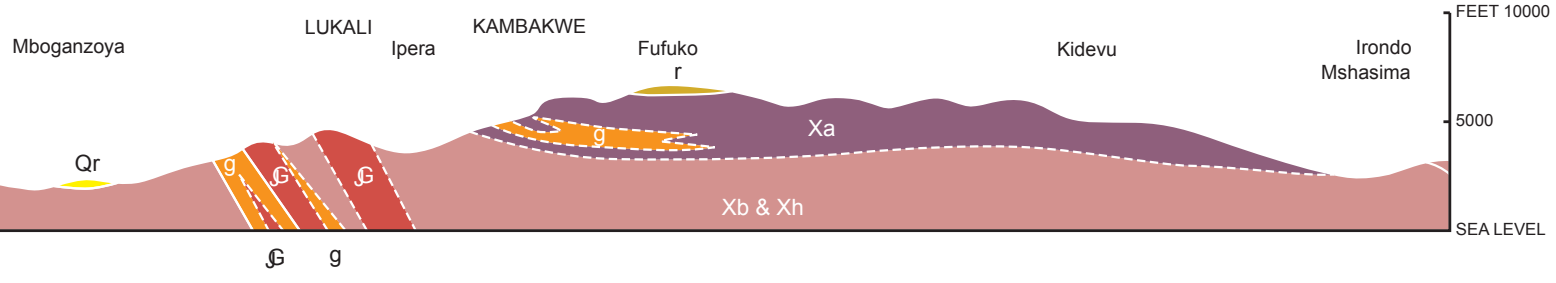

Legend

~	Alluvium	Xg	Migmatitic biotite gneiss and gneissose granodiorite	D	Olivine dolerite
~	'Mbuga' soils	Xgg	Granular quartzo-feldspathic gneiss and migmatitic biotite gneiss	D	Lamprophyre
r	Red-brown soils	Xb & Xh	Biolite gneiss and amphibolite	De	Altered olivine dolerite
r	High-level red earth	Xa'	Kyanite-garnet-biolite gneiss and schist		Dip of metasediments (bedding)
Qc	Plateau earths and highly weathered gneiss	h	Garnet-pyroxene amphibolite		Dip of Foliation
Qf	Calcareous crustal deposits	h	Eclogite (altered)		Strike of Foliation (dip vertical)
	Ferruginous crustal deposits	g	Porphyroblastic gneisses and schists (porphyroblastic migmatite)		Reverse Fault with Dip and direction of Thrust
	Talus	G	Alkali-granite		Joints, Vertical
Sg	Quartzite	G	Alkali-granite, foliated	P	Mines or Prospect working in 1959
So	Crystalline dolomitic limestone	mG	Microgranite	P	Mines or Prospect not working in 1959
Sp	Albite-epidote-chlorite -mica schists	B	Metedolerite and metagabbro	X	Mineral Occurrence not working in 1959

Fig. Tan09 Two geological profiles are shown. Their position is marked as A-A and B-B in the geological map (Fig. Tan10). Section A-A runs across the mining area. In the Profile A-A, the Winza ruby deposit is located in the Kinsasi, Mtindri section, in the area of migmatite rocks. The profile section B-B (further to the South of the "Winza" mine) shows the steep inclination of these rocks (including large foliated alkali-granite, eclogite, garnet-pyroxene amphibolite, metadolerite, metagabbro and migmatite). Profile sections were modified after Whittingham, 1959 (The Geology of the Nyanzwa Area, Quarter Degree Sheet 63 NW Geological Survey of Tanganyika, See Literature) by simplifications of the legend and minor additions. The map belonging to the legend see Fig. Tan10.

rock. The NIR-Raman experienced some limitations for ruby identification due to high fluorescence effects. Difficulties in applying the Field-Raman were noticed with dark-green and black minerals, such as pargasite. For these minerals it was not applicable. A portable computer with an installed software and an attached database enabled us to interpret the Raman spectra of the minerals (Fig. Tan 21). Raman spectra of pargasite and spinel could be obtained later at the University of Berne in Switzerland (Fig. Tan 27).

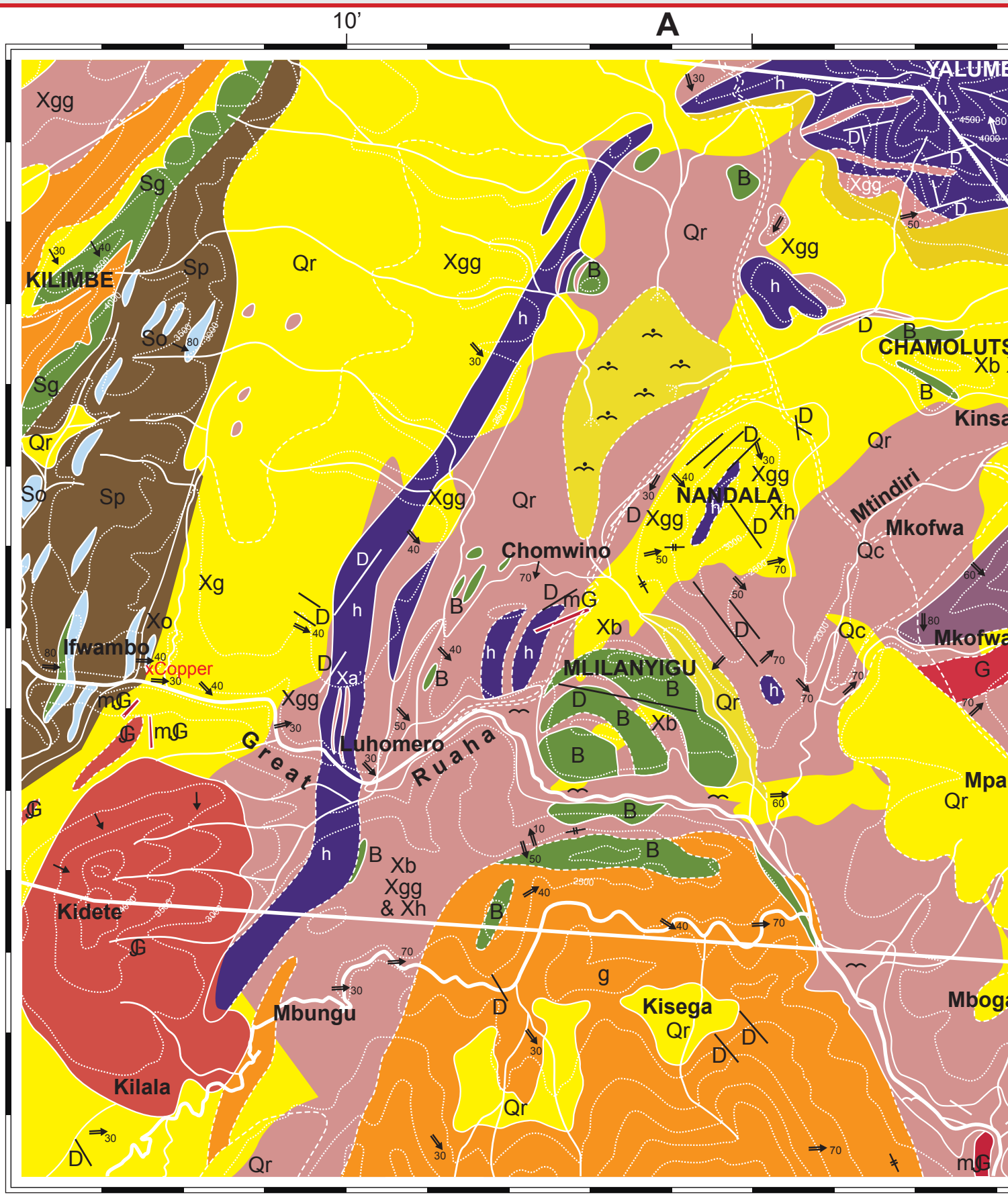

Fig. Tan10 Geological map in the vicinity of the new ruby mine at Winza (Tanzania). Drawn on the basis of a map available from the Geological Survey of Tanzania (Lit Tan38). Note the position of two cross-sections (A-A) and (B-B) (See Fig. Tan09). Note the presence of the following rock types in the vicinity of the mining site (indicated as "Winza"ruby mine in the map): Biotitic gneiss and amphibolites, granular quartzo-feldspathic gneiss and migmatite biotite-gneiss, metadolerite and metagabbro and alkali-granite. To the South East of the "Winza"-mine: Kyanite-garnet-biotite schist and to the North West of the "Winza"-mine: Garnet-Pyroxene

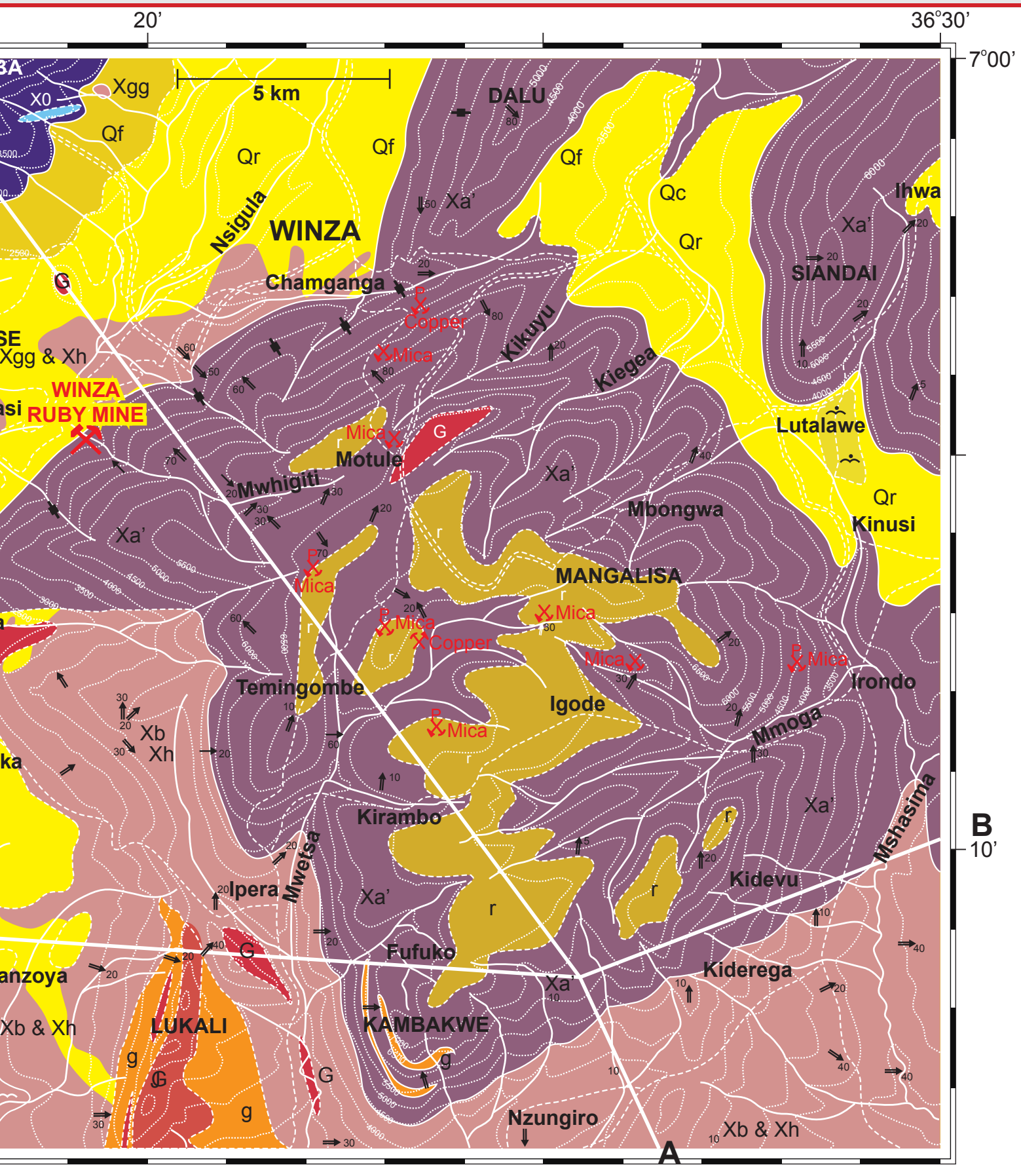

amphibolite and altered eclogite rocks. These rocks are indicative of high-grade metamorphism (high pressures and high temperatures). The outcrops are covered with red-brown soils and ferruginous crustal deposits. Source: Whittingham J.K. (1959). The Geology of the Nyanzwa Area, Quarter Degree Sheet 63 NW Geological Survey of Tanganyika, Printed by the Government Printer Dar es Salaam. Legend See Fig. Tan09. Winza ruby mine is located in the map and the original legend has been simplified.

Fig. Tan11a View in direction to SW to the “Winza” Ruby mine. In the fore ground the small river where the miners wash the ruby-bearing soils (the mine is about 0.5 km away). According to the geological map (Fig. Tan10) the mountain range in the back-ground consists possi-bly of Kyanite-garnet-biotite schist (a high-grade metamorphic rock type).

Fig. Tan11b View to the North West from a different viewing point to the same washing place as shown in Fig. Tan11a. According to the geological map (Fig. Tan11a), the small hill in the background consists of completely different rock types, possibly garnet-pyroxene amphibolites and eclogites. These rocks are also indica-tive of high-grade metamorphism.

Fig. Tan12 The police station tent at the mining camp in Winza. At the point of arrival, we were immediately arrested and the camera equipment was confiscated. After it was verified that we had permission papers from the government, the expedition members were registered in a log book and the passage to the mine was granted.

Fig. Tan13a

Fig. Tan13b

Fig. Tan13c

Fig. Tan13d

Fig. Tan13 Details of living conditions in August 2008 at the mining site that served as our base camp at the Winza mine in Tanzania. We reached the mine by car (Fig. Tan13a) and stayed overnight in primitive huts (Fig. Tan13b). Meals were prepared at an open fire (Fig. Tan13c). Numerous small claims with small hills and open pits surrounded the camp (Fig. Tan13d).

Fig. Tan14a

Fig. Tan14b

Fig. Tan14c

Fig. Tan14 The outcrops were documented by filming and photographing under extremely harsh conditions (in the picture is one of the authors AK). Fig. Tan14b shows one of the authors (AP) and a local geologist Mr. Rogers Sezinga from Mineral Consultancy (Co., LTD). He is elaborating on the formation and structure of large-scale fracture zones and hydrothermal activities in the rocks and their relation to the occurrences of the ruby findings. Ruby samples were obtained by hammering pargasite-garnet rocks into small pieces (Fig. Tan14c).

Fig. Tan15a

Fig. Tan15b

Fig. Tan15c

Fig. Tan15 The general overlook of the mining scene is shown. The main portion of the mine is a hillside deposit with a meter thick weathered surface soil that is underlain by hard rocks. The mining activities are concentrated on numerous small claims (Fig.Tan15a). Fig. Tan15b-c shows the digging on the surface, the sheaving of the soil and its transportation in bags to the washing site at the nearby small river.

Fig. Tan16a

Fig. Tan16b

Fig. Tan16c

Fig. Tan16d

Fig. Tan16 The hard rock appears after one meter of topsoil and reveals the presence of migmatite rocks with round gneiss and amphibolite boulders. Ruby samples were acquired from local miners (in the picture “Masai”) at the spot (Fig. Tan16b, c). Quartz nodules and quartz crystals were also found in the topsoil and collected (Fig. Tan16d).

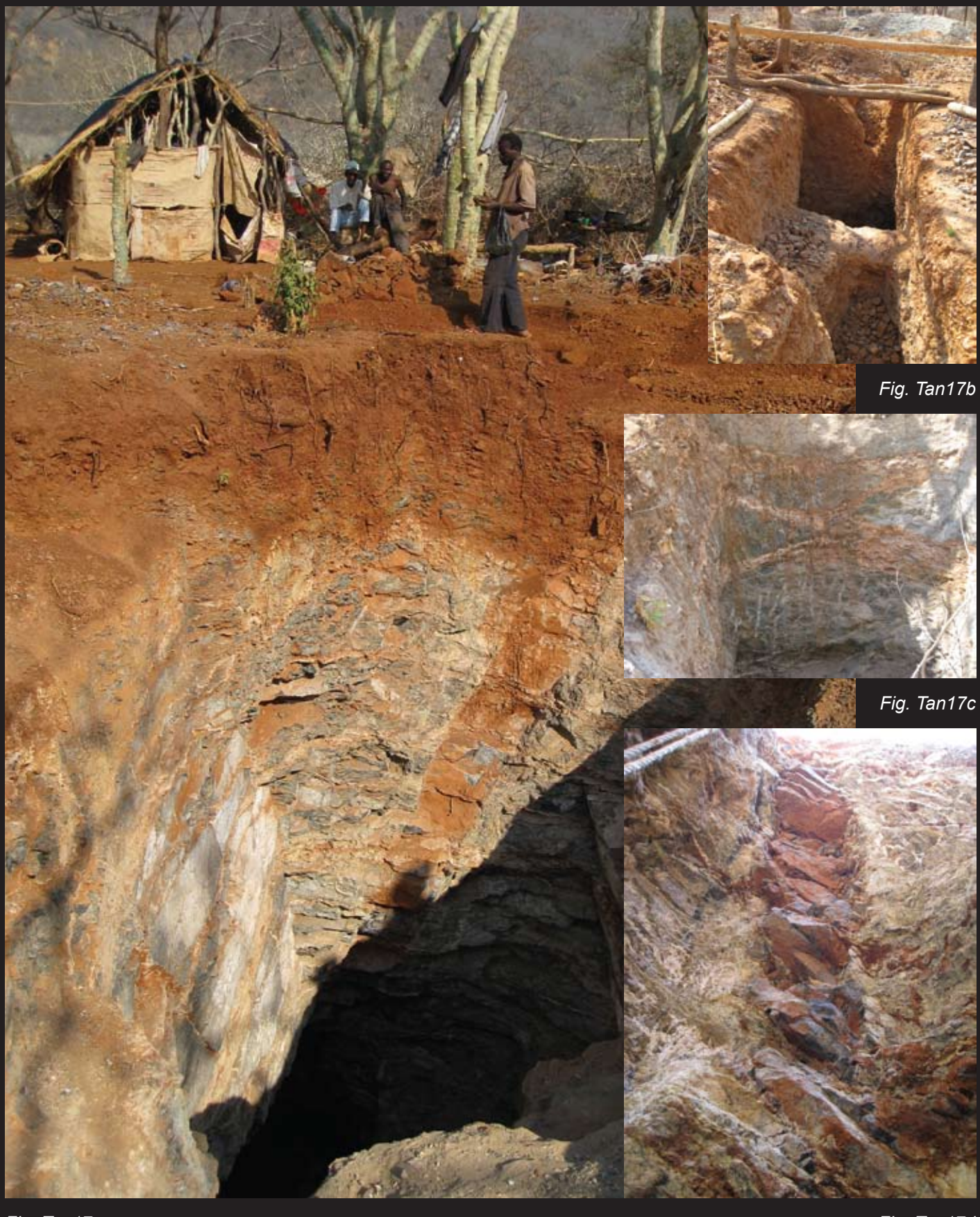

Fig. Tan17b

Fig. Tan17c

Fig. Tan17a

Fig. Tan17d

Fig. Tan 17a, b, c, d Deep shafts were blasted from the hard rock to follow some garnet-corundum dykes that are present in the pargasite rocks (Fig. Tan17a) and hydrothermal alteration zones (Fig. Tan17c). Small open pits and shafts were made at the surface to follow these ruby-bearing zones (Fig. Tan17b, c) One of the authors (AP) climbed more than 10 m down into a shaft and took a picture of the dyke by looking backwards to the surface (Fig. Tan17d). These pargasite-rich rocks locally contained large amounts of corundum as well as garnet. Ruby and sapphire were occasionally found in these zones (See Fig. Tan24a-d).

Fig. Tan18a

Fig. Tan18b

Fig. Tan18c

Fig. Tan18 Details of the field studies are shown. One of the authors (AP) repels down a 15 m deep shaft with the help of a rope and documents the rock formations by filming and photographing (Fig. Tan18c). He is followed by a group of migrant-workers who came from the area of Meralani (Tanzania) (Fig. Tan18b). They applied their experience for mining in the hard rocks using explosives. Two police staff assisted us for guidance and personal protection (Fig. Tan 18a).

Fig. Tan19a

Fig. Tan19b

Fig. Tan19c

Fig. Tan19d

Fig. Tan19e

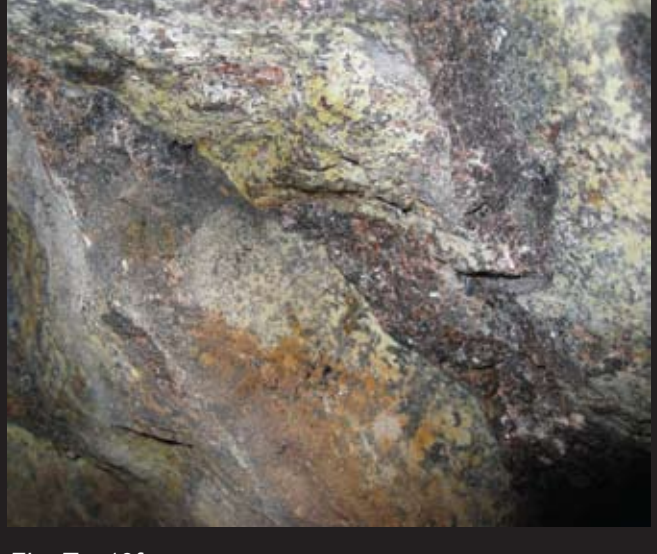

Fig. Tan19f

Fig. Tan19 The miners showed us key outcrops, which enabled us to find the important key samples in a very short time. We were able to sketch details of the rocks in the deep shafts, such as intersections of magnesite-agate veins with corundum-rich dykes (Fig. Tan19a, b). Fig. Tan19c shows the examination with a Geiger counter to check for radioactivity (no radioactivity was detected). Specimens were hammered from the outcrops and labeled (Fig. Tan19d). Fig. Tan19e, f are garnet-rich pargasite rocks.

Fig. Tan20

Fig. Tan20 The GRS field Raman spectrometer is shown which consists of a notebook computer, two different Raman Laser sources (NIR785nm and 532nm), a fiber optic bundle and a hand held objective. The system is portable and battery-supplied. The NIR 785nm Laser is in use while the 532nm, as an exchangeable unit, is hidden in the compartment (the picture has been reconstructed and edited for clarity and confidentiality outside the mining area). In the picture: Whitish veins of agate, carbonate and magnesite.

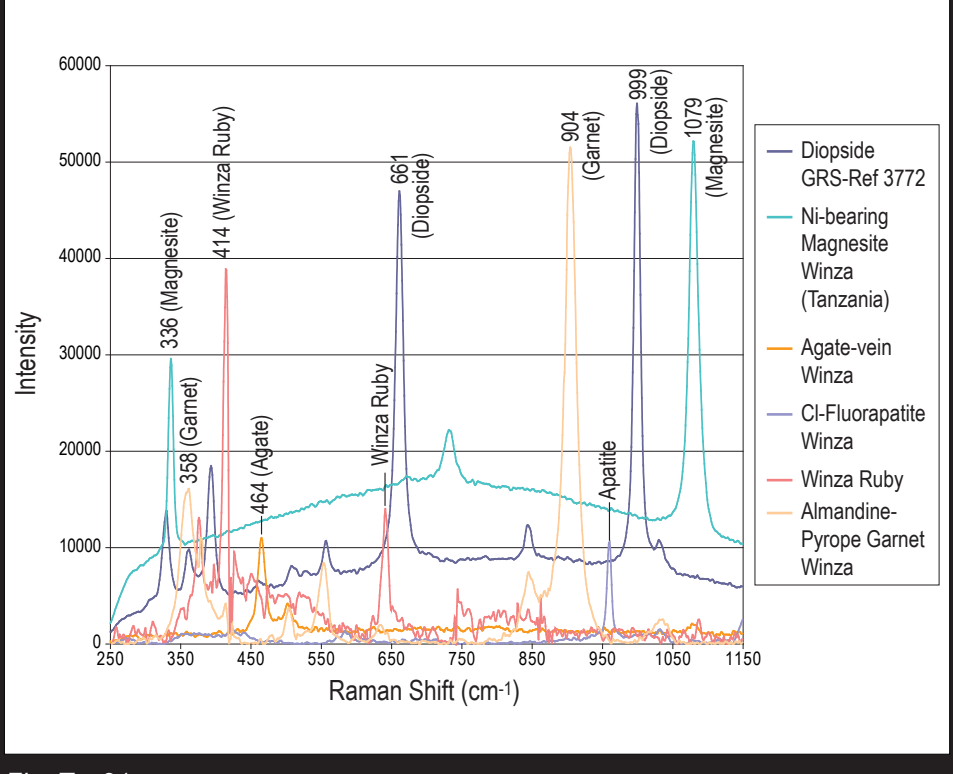

Fig. Tan21

Fig. Tan21 A series of Raman spectra recorded by a portable GRS Raman instrument (NIR Laser). Different minerals could be identified (See spectra). Note that magnesite, quartz, apatite and garnet can be easily differentiated (including other minerals such as zoisite, calcite, aragonite, rutile and spinel). Diopside was not detected in the mine but its spectrum is given for reference purposes (Raman spectra of magnesite and diopside are not background corrected). To obtain a Raman shift signal of certain rubies, the Raman instrument had to be exchanged with the green Laser source. (Fig. Tan26 and Tan27).

Fig. Tan22a

Fig. Tan22b

Fig. Tan22a, b Two minerals were present in veins within the garnet-corundum-pargasite rocks: Aggregated magnesite in folded veins (Fig. 22a) and banded agate veins with outer whitish rims of magnesite (Fig. 22b). This sample was taken from the outcrop of Fig. Tan19a. Later chemical testing by ED-XRF showed that magnesite contains traces of nickel.

Fig. Tan23a

Fig. Tan23b

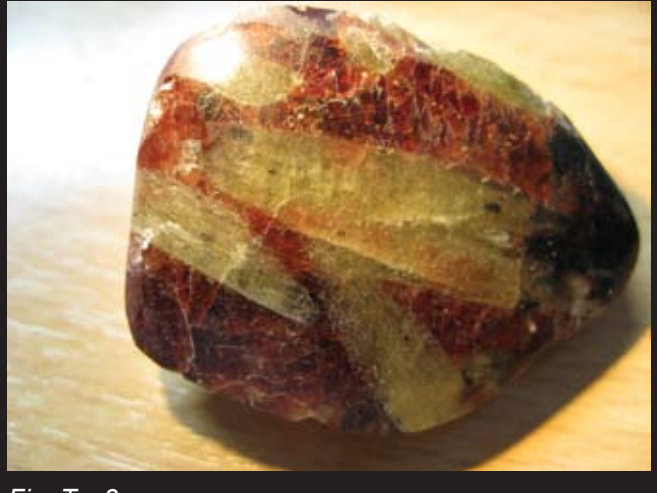

Fig. Tan3c

Fig. Tan23d

Fig. Tan23e

Fig. Tan23 Example of rock types found at the mines: Fig. Tan23a amphibolites with plagioclase spots (does not contain corundum), Fig. Tan23b banded gneiss, Fig. Tan23c garnet nodules that contained large zoisite crystals, Fig. Tan23d a deeply weathered serpentinite and Fig. Tan23e white mica gneiss.

Fig. Tan24a

Fig. Tan24b

Fig. Tan24c

Fig. Tan24d

Fig. Tan24 Corundum was found in various types of amphibolites such as corundum-pargasite rocks or corundum-garnet-pargasite rocks. Fig. Tan24a shows the formation of corundum at the contact zone to a garnet- rich layer within an amphibolite. Corundum was formed across this contact zone and was partially composed of ruby and sapphire (bi-colored). The sapphire part of the corundum crystal was formed on the side of the garnet-rich layer. Fig. Tan24b and Fig. Tan24c show examples of sapphire and ruby crystals that were grown within garnet-rich amphibolites. Long crystal habits were found in these rock types. Rhombohedra ruby shapes were found in another pargasite rock type, e.g. with lower concentrations of garnet (Fig. Tan24d).

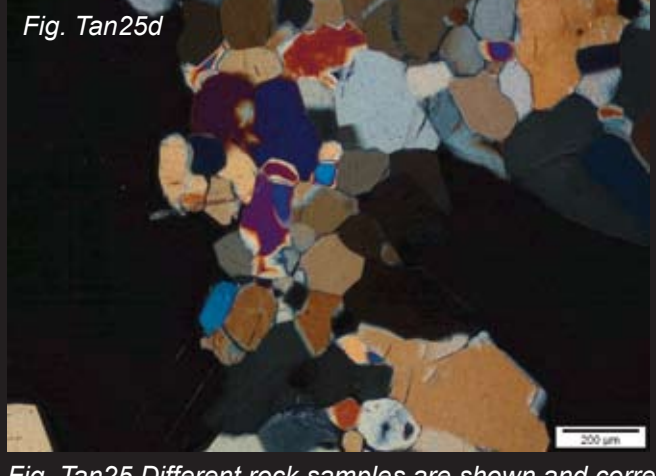

Fig. Tan25 Different rock samples are shown and corresponding thin sections (Fig. Tan25a). A total of 7 different rock cubes were prepared (from the left): 5 cubes with different types of corundum-pargasite-garnet amphibolites (pargasite is green, garnet is brown), a white mica-gneiss and on the right a garnet-pargasite rock with a large ruby (thin section of sample shown in Fig. Tan25a). From this samples a series of thin section were obtained. These sections were studied in a Petrographic Microscope. The minerals were than optically identified and their intergrowth texture was studied. Fig. Tan25c shows one of the rocks in crossed polarized light (left) and non-polarized light (right). Note the mosaic texture of the pargasite minerals with angular grain boundaries forming 120 degrees angels (no plagioclase and no pyroxene detected). Such metamorphic textures are typically found in well-equilibrated rock suites of the amphibolite to granulite facies grade of metamorphism. Further results see Fig. Tan26 and Tan27.

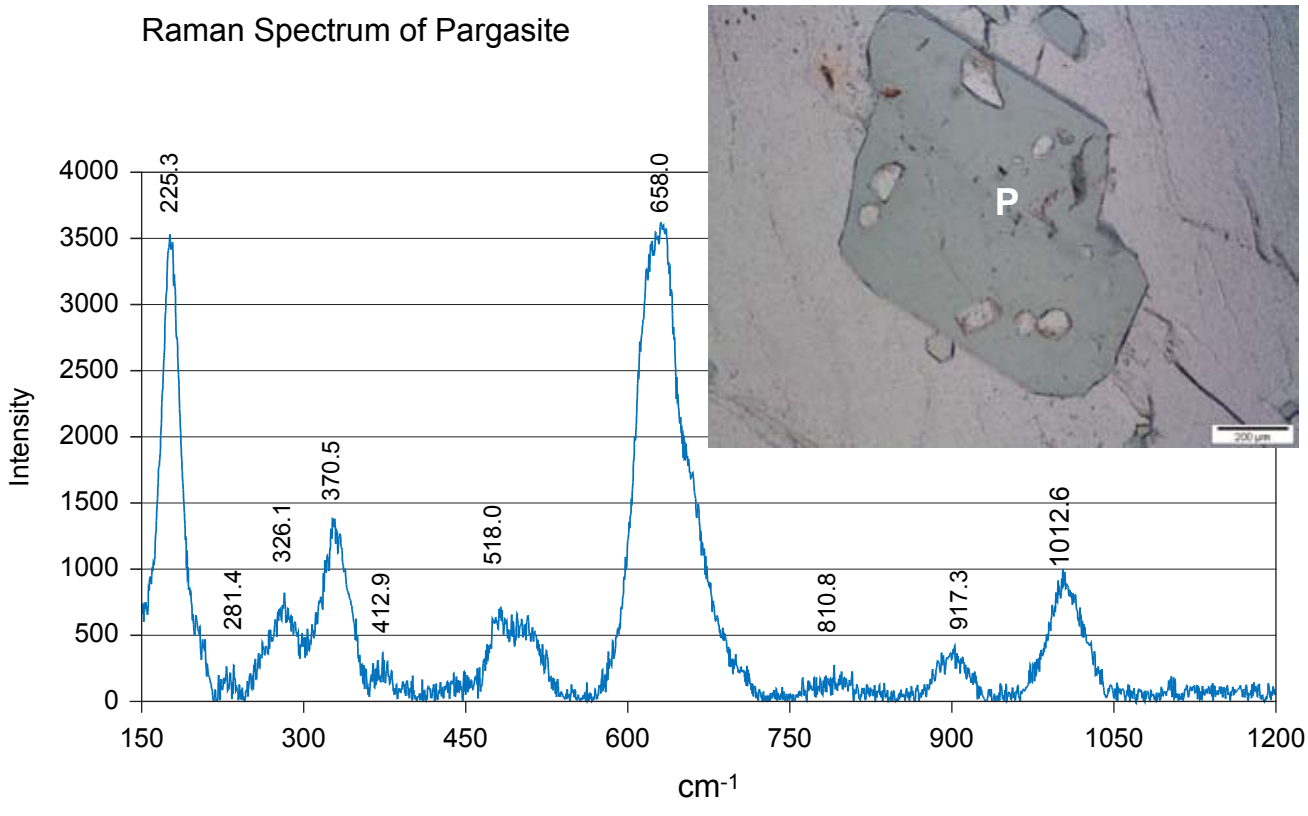

Fig. Tan26 Identification of minerals in thin sections was confirmed by Raman spectroscopy (G. Lambrecht, University of Berne, Institute of Geological Sciences, Research Group Rock-Water Interaction of Prof. L. Diamond). Raman spectrum confirmed pargasite. Micro-photo of the same analyzed green pargasite is inserted (thin section analyses by Ivan Mercolli, University of Berne, Switzerland).

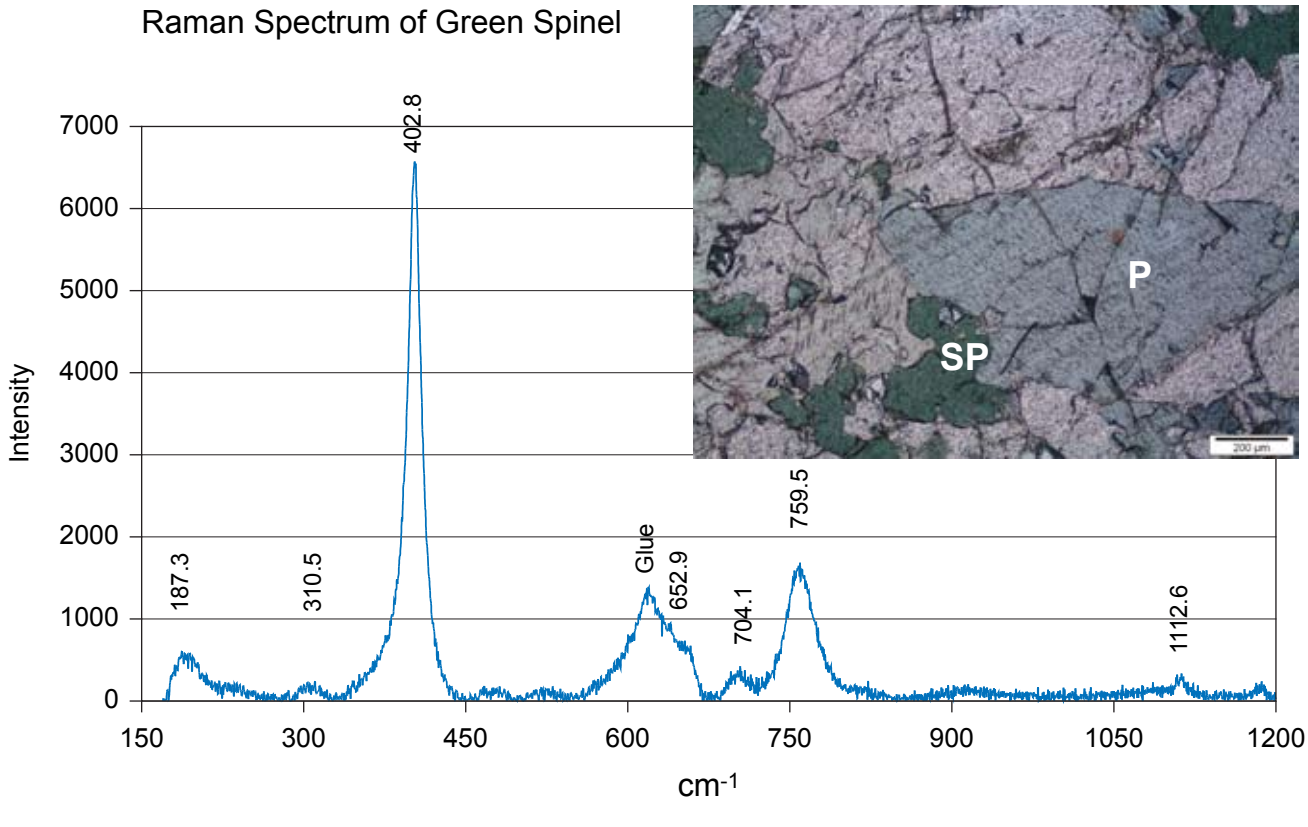

Fig. Tan27 Raman spectrum of green spinel found as a rock-forming mineral in a thin section. Micro-photo of the same analyzed spinel is inserted. (P = Pargasite, SP = Spinel)

Fig. Tan28a

MATERIALS

A large series of rough rubies were acquired directly from the mine. Further material was found on the market in Thailand. The rough materials were polished at GRS and registered in the GRS reference collection. A series of highly valuable faceted rubies from the market were tested in the GRS laboratories (Fig. Tan04). They were also included in this study for comparison with the collected samples from the mining site.

Fig. Tan28b

Fig. Tan28c

Fig. Tan28 Large amounts of rough rubies were available for research. They were acquired at the mining site itself (Fig. Tan28a, b) as well as from African suppliers in Bangkok (Fig. Tan28c).

Fig. Tan29a

Fig. Tan29b

Fig. Tan29c

Fig. Tan29d

Fig. Tan29d

Fig. Tan29 Series of different rough crystals are found at the Winza mine in Tanzania: Fig. Tan29a Long pencil-like habits Fig. Tan29b Rhombohedra habits resembling spinel crystal shapes and Fig. Tan29c Curved teeth-like shapes. The type (a) rubies contain often blackish-blue sapphire skins. The 3-5cm long sapphire/ruby rough crystals have poorly developed outer terminations because they were grown as a rock-forming mineral.

Fig. Tan30a

Sample No. GRS-Ref7330

Fig. Tan30b

Sample No. GRS-Ref7153

Fig. Tan30a, b Two rare example of Winza rubies with idiomorphic habit. Length of long crystal is 9 mm. In contrast, another ruby has negative imprints of other minerals on its surface (Fig. Tan29d). Weight 1.13ct.

Fig. Tan31a

Fig. Tan31b

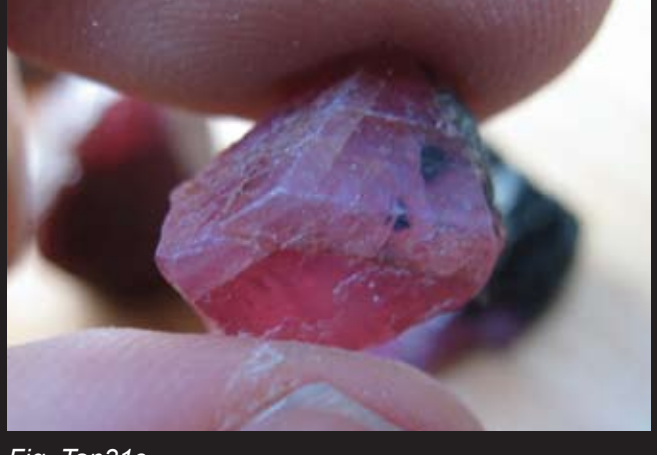

Fig. Tan31c

Fig. Tan31d

Fig. Tan31e

Fig. Tan31 Details of ruby rough crystals from the Winza mine (GRS reference collection). Ruby without blue color zoning is found in pargasite-bearing plagioclase-rich rock (Fig. Tan31a). It was obtained from a miner and proves that the rubies also formed in other rock-types containing plagioclase. A series of different shapes are found: Ruby with large rhombohedra faces resembling octahedral spinel shapes (Fig. Tan31b, c), a ruby crystal with steep pyramids, a ruby core and a sapphire mantle (Fig. Tan31d) and a black sapphire with a pink sapphire mantle (Fig. Tan31e). The inclusion in the black sapphire is a garnet.

Fig. Tan32. An insight in to part of the GRS reference samples from the Winza mine. These rubies have been faceted from our rough for the purpose of this study. The collection comprises over 100 faceted, 300 cabochon, more than 200 rough ruby crystals with polished windows and over 500 rough pieces that are spared of cutting. They remain in the GRS collection as original samples collected from the mine.

BOX TAN01:
MINERAL INCLUSIONS IN WINZA RUBIES IDENTIFIED BY SEM-EDX, ED-XRF, RAMAN AND XRD

Authors

WB

<u>SEM-EDX analysis (Pages 41-48)</u>

Apatite, Pargasite with chemical variations, Green Spinel, Black Spinel, Ca-Mg-Carbonate and Mg-Al-Chlorite.

AP

<u>ED-XRF analysis</u>

Apatite, Pargasite, Xenothim and Zirconolith

AP

<u>Raman analysis (Pages 17, 21 and 38)</u>

at GRS: Apatite, Garnet and Talc (Magnesite, Agate and Zoisite in parent rock).
at University of Bern: Pargasite and Spinel

<u>XRD analysis (Page 41)</u>

Garnet (Pyrope-Almandine) and Pargasite (Cl-Ferro-Pargasite)

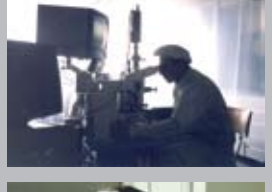

DG

<u>LA-ICP-MS analysis (Pages 93-94)</u>

Pargasite, Apatite and Garnet (with REE)

FP

<u>Optical identifications in the microscope (Pages 33-37 and 39-40)</u>
Apatite, Garnet, Pargasite and Pyrite
<u>Optical property of Pargasite as determined by refractometer</u>
Pargasite x = 1.649, z = 1.670 DR= 0.021, 2A+

<u>Statistics of inclusions in Winza Rubies</u>

Very abundant	*Pargasite*
Abundant	*Spinel and Garnet*
Rare	*Apatite, Pyrite, Xenothim and Zirconolith*

Fig. Tan33 Winza ruby rough crystal is shown. Facets have been polished parallel to the original growth faces. It became visible that a blue color skin is present. A series of fluid inclusion trails are present which are cutting through this color zoning. They are visible as curved red lines inside the blue color zone. For further explanation of this phenomena see Fig. Tan36. Sample No. GRS-Ref7151. Crystal length 26.5 mm, weight 12.81ct.

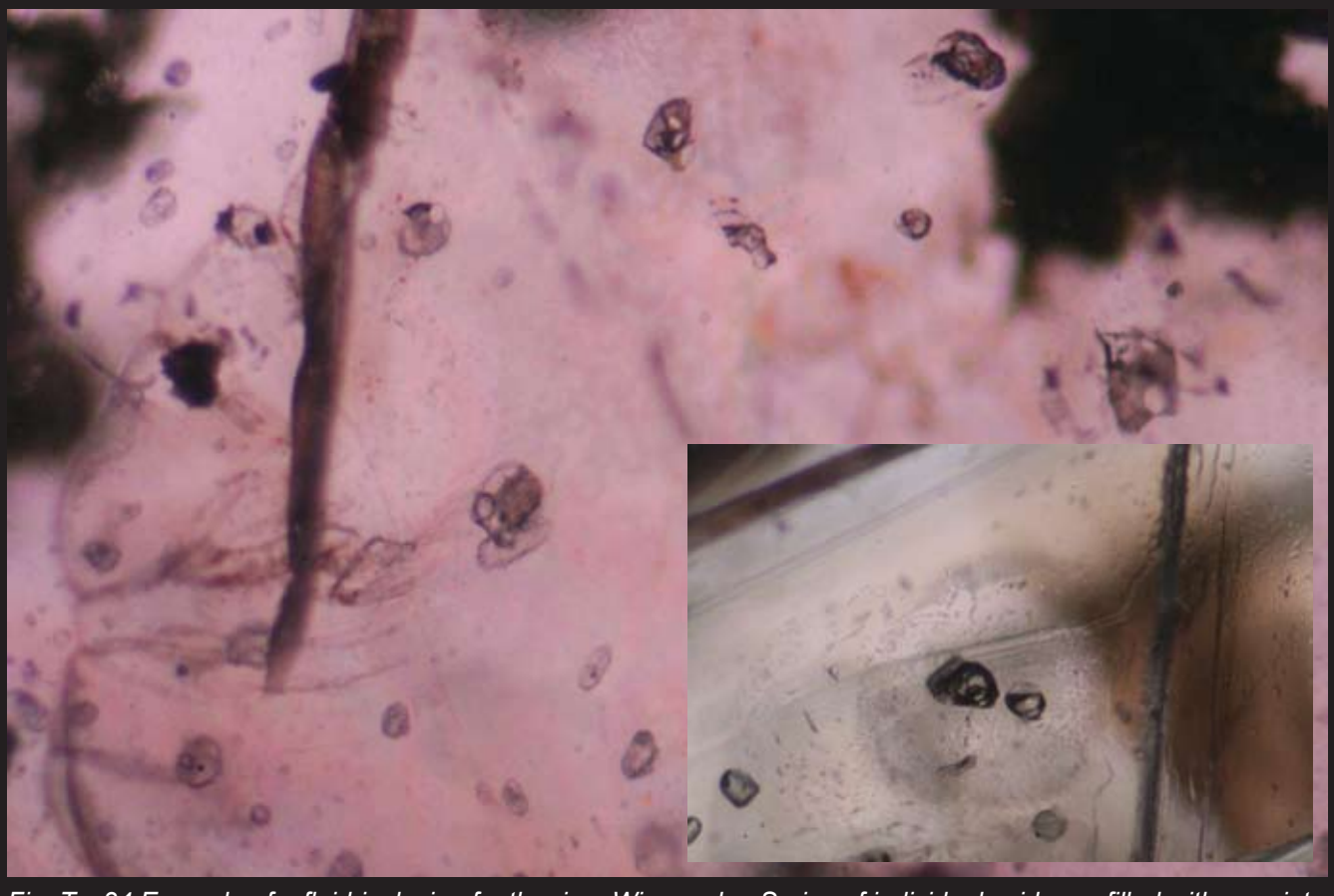

Fig. Tan34 Example of a fluid-inclusion feather in a Winza ruby: Series of individual voids are filled with a variety of solids, vapor and liquid. The solids (or daughter minerals) include black crystals, colorless rectangular solids, solids of monoclinic or triclinic shapes and needles. Inserted picture: Primary fluid inclusion with a surrounding secondary fluid inclusion feather (transmitted and reflected light).Sample No. GRS-Ref7378.

Fig. Tan35a

Fig. Tan35b (Sample No. GRS-Ref7149)

Fig. Tan35a,b Pinkish color patches are present in an otherwise blue color zone. They are concentrated around fluid inclusions.

Fig. Tan36

Fig. Tan36 Color zoning found in rubies from Winza. Pink color halos are present in otherwise blue color zones. These formations are concentrated along fluid inclusions trails and created by a chemical reaction of the fluids with the ruby (Sample No. GRS-Ref7166).

Fig. Tan37 Photo of a faceted purplish-red ruby from Winza with numerous fluid inclusions. The fluid inclusions are entirely filled with whitish daughter minerals. Sample No. GRS-Ref7125. Fiber optic and transmitted light.

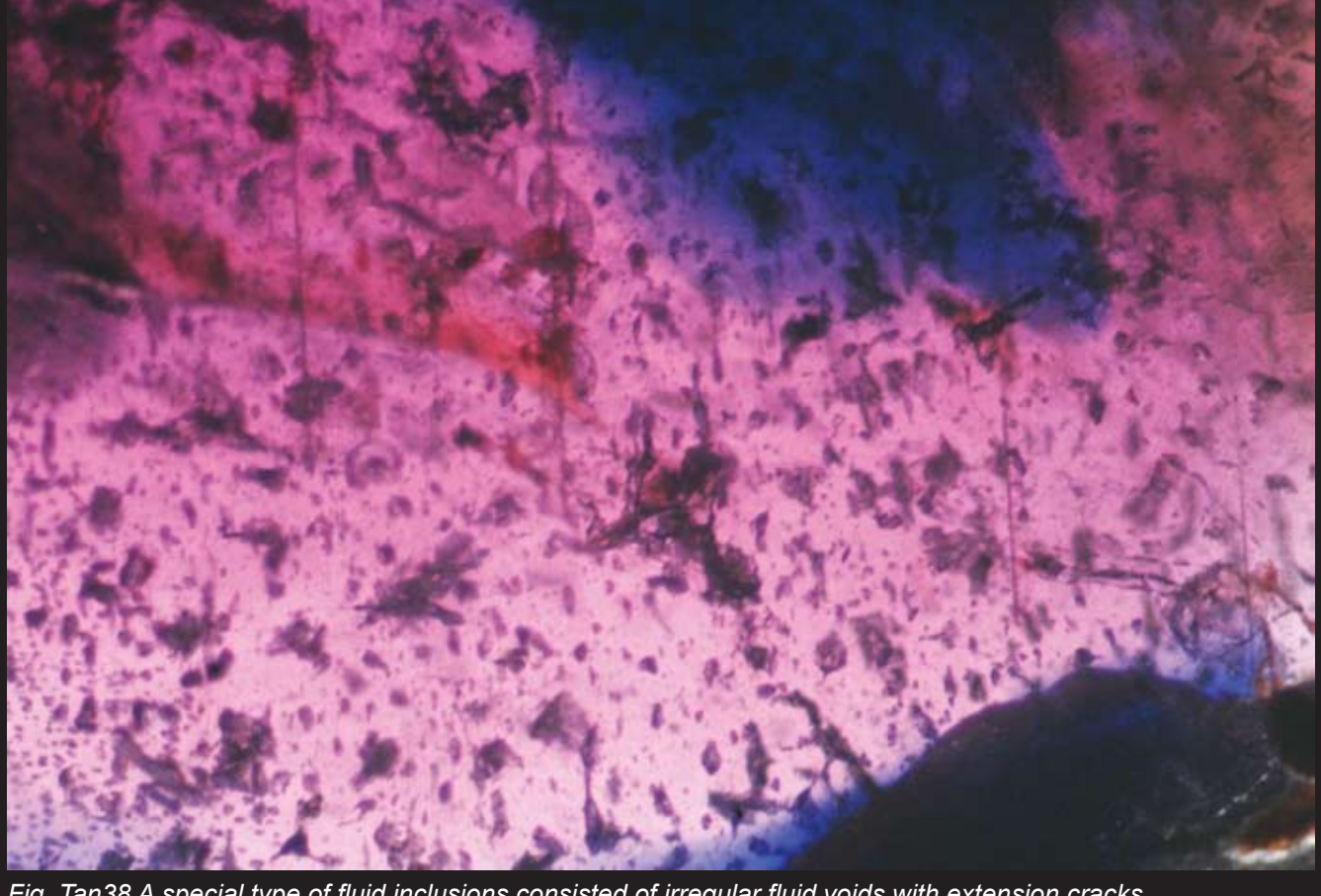

Fig. Tan38 A special type of fluid inclusions consisted of irregular fluid voids with extension cracks. Sample No. GRS-Ref7368

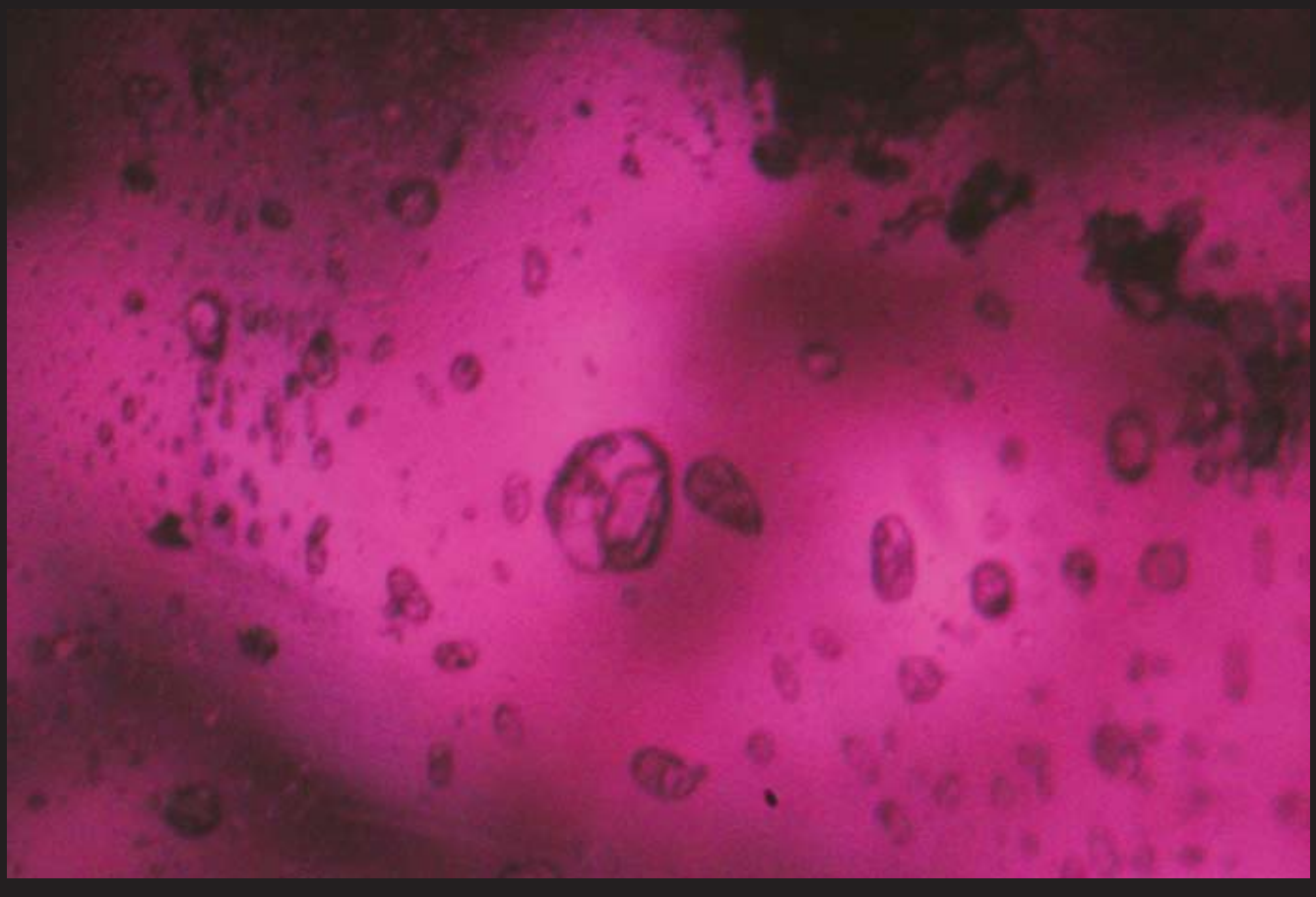

Fig. Tan39a (Sample No. GRS-Ref7379)

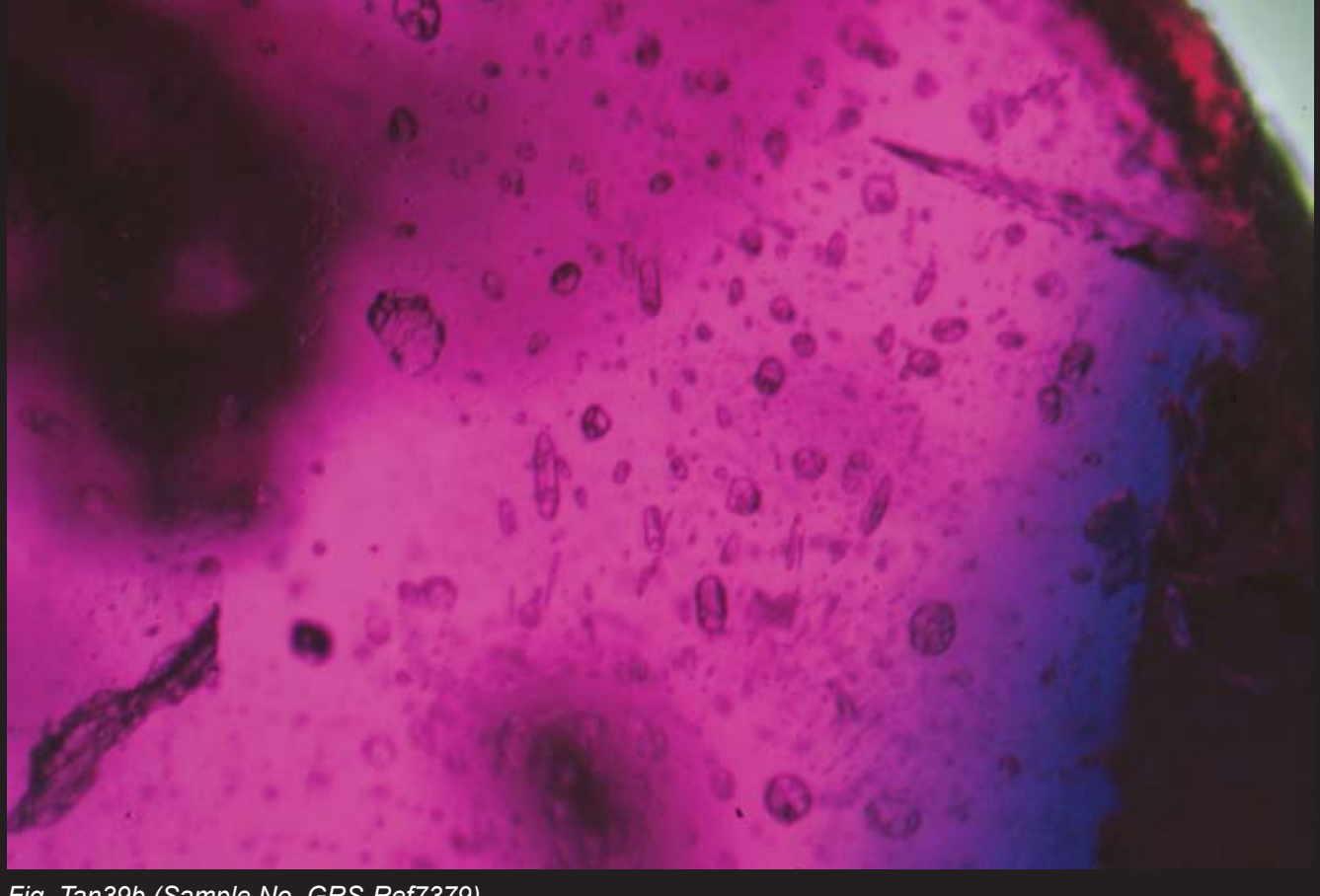

Fig. Tan39b (Sample No. GRS-Ref7379)

Fig. Tan39a, b Examples of fluid-inclusion feathers in rubies. Series of individual voids are filled with a variety of solids, vapor and liquid. The solids (or daughter minerals) include black crystals, colorless rectangular solids, solids of monoclinic or triclinic shapes and needles.

Fig. Tan40a

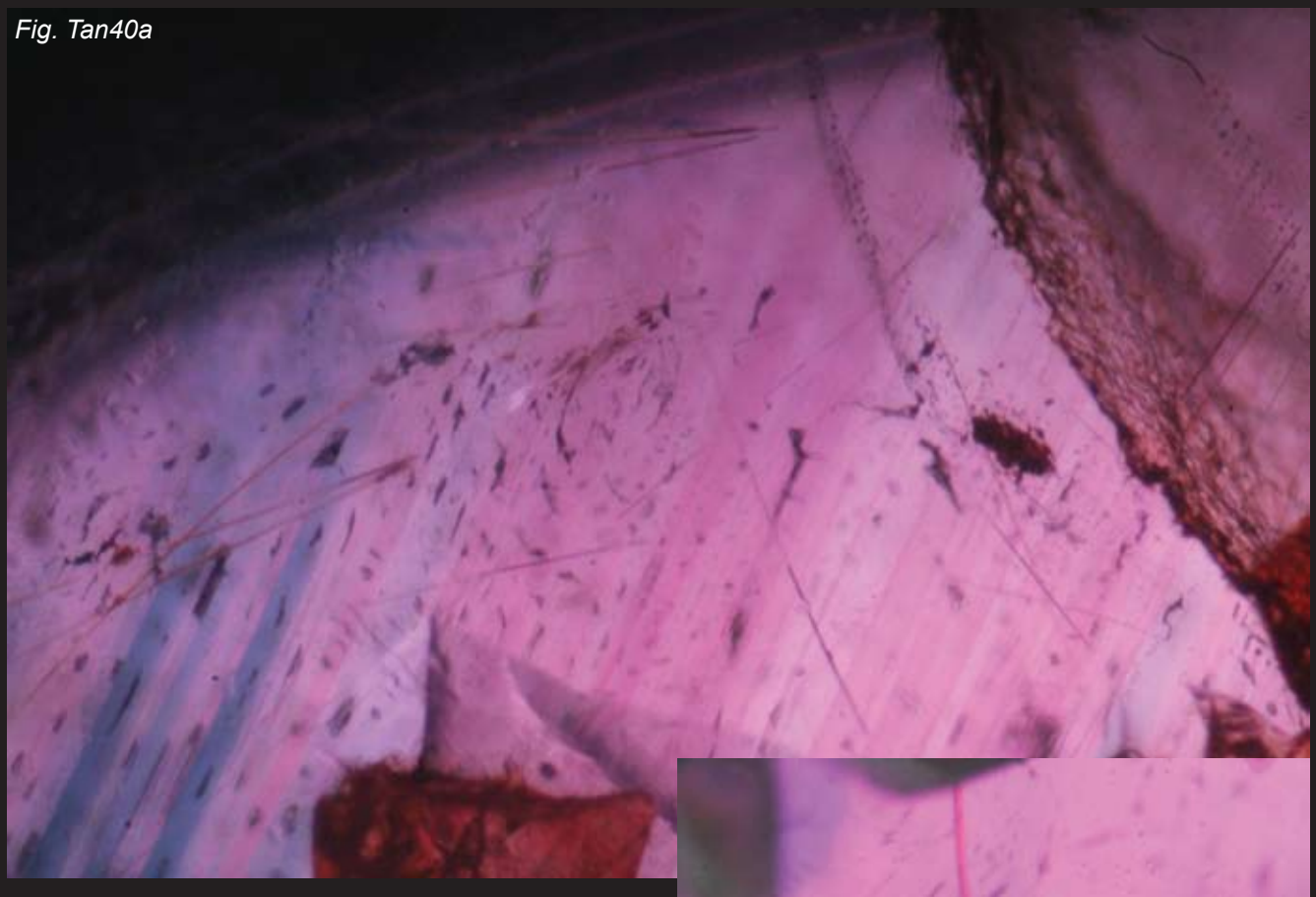

Fig. Tan40a, b Color zoning in a Winza ruby. Series of red and blue color bands were found together with arched orangy needles and fluid inclusion feathers. The needles are hollow tubes. Sample No. GRS-Ref 8321. Hollow tubes are arched (Fig. Tan40b).

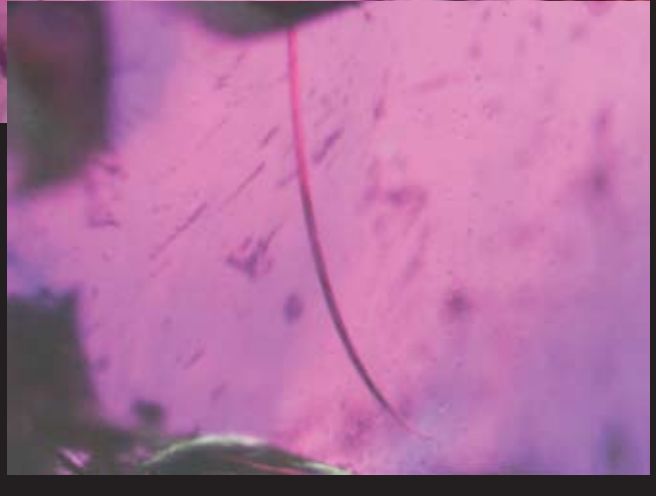

Fig. Tan40b

Fig. Tan41

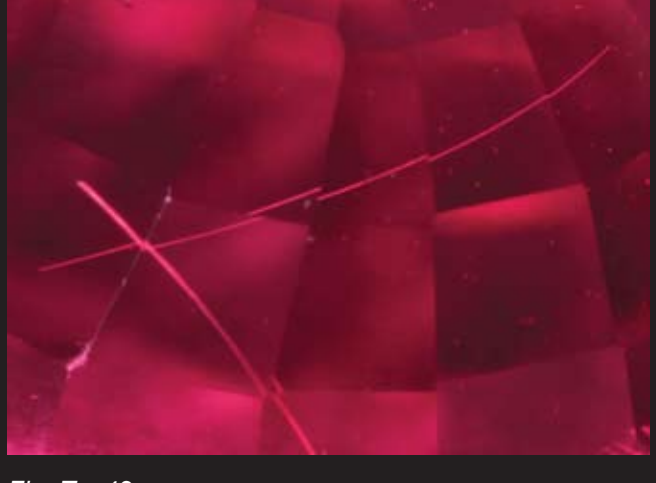

Fig. Tan42

Fig. Tan41 and Fig. Tan42 Faceted rubies with needle like inclusions. The following two different types of needles were found: Flat needles and hair-like needles. The hair-like needles occur in groups and are often curved. They do not follow a special orientation in the ruby crystal.

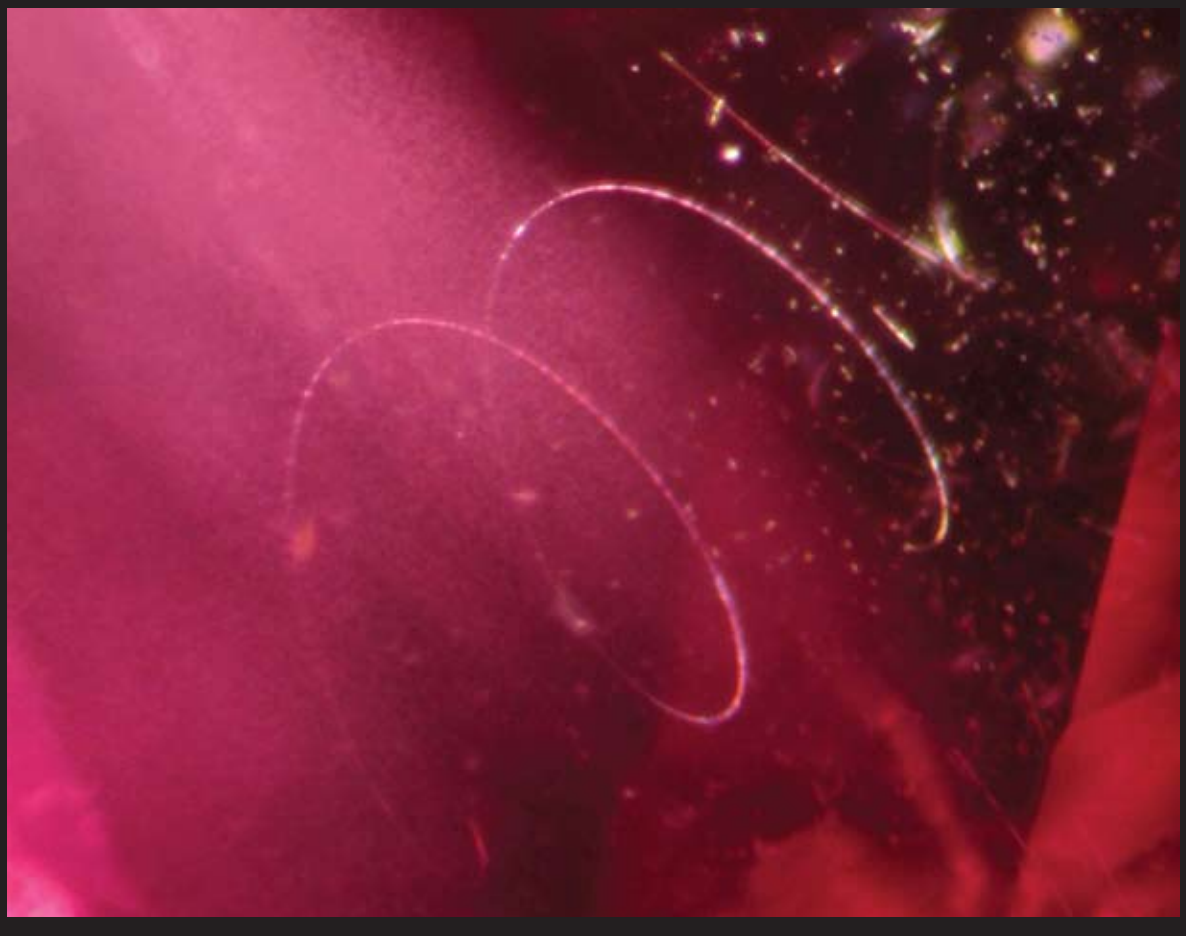

Fig. Tan43a

Fig. Tan43b

Fig. Tan43a, b Arching and spiraling hair-like needle inclusions are found in unheated rubies from Tanzania. In the case of Fig. Tan43a, a hair-like inclusion appears in the form of a spiral (3x360 degrees rotated). No explanation has been found so far to explain this formation.

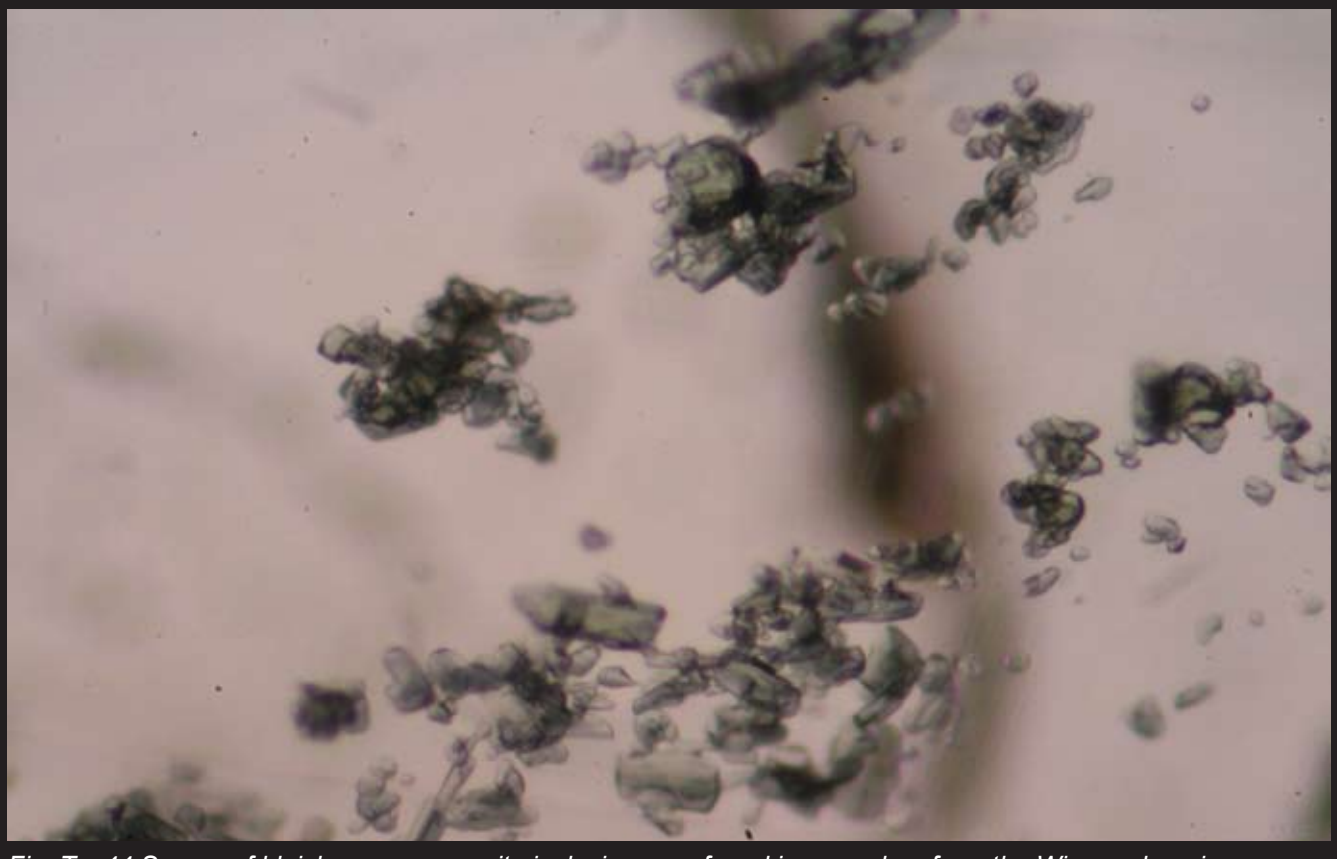

Fig. Tan44 Scores of bluish-green pargasite inclusions are found in corundum from the Winza ruby mine (Tanzania). (Sample No. GRS-Ref7375)

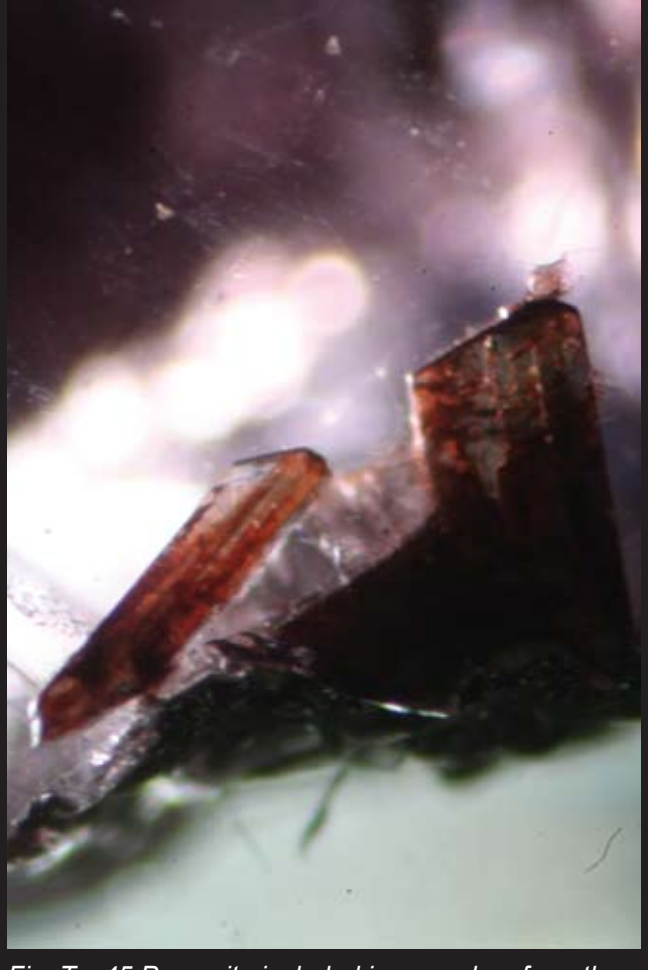

Fig. Tan45 Pargasite included in corundum from the Winza mine that appear orange colored due to surface-oxidation. (Sample No. GRS-Ref7465)

Fig. Tan46 A series of pargasite in a Winza ruby (Transmitted light 40x magnification, White field illumination, Sample No. GRS-Ref7814).

Fig. Tan47 A flat void in a Winza ruby is filled with an aggregate of pargasite. The Cl-pargasite is chemically zoned with more intense colored rims. (Sample No. GRS-Ref1379)

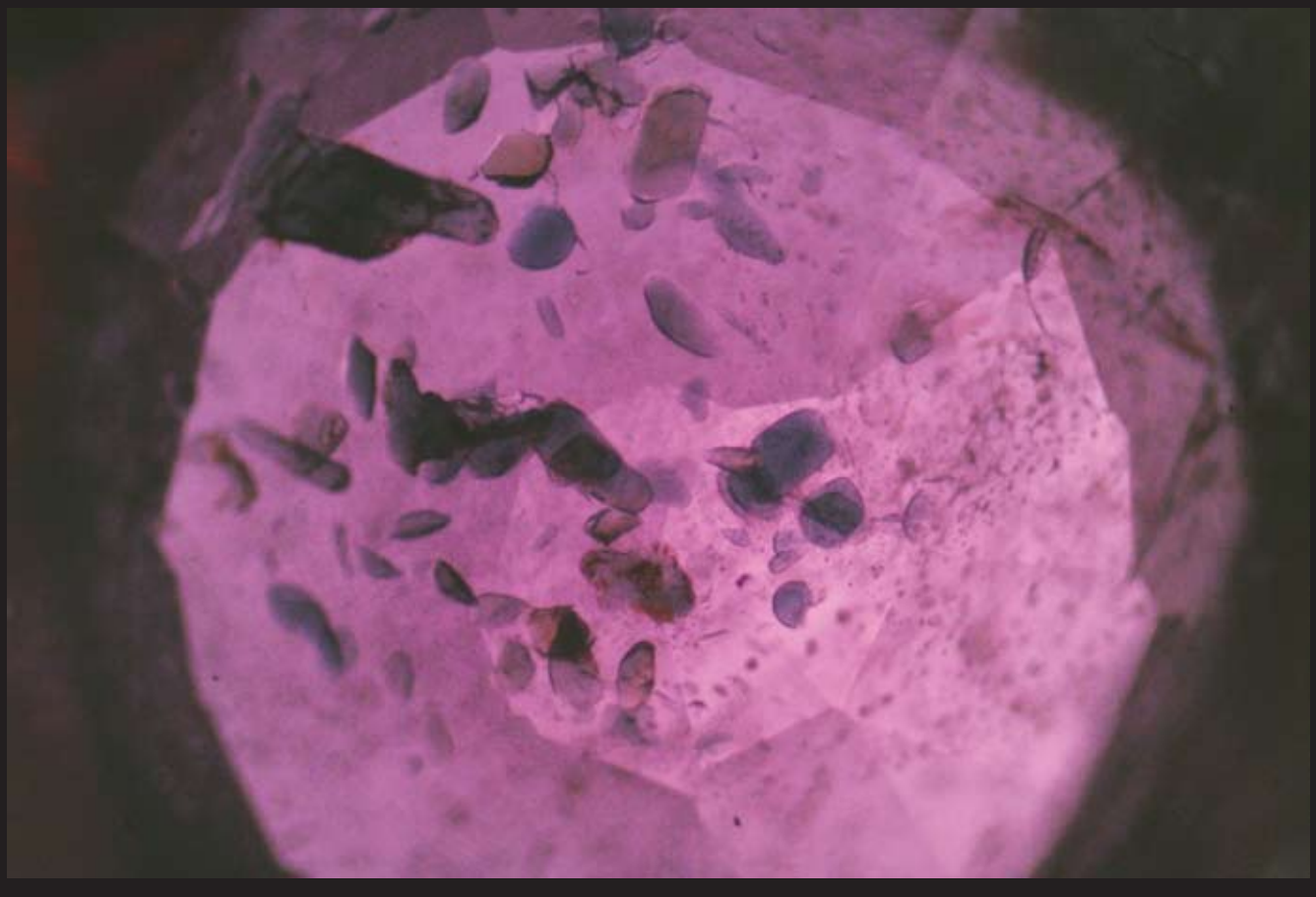

Fig. Tan48 Pargasite inclusions in a Winza pink sapphire. Different colors of the pargasite inclusions are due to different orientation of the minerals (strong dichroism) and/or variations in its chemical composition.

Fig. Tan49 Series of different colored pargasite are included in a Winza ruby. The color is due to strong pleochroism and/or chemical variations in pargasite. (Sample No. GRS-Ref7211)

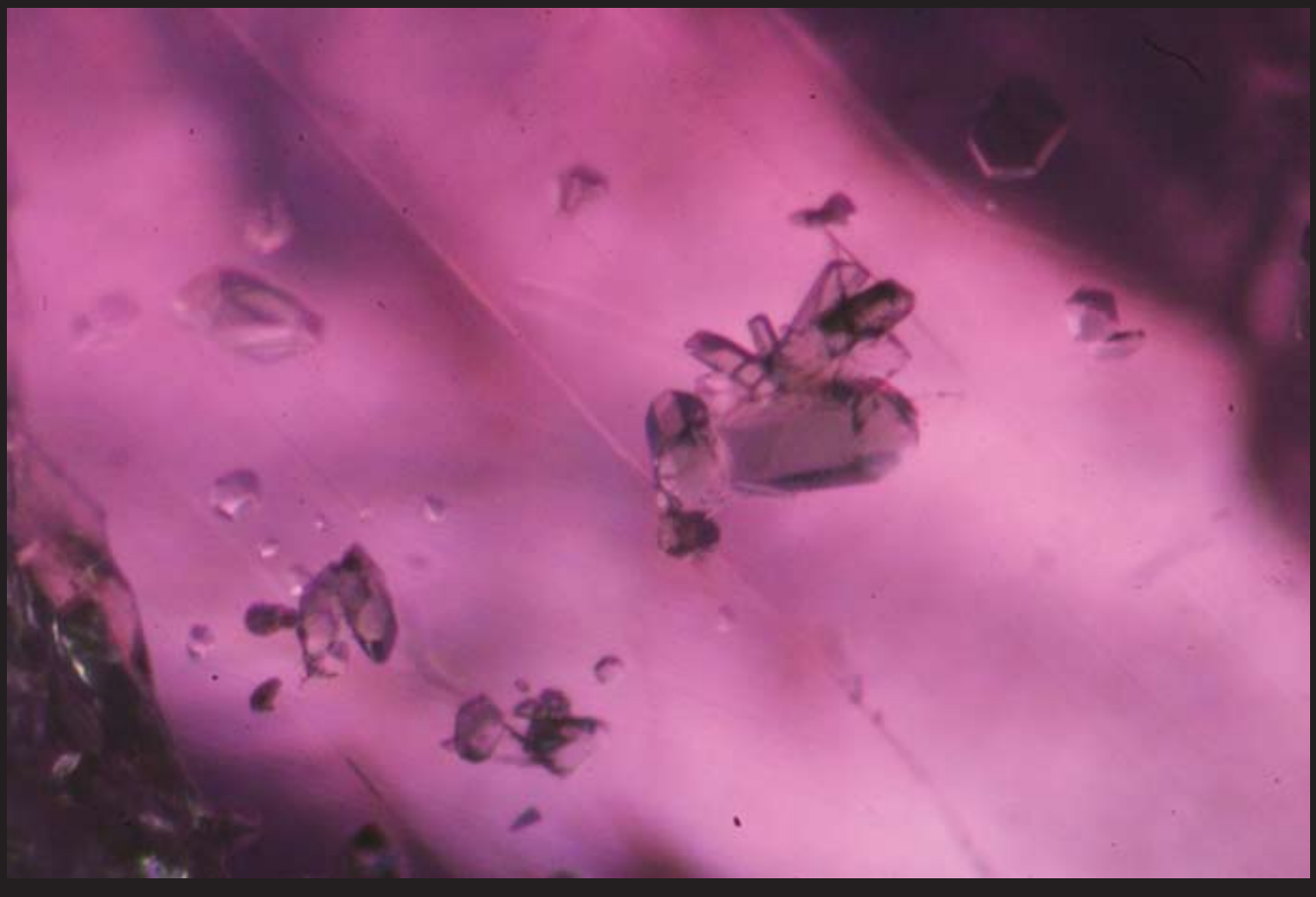

Fig. Tan50 A cluster of pargasite, spinel and rounded colorless inclusions was found in a Winza ruby. (Sample No. GRS-Ref7336)

Fig. Tan51 A series of blue-green pargasite and/or spinel are included in a purple-pink sapphire. Streamers (“comet tails”) are found associated to these solid inclusions. Fiber-optic illumination. Sample No. GRS-Ref8309.

Fig. Tan52

Fig. Tan52 One large garnet has been formed on the tip of a Winza ruby rough crystal. (Sample No. GRS-Ref7347)

Fig. Tan53 Garnet (G, orange-red) and pargasite (P, bluish-green) inclusions are found inside a rough ruby fragment. (Sample No. GRS-Ref7354)

Fig. Tan53

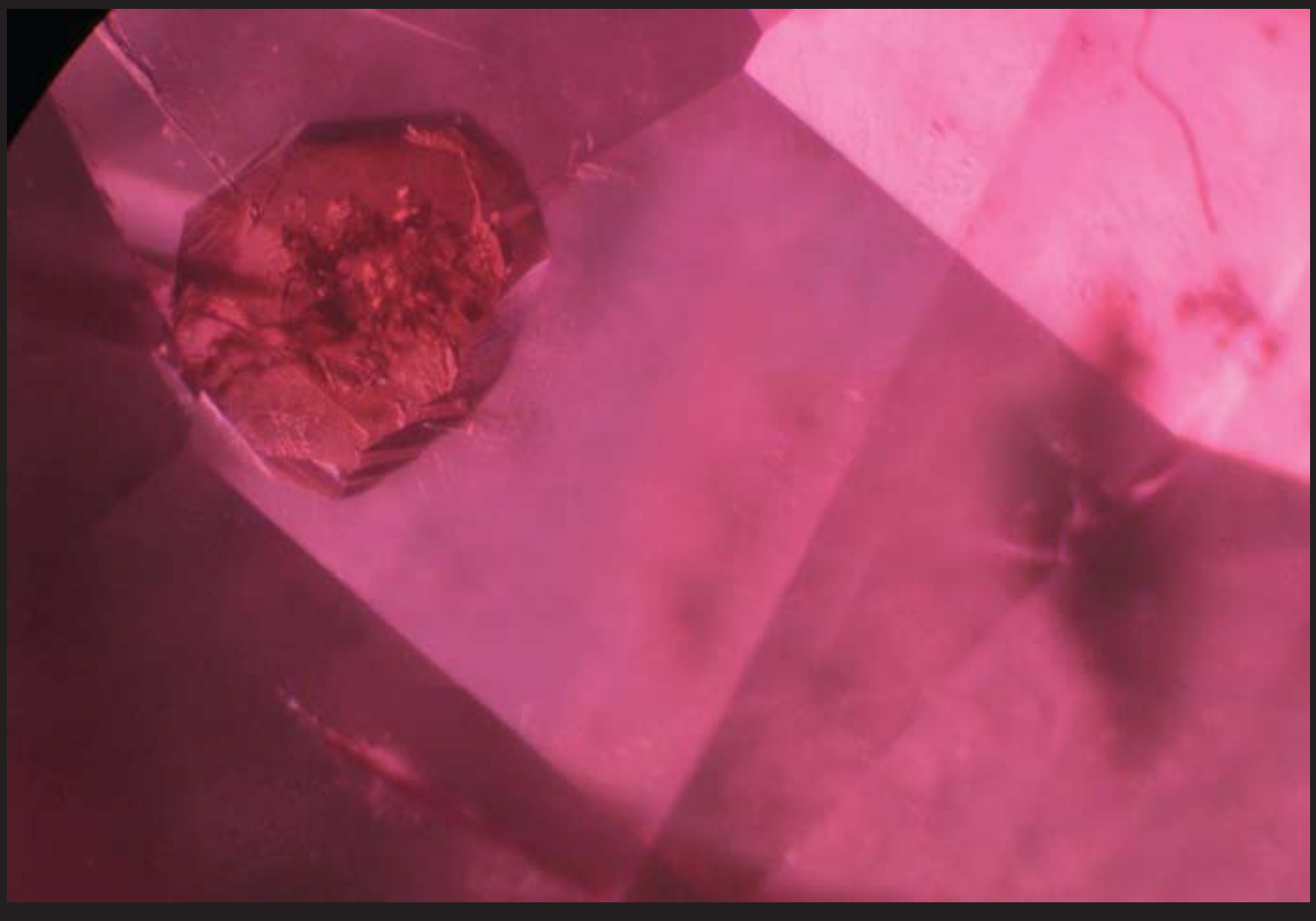

Fig. Tan54 Garnet inclusion in a faceted Winza ruby. The garnet itself contains numerous inclusions.

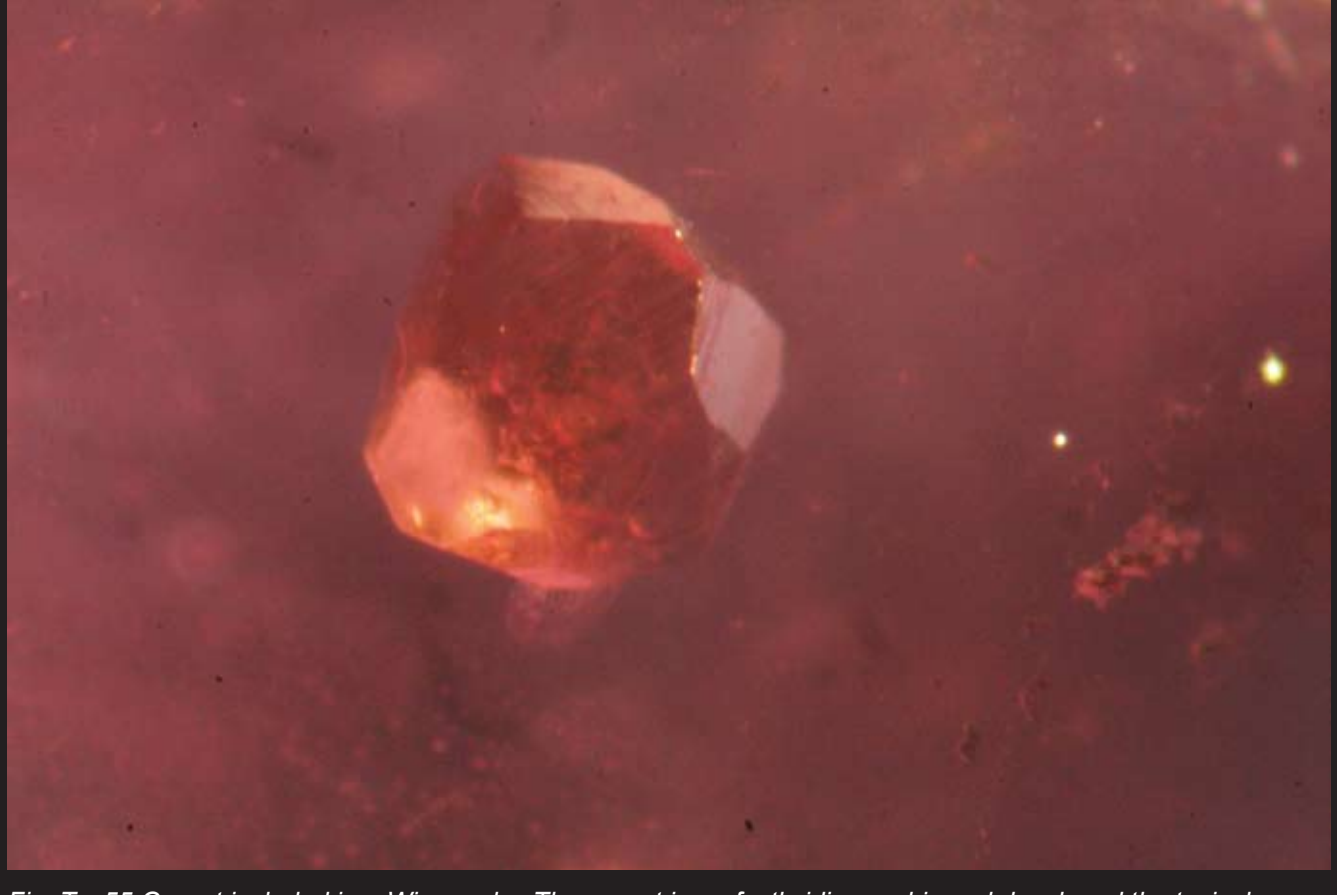

Fig. Tan55 Garnet included in a Winza ruby. The garnet is perfectly idiomorphic and developed the typical pentagon-dodecahedra faces of the cubic system. Fiber-optic illumination. Sample No. GRS-Ref8340.

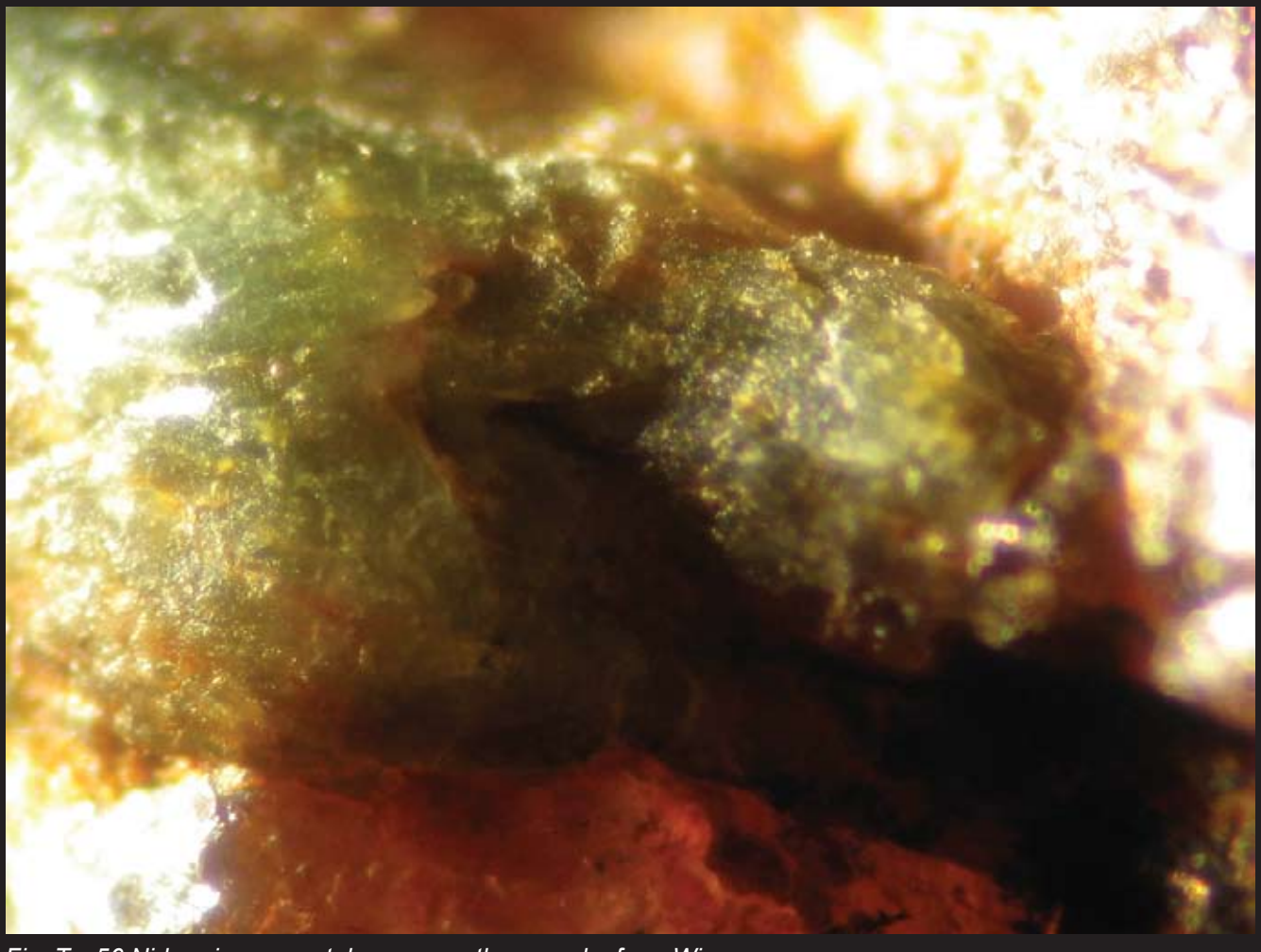

Fig. Tan56 Ni-bearing green talc overgrowth on a ruby from Winza.

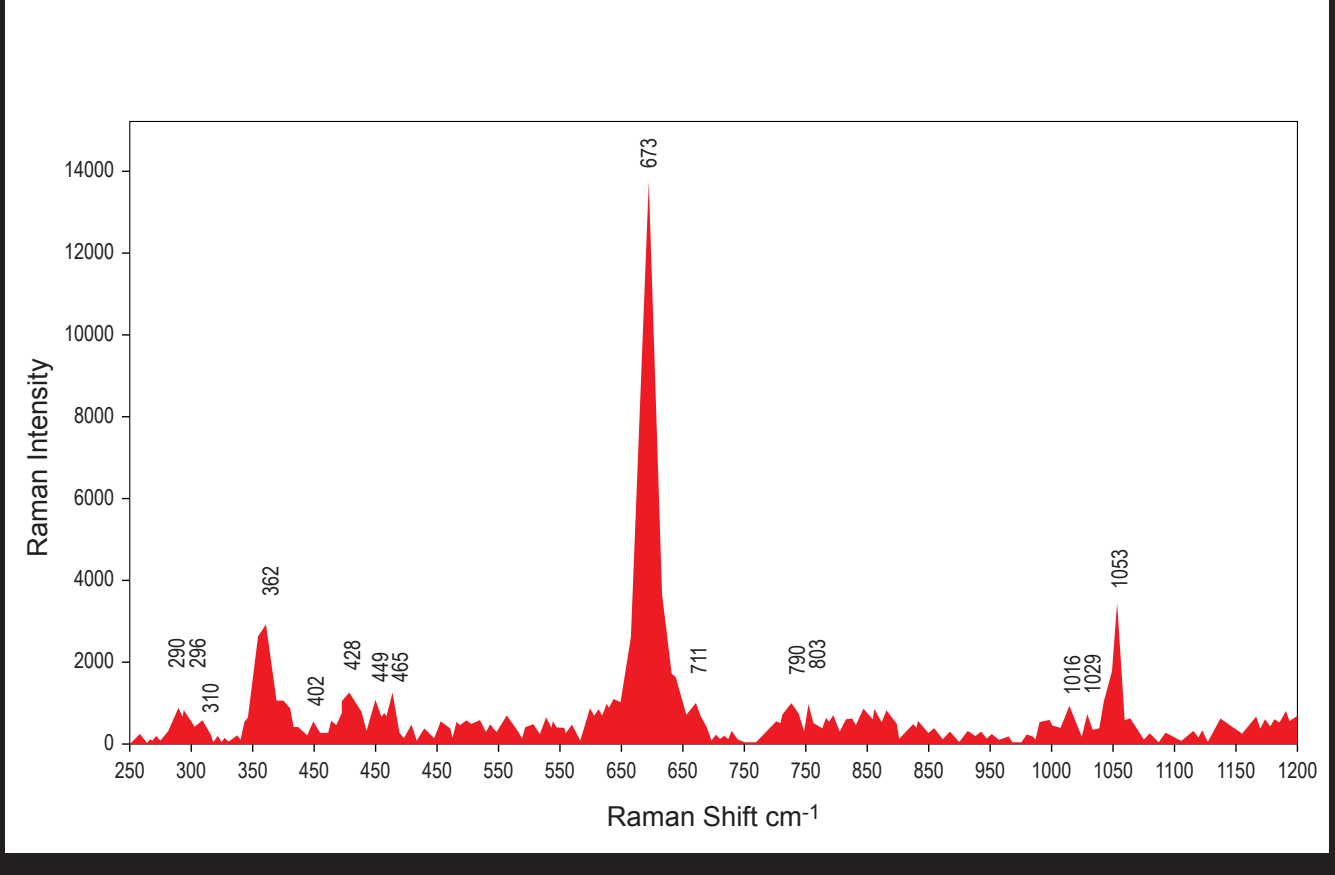

Fig. Tan57 Raman spectra of the same talc that is pictured in Fig. Tan56.

Fig. Tan58 Xenothim inclusion in a Winza ruby is shown (Identification by ED-XRF micro-analysi s). Crystal size is over 1mm. Fiber optic illumination. 15x magnification. Sample No. GRS-Ref7861c.

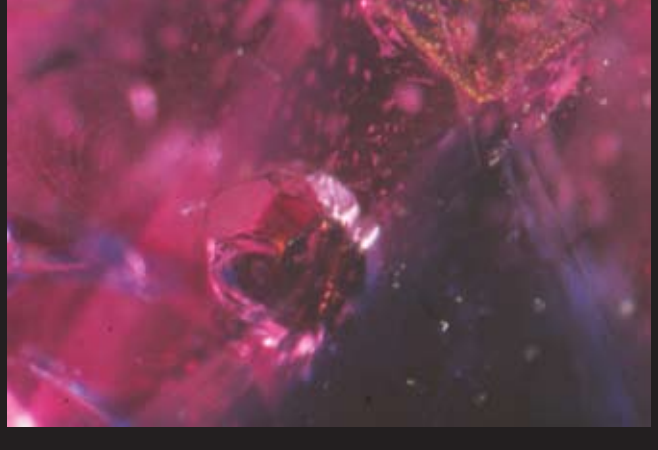

Fig. Tan59

Fig. Tan60

Fig. Tan59 Pyrite was found as an inclusion in a Winza ruby. Sample No. GRS –Ref7118.

Fig. Tan60 Cluster of accessory minerals of orange and colorless color surrounded with tension cracks. This type of inclusion is rarely found. Sample No. GRS-Ref7861a.

Fig. Tan61 One large apatite inclusion was found inside a broken Winza ruby.
(Sample No. GRS-Ref7360, weight 3.04ct)

Fig. Tan61

Fig. Tan62 Colorless crystals with rhombic crystal shape and round colorless crystal inclusions were found in a Winza ruby. 40x magnification. Transmitted light. (Sample No. GRS-Ref7366)

Fig. Tan63

Fig. Tan64

Fig. Tan63 Round blackish magnetite inclusion was present. (Sample No. GRS-Ref7436)

Fig. Tan64 Zirconolith (Identification by Micro-ED-XRF analysis). Sample-No. GRS-Ref 8056. Fiber-optic illumination. Crystal size 0.1 mm.

Fig. Tan65 Irregular shaped transparent and colorless inclusions in purplish-pink sapphire. 30x magnification. Transmitted light. (Sample No. GRS-Ref Tan52)

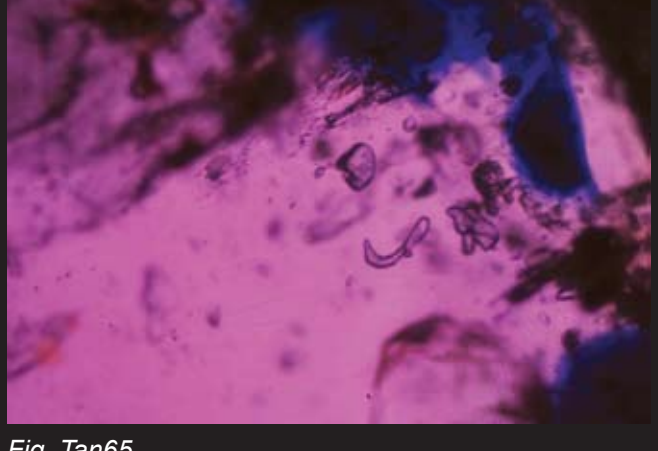

Fig. Tan65

SCANNING ELECTRON MICROSCOPE ANALYSIS (SEM-EDX)

A series of faceted and rough rubies had inclusions that were exposed to the surface. They were suitable for further analyses by SEM-EDX. Most of the samples were coated with carbon. We investigated 6 different ruby samples using a SEM from the University of Berne (Switzerland). The inclusions were analyzed using the different detectors of the instrument (See Box TAN02). SE images were made to obtain sharp images of high magnification. BSE images provided data that allowed us to visualize minerals with different chemical contrasts. The chemical analysis of the inclusions could be measured for particles of 5-10 micron in size. To document the approximate chemical composition of the inclusions, representative chemical spectra are included in this report. Quantitative chemical calculations helped for identification purposes. These semi-quantitative data are not shown here.

BOX TAN02: SEM ANALYSIS

Fig. Tan66 The SEM instrument and operation console of the University of Berne, Earth Science Department, Switzerland. To the left details of the SEM (Zeiss EVO 50): An opened sample chamber, surrounded by a variety of detectors, such as Secondary Electron Detector (SE), Backscattered Electron Detector (BSD) and an X-Ray Detector (EDX) with a Polymer Window (S-UTW) for micro-chemical analysis. To the right the SEM (Zeiss EVO 50 equipped with SmartSEM acquisition software) operated by Dr. Marco Herwegh and one of the authors (WB).

BOX TAN03: CRYSTALLOGRAPHY OF PARGASITE AND GARNET INCLUSIONS

The amphibole inclusions have been tested by X-ray analysis at the Group of Mineralogical Crystallography at the Institute of Geological Sciences of the University of Berne (Prof. Th. Armbruster). They were identified as:

Cl-bearing pargasite-ferropargasite with the simplified average composition (derived from structural analyses):

$Na_{0.75}\ Ca_2\ (Mg_{2.68}Fe_{1.09}Al_{1.23})\ (Al_2Si_6O_{22})\ (OH_{1.67}Cl_{0.33})$.

The unit cell dimensions were determined as:

a = 9.8103(49) b = 18.0094(8) , c = 5.3270 A, beta = 105.058(2),

Volume = 908.85.

The garnet inclusions have been tested by X-ray analyses with the following result:

They were found to be ***almandite-pyrope*** mixed garnets
with the lattice parameter: a = 11.520(4)

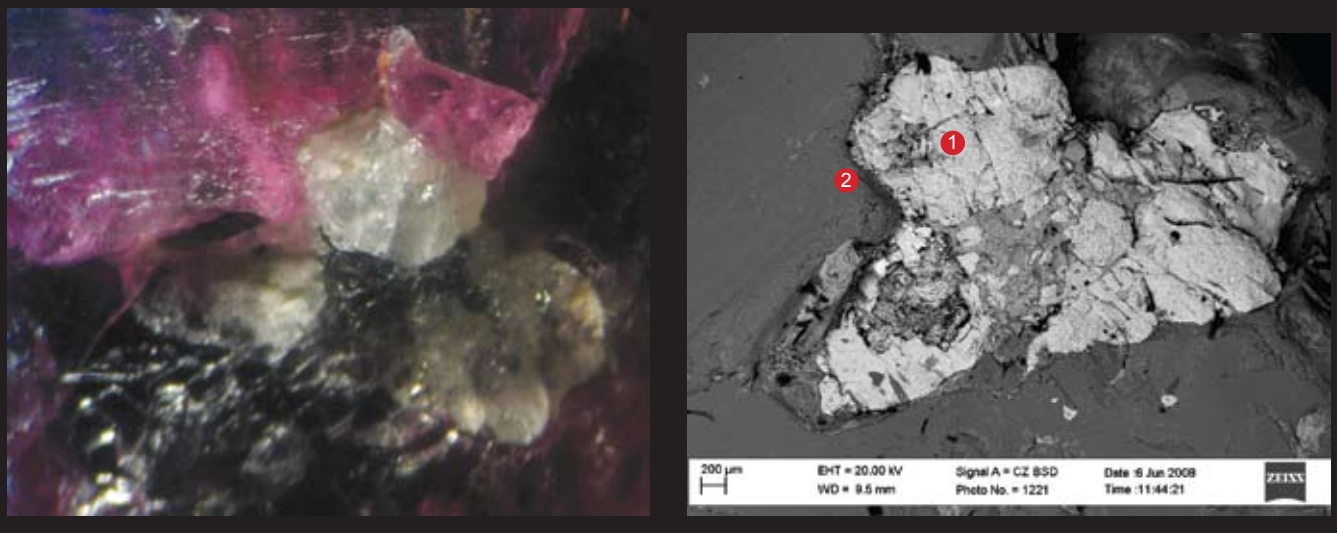

Fig. Tan 67a,b Microphotograph of apatite inclusion as seen in the microscope (left) and the same inclusion as seen by SEM-BSE (right). Note that apatite produces a high contrast in the SEM-BSE image due to its different chemical composition than the surrounding ruby matrix. Sample No. GRS-Ref Tan15.

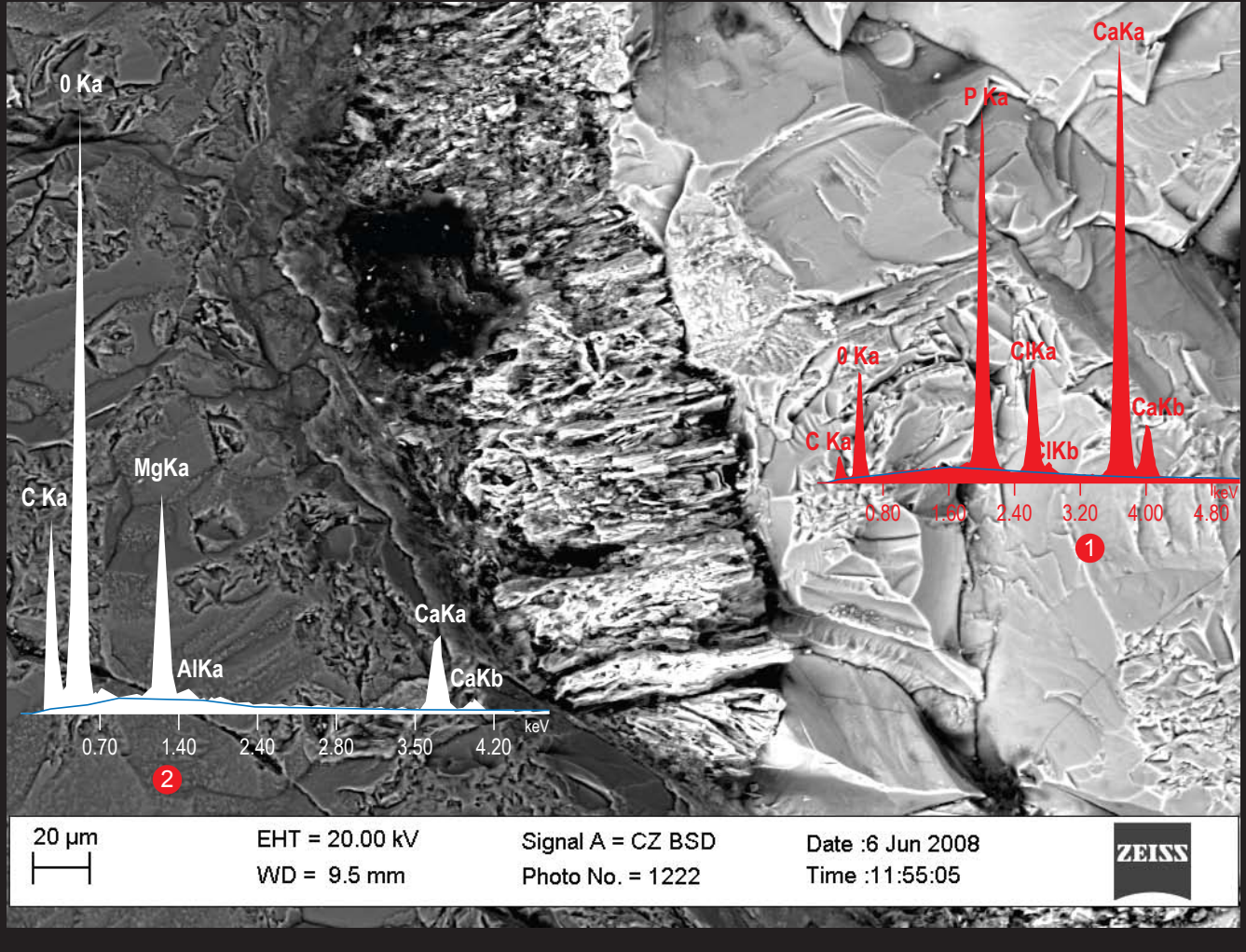

Fig. Tan68 Enlarged SEM-BSE image of Fig. Tan76b. The inclusions in a "Winza" ruby were identified as Cl-bearing apatite (No. 1). Chemical compositions see SEM-EDX spectra. A carbonate (spectrum No. 2) rim was found between apatite (No. 1) and the ruby. The carbonate represents a reaction rim around the apatite crystals and contains high concentrations of magnesium. Apatite was confirmed by Raman analysis.

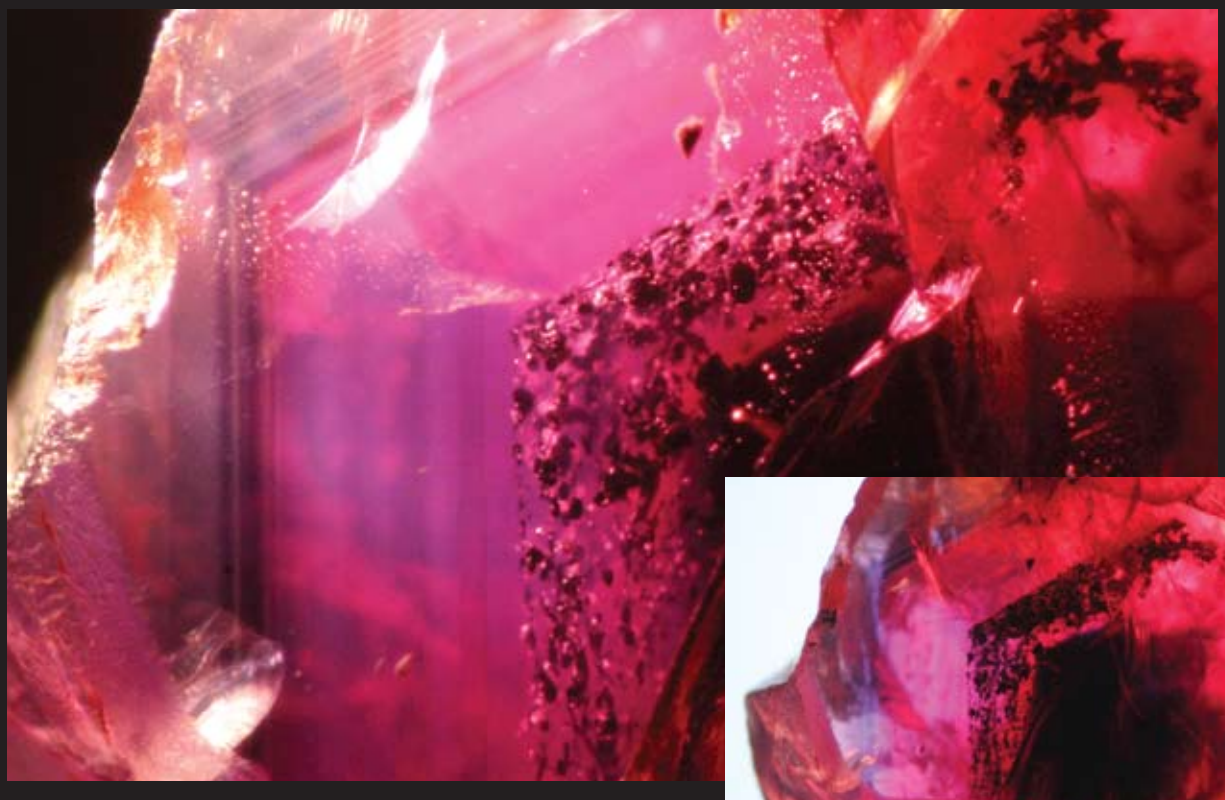

Fig. Tan69

Fig. Tan70

Fig. Tan69 A section perpendicular to the c-axis of a ruby crystal is shown. Different illumination and slightly more magnified than Fig. Tan70 (20x, fiber optic illumination). Note: Mineral inclusions were deposited at particular growth stages of the ruby (see also color-zoning confined to growth faces). Sample No. GRS-Ref Tan07.

Fig. Tan70 Same sample as in Fig. Tan69 is shown. A window was polished to expose mineral inclusions to the surface. Note the hexagonal alignment of mineral inclusions along the early growth stage of the ruby (transmitted light).

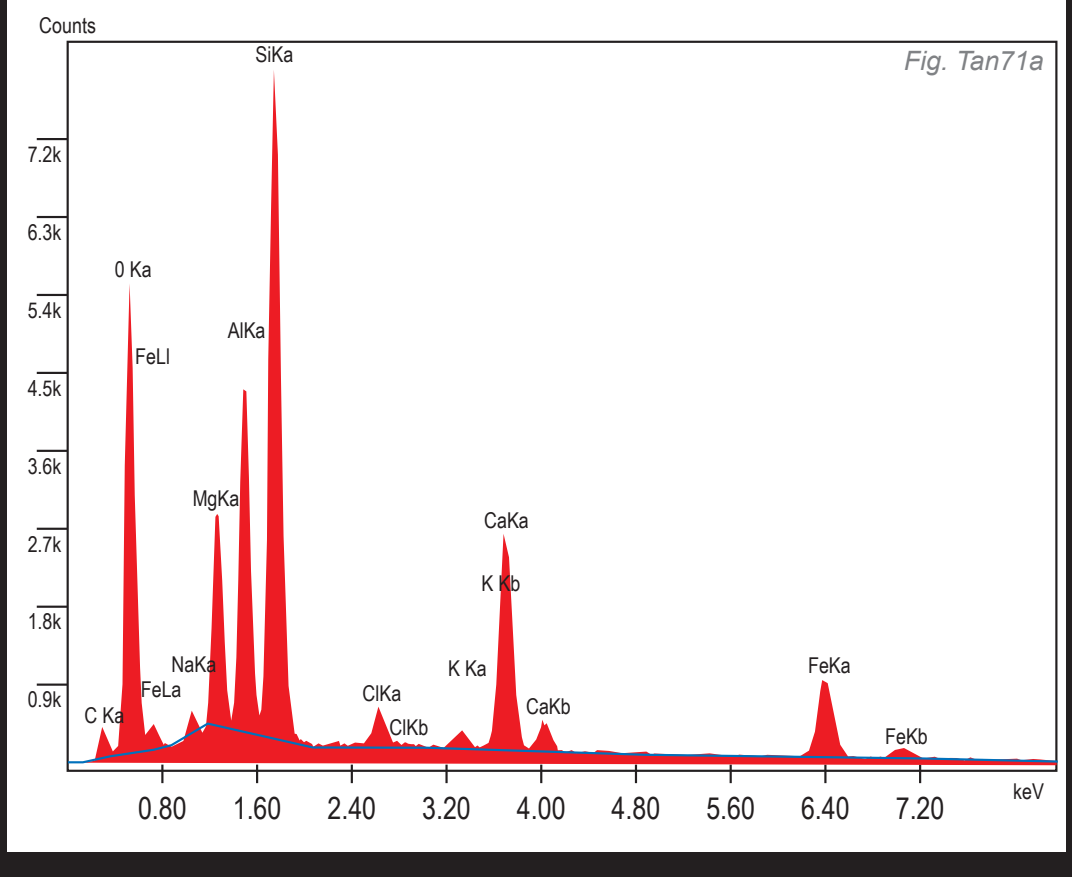

Fig. Tan71 SEM-EDX chemical analyses identified No. 1 of Fig. Tan72a,b as pargasite. SEM-EDX analysis of a pargasite inclusion (See SEM-EDX spectrum) confirms the finding of the XRD analyses (See Box Tan03). Such as the presence of chlorine (Cl) in the chemical composition of pargasite.

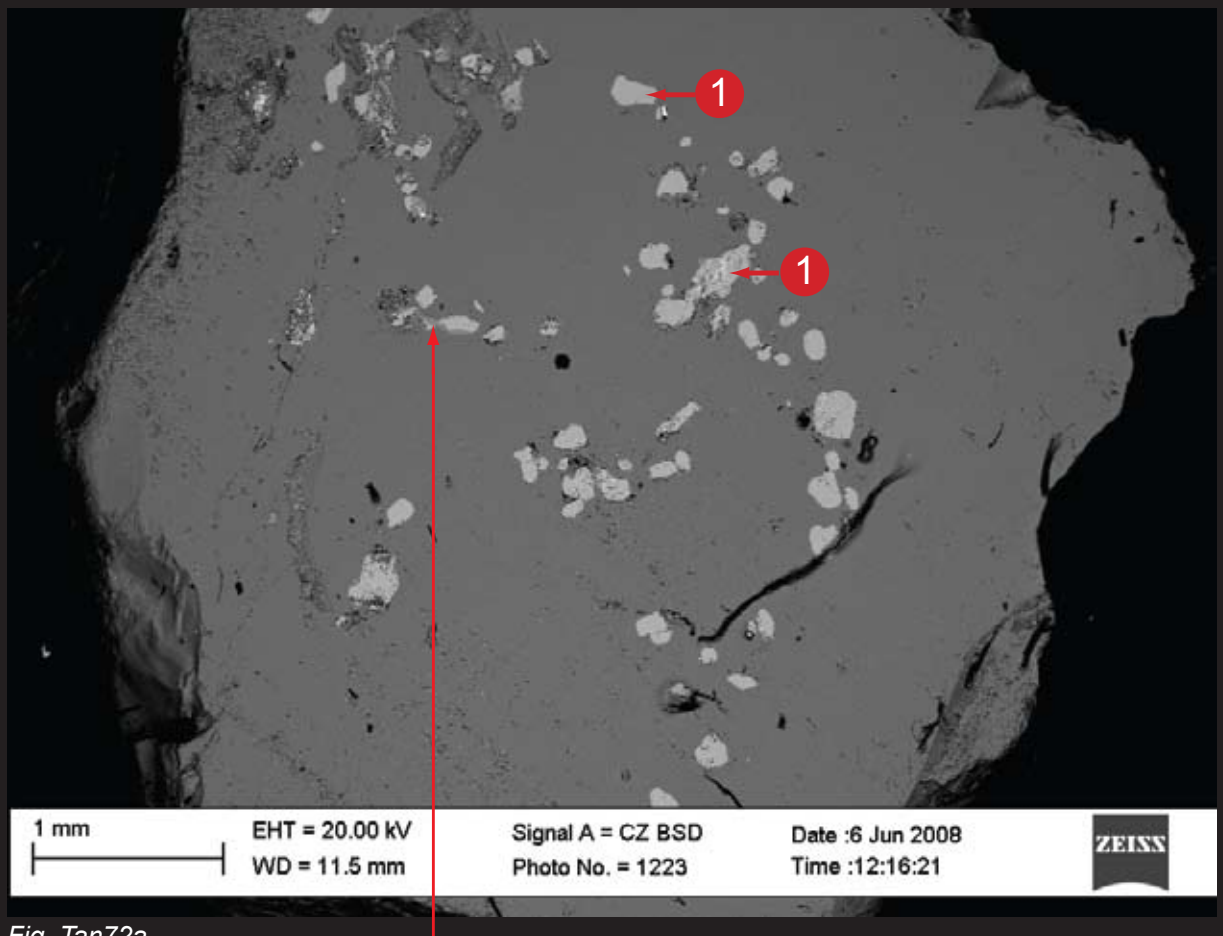

Fig. Tan72a

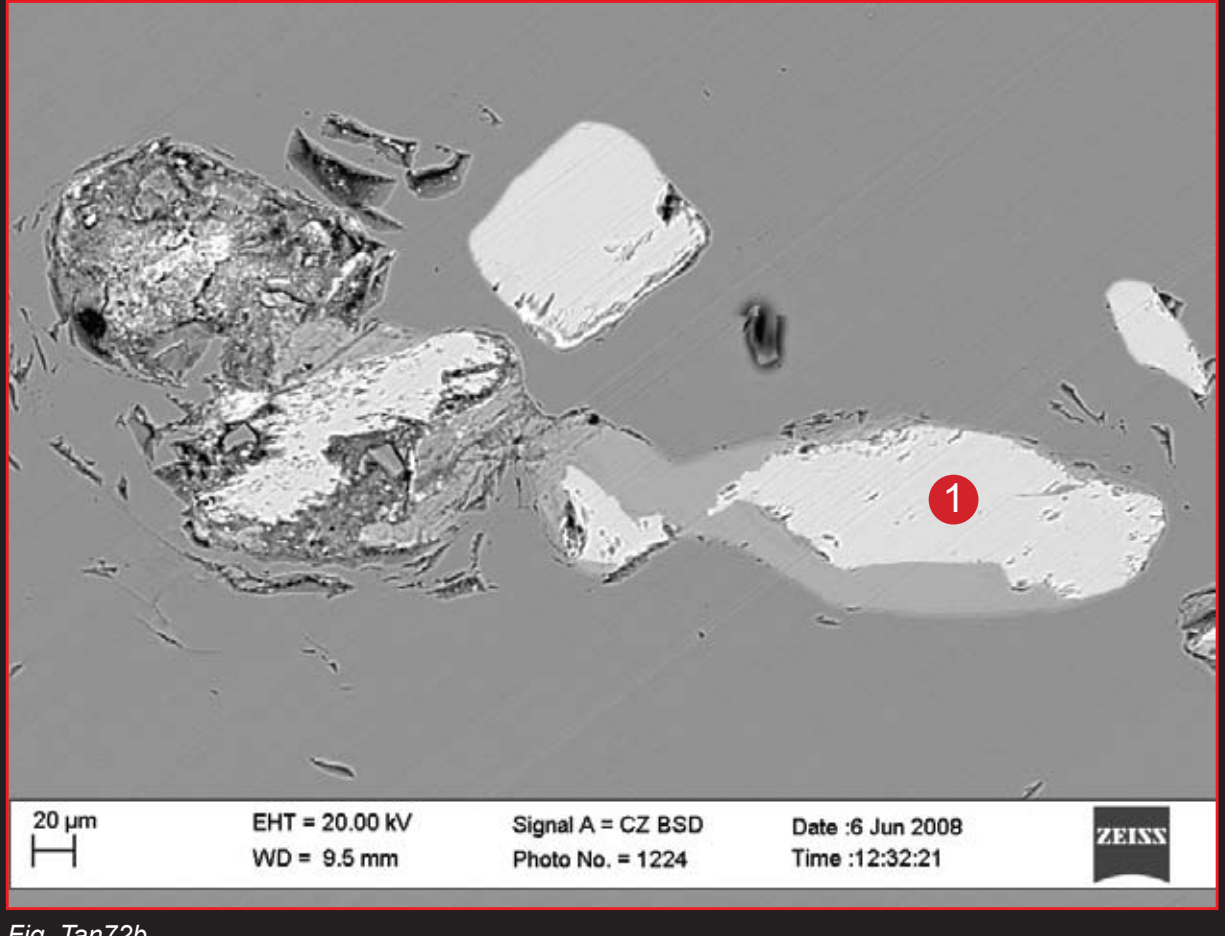

Fig. Tan72b

Fig. Tan72a, b. Two SEM-BSE images of the same sample as in Fig. Tan69 and Tan70. No. 1 are pargasite inclusions.

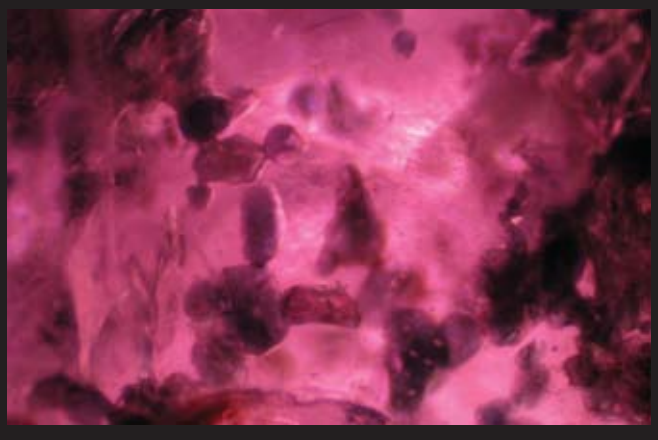

Fig. Tan73 Opaque and bluish-green mineral inclusions in a ruby from the Winza mine in Tanzania. The ruby was faceted and a series of these inclusions reached the surface and were accessible to SEM analysis as shown below.
Sample No. GRS-Ref Tan16.

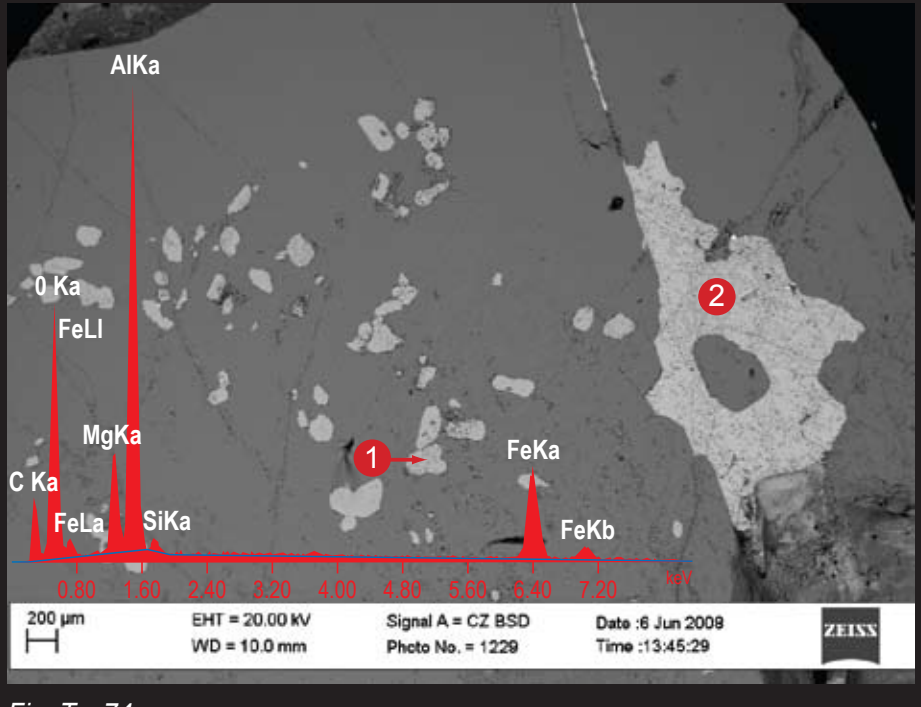

Fig. Tan74a

Fig. Tan74a, b Pargasite (1) and spinel (2) inclusions (see Fig. Tan73) were identified by SEM-EDX-analysis. The back-scattered picture shows different shades within the pargasite inclusions indicating that these minerals have unequal density (3 and 4). The EDAX examination shows that they are slightly varying in chemistry (more concentrations of heavier elements in the more bright part of the picture).

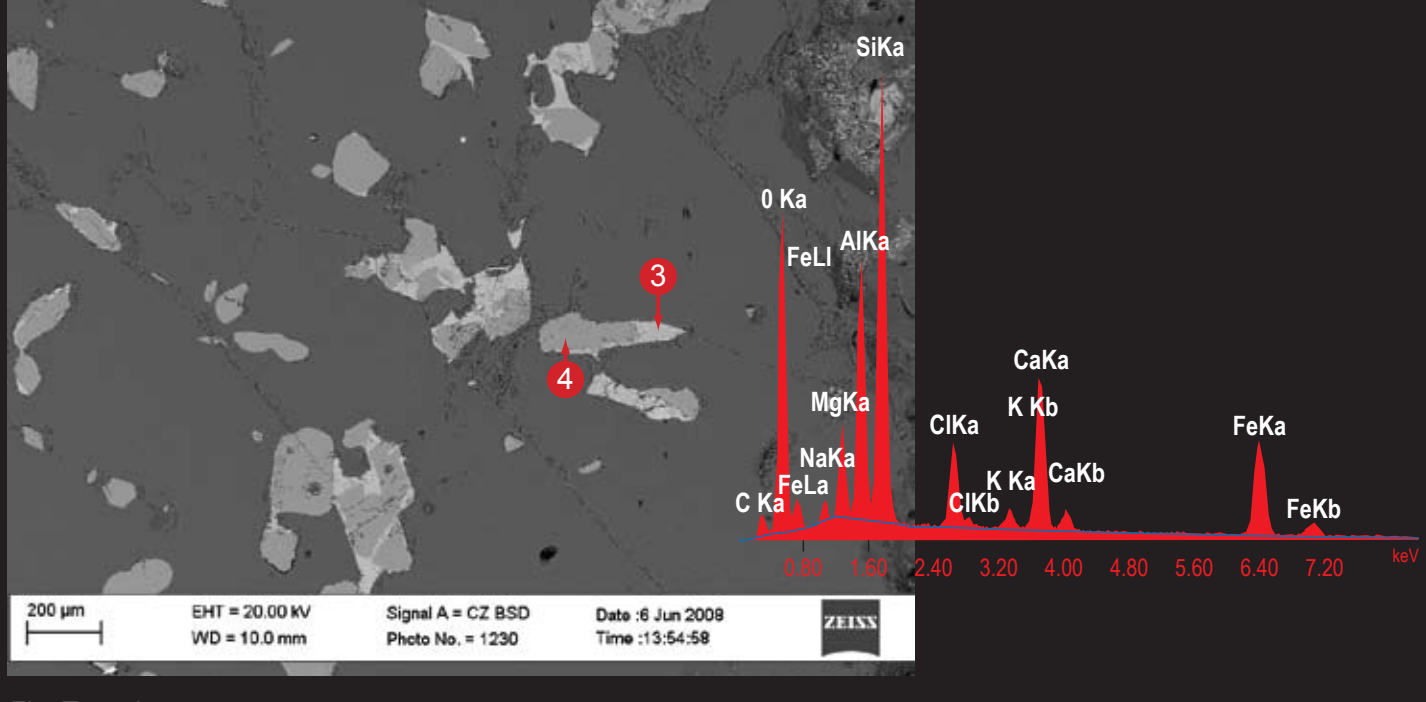

Fig. Tan74b

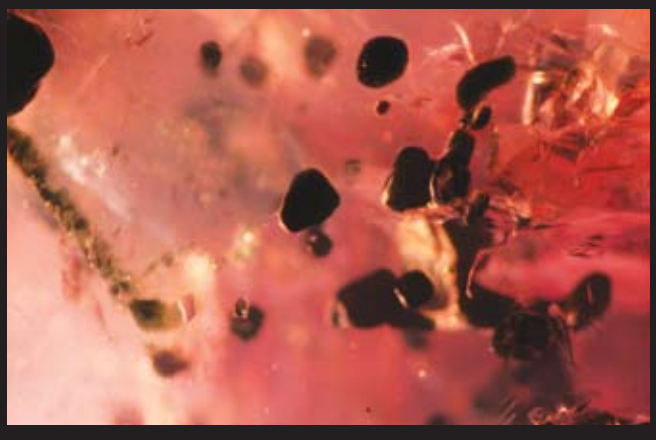

Fig. Tan75 Black spinel inlcusions

Fig. Tan76 Green spinel inclusions

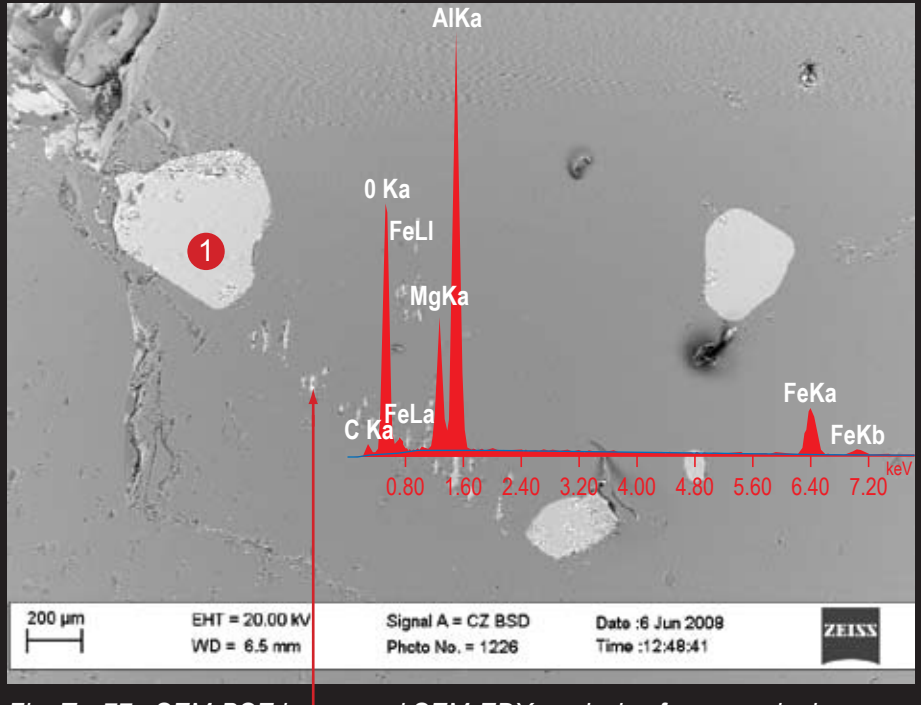

Fig. Tan77a SEM-BSE image and SEM-EDX analysis of green spinel

Micro photograph of a Winza ruby with isolated black inclusions (Fig. Tan75) adjacent to a trail of green inclusions (Fig. tan76). The sample was polished to the level of the inclusions for the purpose of further identification by SEM analysis (Fig. Tan77a and tan77b). Sample No. GRS-Ref Tan17.

SEM-EDX analysis identified them as Mg-Al-spinel (green), Fig. Tan77a and spinels of mixed Fe-rich chemical compositions (black), See Fig. Tan77b.

Fig. Tan77b SEM-BSE image and SEM-EDX analysis of black spinel

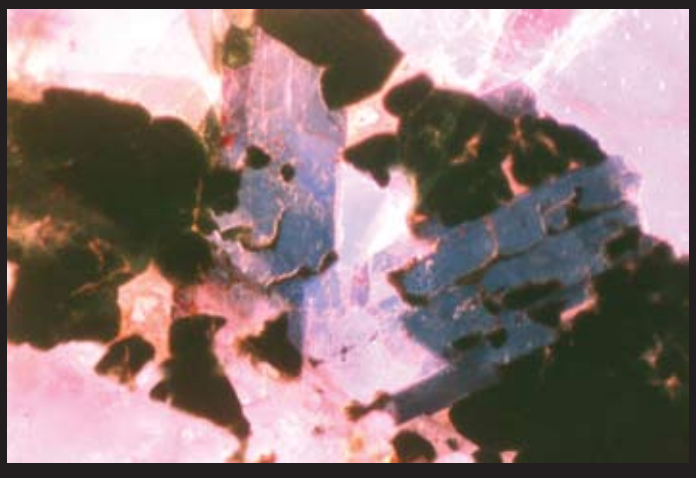

Fig. Tan78 Microphotograph of a flat aggregate of blue and green minerals as seen in transmitted light. They were originally found as a large inclusion cluster in a ruby and were exposed to the surface by parting the stone. This mineral aggregate could be analyzed by SEM-EDX analysis and were identified as pargasite, chlorite and spinel as shown below. Sample No. GRS-Ref Tan01.

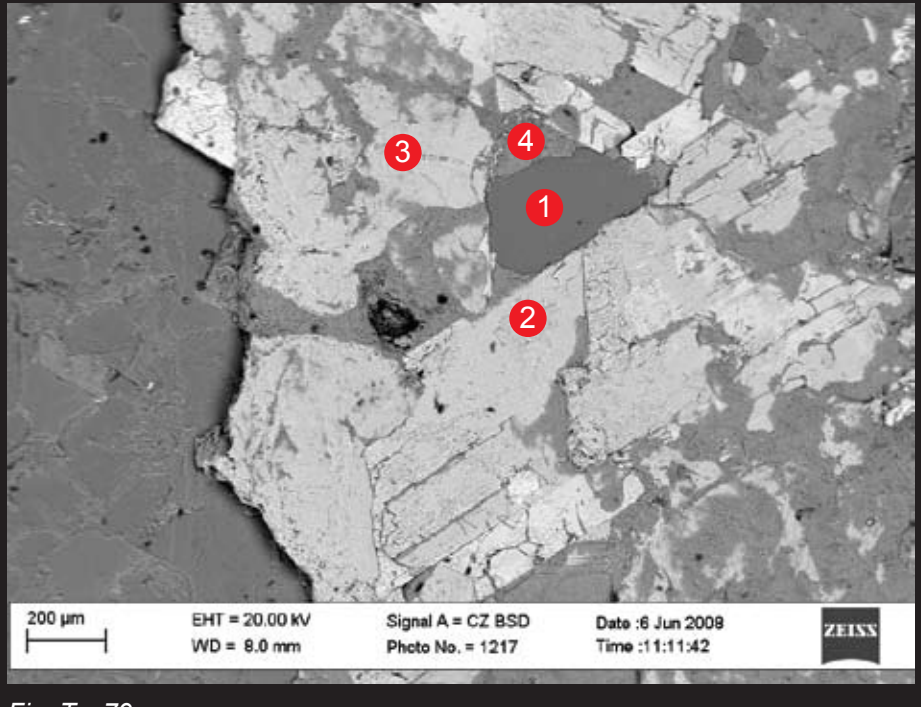

Fig. Tan79a

Fig. Tan79a, b SEM-BSE image of the inclusions of Fig. Tan74. Different grey tones were obtained for different mineral phases. The dark grey part of the SEM-BSE image is corundum (1); other grey shades are pargasite (2,3), chlorite (4, Fig. Tan80b) and spinel (No. 5, See Fig. Tan80c). Comparison of the microscopic and the SEM analysis revealed the following results: The blue phase in the microscopic picture (Fig. Tan78) was identified by SEM-EDX as Cl-bearing pargasite (See Fig. Tan80a). The green phase was also identified as pargasite but with a slightly different chemistry. Small rims of chlorite were present (Fig. Tan80b).

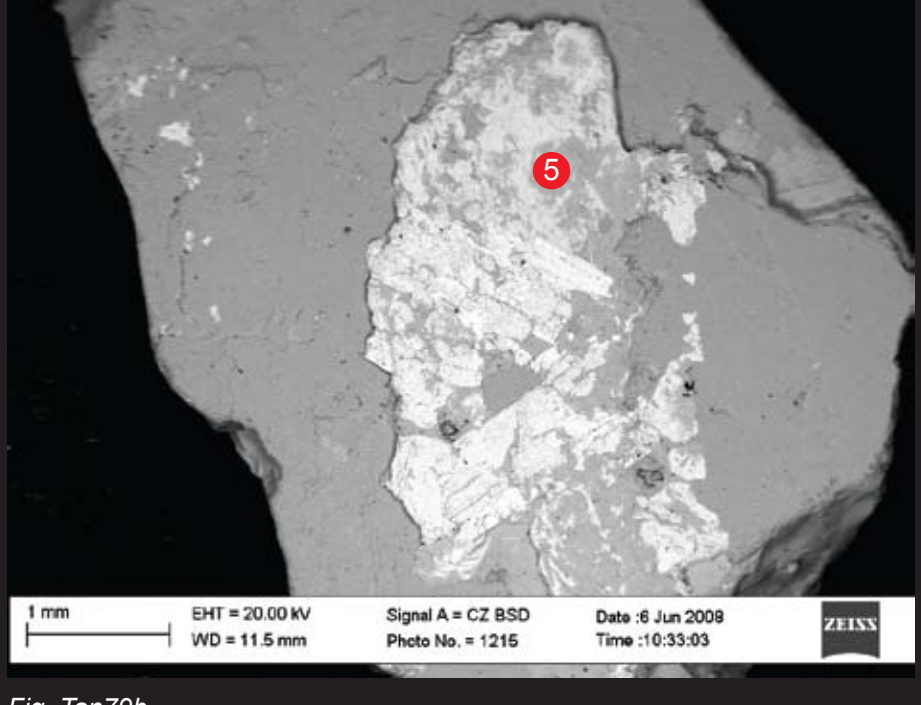

Fig. Tan79b

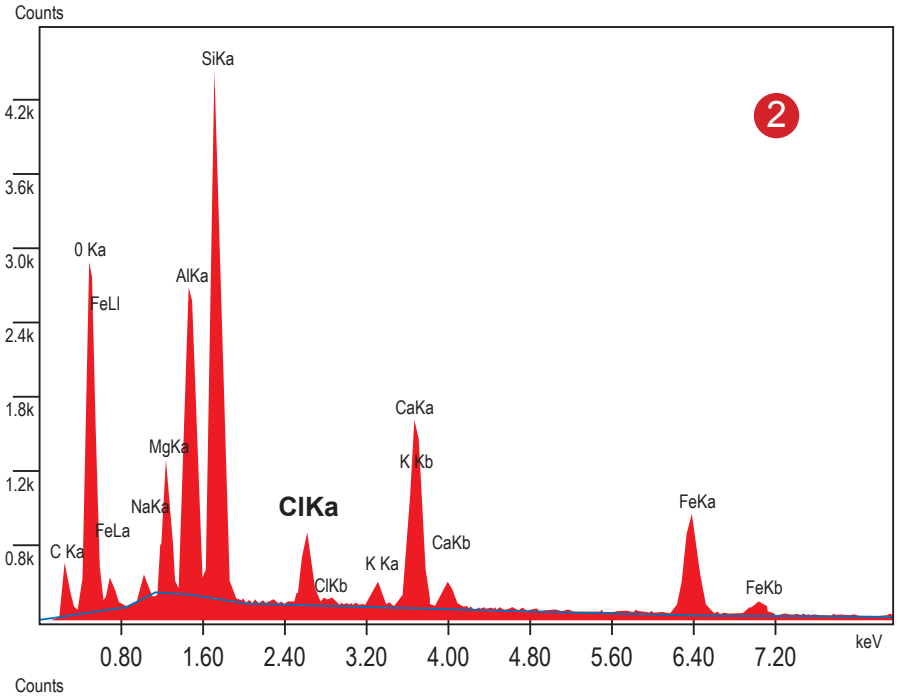

Fig. Tan 80a
SEM-EDX spectrum of bluish pargasite. Note chlorine (Cl) content.

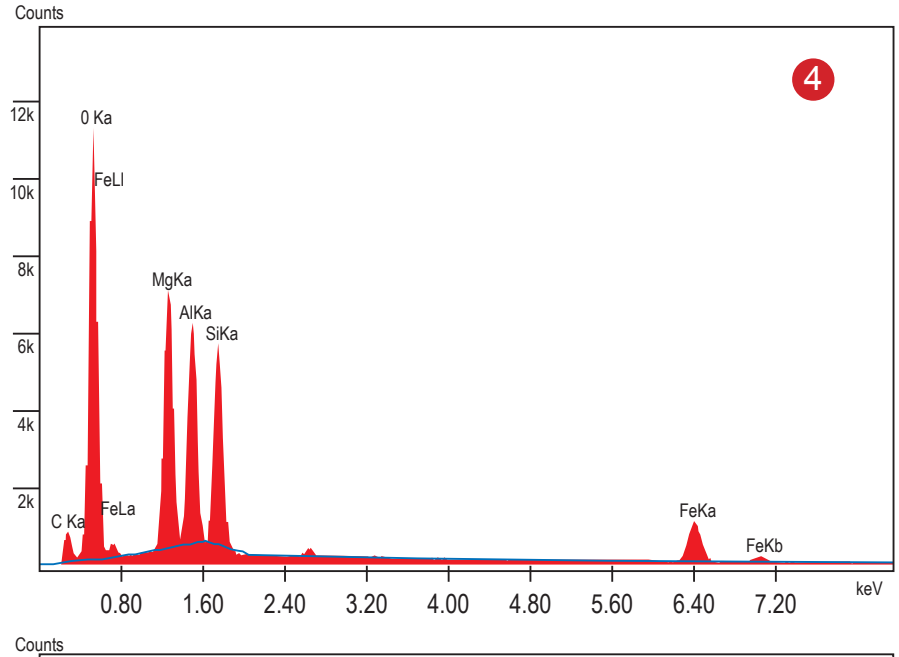

Fig. Tan 80b
SEM-EDX spectrum of chlorite

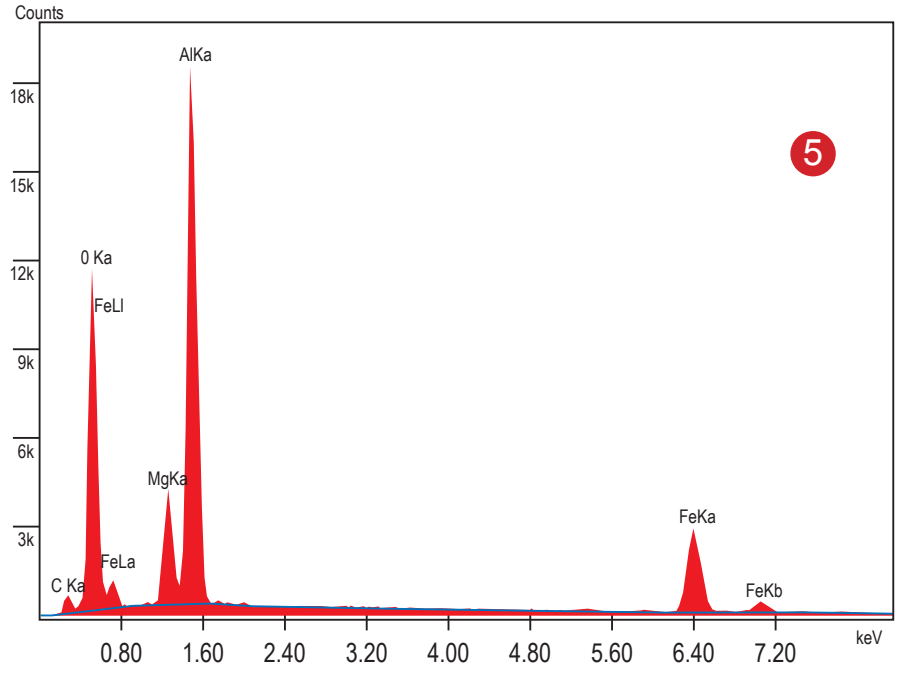

Fig. Tan 80c
SEM-EDX spectrum of spinel

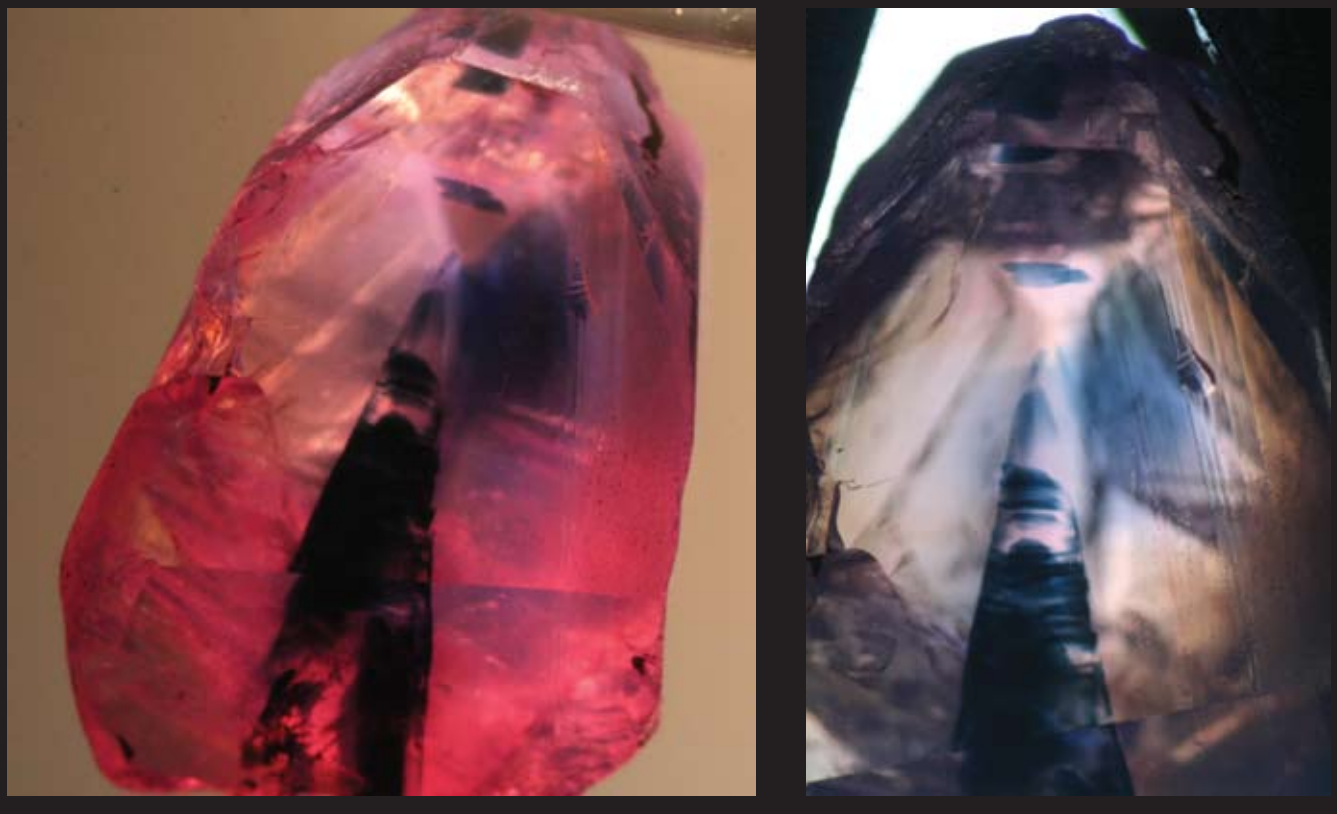

Fig. Tan81 An example of a Winza ruby with perfect terminations is shown. The ruby was cut in half along the c-axis to expose its internal growth structures and color zoning. A blue "pencil"-like core was formed and dramatic changes in habit occurred with continuation of the crystal growth. Left: Fiber optic illumination and right transmitted light. A red core is seen in transmitted light. Sample No. GRS-Ref7475.

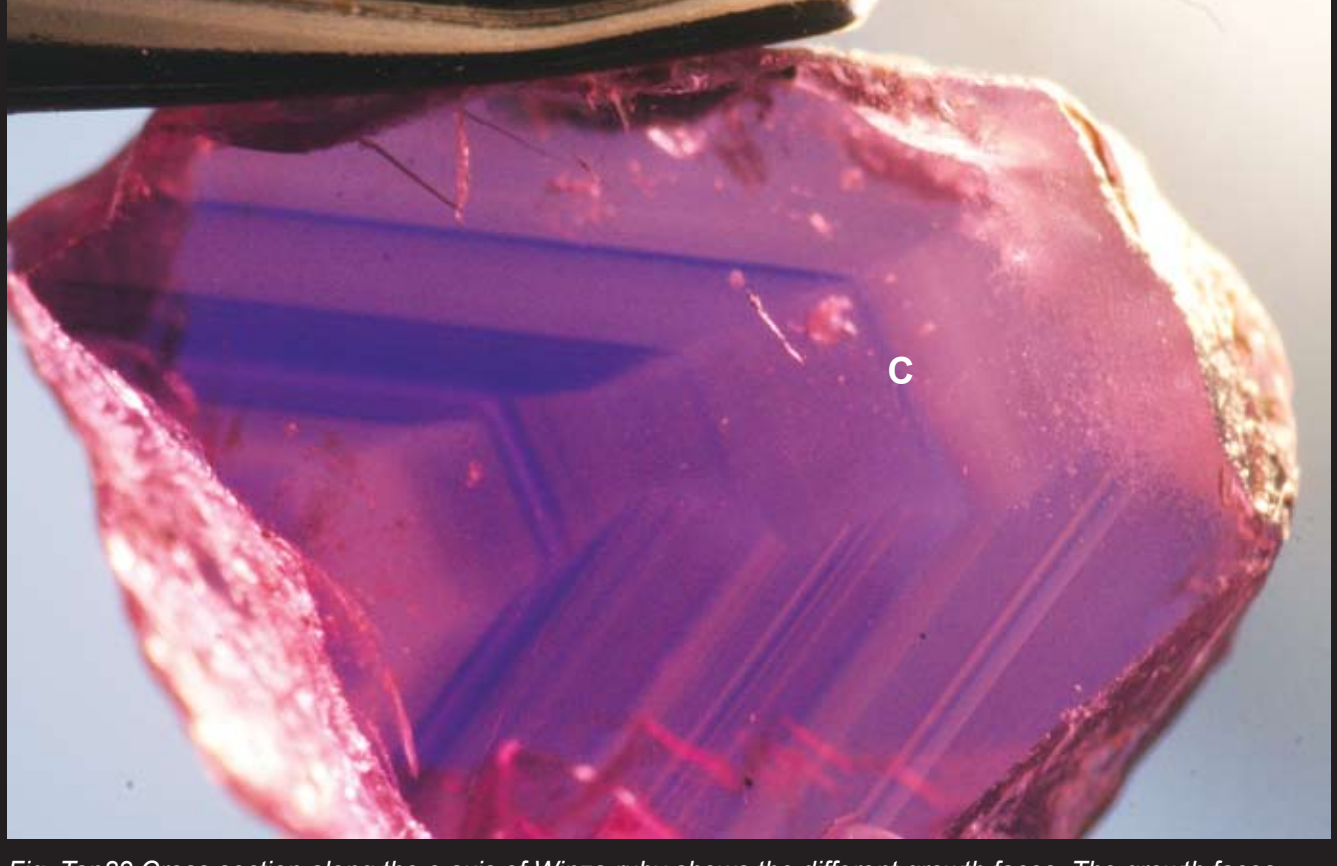

Fig. Tan82 Cross section along the c-axis of Winza ruby shows the different growth faces. The growth faces include a base (c), pyramids and rhombohedra growth faces. Intensive color zoning occurred as the crystal was growing: Initial pinkish-red core (left corner), followed by an orange layer, a blue layer, a pink layer and towards the end of the crystal growth, the color-layers oscillated with numerous repetition of this scheme. Blue zones are found in zones with less particles and vice versa (see picture in reflected light Fig. Tan83).
Sample No. GRS-Ref7152.

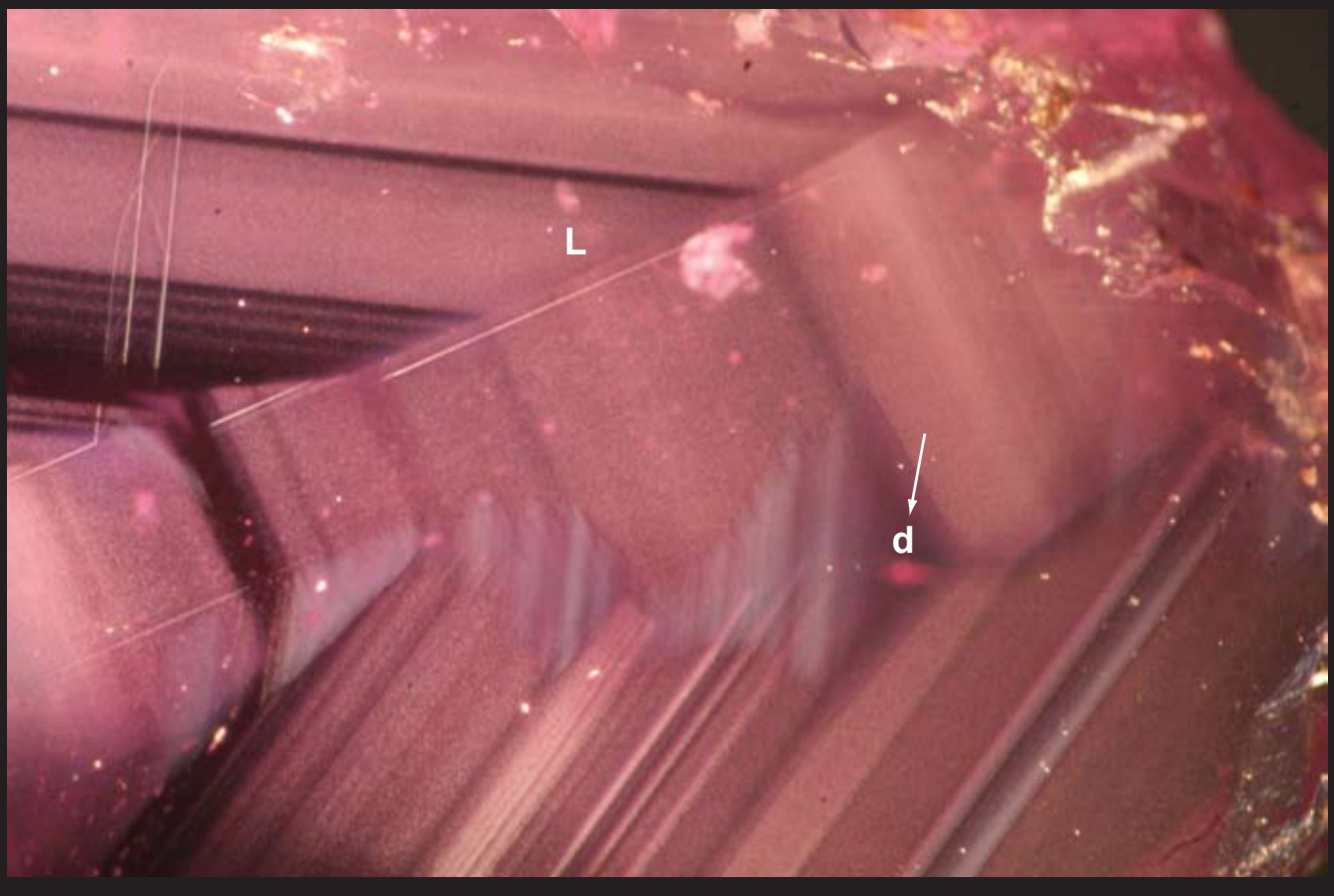

Fig. Tan83 Cross section parallel to the c-axis of a Winza ruby (slightly rotated along the c-axis in comparison to Fig. Tan82). This crystal termination feature appeared and disappeared during crystal growth (d). Occasionally forming triangular patterns in the ruby (see arrow). Picture in reflected fiber optic light that enhanced the presence of micro particles. In direction of the c-axis a whitish line was present in the ruby (L). Sample No. GRS-Ref7152.

Fig. Tan84a

Fig. Tan84b

Fig. Tan84a, b Micro-photo with detail on growth structures is shown in reflected light. The lightening did enhance the presence of micro particles in the Winza ruby. A white line became visible of the shape of “Sky scrapers” (S, Fig. Tan84a). A picture in the transmitted light made the color oscillations visible that occur in addition to the presence of micro-particles (Fig. Tan84b). Sample No. GRS-Ref7152.

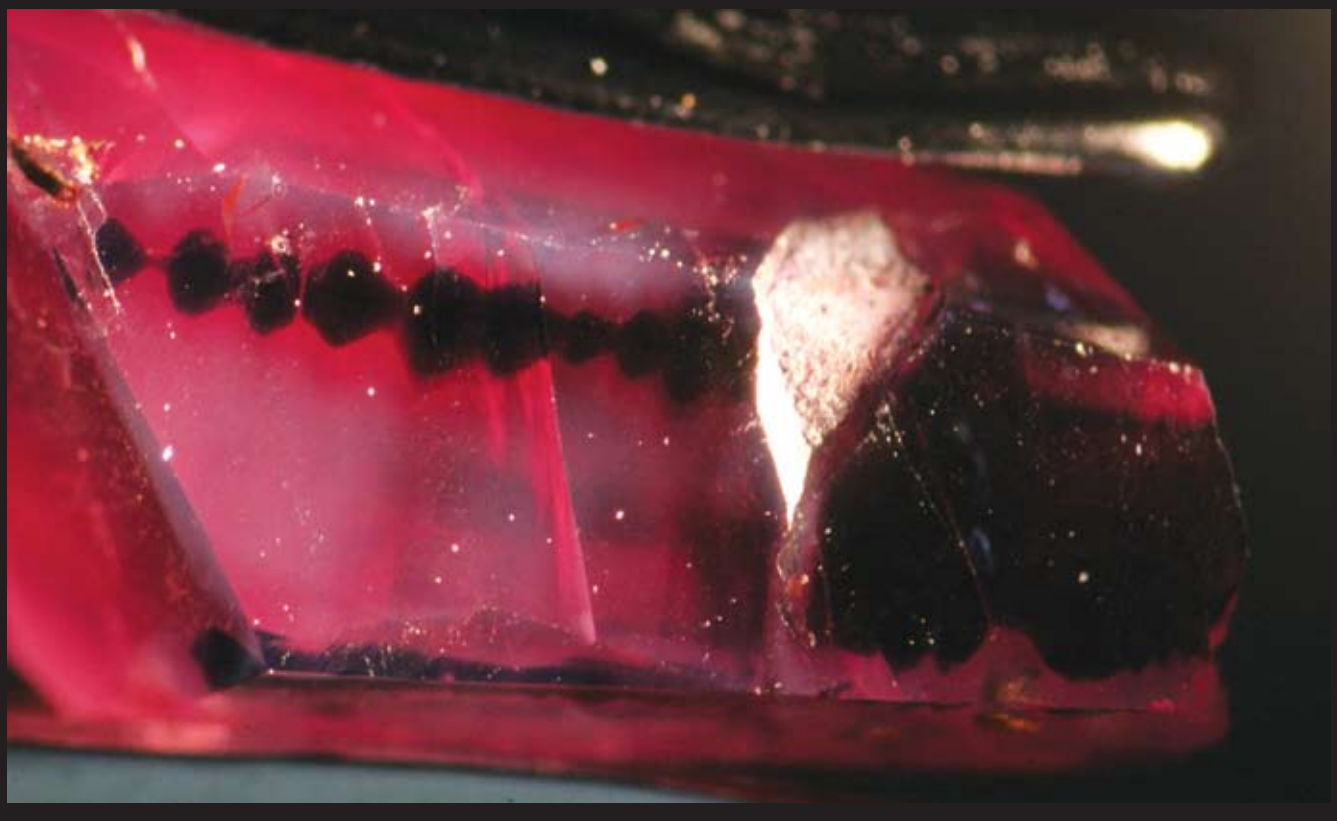

Fig. Tan85a

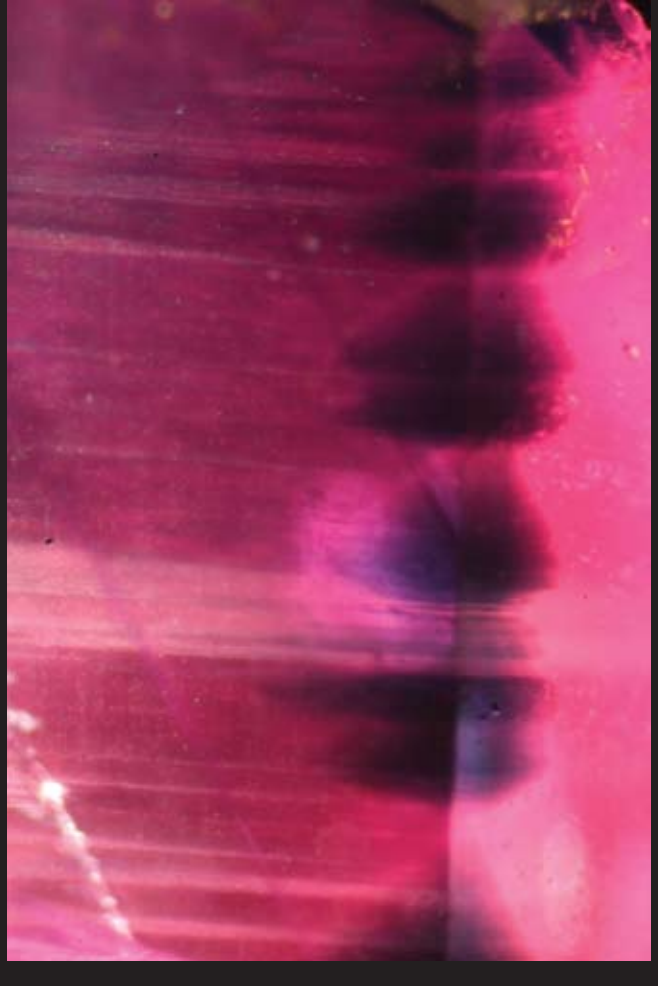

Fig. Tan85b

Fig. Tan85c

Fig. Tan85a, b, c Photo of rough “Winza” rubies. The surface of the rough crystals was polished to expose black and milky color zoning. Sample No. GRS-Ref7574.

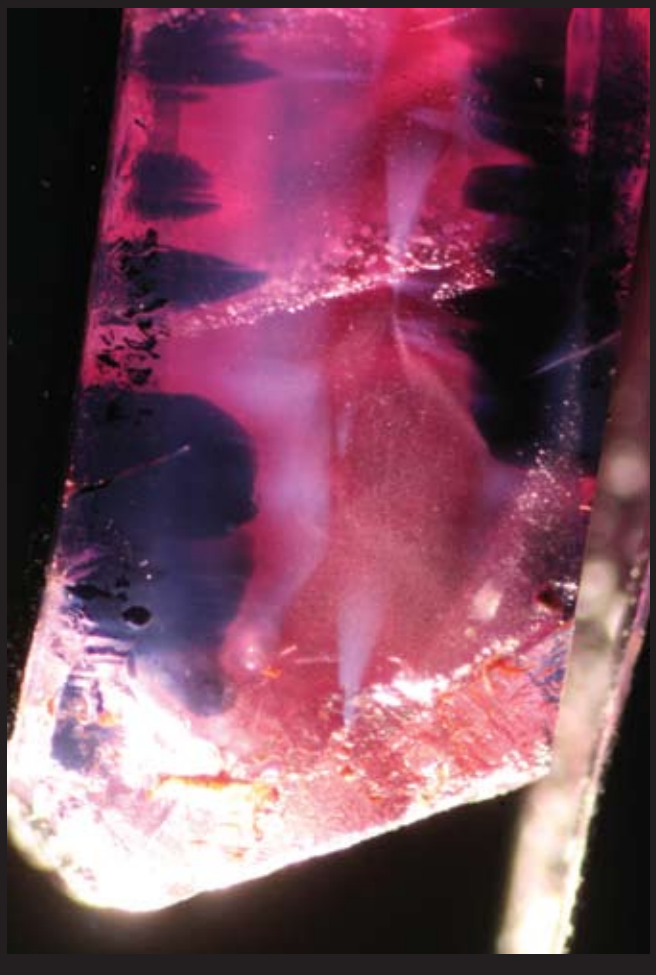

Fig. Tan86a

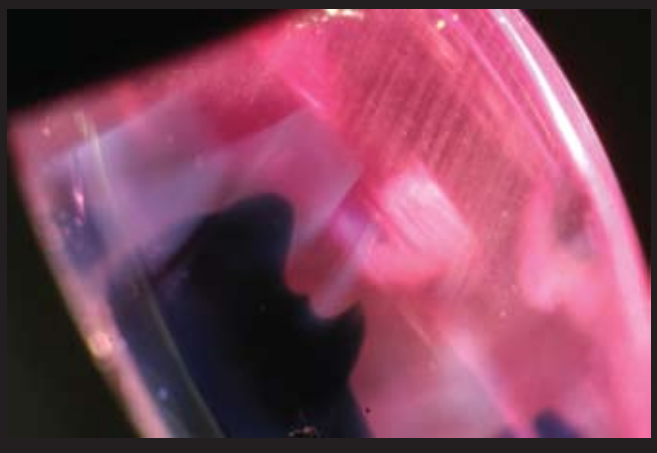

Fig. Tan86b

Fig. Tan86a,b Blue color zoning found in a cabochon ruby. An intense blue color-zone is present which fades laterally into a whitish zone and finally into a growth sector with numerous sub-microscopic particles. Sample No GRS-Ref7453 (Tan38). Crystal length 8mm.

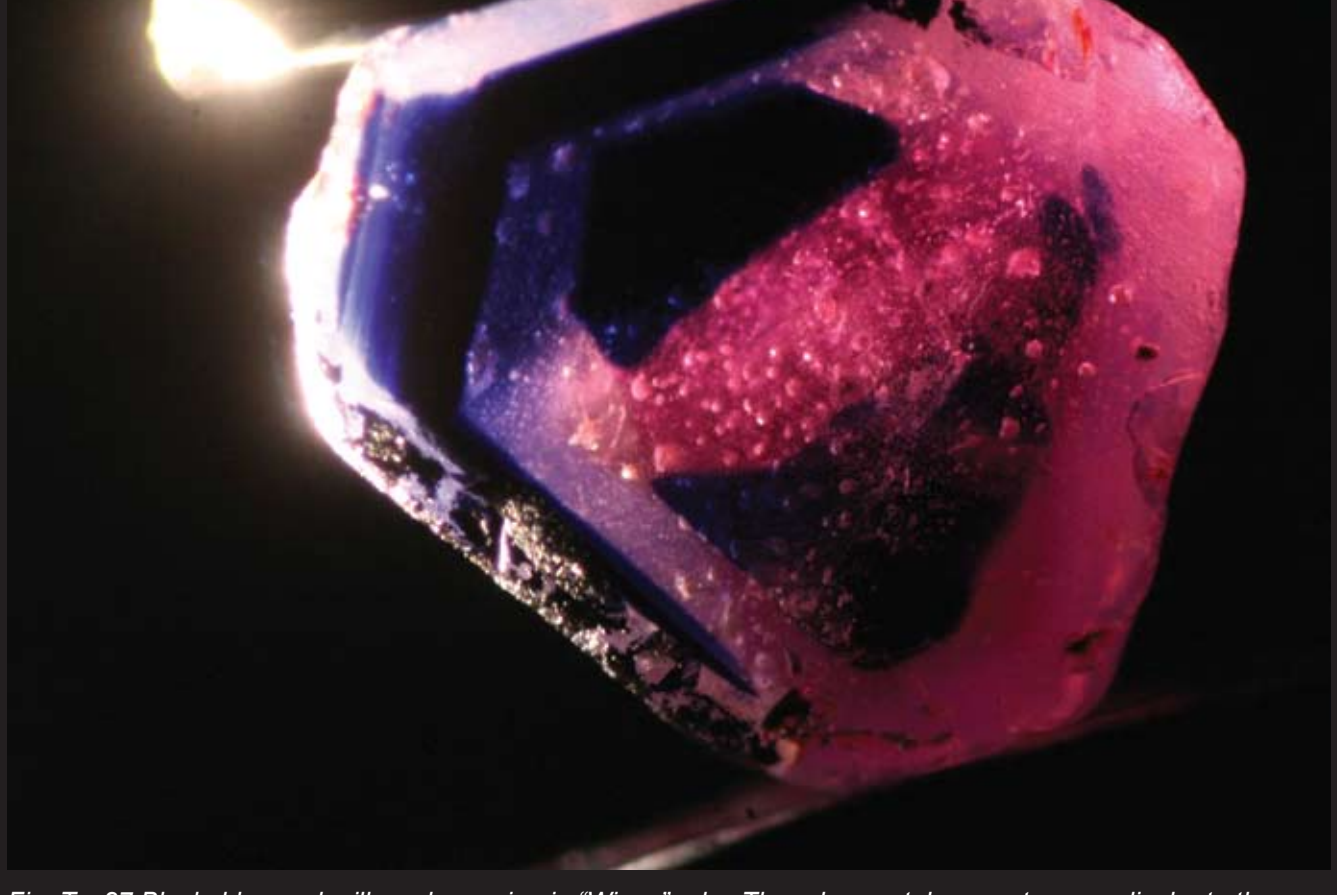

Fig. Tan87 Black, blue and milky color zoning in “Winza” ruby. The ruby crystal was cut perpendicular to the c-axis and polished. Sample No. GRS-Ref7510 (diameter 5mm).

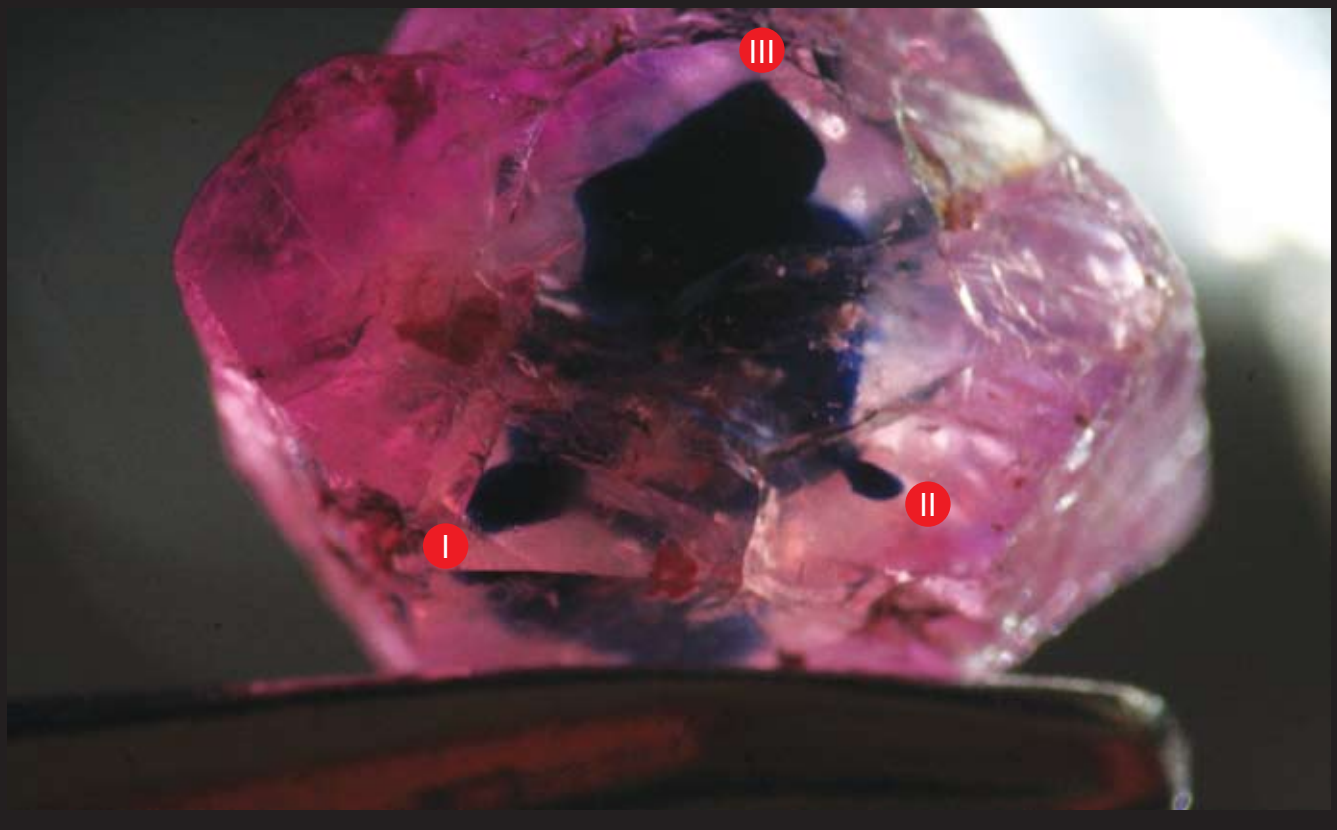

Fig. Tan88 A Winza ruby with rhombohedra shape is shown. The polished window exposes the internal growth structures. The core of the crystal shows an extremely complicated internal growth structure with a series of different blue color zones. Three color-zones have been formed in the shape of “Tornados” (twisted and bended color-pipes) pointing towards the outer faces of the crystal (see I, II, III). Sample No. GRS-Ref7455, weight 1.43ct.

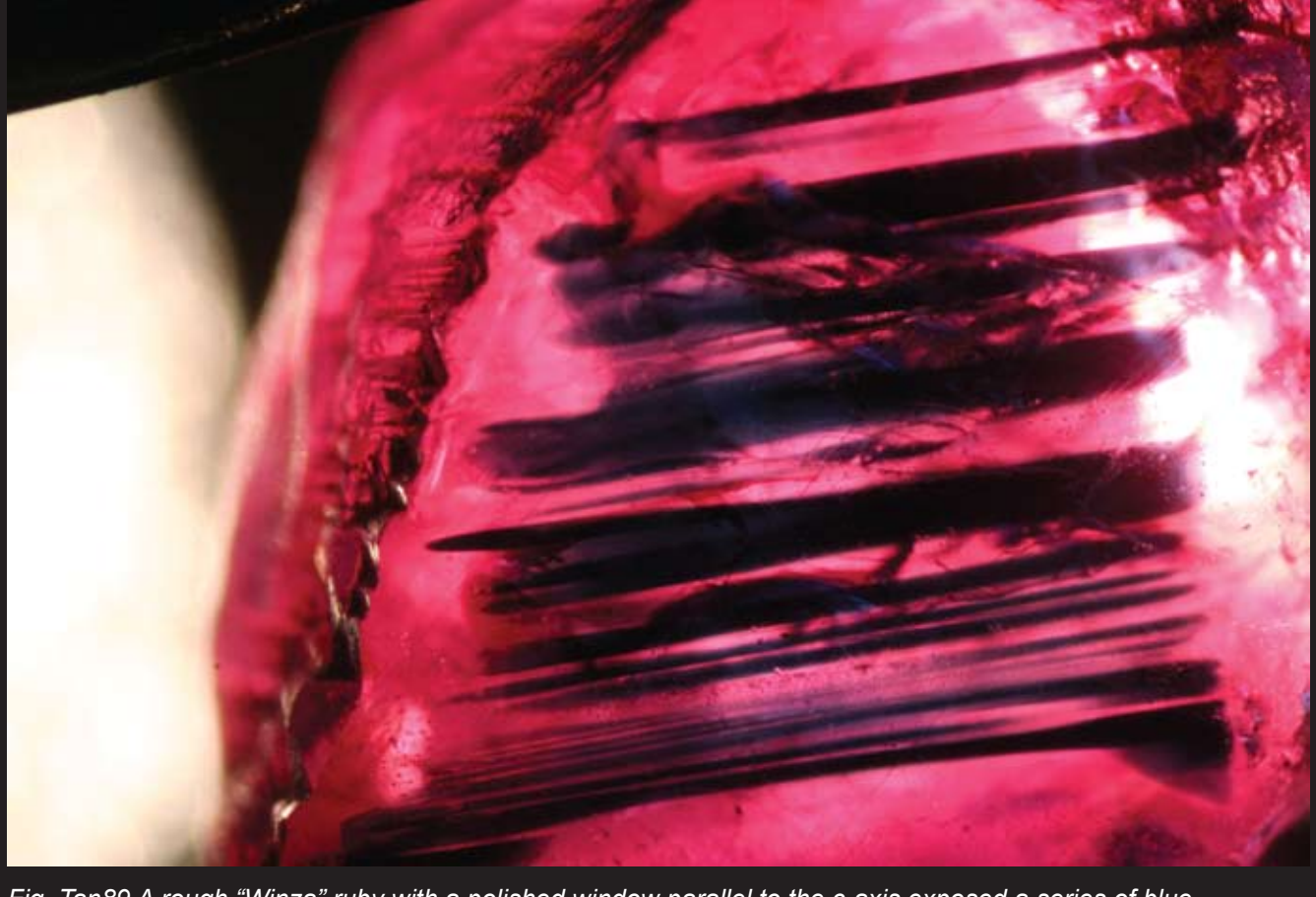

Fig. Tan89 A rough “Winza” ruby with a polished window parallel to the c-axis exposed a series of blue color-zones. Sample No GRS-Ref7501 (Tan56), weight 4.04ct.

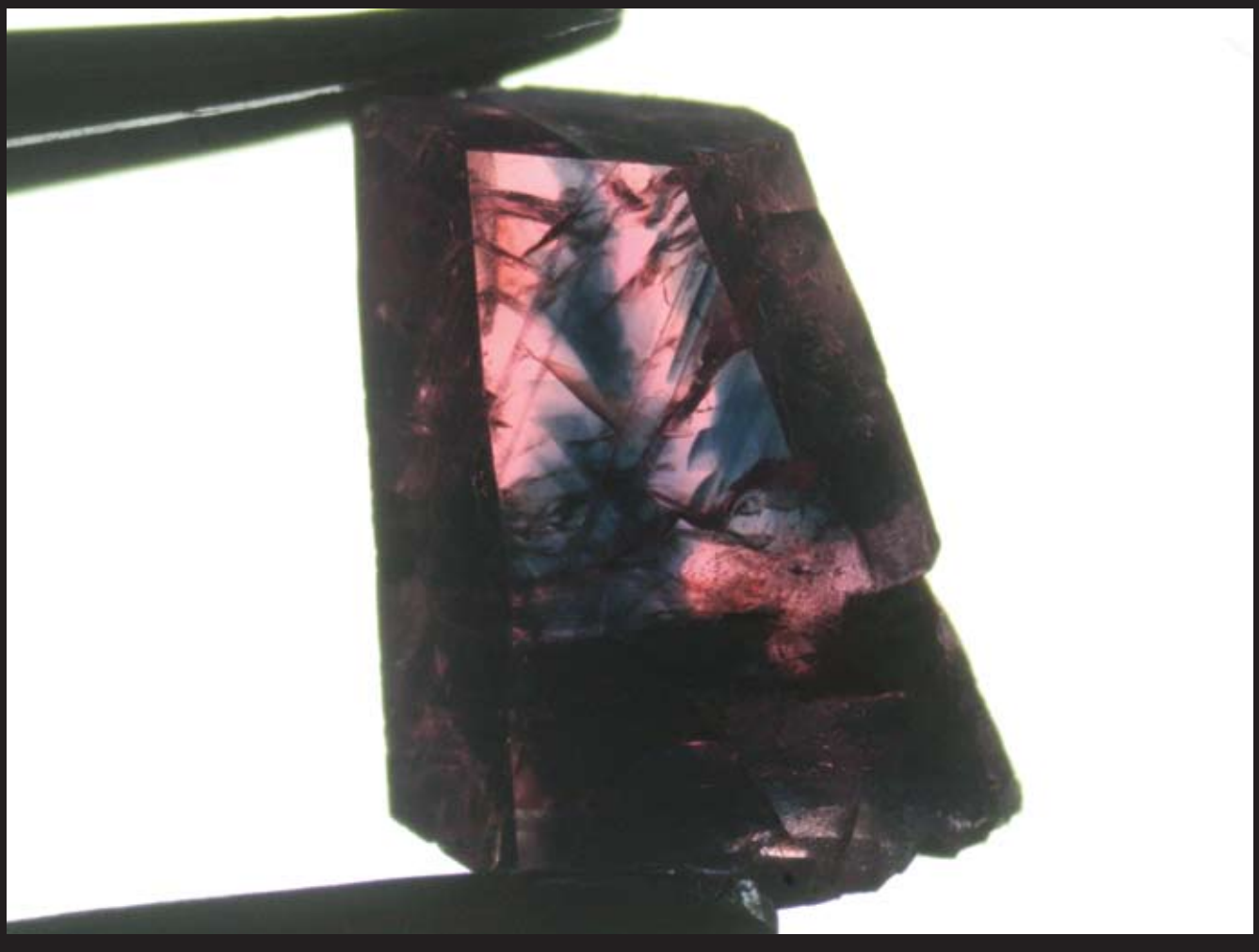

Fig. Tan90 Winza ruby rough with 3 polished windows parallel to the outer crystal faces. A complicated internal color zoning can be seen, which occurs in different screw-like patterns around a pink core. Sample No. GRS-Ref7458, weight 3.73ct, length 7.8mm.

Fig. Tan91 Winza ruby rough with two polished windows is shown. Two different type of blue color zoning are found in this crystal. A series of triangular blue color zones resembling “shark teeth patterns”, are arranged along the c-axis and an outer blue zone, which is formed parallel to a steep pyramid in the ruby. Sample No. GRS-Ref7557, weight 3.14ct, length 10.5mm.

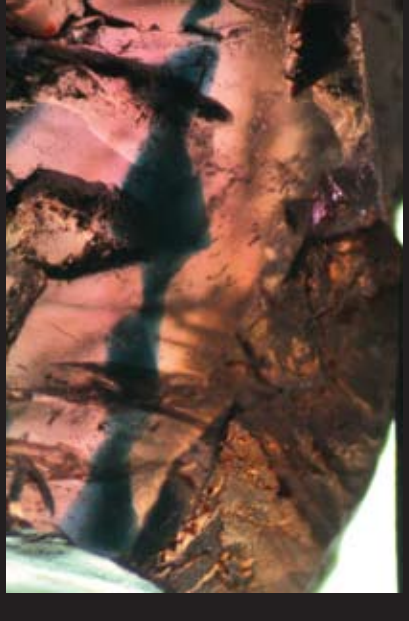

Fig. Tan92 The color distribution in the core of a Winza ruby. The complicated pattern resembles a twisted feature in the shape of a “screw”. The outer mantel is of orange color. Sample No. GRS-Ref7456, weight 2.50ct.

Fig. Tan93 A rough “Winza” ruby has been cut perpendicular to the c-axis. The ruby is composed of a red core and a milky rim. Every second corner, a blue triangular color zone is found parallel to rhombohedra growth faces. Sample No GRS-Ref Tan22.

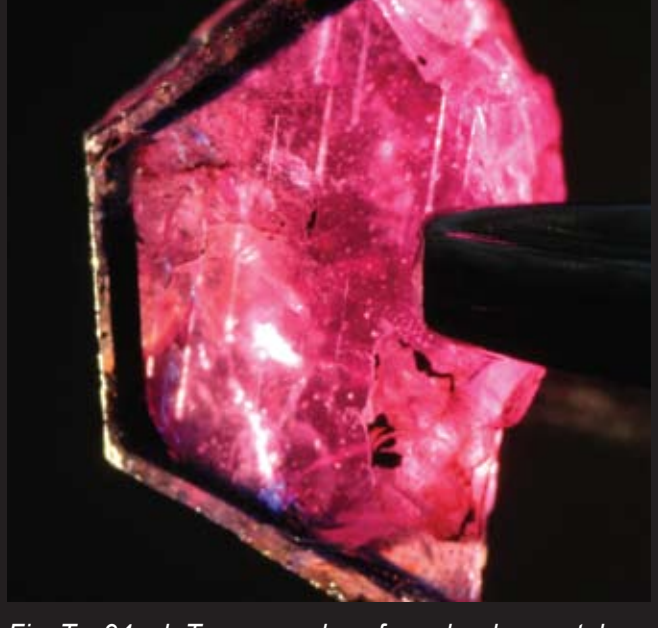

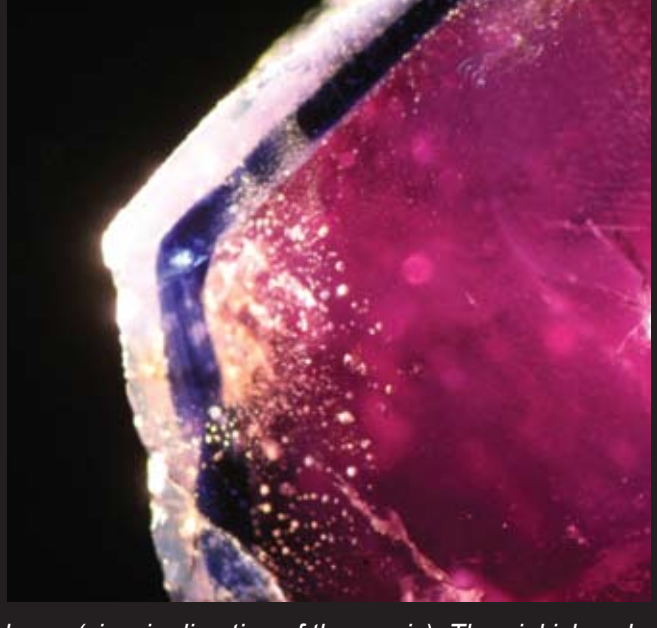

Fig. Tan94a, b Two examples of rough ruby crystals are shown (view in direction of the c-axis). The pinkish-red core is followed by a layer of blue color in the mantel of the crystal. The outermost layer consists of a milky-white rim. (Right) Sample No GRS-Ref7484 (Tan39), weight 4.13ct.

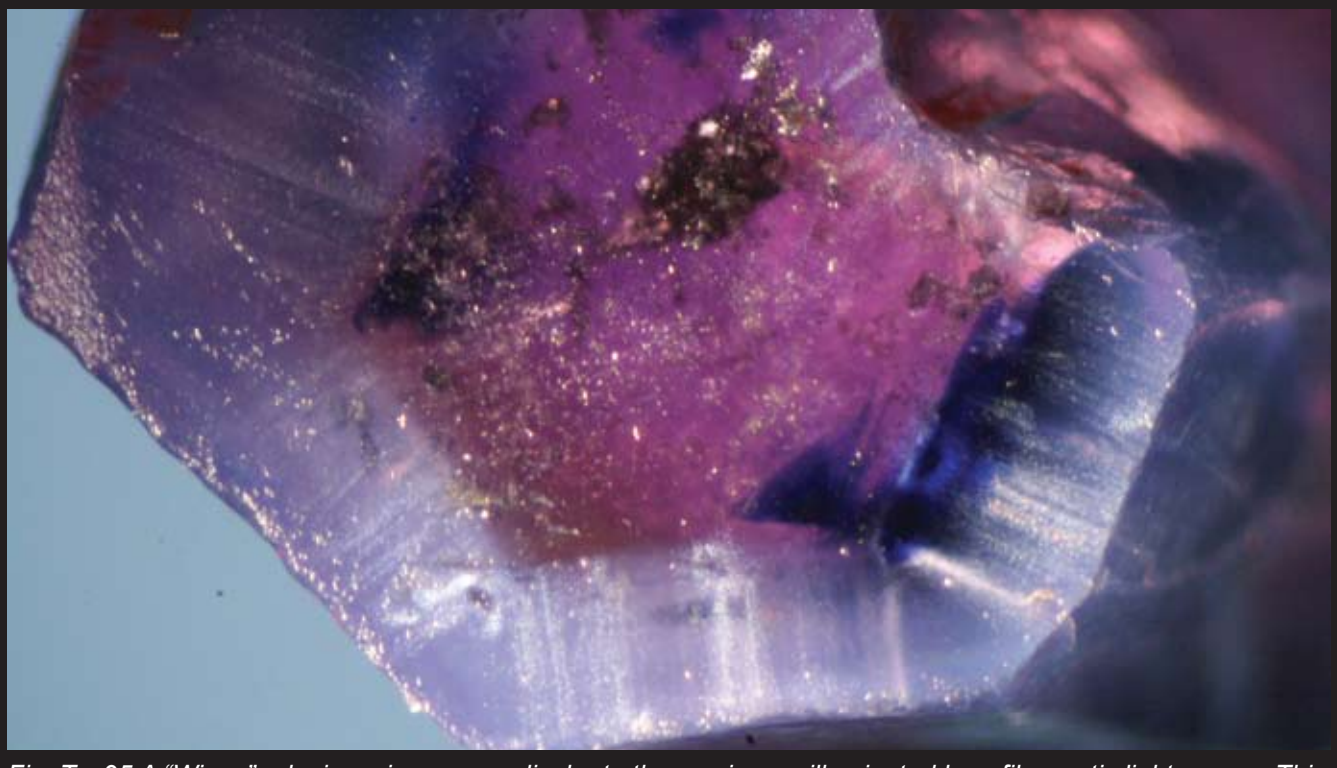

Fig. Tan95 A “Winza” ruby in a view perpendicular to the c-axis was illuminated by a fiber optic light source. This illumination visualized series of “streamers” and “comet tails”. They are nucleated at the ruby to milky sapphire rim contact zone where a series of solid and primary fluid inclusions are found. Sample No GRS-Ref7508 (Tan63), weight 1.00ct.

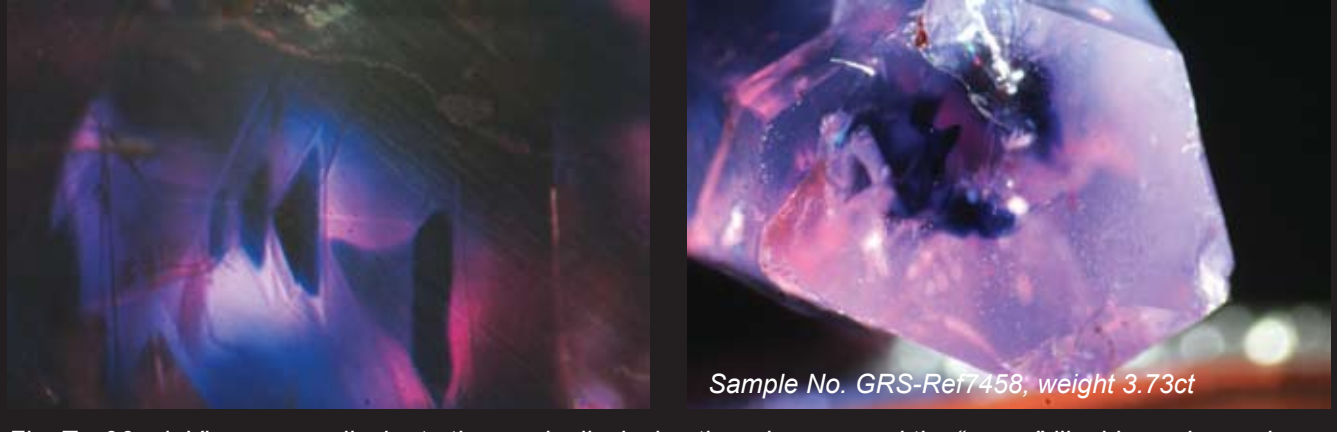

Fig. Tan96a, b View perpendicular to the c-axis displaying the ruby core and the “screw”-like blue color zoning around it. The rim consists of a velvet pink sapphire with numerous submicroscopic particles.

Fig. Tan97a, b These “Winza” rubies are characterized by red core and “screw”-like blue color zoning around it. Individual blue growth zones are identified as rhombohedra growth faces. This growth faces are pointing in the opposite direction than the growth faces of the outer crystal. The direction of growth was 180 degrees rotated during the formation of these crystals. The crystal on the right has a triangular orange-colored zone.

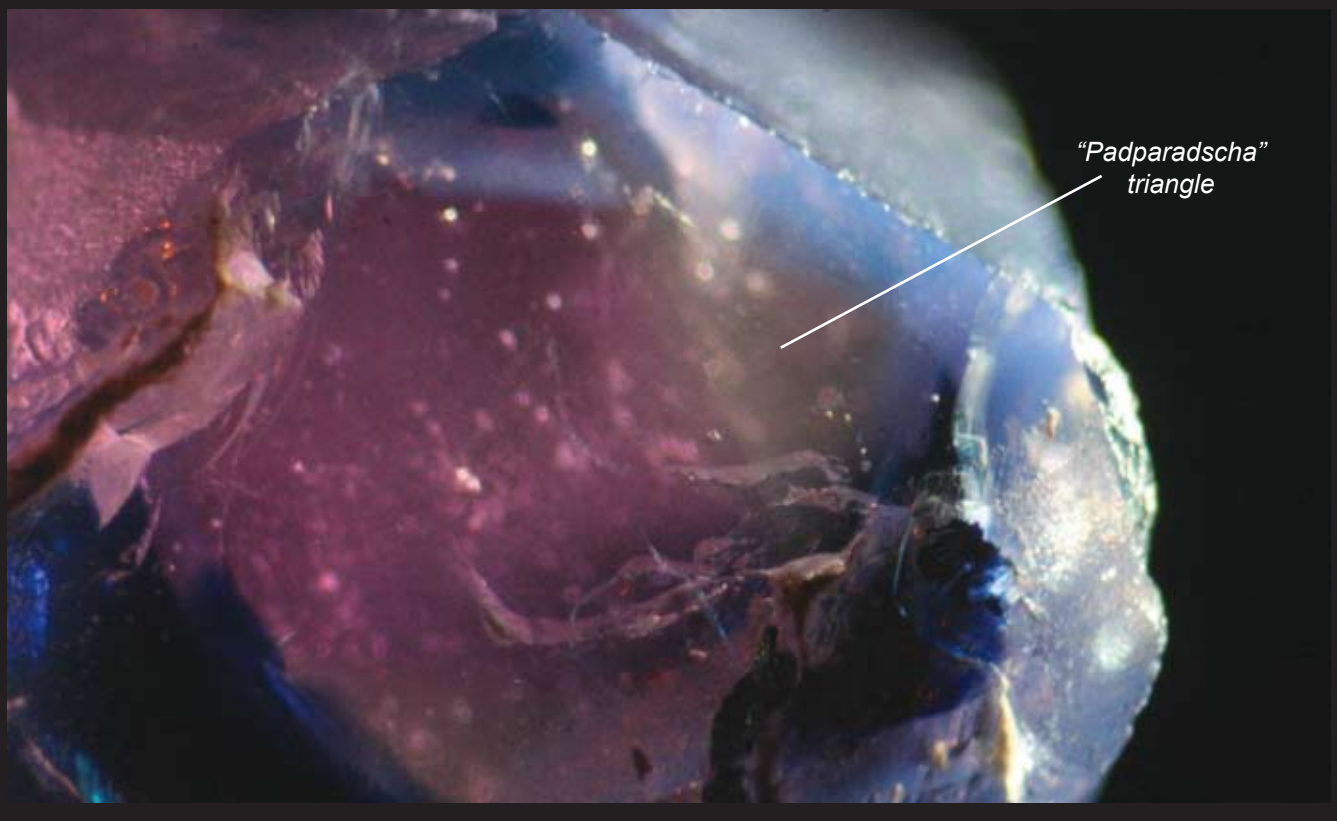

Fig. Tan98 Example of the complicated color zoning observed in a “Winza” ruby. The crystal consists of a pinkish-red core (I), triangular orange-pink (”Padparadscha”)-sectors (II), triangular blue color zones (III) and a milky rim (IV). Triangular blue and orange zones are alternatively formed in different corners of the crystal (view parallel to the c-axis). Sample No GRS-Ref7509, weight 0.76ct.

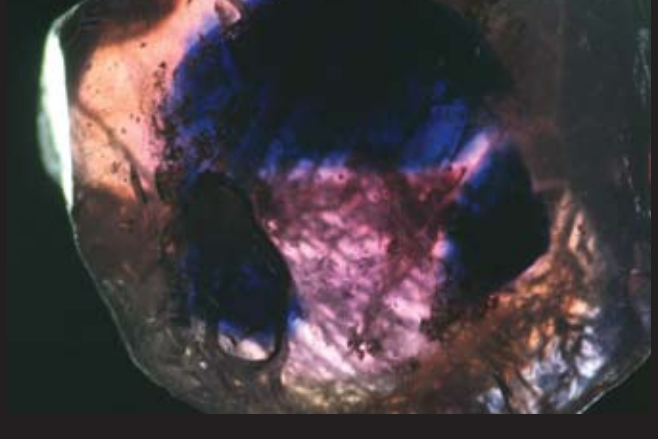

Fig. Tan99a (Sample No GRS-Ref7478, weight 3.94ct)

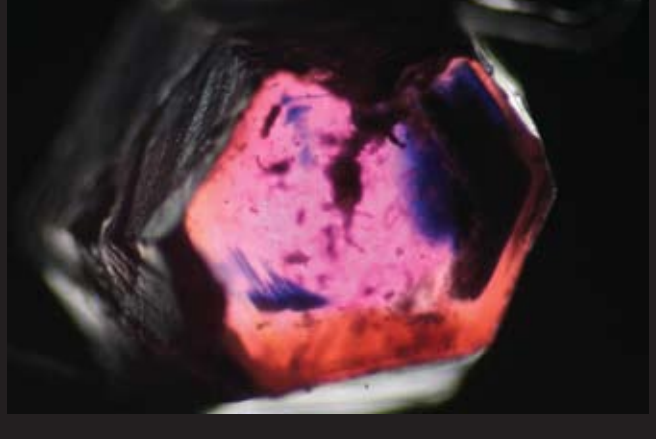

Fig. Tan99b (Sample No GRS-Ref7508, weight 1.00ct)

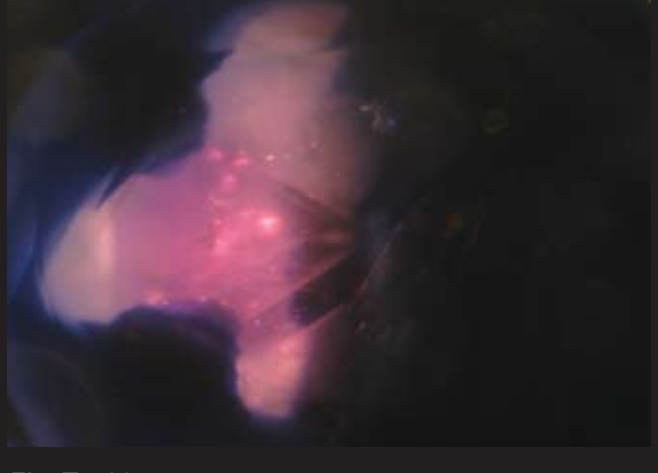

Fig. Tan99c

Fig. Tan99a, b, c Winza ruby rough crystal is shown with a polished window perpendicular to the c-axis. View in direction of the c-axis. It is visible that the ruby is internally composed of a pink sapphire/ruby core, blue sapphire zones in three different directions, orange-pink growth sectors (“Padparadscha”-color), an outer orange brown color rim (appears milky in reflected light) and a outermost blue sapphire rim (left).

Fig. Tan100a (Sample No. GRS-Ref7487 (Tan42), weight 3.85ct)

Fig. Tan100b (Sample No GRS-Ref7507, weight 2.13ct)

Fig. Tan100a, b Orange color zones are found in triangular growth sectors (a). A magnified portion of a particular color zoning found in a Winza ruby shows a sector with intersection of an orange, blue and pink color zone (b).

Fig. Tan101 Blue color zones found in a faceted ruby from Winza. A blue color zoning was found that resembles “Insect Antennas”. Fiber-optic illumination. Sample No. GRS-Ref8308.

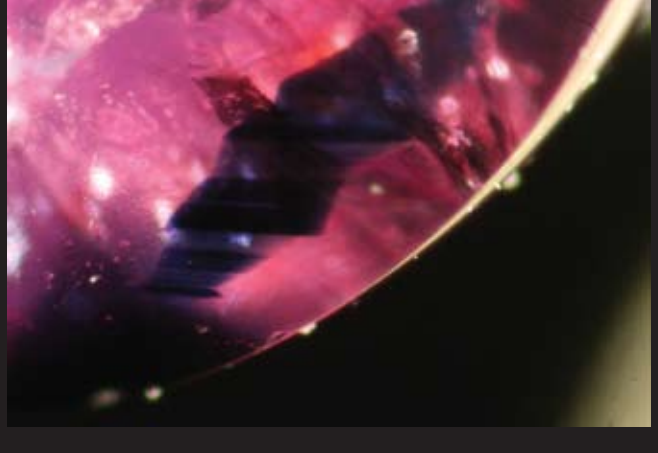

Fig. Tan102

Fig. Tan103

Fig. Tan102 Color zoning in a Winza ruby. Inside structure of isolated blue color patch was visible. The “twisted” appearance of some color zones is due to oscillation in size and blue color intensity of this particular growth face. The color zone varies in size and color intensity. If viewed in other directions this zones appears as curved and “twisted”.
Sample No. GRS-Ref8324.

Fig. Tan103 Example of a complicated blue color zoning in a cabochon ruby with isolated patches and irregular distributions. Sample No. GRS-Ref8057.

Fig. Tan104

Fig. Tan104 A series of blue color zones in a ruby were curved. This indicates deformation of the corundum lattice after its formation.

Fig. Tan105 Winza Ruby in a special view shows blocks of color zones. A fluid feather cuts through the complicated growth and color zoning. Transmitted light. Sample No. GRS-Ref8058.

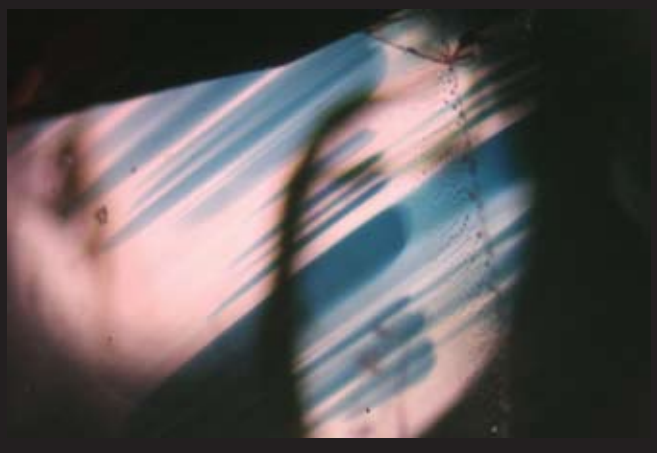

Fig. Tan106 Blue color zoning in a cabochon ruby that appears like a series of discs. Note: the presence of a fluid feather in a direction perpendicular to this color zoning. Sample No GRS-Ref8313.

Fig. Tan107 Angular milky color zoning. Sample No. GRS-Ref8061.

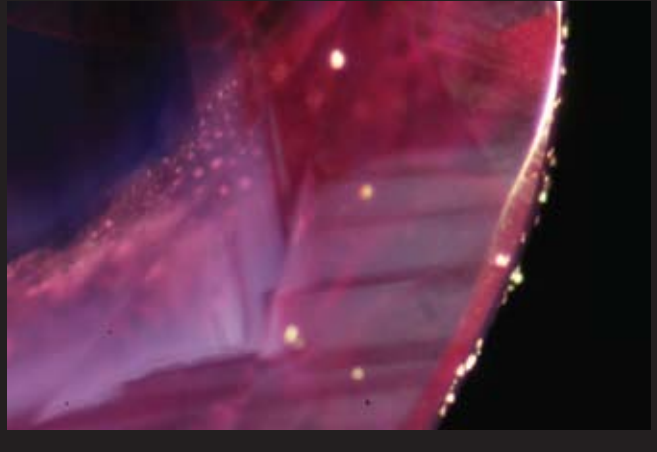

Fig. Tan108 Blocks of white color zones adjacent to an intense blue color zone in a faceted ruby from Winza. In the transition zone between the blue and milky zone is a fluid feather. Sample No. GRS-Ref A.

Fig. Tan109 Fancy sapphire from Winza with color zoning. In this case the color zoning is an oscillation between orange-pink (“Padparadscha” color) and blue sapphire layers. Sample No. GRS-Ref8215.

Fig. Tan110 Blue color zoning in fancy sapphire shows a repetition of distinctive blue color zones in the arrangement of “Dominos”.

INCLUSION FEATURES IN RUBIES FROM “WINZA” (TANZANIA)

Fig. Tan111a

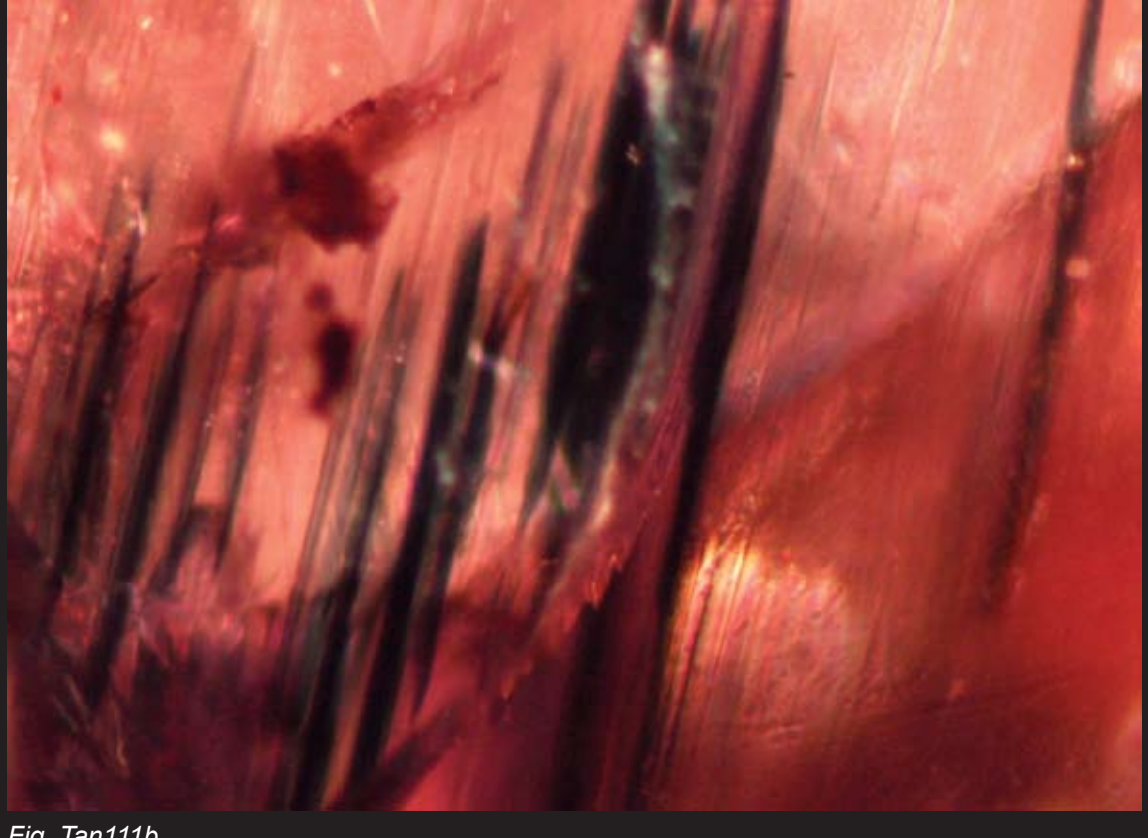

Fig. Tan111b

Fig. Tan111a, b Extremely small color-bands were present in faceted rubies. This color zoning was found in rubies spared of thermal enhancement.

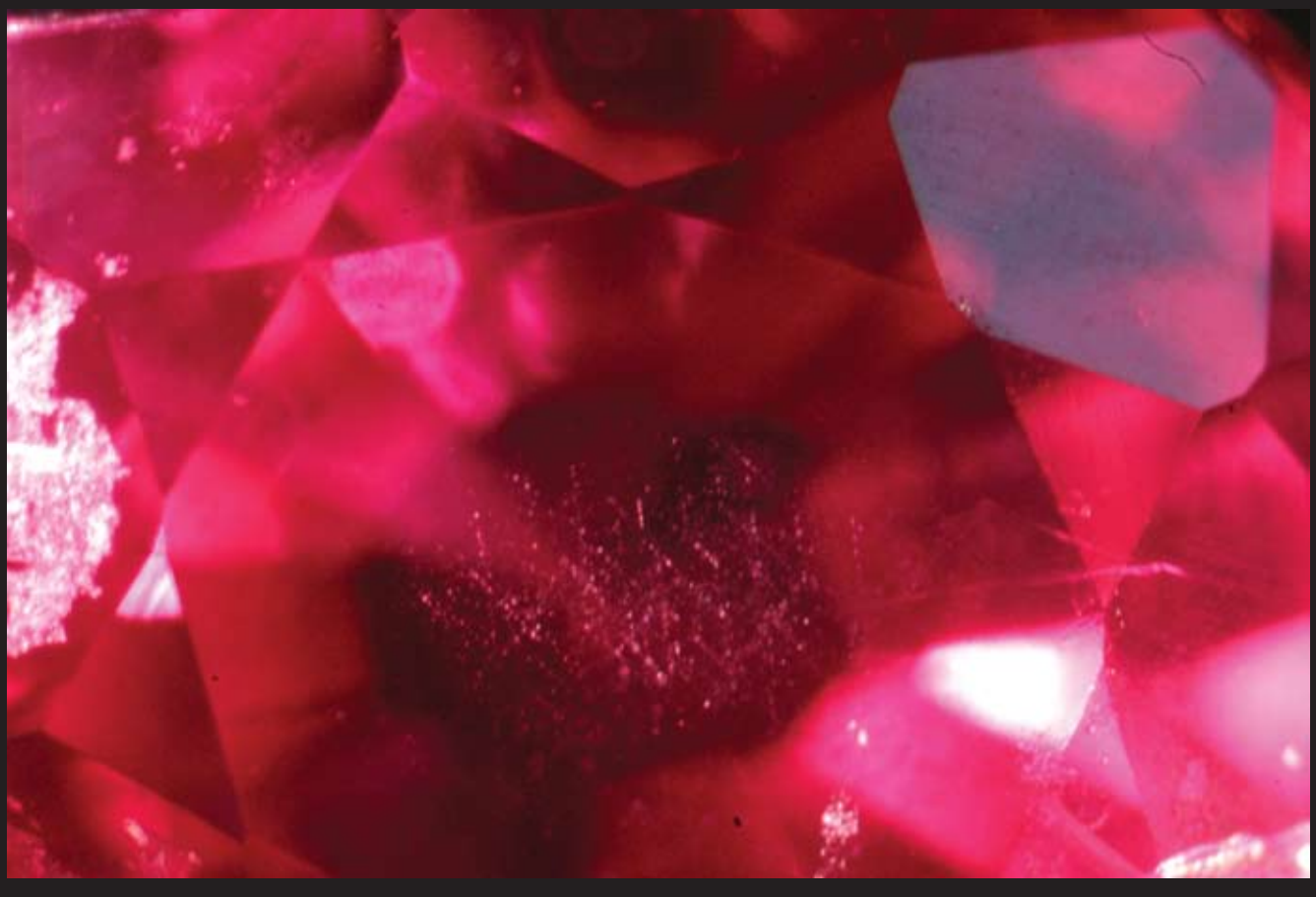

Fig. Tan112 Photo of a 0.8ct faceted Winza ruby with oriented dotted lines directly under the table. Sample No. GRS-Ref7858b. Fiber-optic illumination.

Fig. Tan113 Micro-particle inclusions resembling “Snow Flakes”. Fiber-optic illumination. Sample No. GRS-Ref7861b.

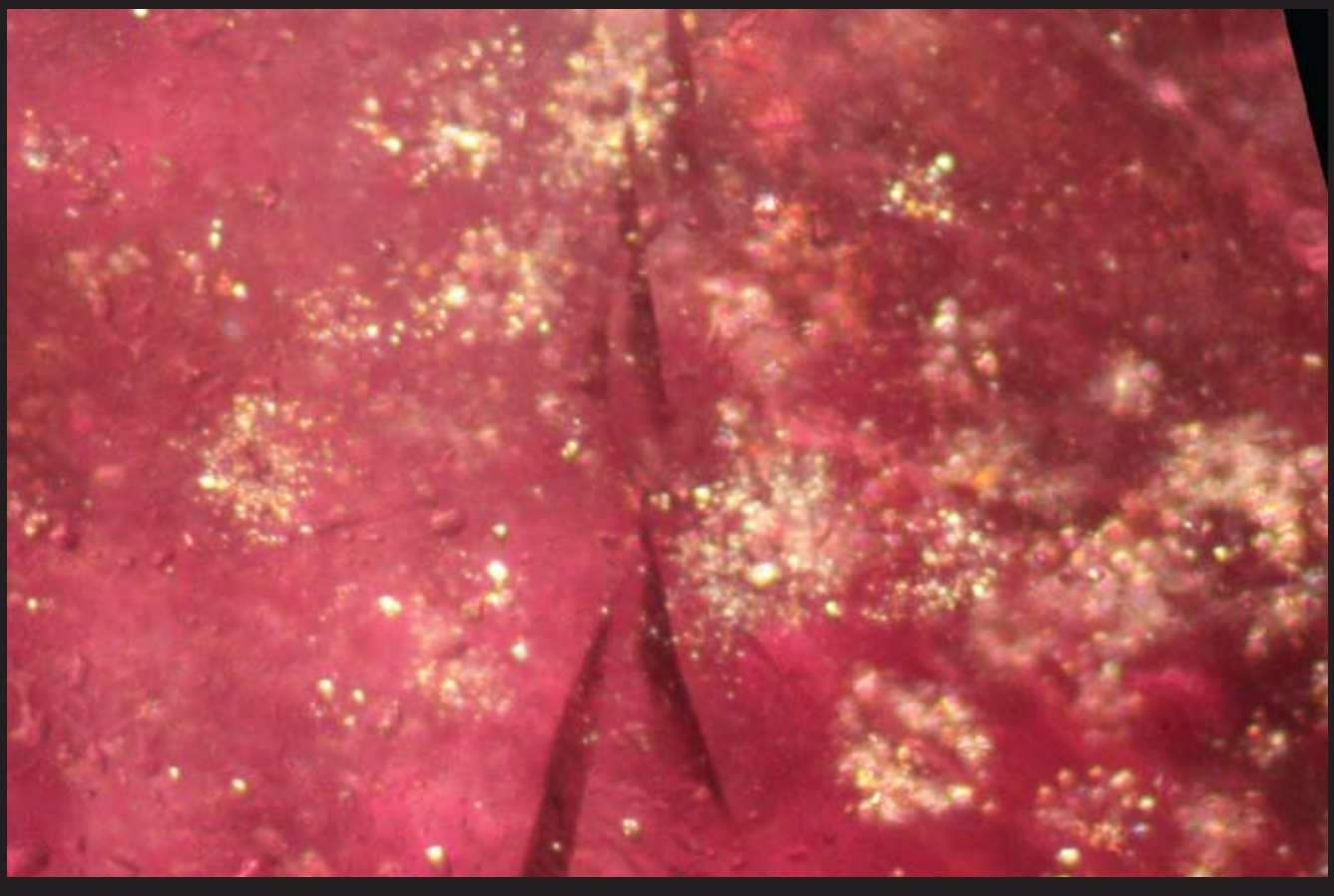

Fig. Tan114 Small particles in a faceted ruby from Winza. Clusters of pinpoints are arranged around a central dark point, resembling “star galaxies”. 60x magnification.

Fig. Tan115 A “comet tail” is formed at the surface of an opaque inclusion. Fiber-optic illumination, 60x magnification.

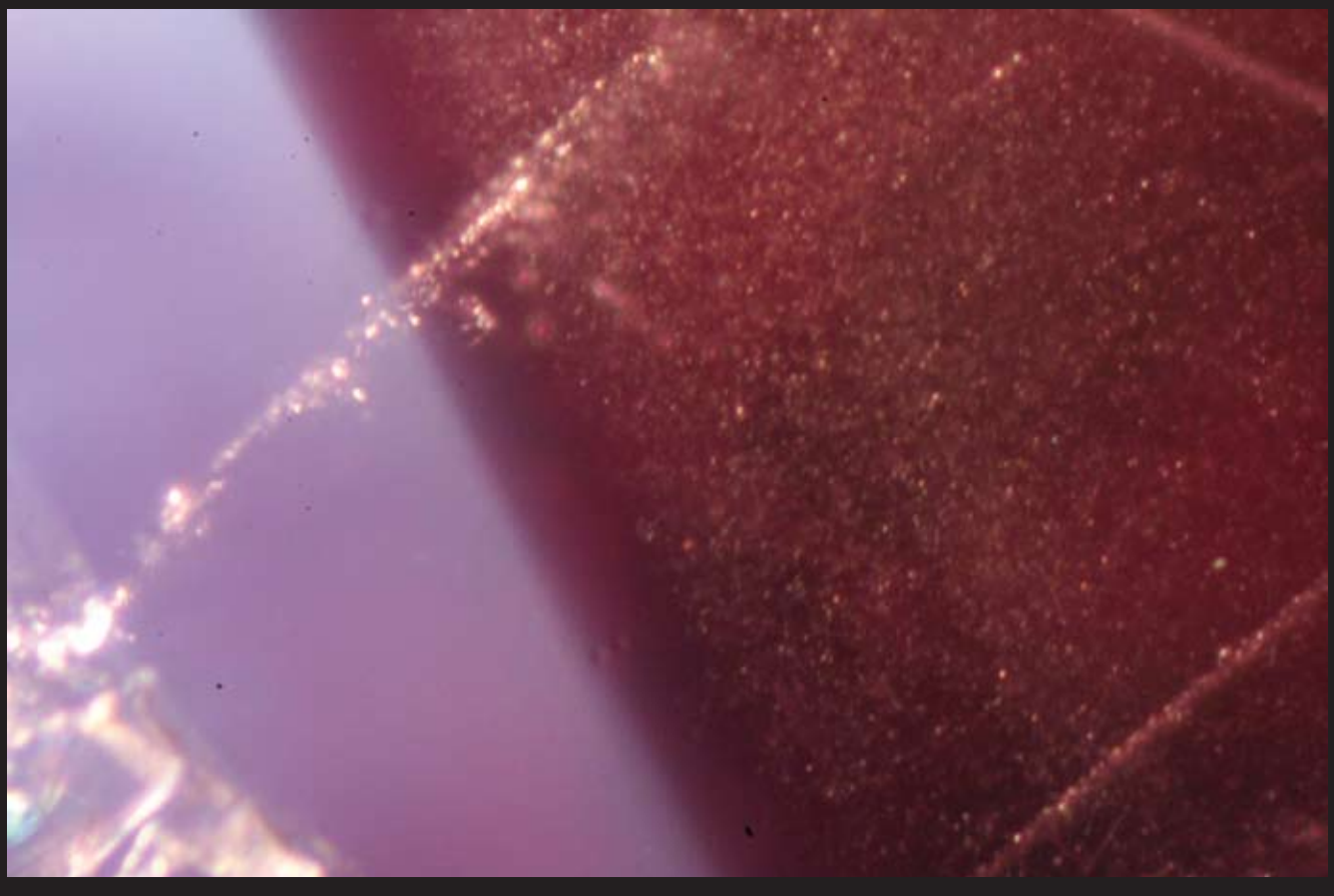

Fig. Tan116 Concentrations of pinpoints and whitish particles. Sample No. GRS-Ref7500 (Tan55), weight 2.17ct.

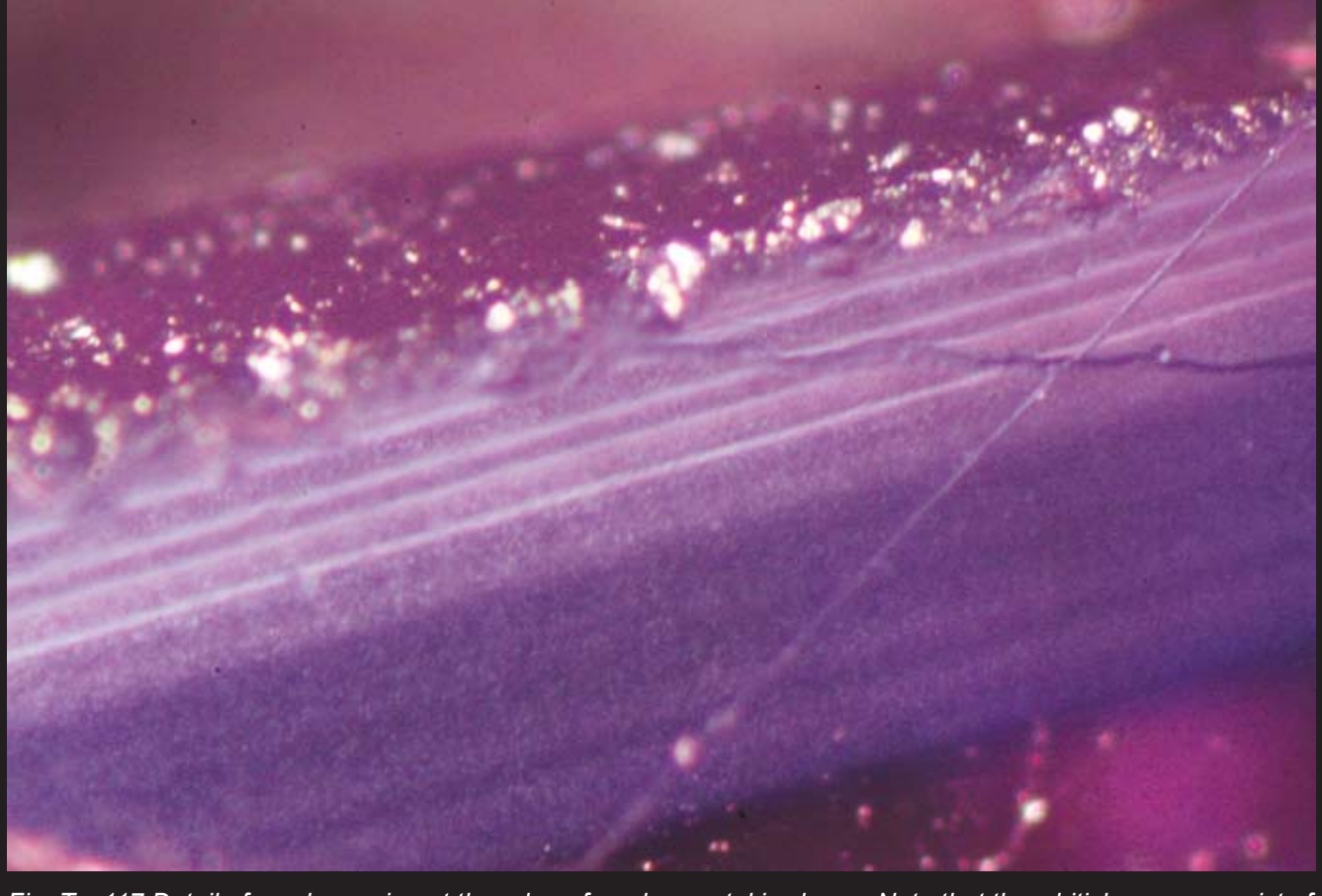

Fig. Tan117 Detail of a color zoning at the edge of a ruby crystal is shown. Note that the whitish zones consist of whitish particles. The concentration of sub-microscopic particles oscillates towards the end of the crystal growth. Sample No. GRS-Ref7498 (Tan53), weight 3.78ct.

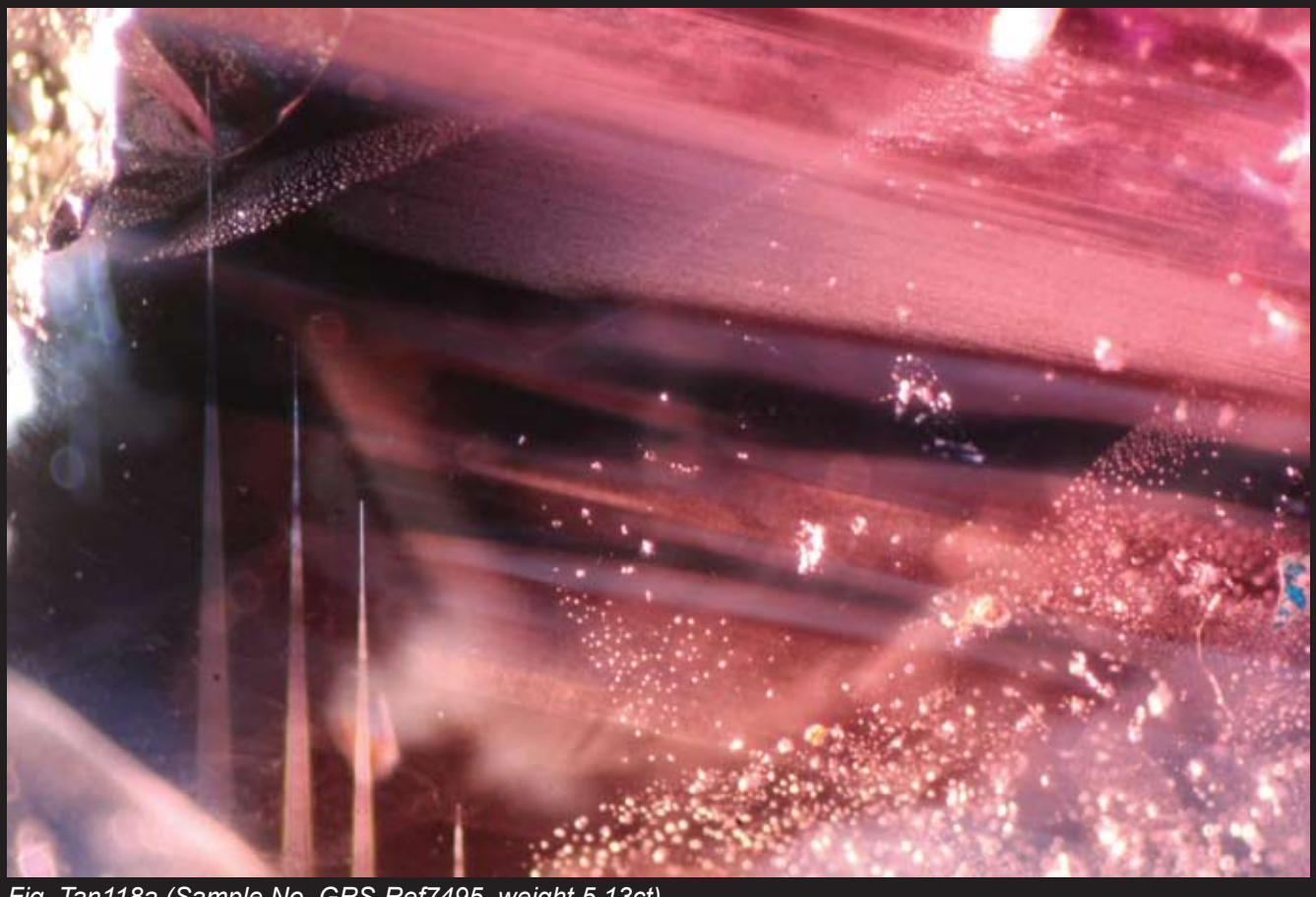

Fig. Tan118a (Sample No. GRS-Ref7495, weight 5.13ct)

Fig. Tan118b (Sample No. GRS-Ref7506, weight 1.19ct)

Fig. Tan118a,b Alternation of blue color zoning and milky zones. The blue color zones are laterally fading and are replaced by layers of submicroscopic particles. Fiber-optic illumination.

Fig. Tan119 Oriented pinpoints in a faceted sapphire. A color whole is present in the sapphire and pin point rutile particles are present in the typical crystallographic orientation inside the color window. No long rutile needles were found. Fiber-optic illumination. Sample No. GRS-Ref8195.

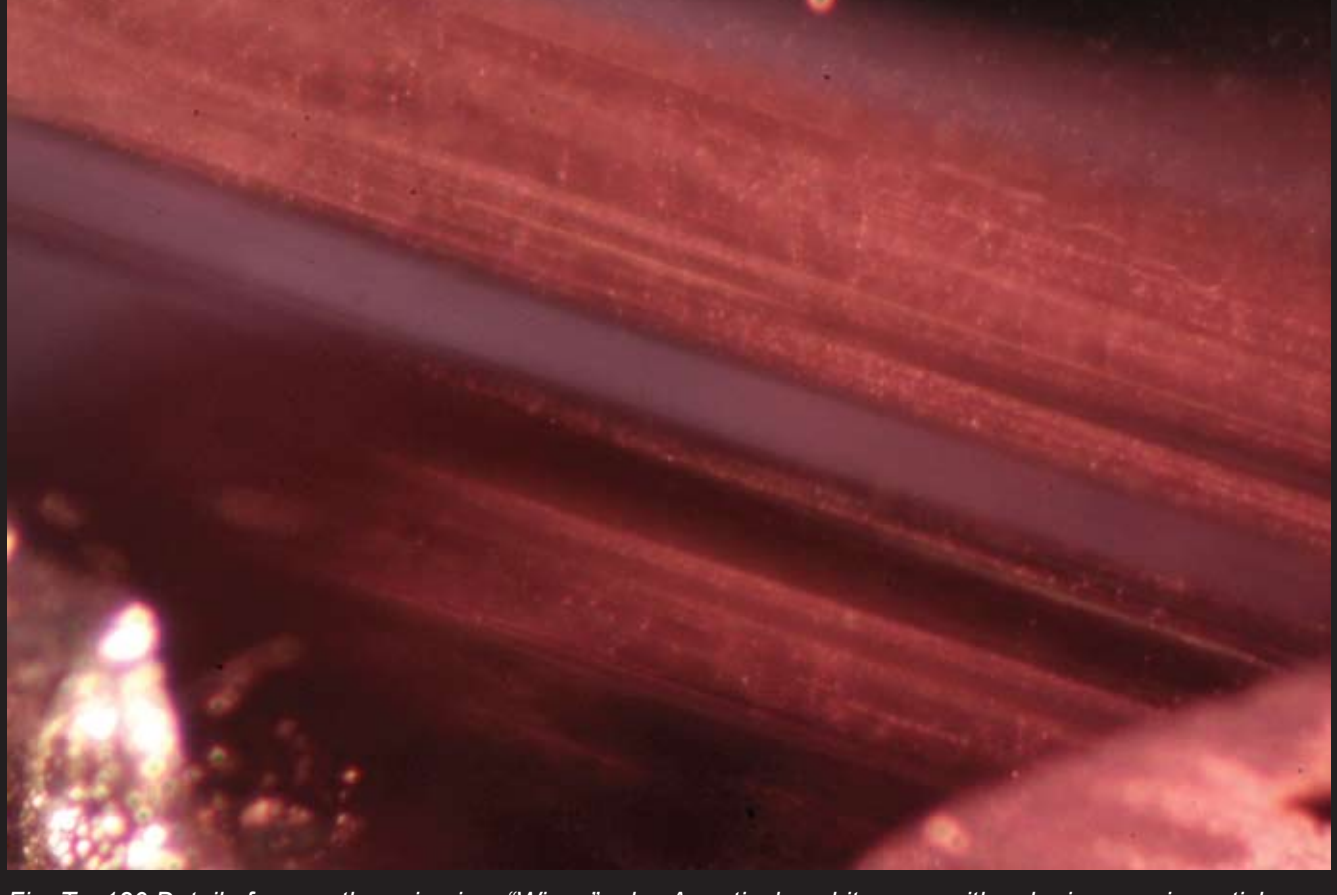

Fig. Tan120 Detail of a growth zoning in a “Winza” ruby. A particular white zone with submicroscopic particles occurred in inside layers of isolated pinpoints and dust-like particles. Fiber-optic illumination. Sample No. GRS-Ref7495, weight 5.13ct.

LA-ICP-MS ANALYSES

Chemical analyses of the rubies from this new deposit were carried out by LA-ICP-MS at the research group for Trace Elements Micro-analysis at the Laboratory of Inorganic Chemistry, ETH Zurich (Prof. D. Günther) and by ED-XRF analysis at the GRS laboratory (Fig. Tan134). The LA-ICP-MS data are shown in Fig. Tan121-122, Fig. Tan125-133 and Tab. Tan02. The methods are described in Lit.Tan16-18 and an explanation of the methods is given in Box Tan04.

8 Rough ruby samples were cut half and a window facet was polished exposing the internal characteristics of a ruby. Across a selected profile, a series of LA-ICP-MS measurements were carried out that resulted in a line of approx. 50-80 craters. Each crater provided chemical analyses of the following elements: Li, Be, B, Na, Mg, Al, Si, K, Ca, Sc, Ti, V, Cr, Mn, Fe, Co, Ni, Cu, Zn, Ga, Ge, Rb, Sr, Zr, Nb, Mo, Ag, Sn, Sb, Cs, Ba, La, Ce, Pr, Nd, Sm, Eu, Gd, Tb, Dy, Ho, Tm, Yb, Lu, Hf, W, Pb, Bi, Th and U. Phosphorus (P) and Fluorine (F) could not be measured. Chlorine (Cl) was not measured in this quantitative approach. A total of over 500 analyses were carried out on various samples. The concentration of the elements are shown in dependence on their position in the sample (Fig. Tan 125-133). Please note that every zero shown in the graphs represent concentrations equivalent to the detection limits. REE detection limits achieved in this study were 0.09 to 0.008 ppm, transition metals Ti, Cr, V, Mn, Cu, Zn, Ga were approx. 0.1-1ppm, Na 1-10 ppm, Si, K, Ca were approx.100 ppm.

From this chemical analysis, the majority of the concentrations of the trace elements represent their limits of detection (LOD). The rubies had concentrations of magnesium (Mg), chromium (Cr), vanadium (V,) titanium (Ti), manganese (Mn), iron (Fe) and gallium (Ga) as in most of the natural rubies (see Lit Tan14, 23, 24, 26, 30). Beryllium (Be) concentrations above LOD were not found. However, the additional presence of traces of nickel (Ni) was detected (Fig. Tan121a). Such high concentrations of Ni in corundum have so far only been detected in natural rubies found as inclusions in diamonds (Lit Tan21). Furthermore, Ni concentrations have been also reported in synthetic corundum (Lit Tan31, 36). The measured concentrations of the trace elements Cr, V, Ti, Fe and Ni are variable and correlated with different color zones. Blue color zones are enriched in Ti (along with high levels of Fe), orange color zones are rich in Mg and Fe (at lower level of Ti and Cr) and ruby contains high concentrations in Cr. A number of additional elements were found in the rubies including the elements Li, Si, Na, Ca, K, Ba, Rb, Sr, Cu, Zn, La, Ce, Sb, Nb, Ag, Mo, Zr, Bi, U, Th and Pb. These chemical trace elements in the rubies might be the result of contamination by inclusions. Inspection of the measured points in the microscope revealed that these trace elements were detected in areas of the rubies that had numerous sub-microscopic fluid or mineral inclusions. The Ni-concentrations in the rubies, however, are correlated with color zoning and are therefore clearly a trace element present within the ruby matrix (Figs. Tan126d, 127c, 128, 129c, 130d, 131c and 132c). Nickel-concentrations are also correlated to the trends of other trace elements in the rubies, such as V (Fig. Tan121a).

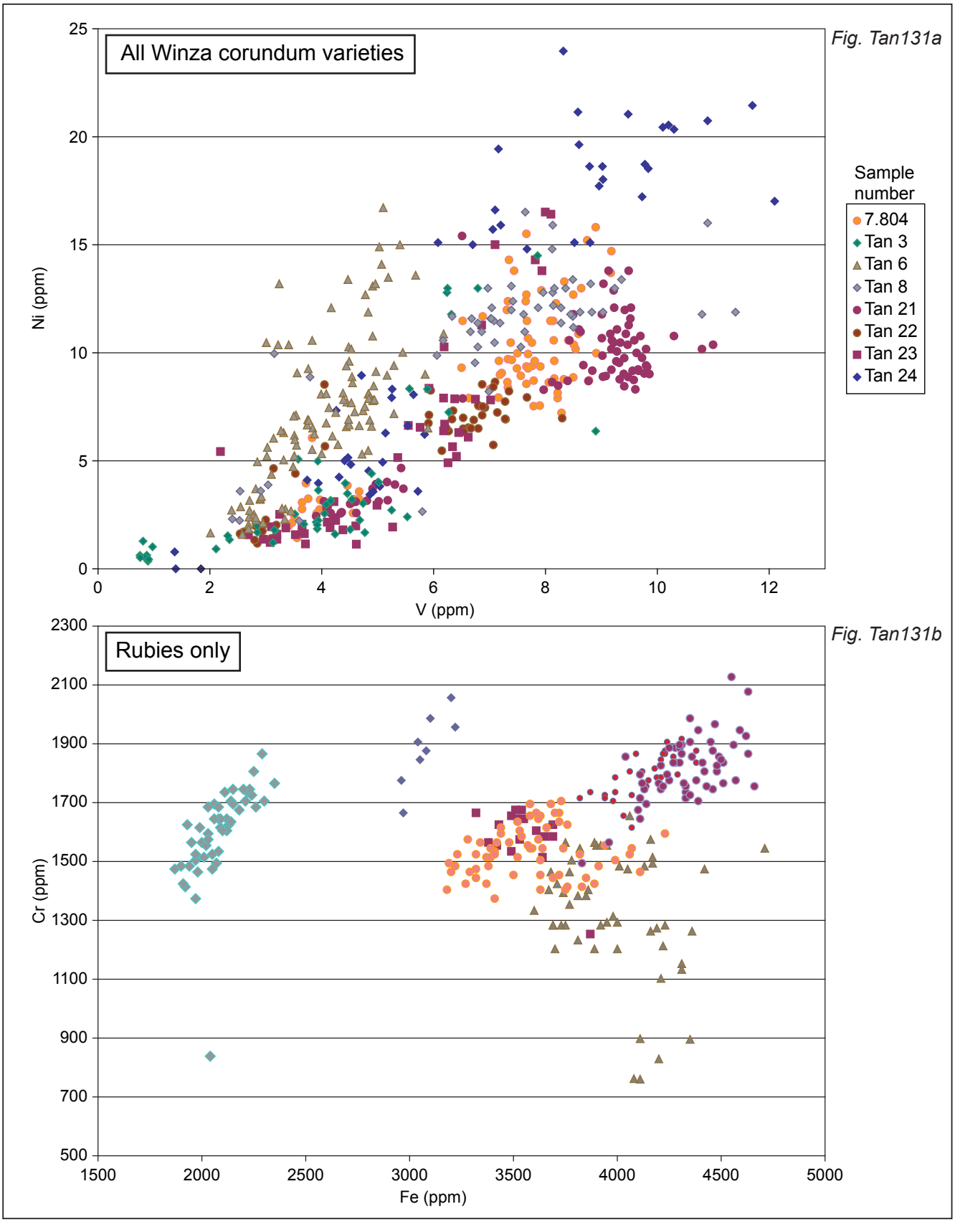

Fig. Tan121a, b Trace element concentrations of chromium (Cr) iron (Fe), vanadium (V), nickel (Ni) and rubies from “Winza” (Tanzania) are shown for 7 samples (other elements see also Tab. Tan02). The analyses of blue and orange color zones are only shown in Fig. 121a. Note that differences are found in chemical compositions within one particular sample and also between different samples. Increasing Ni-concentrations are correlated with increasing V-concentrations in the rubies (Fig. Tan131a). Fe- and Cr-concentrations are not correlated (Fig. Tan131b). Strong variations in Fe-concentrations occurred independent of Cr-concentrations. Major variations in Fe-concentrations are sample dependent.

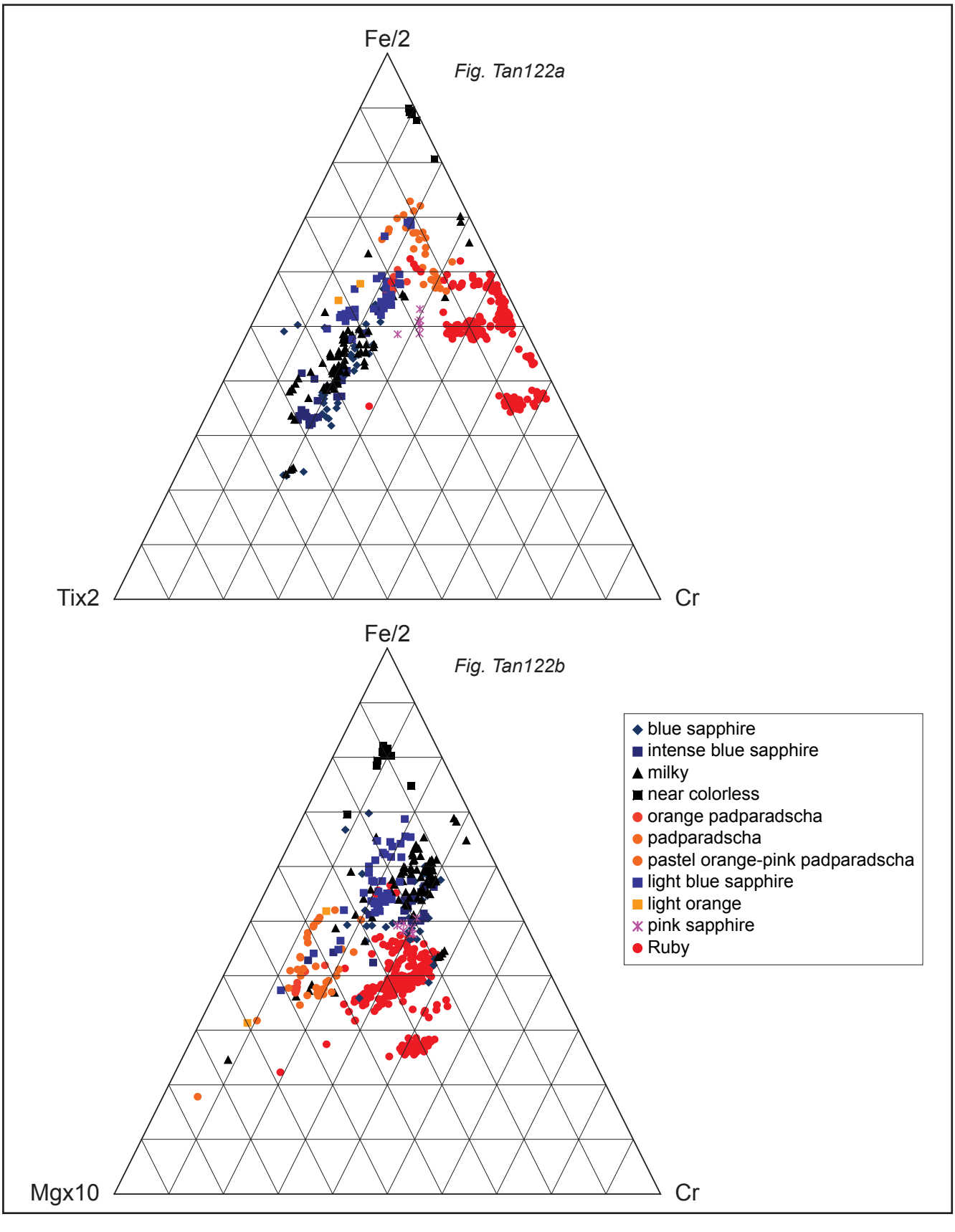

Fig. Tan122a, b Contains the chemical compositions of the Winza corundum including the analysis of the different color zones. They can be correlated to growth sectors and color zoning. The high variability of the chemistry is due to differences within the corundum crystal itself as well as between the samples (See Fig. Tan125-Tan133). Major differences were found in the concentrations of Mg, Ti, Cr and Fe concentrations: Ruby is high in Cr and variable in Fe and low in Mg and Ti concentrations. Sapphire colors are variable in Fe, high in Ti and low in Mg concentrations. Padparadscha-colors typically have relatively high Fe, high Mg, low to intermediate Cr and low Ti- concentrations (See also Tab. Tan02).

BOX TAN04: LA-ICP-MS CHEMICAL ANALYSIS

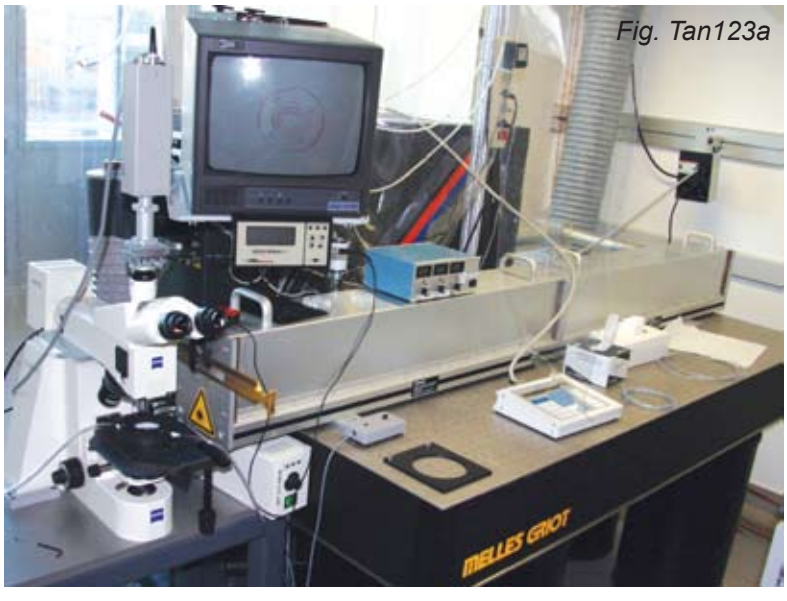

Fig. Tan123a


Fig. Tan123b

Fig. Tan123a, b Laser Ablation Mass Spectroscopy (LA-ICP-MS) at the Laboratory for Inorganic Chemistry, ETH Zurich, Switzerland (Prof. D. Günther)

EXPLANATION OF THE METHOD

Fig. Tan124 The laser ablation technique (LA) uses a 193 nm excimer laser (1) that is imaged onto the sample surface via optical lenses and a petrographic microscope (2). The laser is ablating (carrying away) the material (crater diameter 4 to 80 µm) (3). The mobilized material (particles) is suspended in a carrier gas (4) and transported via transport tube into an Inductively Coupled Plasma Mass Spectrometer (ICP-MS) (5). The laser-generated aerosol particles (except those that cannot be ionized, such as fluorine), are vaporized, atomized and ionized within the ICP. The formed ions are then transferred to the mass spectrometer and separated by their mass, divided by charge (5). The detector allows measuring major, minor and trace elements within a single analysis (9 orders of magnitude). Very light elements, such as boron, lithium or beryllium, can be detected, along with a large series of other elements at concentrations of less then 1 ppm. The quantification at low concentrations is possible by LA-ICP-MS due to a matrix-independent calibration, including special computer analysis and software (6).

INSTRUMENT

Lambda Physics GeoLas Q with PE/Sciex Elan 6100 DRC

Fig. Tan124

EXPERIMENTAL

The ablation craters on the rubies were placed along a profile. For each measurement, the background signal was recorded for 30 seconds, and then the ablation of the rubies was carried out for a period of 30-50 seconds. NIST 610 glass standard was used as external standard for calibration and analyzed using the same parameters as applied to the rubies.

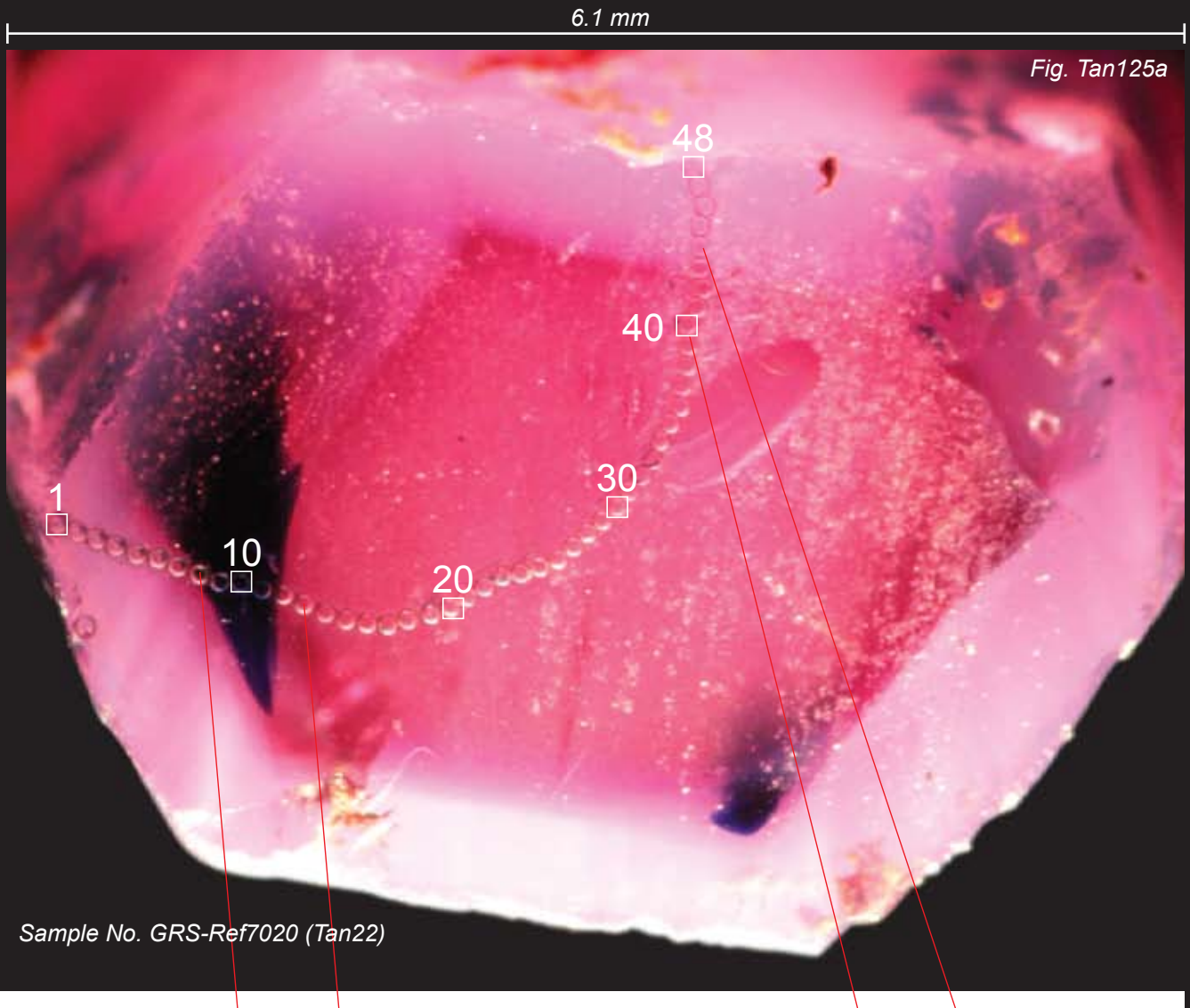
6.1 mm
Fig. Tan125a
48
40
30
1
10
20
Sample No. GRS-Ref7020 (Tan22)

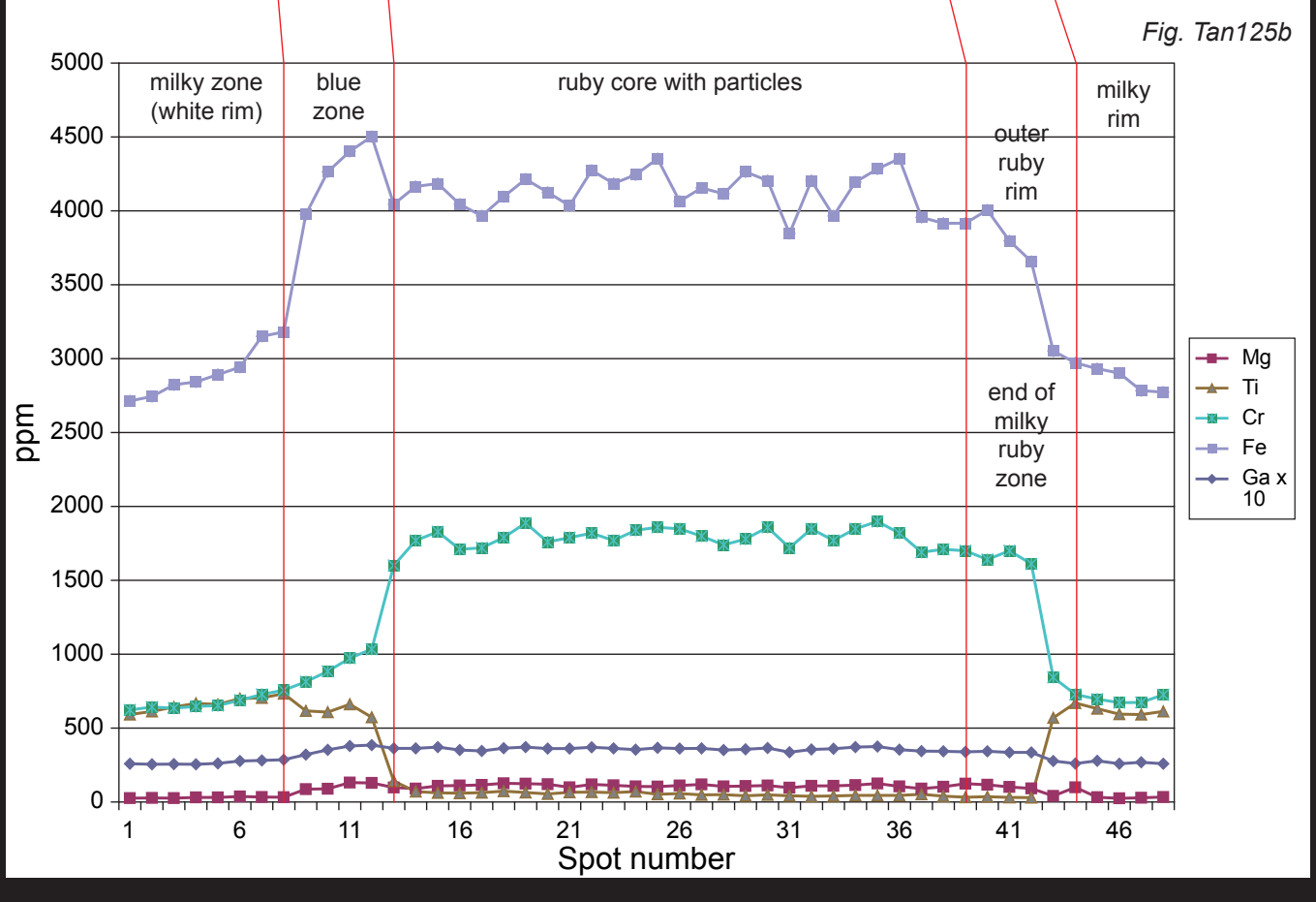
Fig. Tan125b
milky zone (white rim)
blue zone
ruby core with particles
milky rim
outer ruby rim
end of milky ruby zone
ppm
5000
4500
4000
3500
3000
2500
2000
1500
1000
500
0
1
6
11
16
21
26
31
36
41
46
Spot number
Mg
Ti
Cr
Fe
Ga x 10

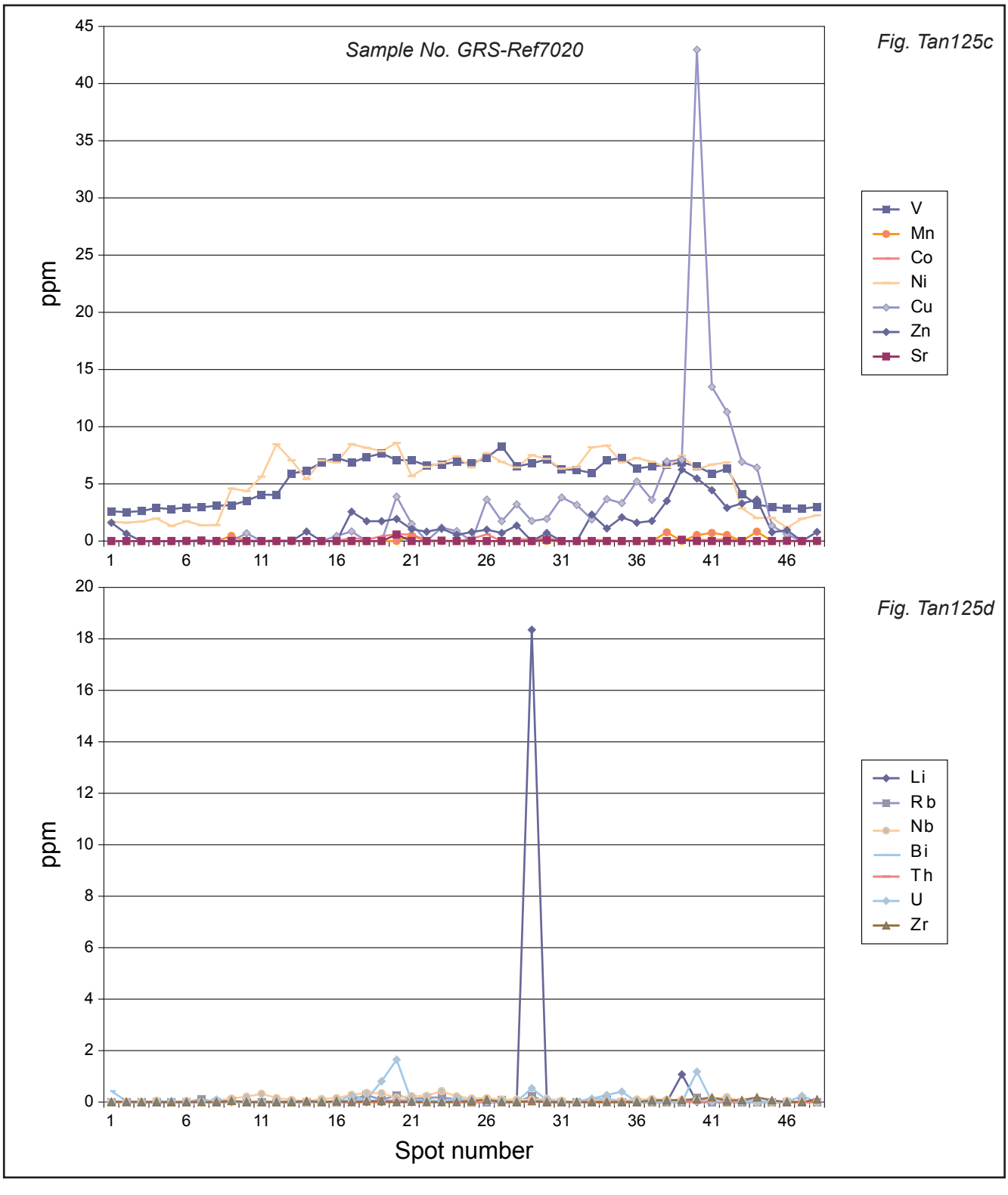

Fig. Tan125a, b, c, d A rough ruby sample with pinkish-red ruby core, triangular blackish-blue color zoning and milky rim as seen in fiber optic light (sample GRS-Ref Tan22). 48 Laser ablation craters represent the position of the analysis. The graphs show the concentrations of chemical elements in a profile across the ruby (in ppm) (Fig. Tan132a, b, c). The concentrations of the trace elements Mg, Ti, Fe, Cr, V and Ni are correlated with the color zoning. The ruby core is highest in Fe, Cr and Mg. The blue zone (point 10) is highest in concentrations of Fe, Ti and depleted in concentrations of Cr. Ni and V. The milky rim is characterized by lower concentrations of Fe, Cr and Mg, at high levels of Ti. Ni and V concentrations are highest in the ruby core. As expected, Ga concentrations are not correlated with the color zoning (Fig. Tan132a). Li and U concentrations are erratic and related to the presence of sub-microscopic particles or fluid inclusions in the ruby (Fig. Tan132a), which are not correlated with color zoning. Higher concentrations of Cu were found in the transition zone between the core and the milky rim. As they occur only on one side of the sample, these concentrations are also interpreted as the result of contaminations by micro-particles.

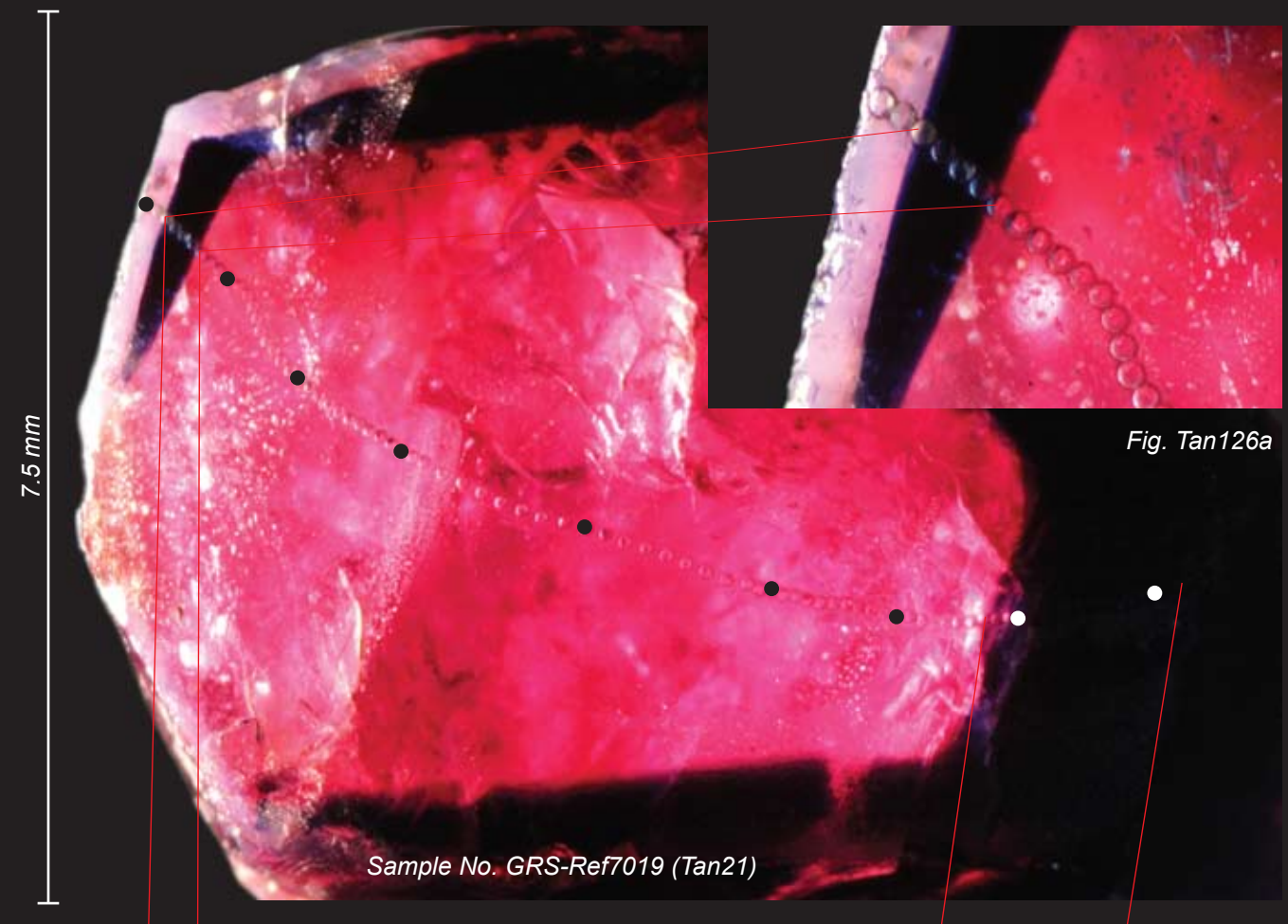

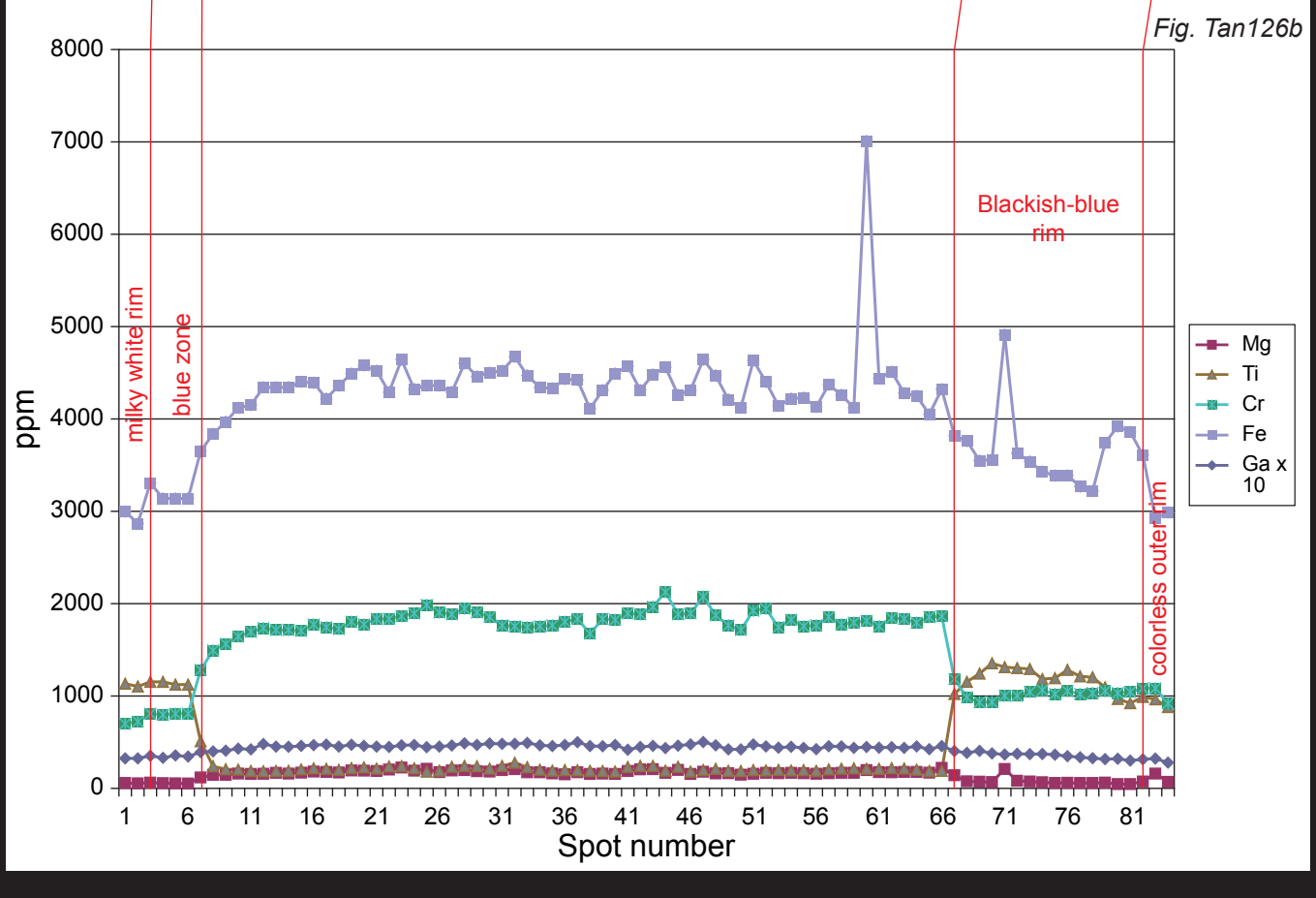

Fig. Tan126a shows a rough ruby sample with a ruby core of an intense blackish-blue colored sapphire rim and a narrow outermost colorless milky rim in a section perpendicular to the c-axis (fiber optic light illumination). 84 laser ablation craters represent a profile across this color zoning.

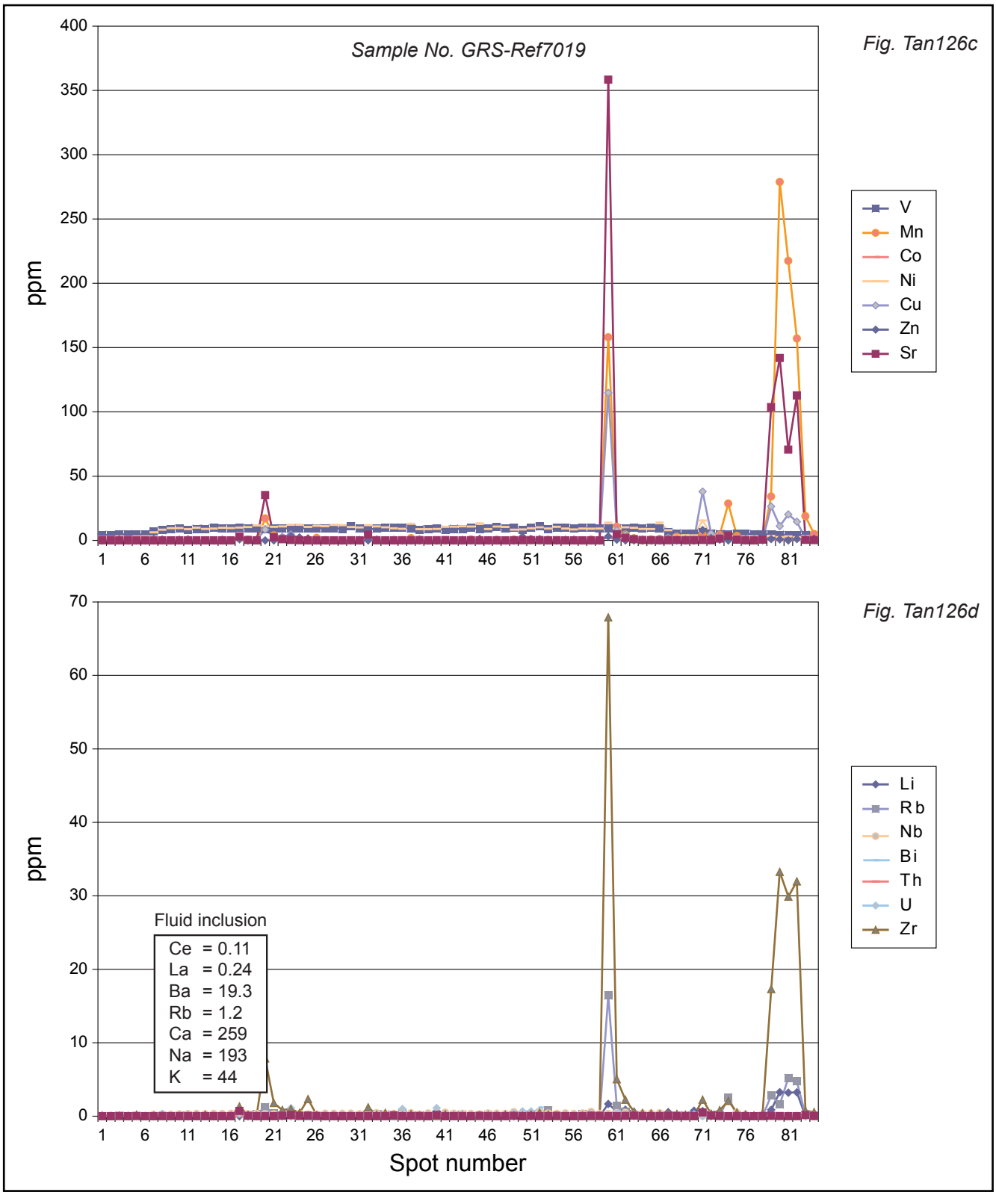

Fig. 126b, c, d Concentrations of other trace elements measured at the same positions are shown (see Fig. Tan126a). In a few isolated measuring positions, some element concentrations typically not found across the profile were detected above LOD (Pt.60 and 78-82, elements Sr, Mn, Cu, Zn, Zr, U and Li). Most of these element concentrations were found in the blackish to milky outer zone. They are interpreted as contamination by inclusions as they were only found on one side of the ruby crystal. An isolated increase of the trace element concentrations of Ce, La, Ba, Rb, Ca, Na, and K was found in the core of the ruby (Pt.60). The control in the microscope revealed that these elements were measured from an ablation crater that has partially ablated a fluid inclusion. These element contaminations are therefore attributed to the contents of a fluid inclusion, such as different salt minerals, other solid daughter minerals or liquids.

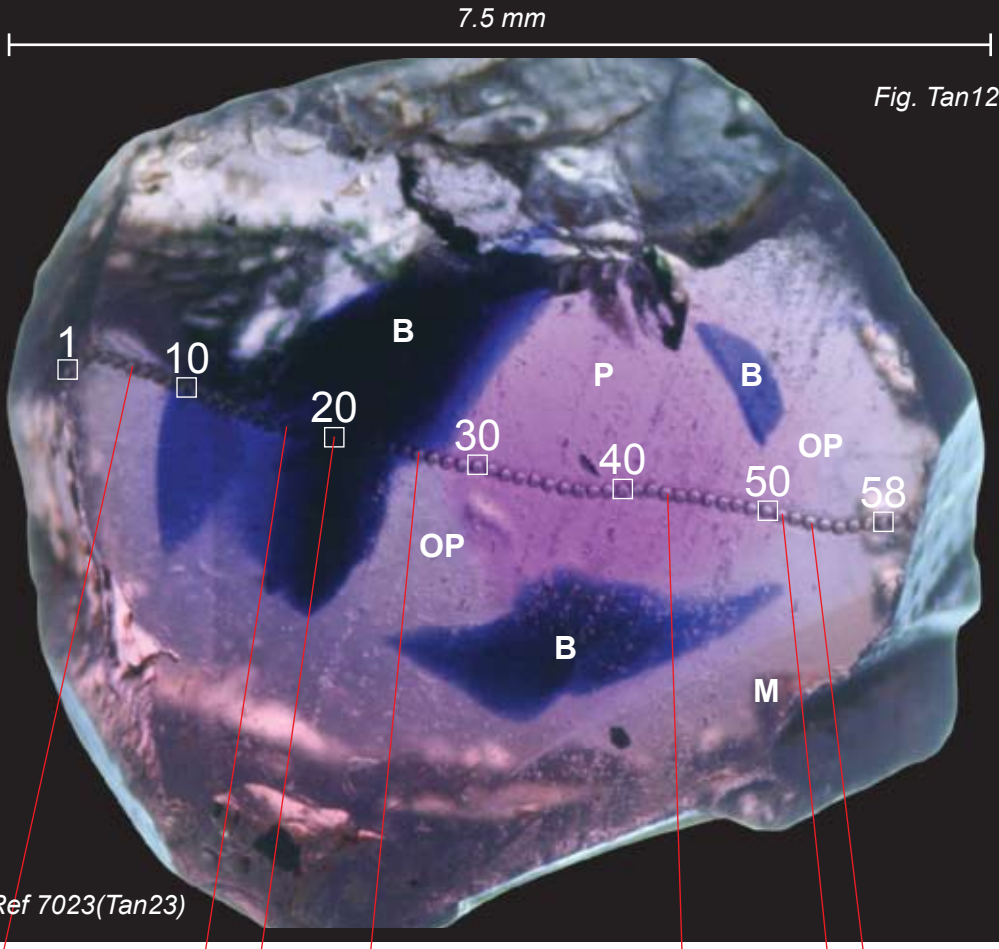

Sample No. GRS-Ref 7023(Tan23)

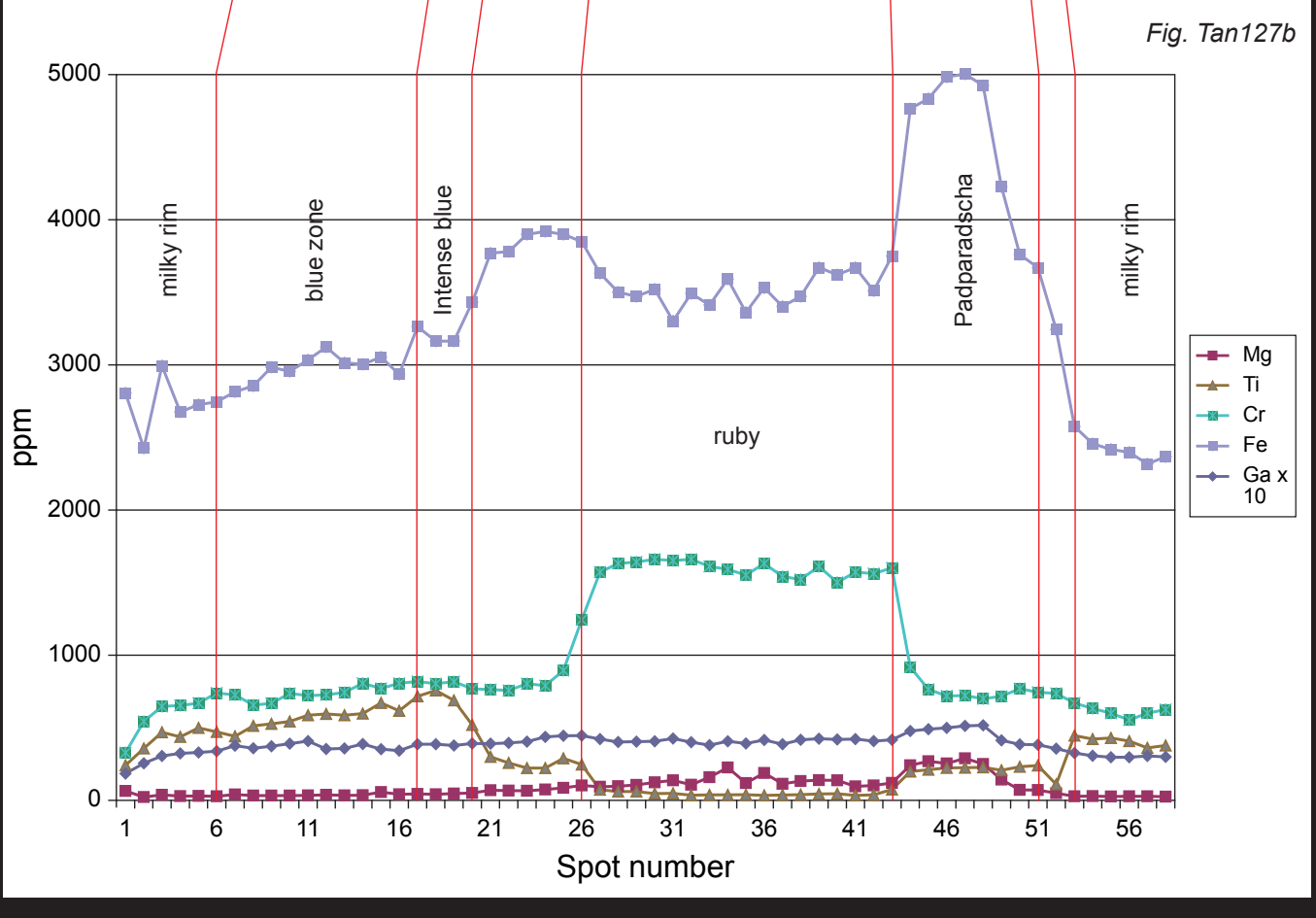

Fig. Tan127a Rough multi-colored "Winza" sapphire with a pink sapphire core (P), blue sapphire rim in 3 sectors (B), orangey-pink sapphire ("Padparadscha", OP) in 3 sectors and an outer milky-brownish rim (M). View in direction of the c-axis. A polished window was applied to the rough sample for analysis. A series of laser ablation craters mark the positions of the LA-ICP-MS analysis.

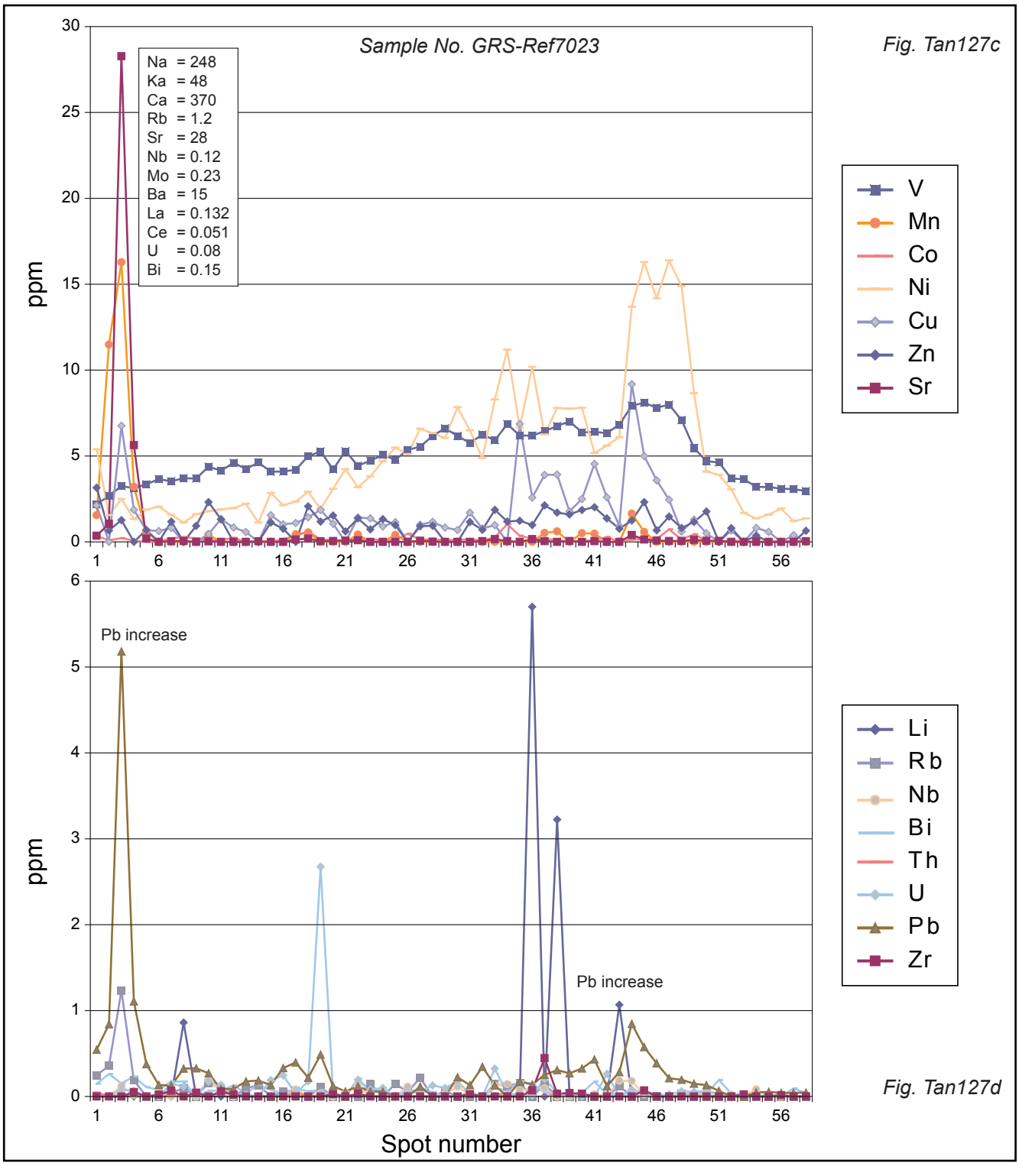

Fig. Tan127b (left page) *Concentrations of elements across a profile of a rough “Winza” sapphire with color zoning in sectors. The element concentrations of Mg, Ti, Cr and Fe are correlated with color zoning. Ga concentrations are not correlated with the pink and blue color zoning. A slight increase of element concentrations can be noticed in the “Padparadscha”-sector and a general decrease of element concentrations can be seen in the milky rim.*

Fig. Tan127c, d Additional elements are graphically shown in the same profile as Fig. Tan127b. Ni and V are highest in the “Padparadscha” growth sector. These elements are part of the chemical composition of the sapphire. Other element concentrations including Co, Cu and Zn are not correlated with the color zoning. Concentrations of Li, U and Pb occurred at some isolated positions and are not correlated to each other. These elements are interpreted as contaminations by micro-particles or fluid inclusions. An increase in these contaminations by inclusions occurred at the transition of the pink core to the rim and within the milky outer rim. Rare earth elements (La, Ce) and a series of other elements were detected in the milky zone. They are also interpreted as contaminations by inclusions. The inserted box in Fig. Tan134c includes further elements (in ppm) at an isolated measuring point.

7 mm

Fig. Tan128a

Sample No. GRS-Ref7533 (Tan24)

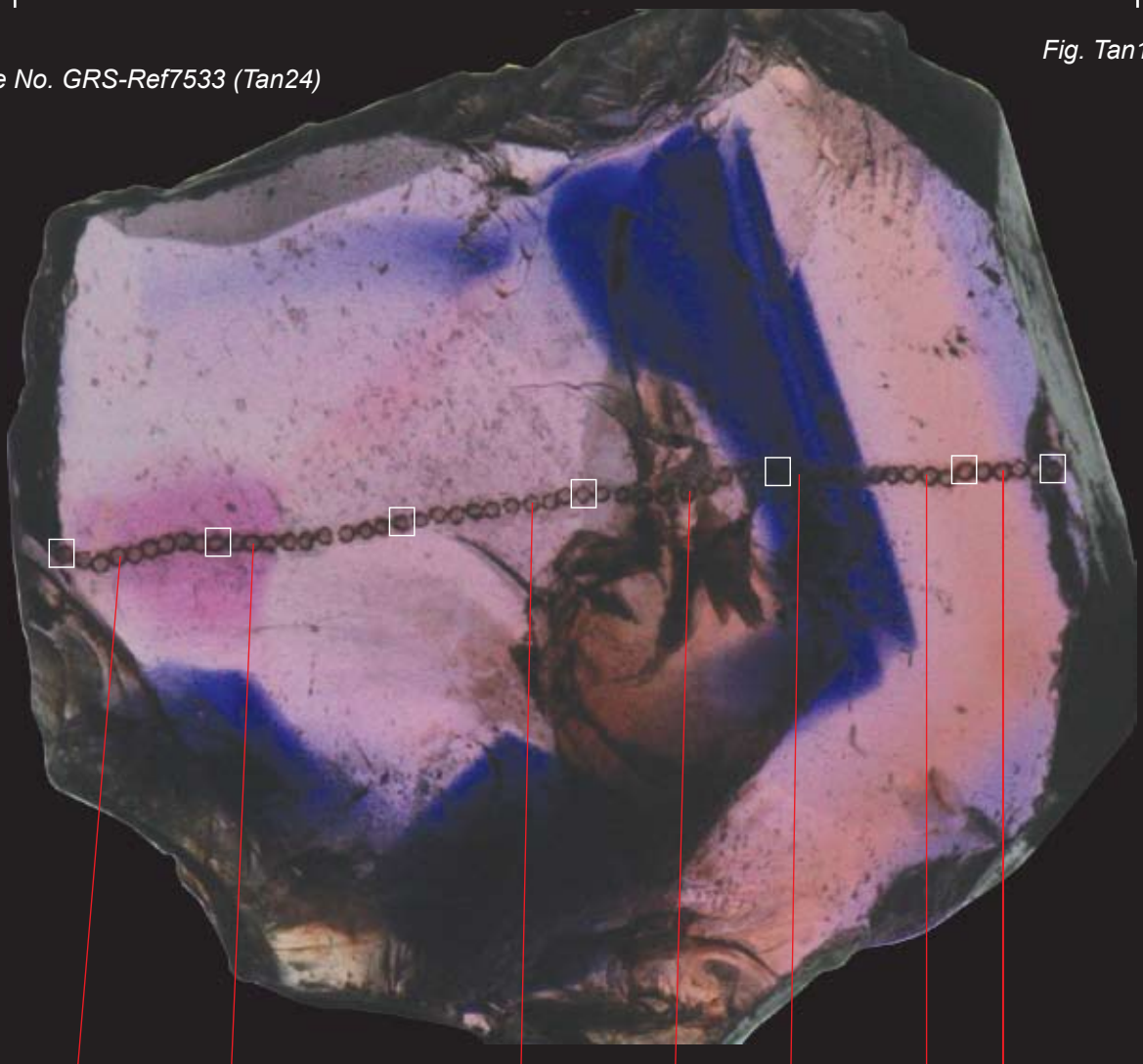

Fig. Tan128b

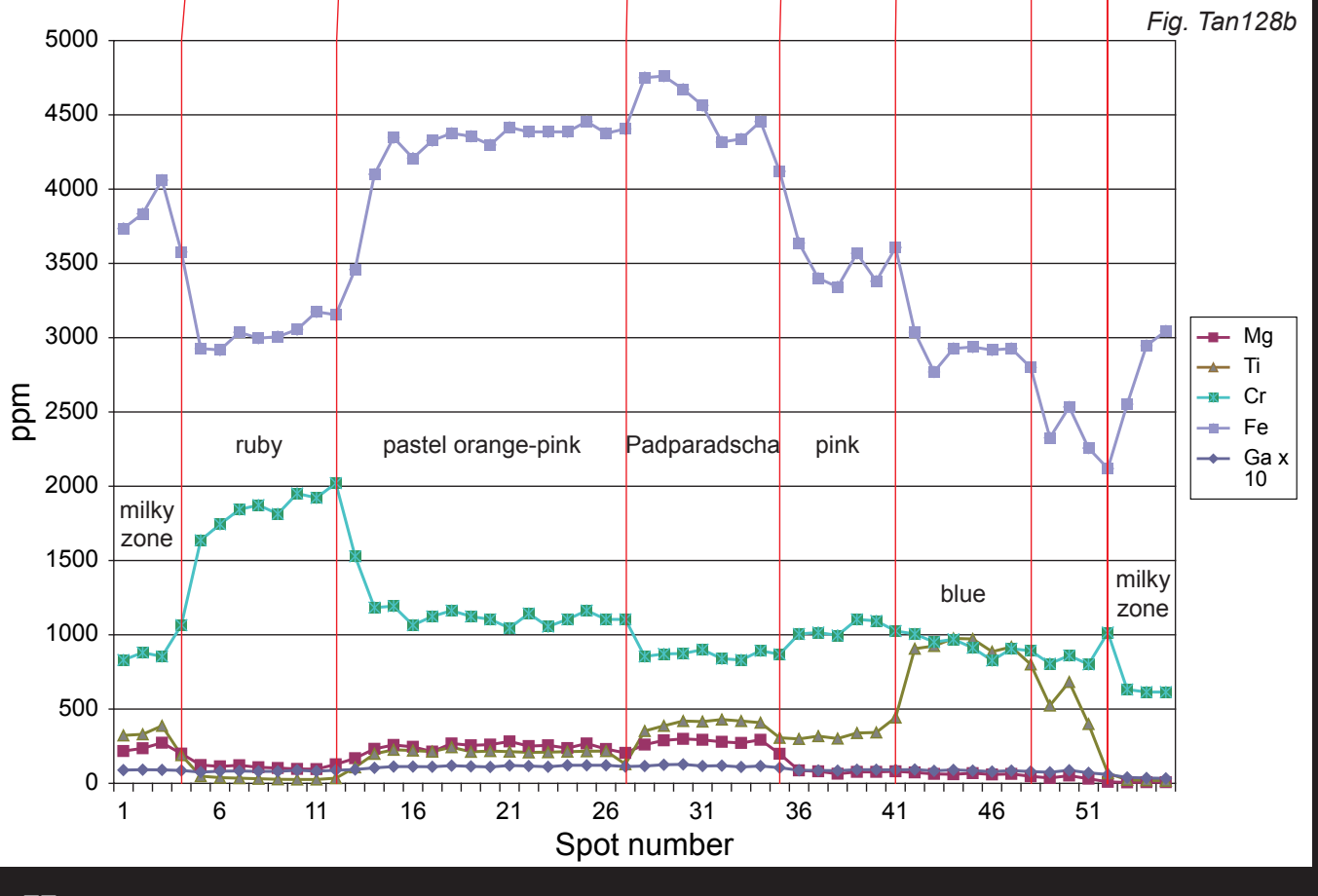

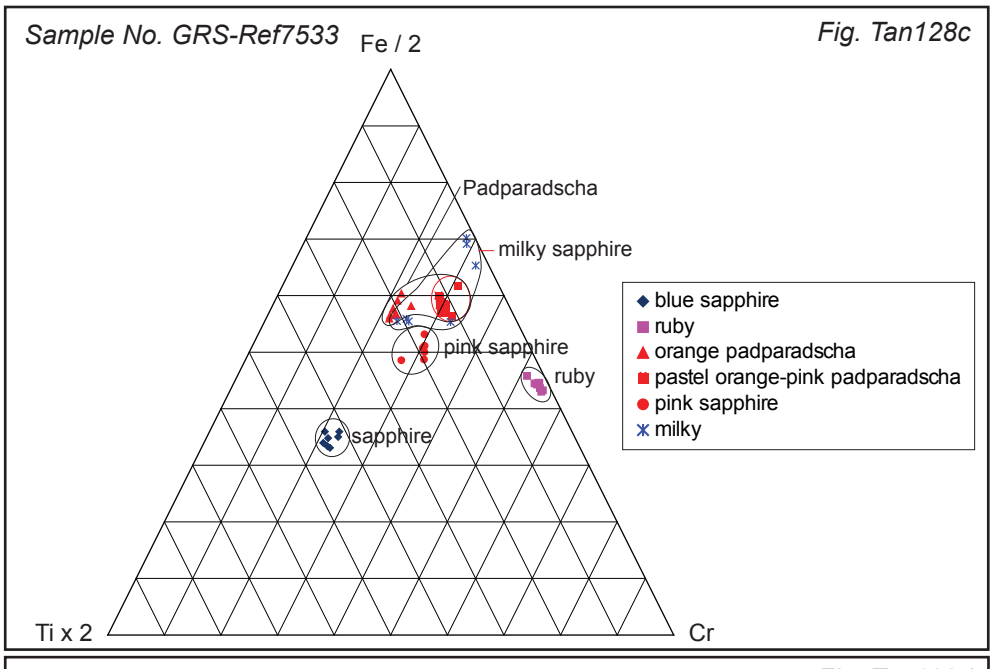

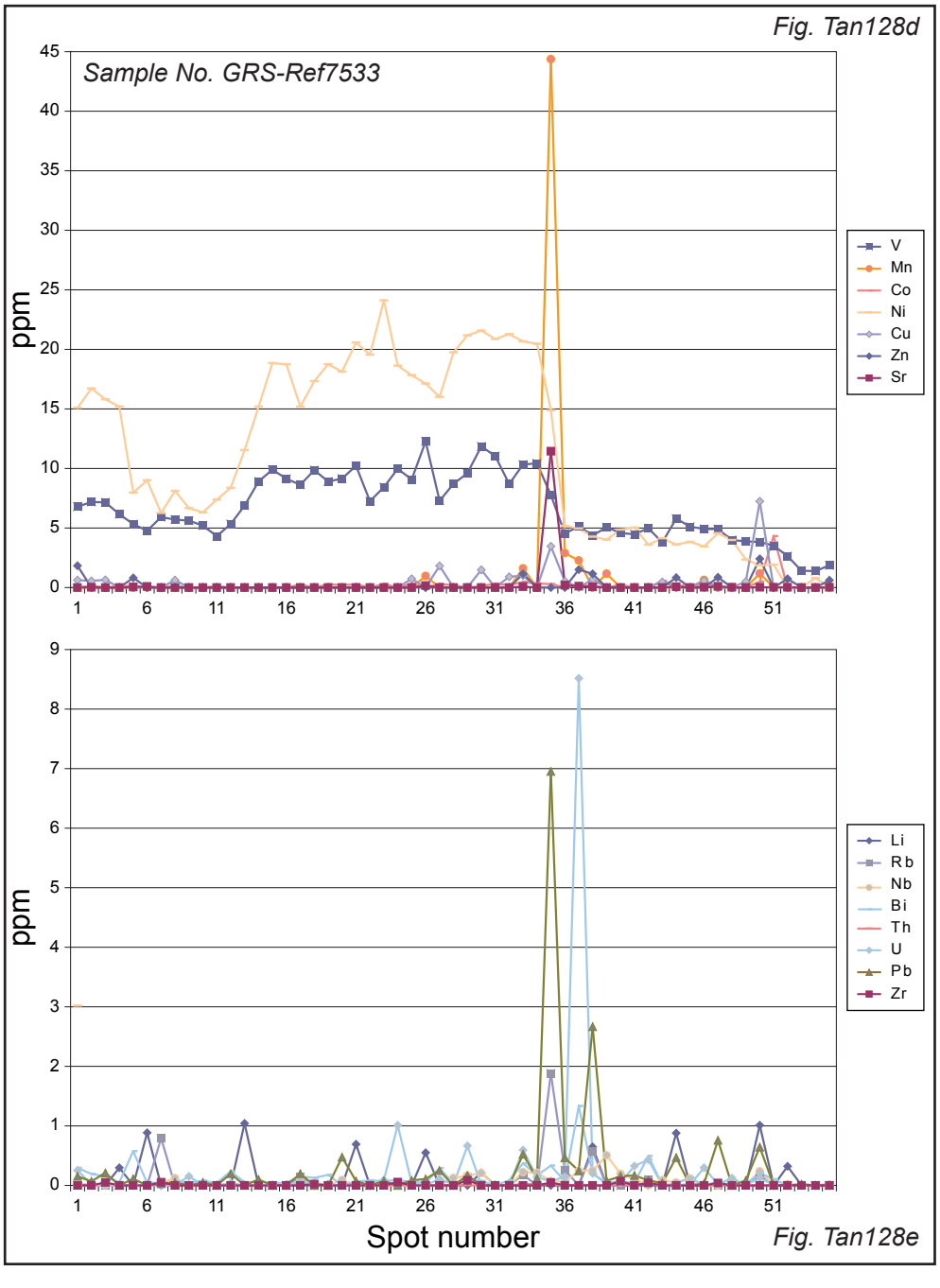

Fig. Tan 128a (page 77) Photograph of a multi-colored sapphire from Winza with color zoning. Note the small ruby core and the sector of "Padparadscha"- and blue sapphire zone. Laser ablation craters are visible and they have been correlated with the individual analyzed spots.

Fig. Tan128b (page 77) shows the element concentrations of Fe, Ti and Cr in correlation with the color zoning (e.g. see field of sapphire composition is found at intermediate Fe and high Ti and ruby composition at high Cr and Fe and low Ti). Triangular plot of the elements of different color zones are summarized in Fig. Tan128c

Fig. Tan128d shows the element concentrations Ni and V that correlate with the color zoning. Other trace elements concentrations are due to contamination with solid or fluid inclusions (e.g. Mn, Cu, Zn, Rb, Sr and Pb at point 35, and U at point 37, see Fig. Tan128d,e).

12.3 mm

Sample No. GRS-Ref7004 (Tan06)

Fig. Tan129a

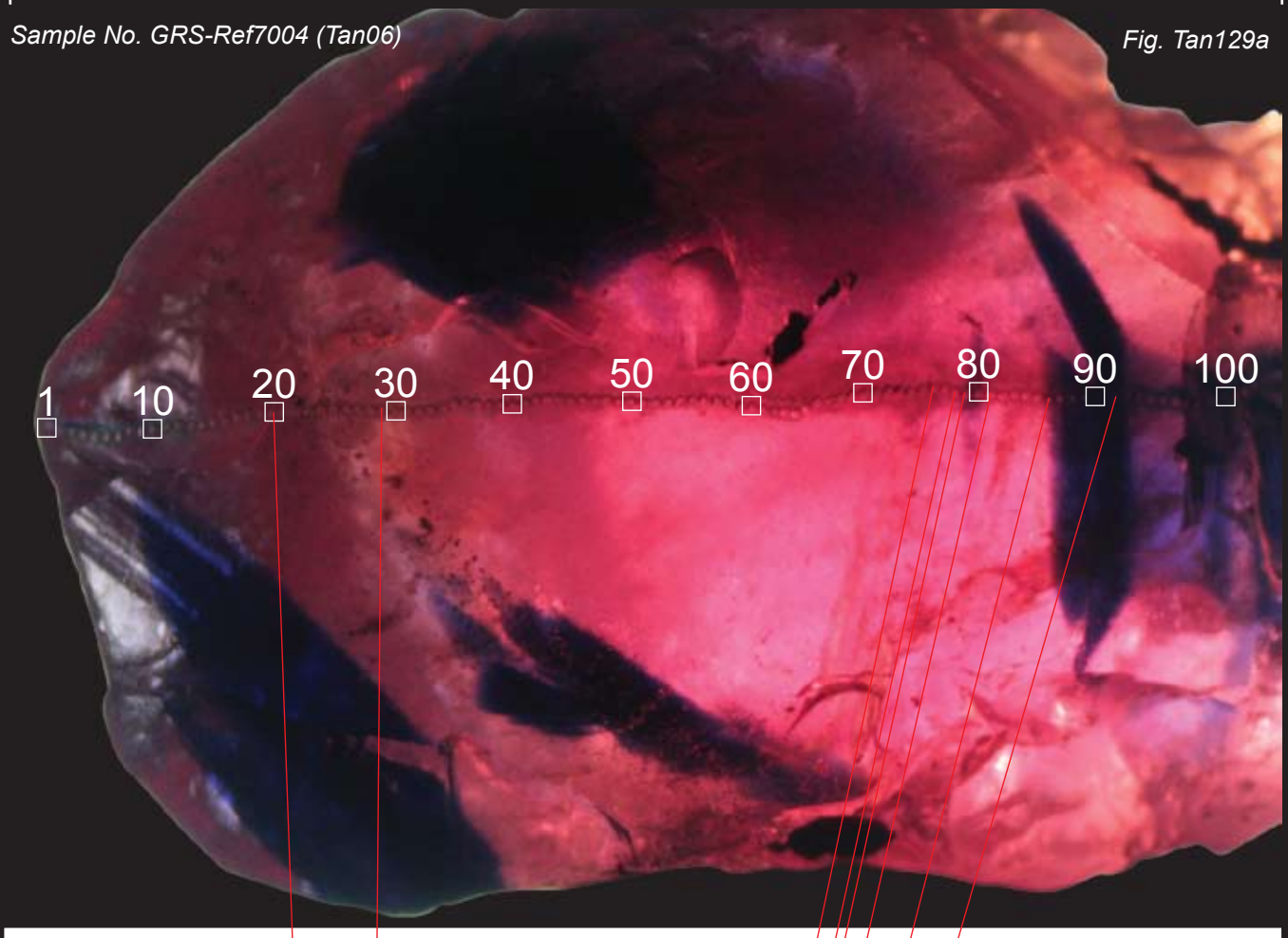

Fig. Tan129b

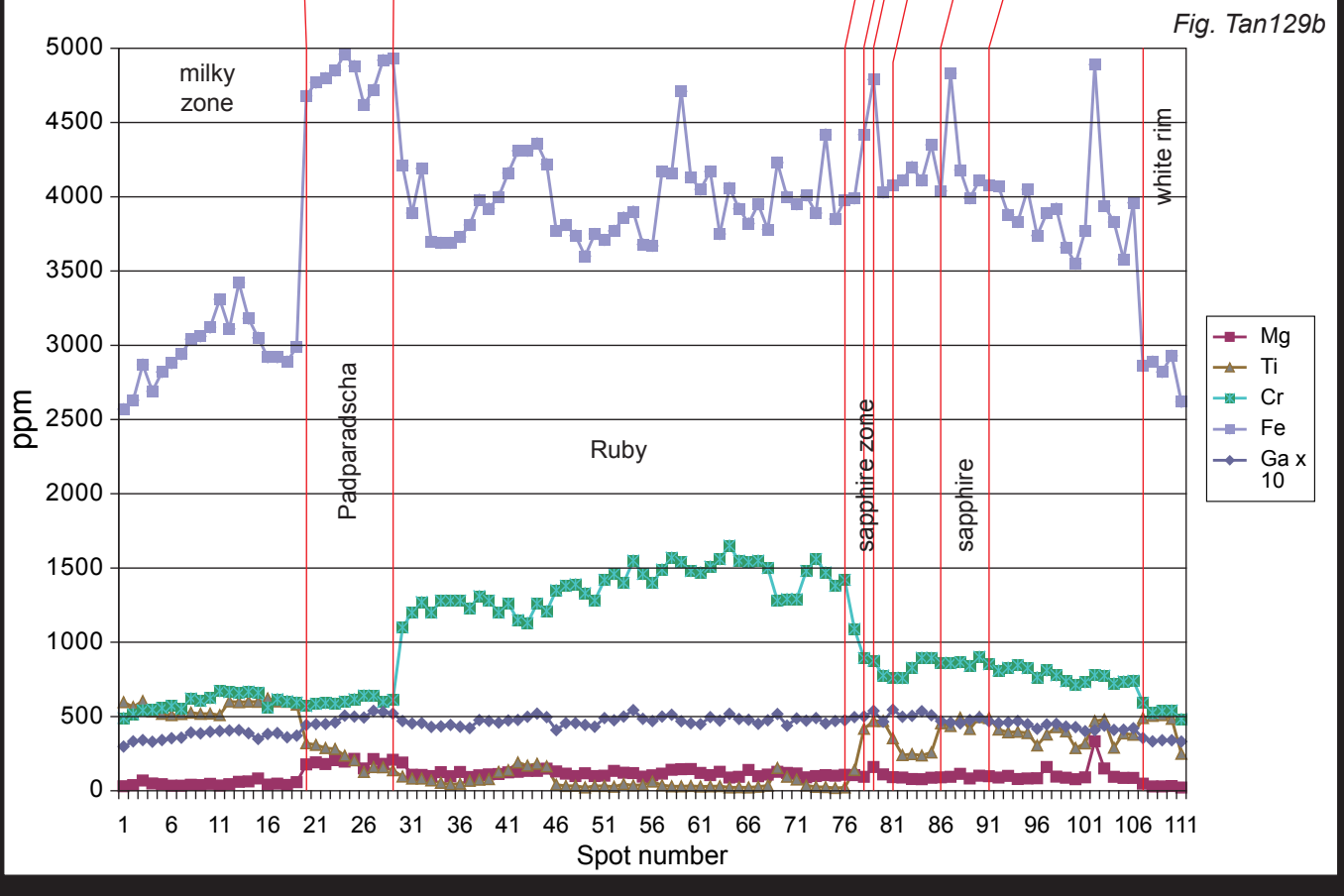

Fig. Tan129a Photograph of a multi-colored sapphire from Winza with color zoning. Note the occurrence of isolated triangular color sectors at the rim of the ruby (further detail see graph). The ruby contains submicroscopic particles and fluid inclusions. Laser ablation craters were correlated with the individual chemical analysis. Fig. Tan129b Trace elements Mg, Ti, Cr, Fe, Ti, V, Ni and Ga are incorporated in ruby and sapphire.

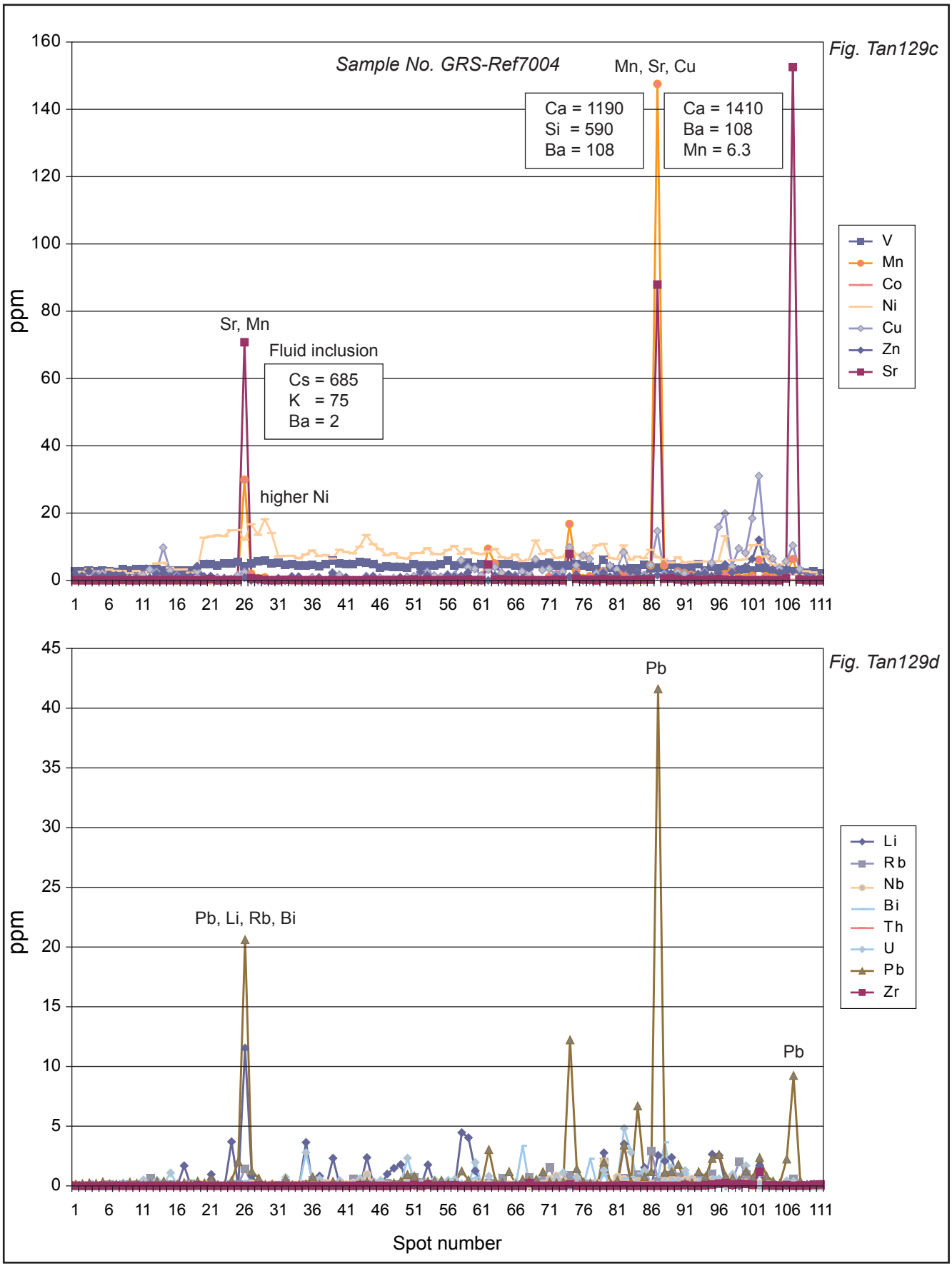

Fig. Tan 129c Trace elements Mg, Ti, Cr, Fe, Ti, V, Ni and Ga are incorporated in ruby and sapphire. The following elements were detected due to the ablation of fluid inclusions: Li, Rb, Sr, Mn, K, Ca, Ba, Pb and Bi without Si. Another contamination of unknown inclusions includes the Mn, Cu, Pb, Ba, Ca and Si concentrations. Inserted boxes give additional details on element concentrations at the 3 measuring points (in ppm). The contaminations are concentrated at the transition of the ruby core to the rim on both sides of the measured profile.

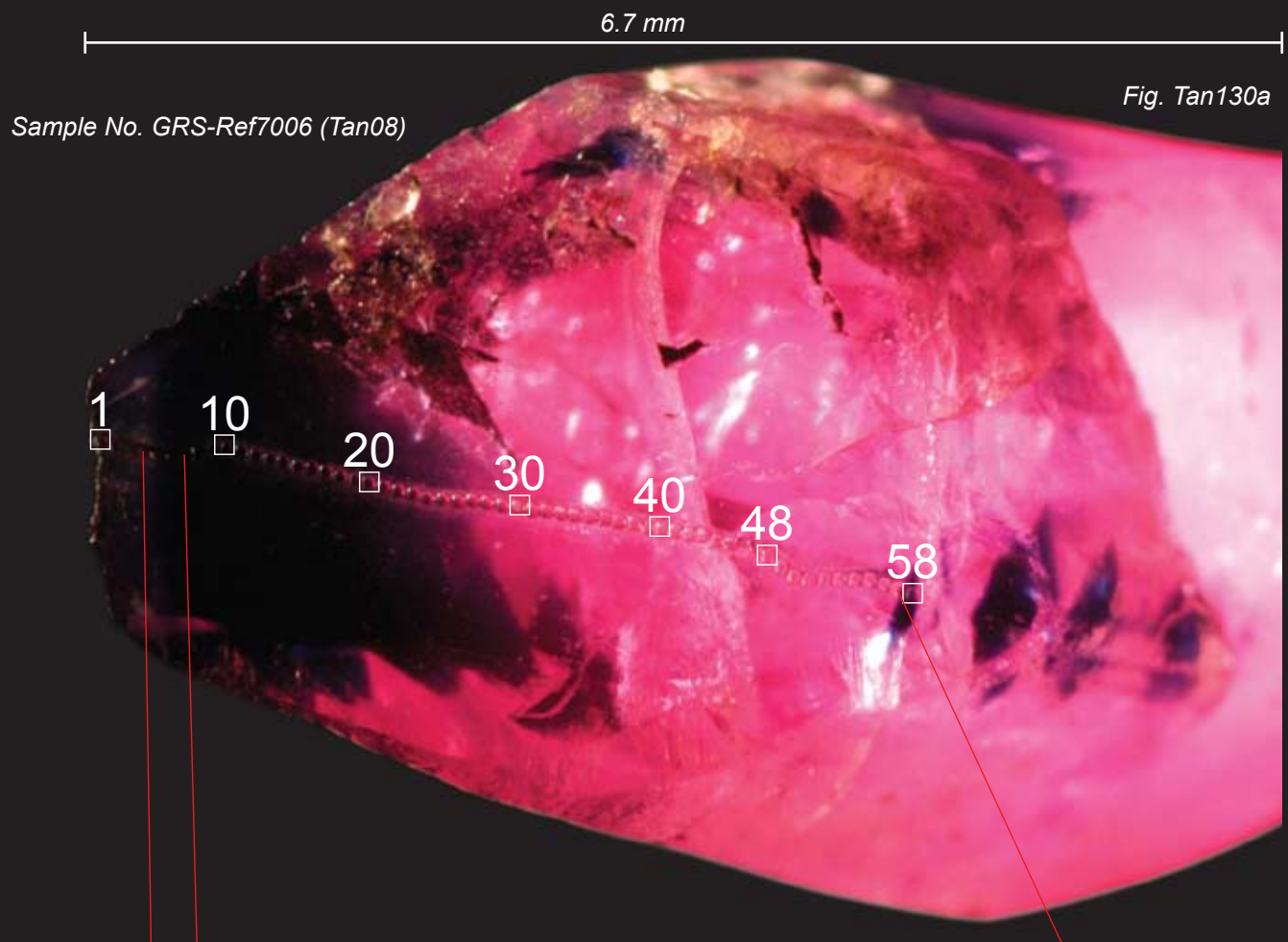
6.7 mm
Sample No. GRS-Ref7006 (Tan08)
Fig. Tan130a
1
10
20
30
40
48
58

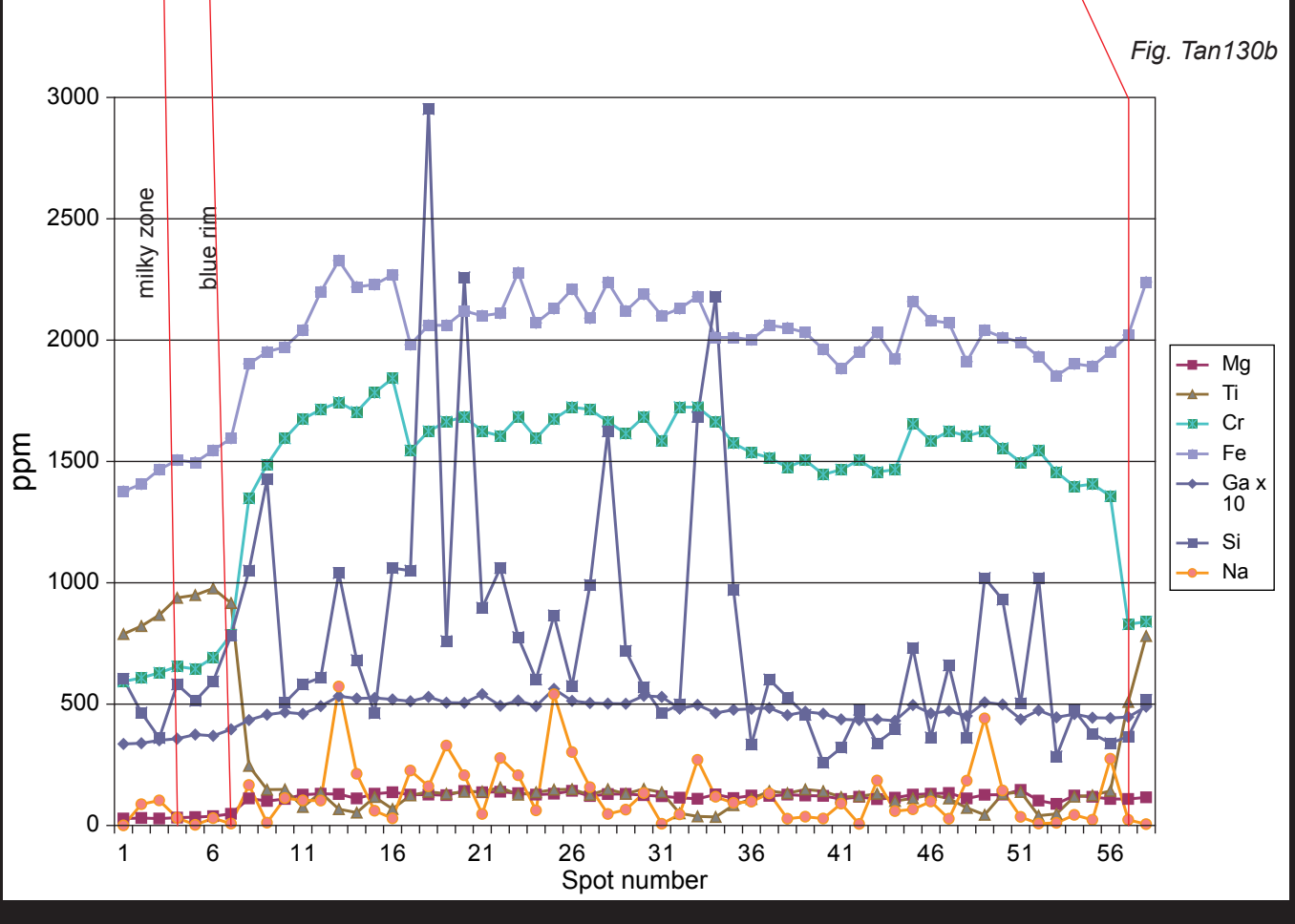
Fig. Tan130b
ppm
3000
2500
2000
1500
1000
500
0
milky zone
blue rim
1
6
11
16
21
26
31
36
41
46
51
56
Spot number
Mg
Ti
Cr
Fe
Ga x 10
Si
Na

Fig. Tan130c

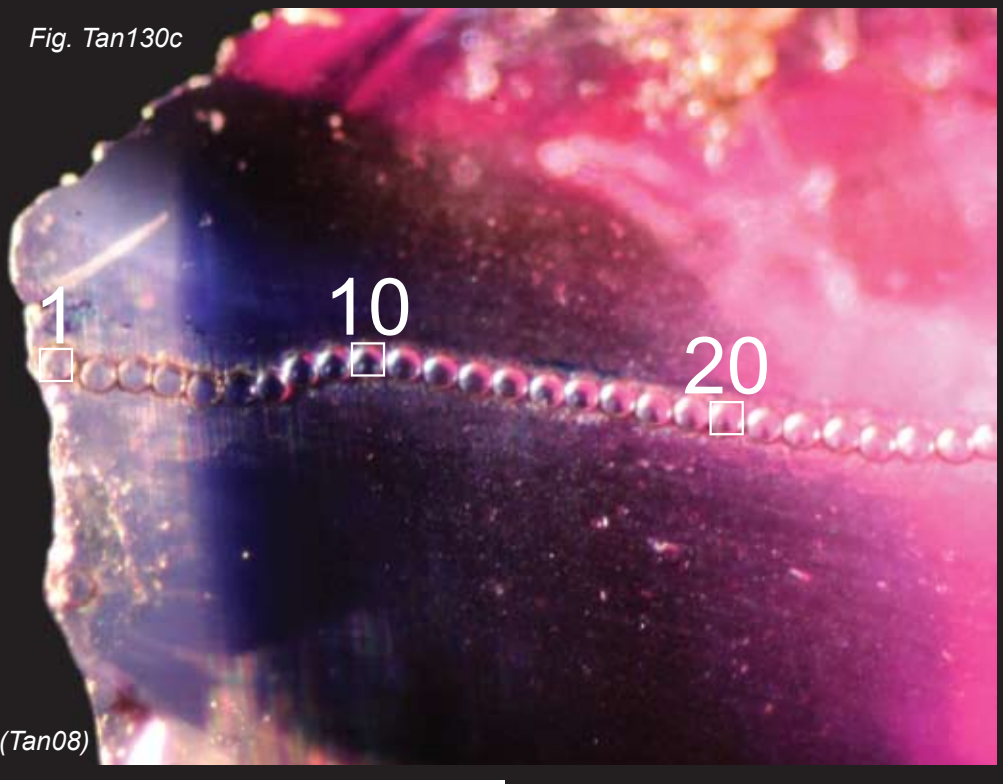

Sample No. GRS-Ref7006 (Tan08)

Sample No. GRS-Ref7006 Fig. Tan130d

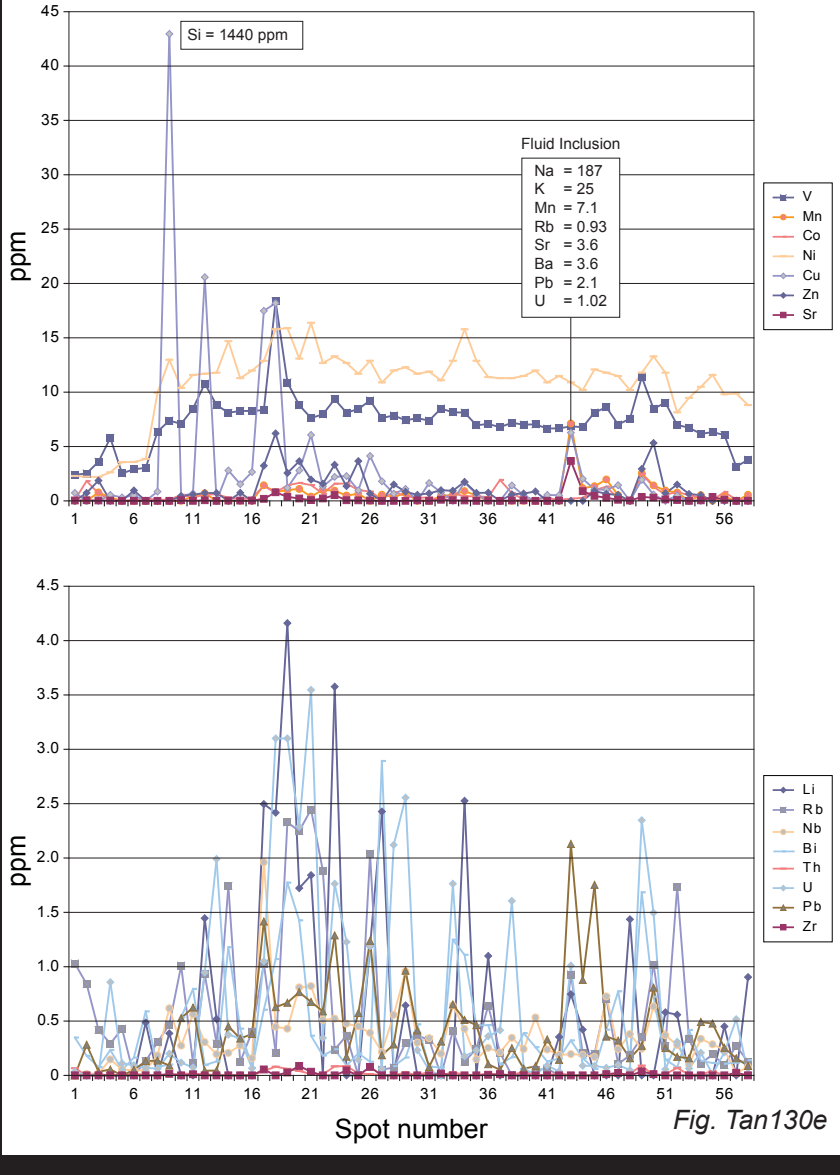

Fig. Tan130e

Fig. Tan130 Ruby rough crystal cut perpendicular in an angel of about 40 degrees to the c-axis. The internal color zoning is visible (Fig. Tan130a). Towards the rim of the crystal, the abundance of micro-particles is made visible by use of an oblique fiber optic illumination (Fig. Tan130b). The trace elements show the general distribution of Cr, Ti, Fe, V, Ni and Mg in relation to the color zoning as found in other sections (Fig. Tan130b). Note: Decreasing Ni-concentrations in the outer rim (Fig. Tan130d). Additional high concentrations of Si and Na are not correlated to this color zoning and are therefore, related to mineral or fluid inclusion contaminations. As can be seen in the microscope, the numbers of particles increases towards the left of the profile (Fig. Tan130c). This correlates well with increasing concentrations of the elements Li, Ca, Na, Rb, Sr, Cu, Zn, Nb, Pb, Bi, U and Th (Fig. Tan 130e).

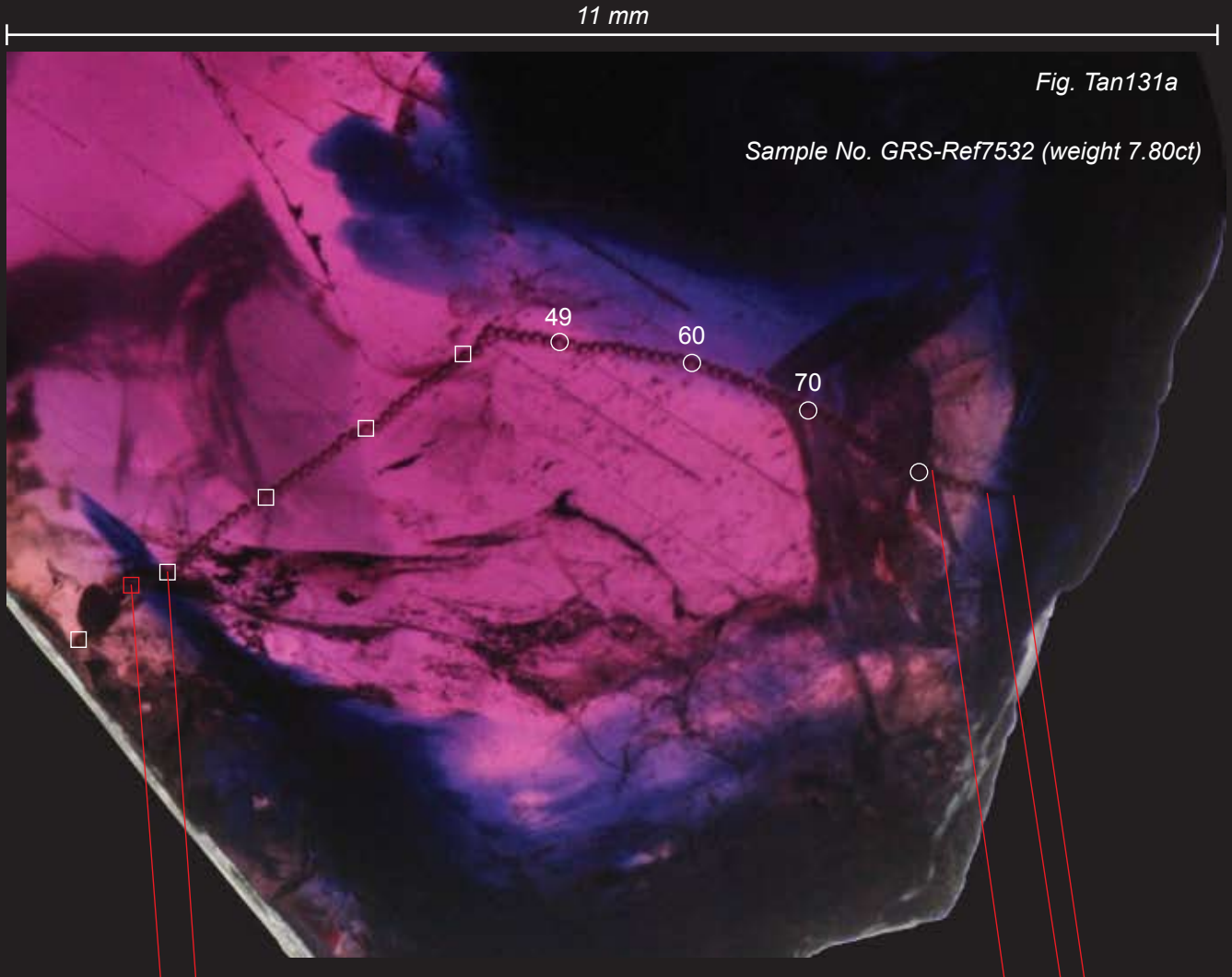
11 mm
Fig. Tan131a
Sample No. GRS-Ref7532 (weight 7.80ct)
49
60
70

Fig. Tan131b

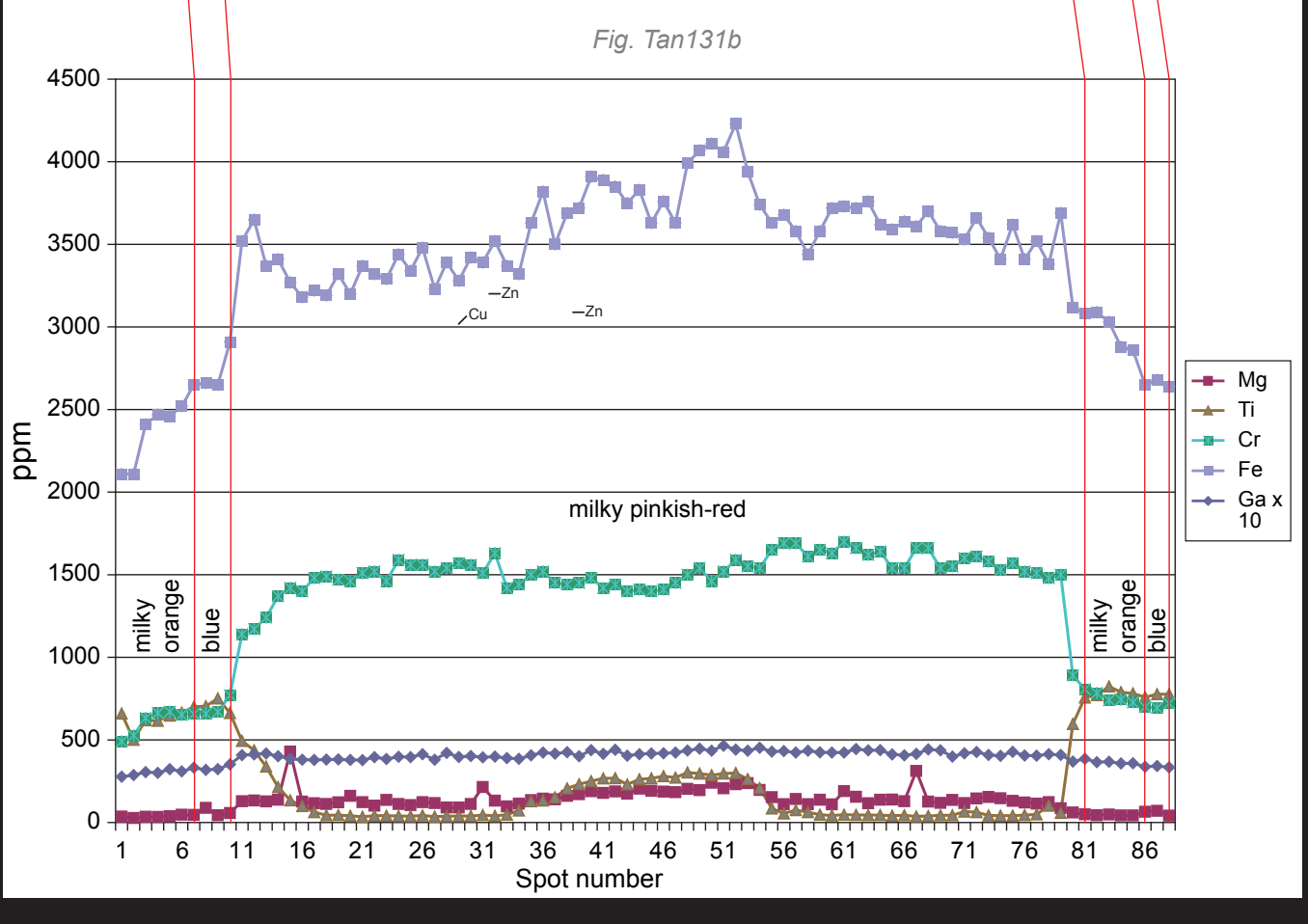
ppm
4500
4000
3500
3000
2500
2000
1500
1000
500
0
Zn
Cu
Zn
milky pinkish-red
milky
orange
blue
milky
orange
blue
Mg
Ti
Cr
Fe
Ga x 10
1
6
11
16
21
26
31
36
41
46
51
56
61
66
71
76
81
86
Spot number

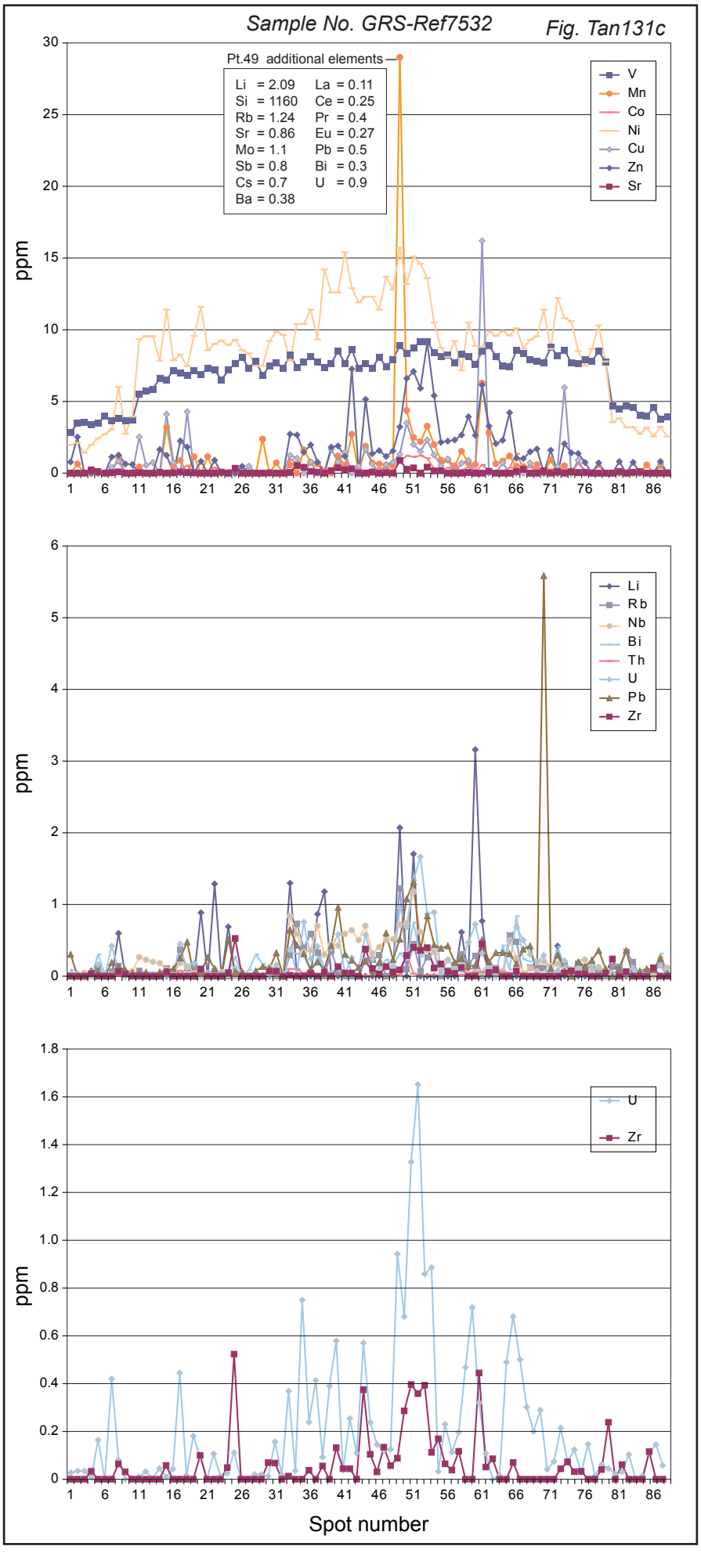

Fig. Tan131a, b, c, d
Microphotograph of a rough ruby. One window was polished perpendicular to the c-axis. A color zoning is seen with a red core and blue outer rim. The sample contains numerous pinpoint particles. The craters of the LA-ICP-MS analysis are visible (Fig. Fan131a) and the measured concentrations of the elements are shown in a graph below (Fig. Fan131b). Additional element concentrations (in ppm) are inserted in a box (Fig. Tan131c, spot No. 49). The general trend in the trace elements Mg, Ti, V, Cr, Fe and Ni correlates well with the color zoning. Other element concentrations such as Mn, Cu, Zn, Li, U, Pb, Nb, Zr and REE (La, Ce, Pr, Eu) are attributed to contamination by the solid and fluid inclusions.
(Fig. Tan131c, d, e)

Fig. Tan131d

Fig. Tan131e

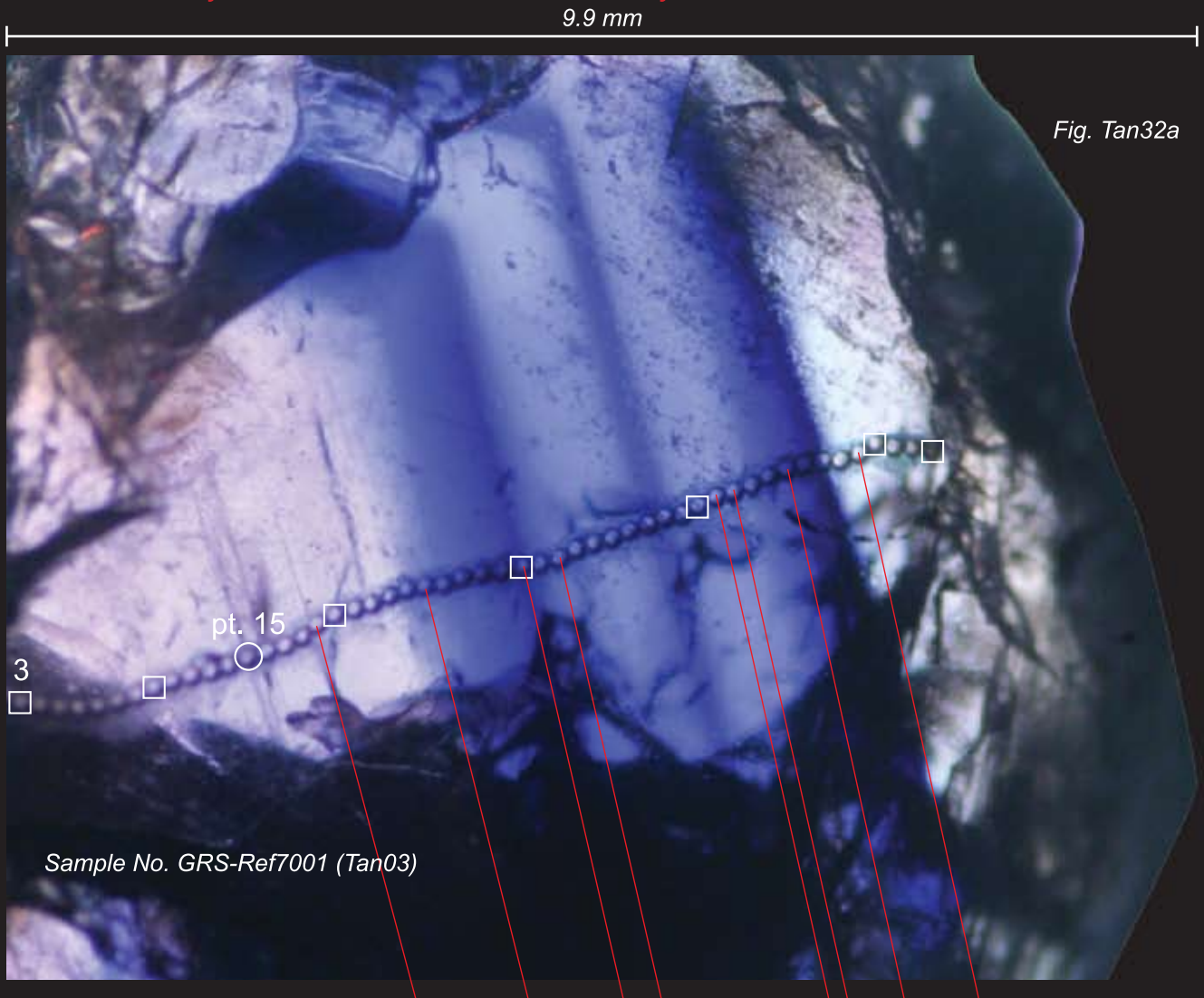
9.9 mm
Fig. Tan32a
pt. 15
3
Sample No. GRS-Ref7001 (Tan03)

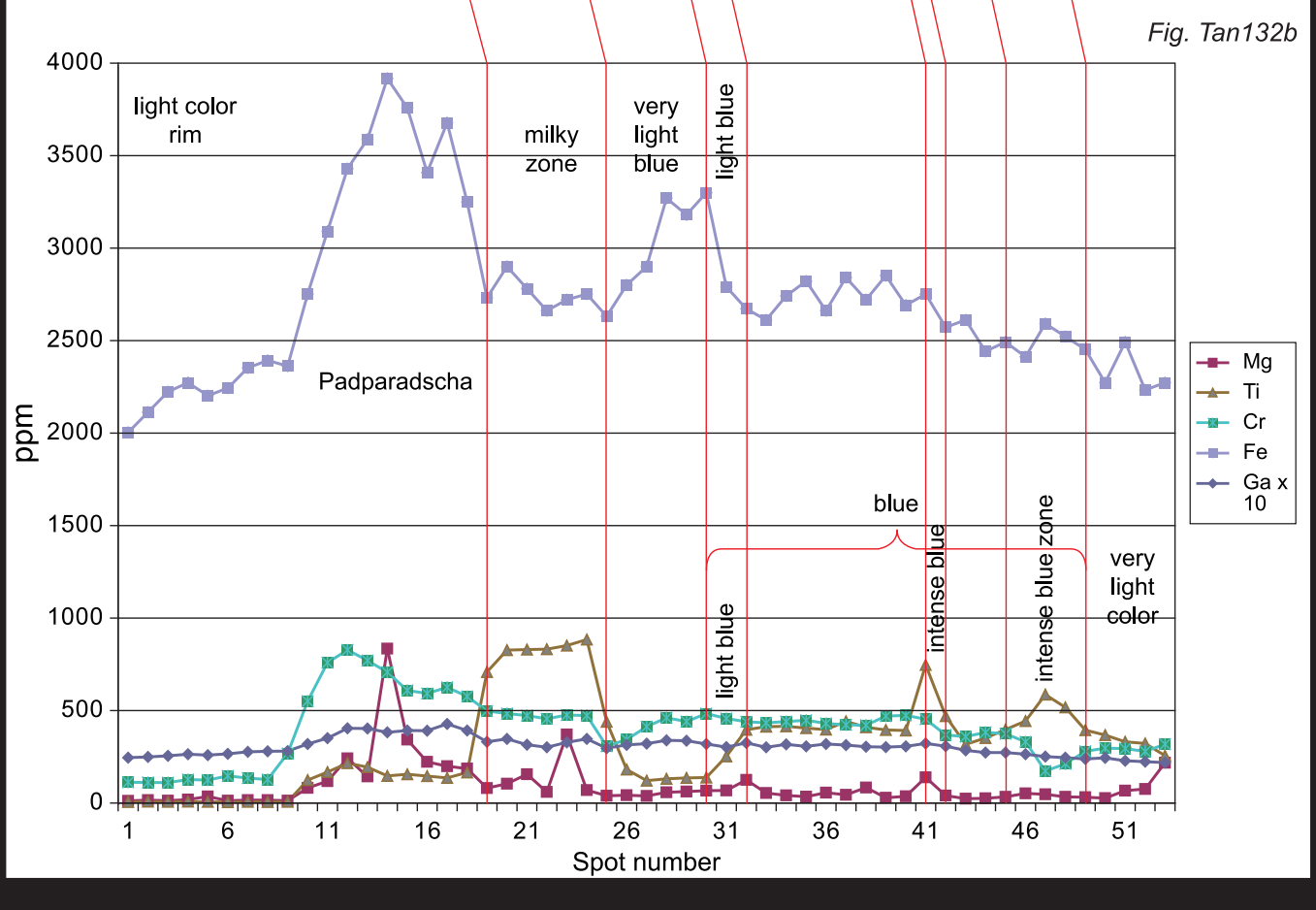
Fig. Tan132b
light color rim
milky zone
very light blue
light blue
Padparadscha
blue
light blue
intense blue
intense blue zone
very light color
ppm
Spot number
Mg
Ti
Cr
Fe
Ga x 10

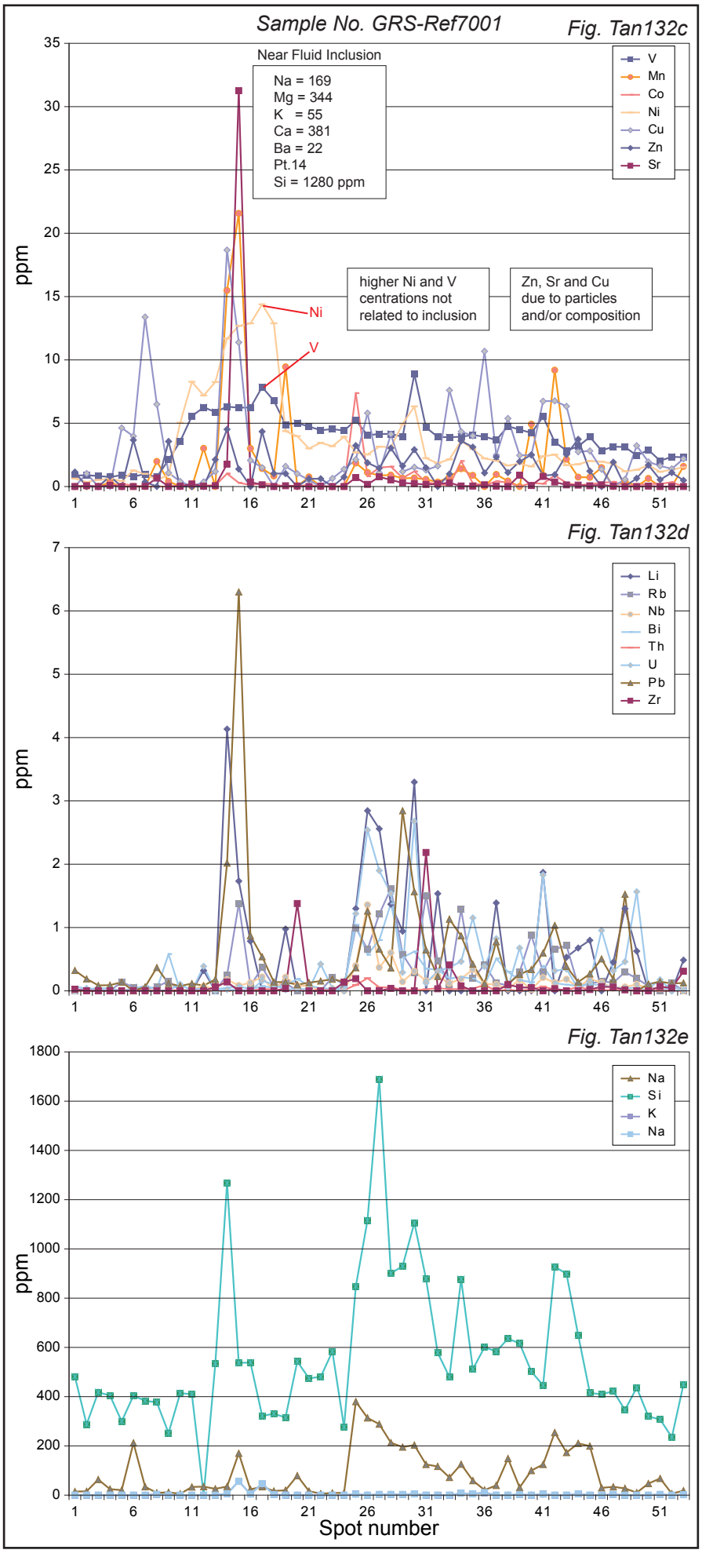

Fig. Tan132 A rough ruby has been cut perpendicular to the x-axis. The left side of the crystal represents the core and the right side the rim of the original crystal. A complicated color zoning is visible. The measured points are positioned on the transition of a “Padparadscha”-sector to the oscillating blue color zoning (see LA-ICP-MS craters, Fig. Tan132a). The Padparadscha”-sector is characterized by high Fe, Mg, Ni, and V, intermediate Cr and low Ti (Fig. Tan132b). The oscillation of blue sectors is correlated with variations in Ti-concentrations at high Fe-concentrations. The Cr-concentration decreased in a strong blue color band (pt. 47, Fig. Tan132b). With the appearance of a blue zone (from left to right), a sudden increase of the contamination by Li, Rb, Sr, Cu, Zn, Mn, Nb, U, Th and Pb occurs (Fig. Tan132c,d). These trace element concentrations in this part of the crystal are found in areas with numerous particles. The contaminations are correlated with an increase of Si, Na and K (Fig. Tan132e) and are interpreted as micro-particles of silicates.

BOX TAN05: HOW IS A POSITIVE EU ANOMALY FORMED BY MAGMATISM

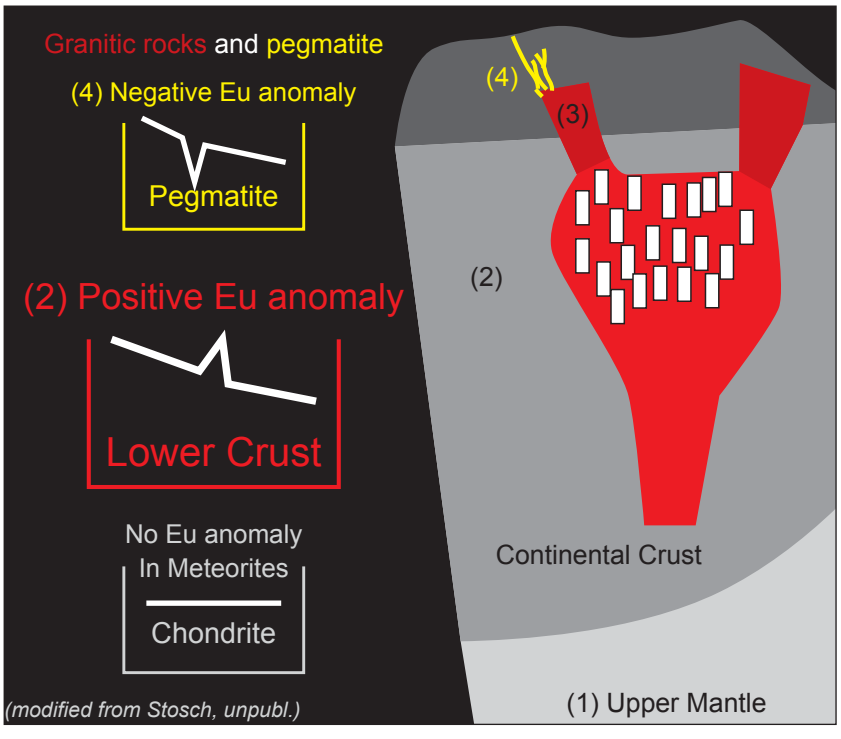

SIMPLIFIED MODEL FOR THE EXPLANATION OF EU-ANOMALIES IN THE CONTINENTAL CRUST

1. REE-bearing rock forms magma (no Eu anomaly)

2. Accumulation of plagioclase and formation of anorthosite (positive Eu anomaly in rock)

3. Removal of remaining magma to higher levels of the Earth's crust. Pegmatite derived from anorthosite is depleted in plagioclase (negative Eu anomaly)

4. Further crystallization of minerals in the pegmatite distributes the remaining REE preferable into some minerals containing Ca^{2+}.

REE CONCENTRATIONS IN MINERAL INCLUSIONS

REE concentrations are useful for the reconstruction of the origin of rocks (See Box Tan05 and Lit Tan 27. It was possible to detect REE concentrations in pargasite, garnet and apatite inclusions (Tab. Tan01 and Fig. Tan133). It can be seen in Fig. Tan133, that a positive Europium (Eu)-anomaly was present in both garnets as well as pargasite. This positive Eu anomaly, however, was not present in apatite and a negative Cerium (Ce) anomaly was present.

ED-XRF CHEMICAL ANALYSES OF RUBIES

Rubies of different origins have been measured by ED-XRF. As it shown in Fig. Tan134, it is possible to distinguish Winza rubies from rubies of various other origins on the basis of Cr, Fe and Ga-concentrations.

LIBS TESTING

LIBS testing of rubies and blue zones in rubies from Tanzania showed no concentrations of beryllium. Magnesium concentrations are similar those in sapphires from Sri Lanka and Madagascar.

The magnesium concentration in rubies (specially in blue zones) is generally higher than those of basaltic origin.

HEAT-TREATMENT OF WINZA RUBIES AND FTIR ANALYSIS

A series of Winza rubies have been experimentally heat-treated in Chantaburi and Bangkok (see Lit Tan07). These samples have been subjected to commercial heat-treatment normally used for Burmese rubies (high temperature treatment) and Mong Hsu rubies (so-called "warming" in the trade, used for removal of blue color zones). Heat-treatment created intense orange zones in the Winza rubies and also reduced transparency of the stones. Therefore, the conventional heat-treatment techniques used in the trade for other ruby types could not be applied for Winza rubies. However, that may change in the future. A series of FTIR analyses have been made of rubies before and after heat-treatment. This enabled us to establish a test for detection of heat-treatment of Winza rubies. As it shown in Fig Tan.135, we were able to distinguish heat-treated from unheated rubies based on FTIR-analysis. The FTIR-spectra of unheated Winza rubies can also be used to distinguish them from their synthetic and natural counterparts (e.g. Lit Tan30, 32, 36).

UV-VIS-NIR ANALYSES

The Winza rubies have absorption spectra typical for iron-rich rubies that have been formed in volcanic rocks, such as Siamese rubies. UV-VIS spectroscopy can be used to distinguish Winza rubies from natural and synthethic counterparts (see Fig. Tan136 and compare with Lit Tan26)

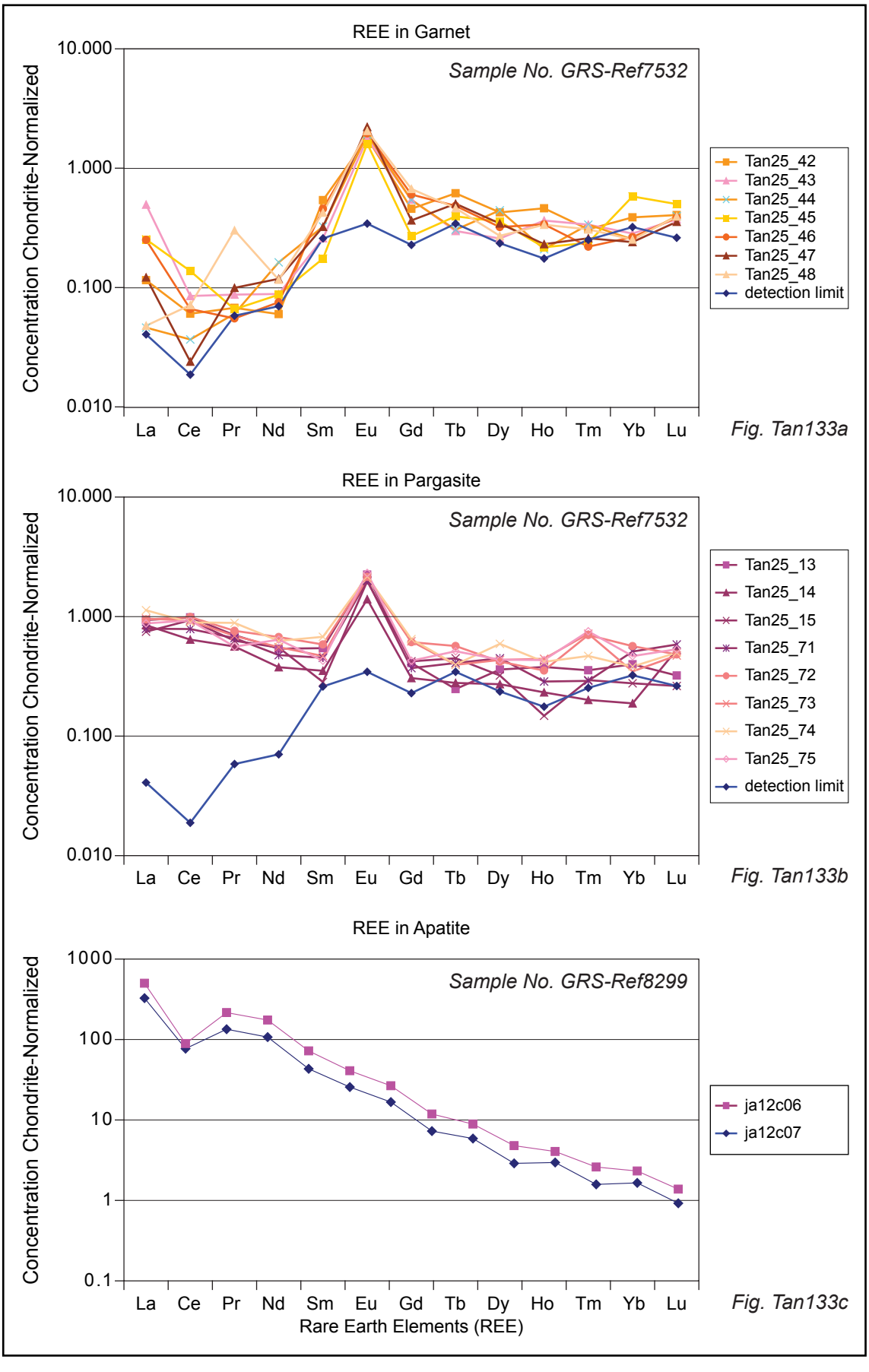

Fig Tan133a, b, c Normalized rare earth elements (REE) concentrations in pargasite, garnet and apatite. Pargasite and garnet were present as inclusions in the same ruby from "Winza" (Tanzania) whereas the apatite inclusion was found in another sample from a different outcrop. Note the positive Europium (Eu) anomaly in pargasite and garnet and the negative Cerium (Ce) anomaly in apatite. The curve for detection limits is included (other element concentrations see Tab. Tan01).

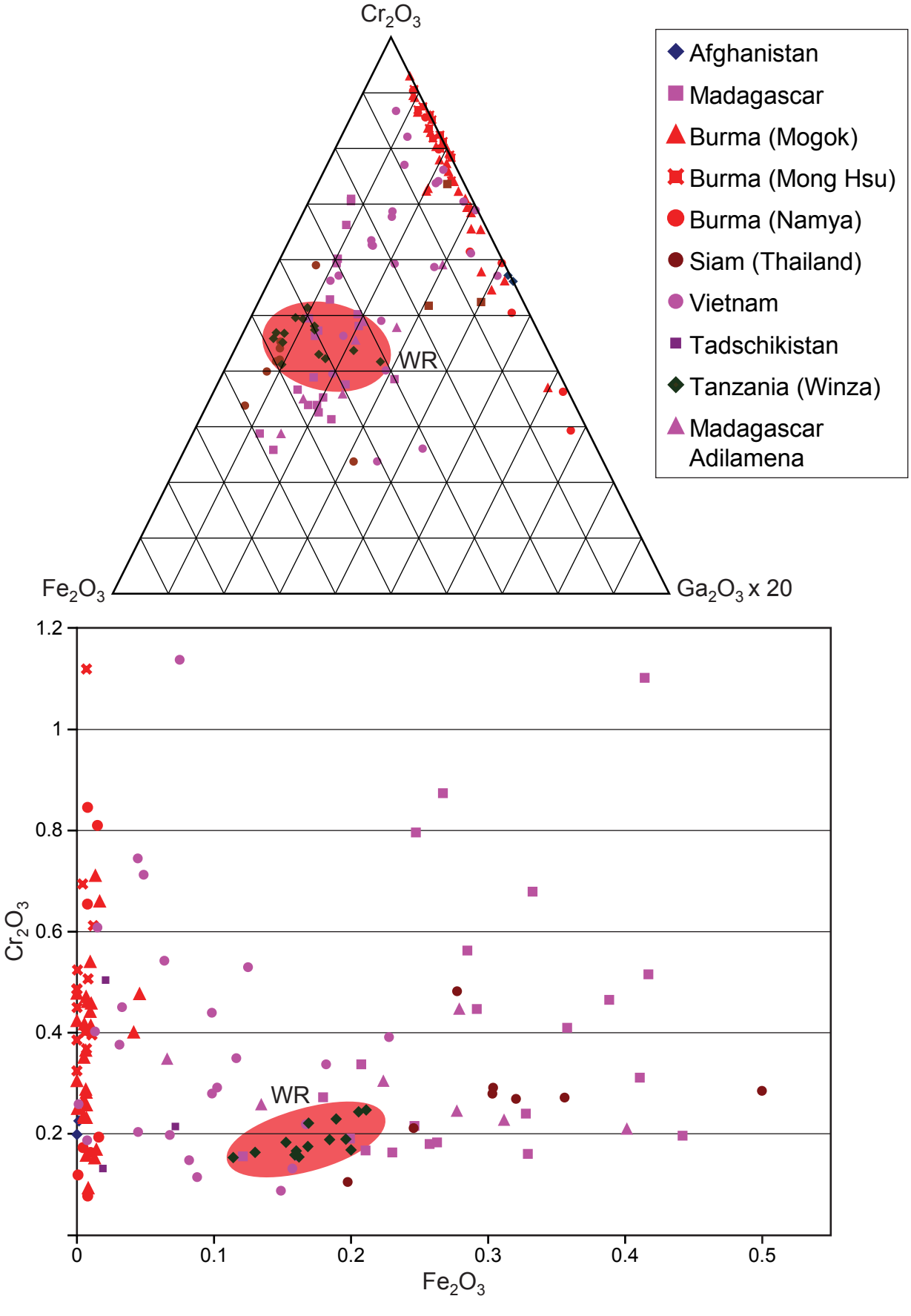

Fig. Tan134 Chemical compositions in wt% of “Winza” rubies (WR) in comparison to rubies from other origins. The field of Tanzania rubies is highlighted. Note equal iron and chromium concentrations are typical for the new Tanzania rubies. The Cr/Fe-ratio may vary slightly and result in different color varieties. Winza rubies can be distinguished easily from rubies of other origins, including Burma, Vietnam and Tajikistan. Sample from the GRS collection. Methods see Lit Tan26.

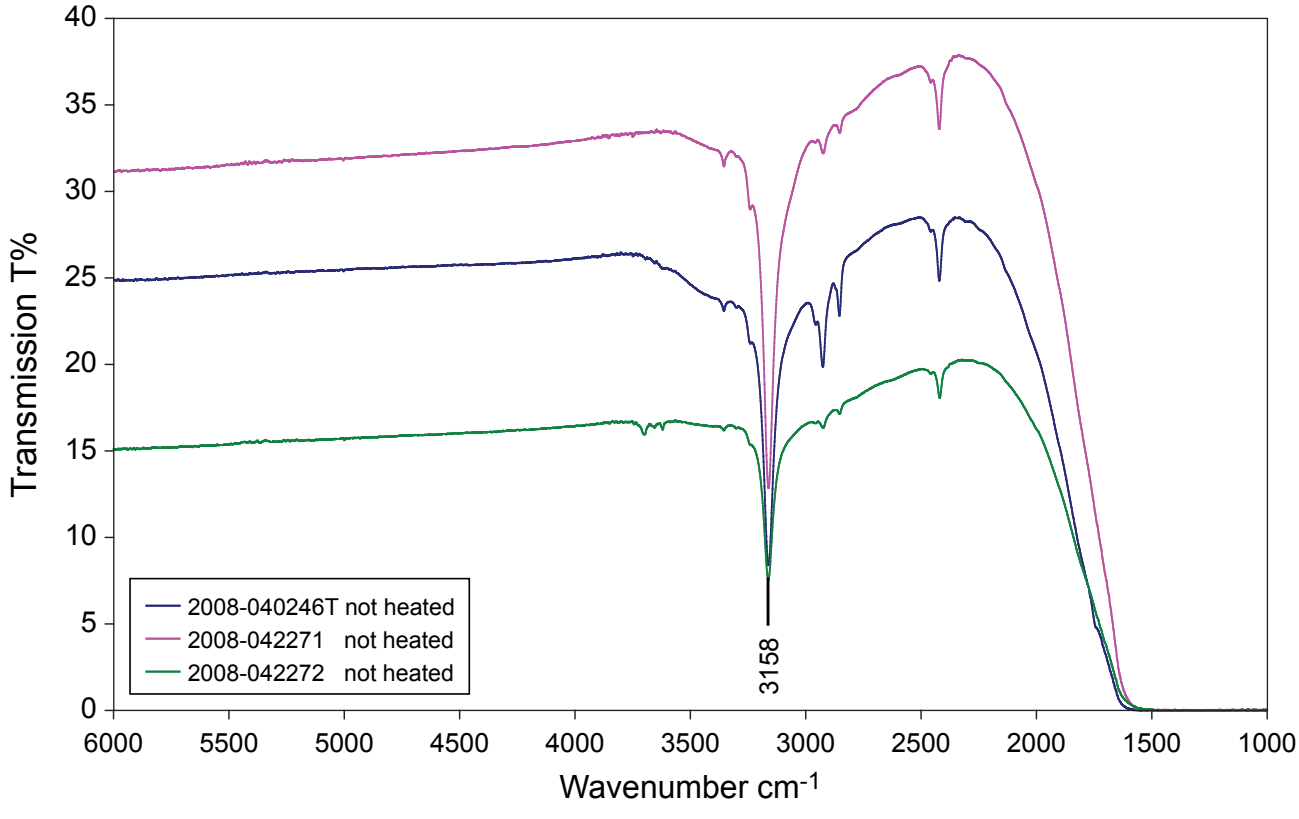

Fig. Tan135a FTIR-spectra of unheated Tanzania rubies showed a series of absorption lines related to sub-microscopic mineral inclusions. Methods see Lit Tan27.

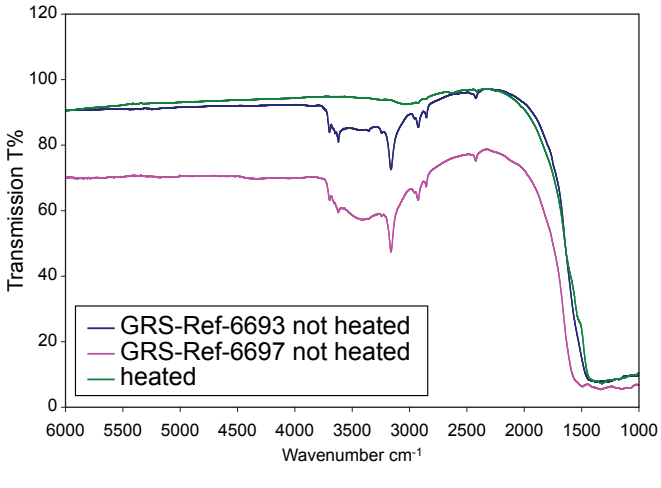

Fig. Tan135b FTIR-spectra of 2 unheated and a heated Tanzania ruby. A Winza ruby was heat-treated and showed no distinct FTIR- lines. The typical absorption lines of unheated rubies were extinct by the heat-treatment.

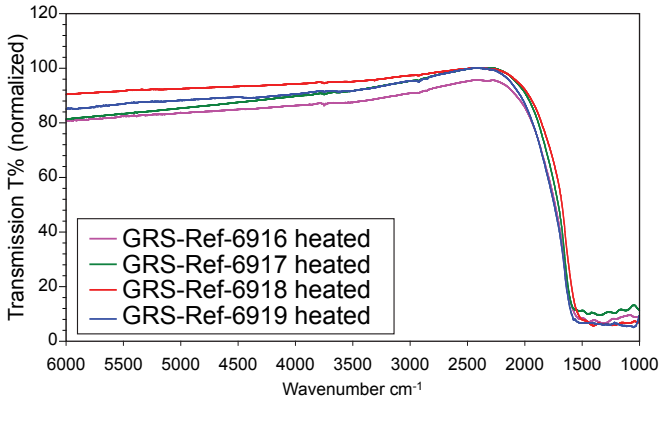

Fig. Tan135c FTIR spectra of heated Tanzania rubies. Note the difference to the spectra of unheated Tanzania rubies Spectra Fig. Tan135a, b.

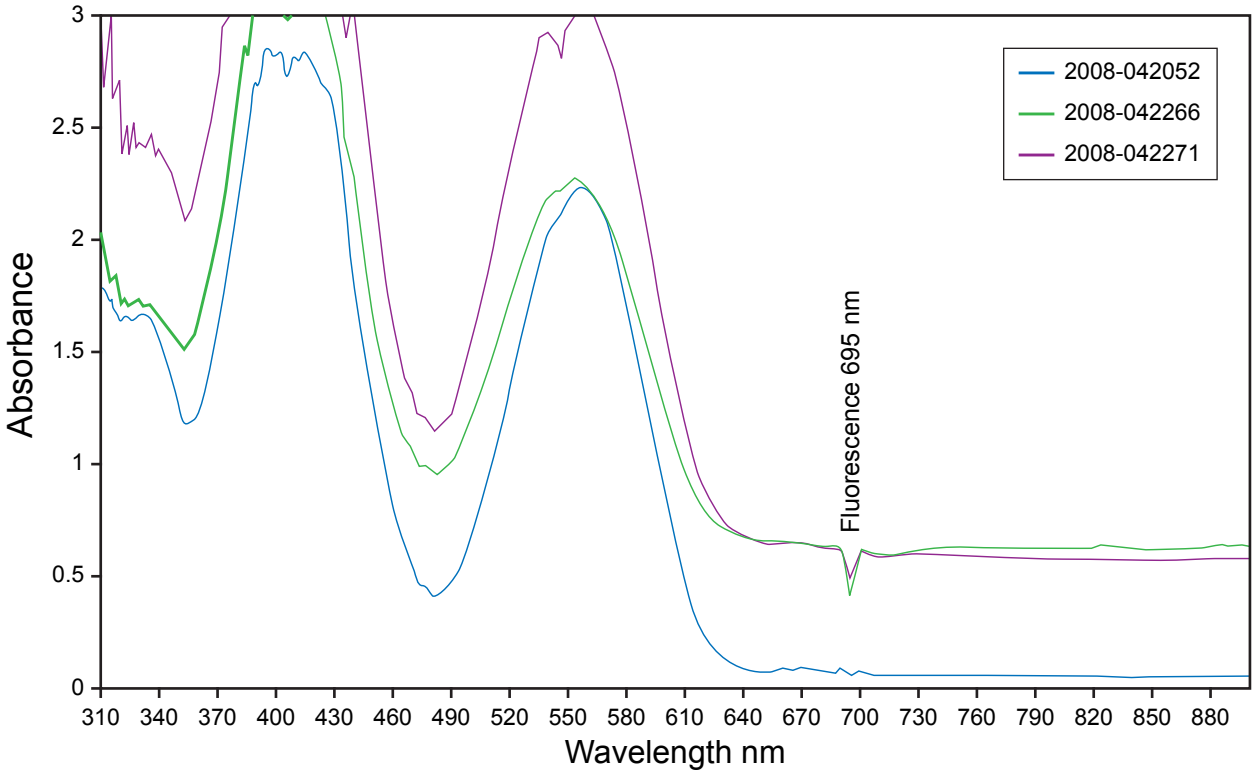

Fig. Tan136 UV-VIS-NIR spectroscopy is characterized by an absorption spectrum with a narrow UV-transmission and the position of absorption edges in the visible region of the spectrum. It mostly resembles those of some Thai rubies but is distinctively different to absorption features found in rubies from other origins, such as Burmese rubies (Lit Tan.). Thai rubies and "Winza"- rubies, however, can be easily separated by inclusion and FTIR infrared analysis.

FORMATION CONDITIONS

Based on field evidences "Winza" rubies are formed in garnet-pargasite rocks. Thin section analyses revealed that these rocks are highly metamorphosed rocks of upper amphibolite to granulite facies metamorphism. The inclusions in the rubies confirm this observation by the frequent presence of the pargasite and garnet inclusions. Detailed chemical analysis of these inclusions revealed the presence of REE concentrations in apatite, pargasite and to a lesser extent in garnet. The normalized REE pattern of these minerals revealed a prominent positive europium (Eu) anomaly. It is interesting to note that the negative Eu-anomaly cannot be found in apatite inclusions but a negative Ce-anomaly is present. According to the CART tree for discrimination of apatites (Lit Tan12), the Winza apatite would be classified as derived from fluids equilibrated with poorly differentiated carbonatite melts. When plotted in the discrimination figures (Fig. Tan137), the chemical composition of Winza apatite is close to the field of apatite found in both lherzolite and carbonatite. However, only ultramafic rocks (no carbonatites) have been found in the direct vicinity around the mine. Carbonatites do occur in Tanzania in other localities (Fig. Tan08)

A positive Eu-anomaly traditionally indicates that the rocks originated from residual rocks possibly from the upper mantle to the lower Earth crust (e.g. Lit Tan19, 24 and Box Tan05).

Negative Eu-anomalies and negative Ce-anomalies may also be solely produced by metamorphic fluid/rock interactions during metamorphism (Lit Tan22). Eu and Ce anomalies can be variable during metamorphism involving migmatitic hydrothermal fluids from different sources. Different generations of minerals may well show different Eu- and Ce-anomalies (positive and negative) due to changes in metamorphic formation conditions (see Lit for discussion on changes in oxidation state of Eu and Ce during metamorphism).

The REE patterns suggest that the analyzed apatite does not belong to the same mineral generation as the garnet and pargasite mineral inclusions. This in not surprising as apatite was found in a different sample (pargasite and garnet are from the same sample) and originated from a different outcrop.
The geological field evidences and the inclusion analysis support the model that fluid/rock interactions rather than magmatic processes have produced the REE patterns. Fluids were present in all stages of the formation of the rubies. A large variety of different fluid inclusions were found including primary, pseudo-secondary and secondary generations at all different stages of the ruby formation. However, it may not be excluded that both processes (magmatic and metamorphic) were responsible for the REE patterns.

In comparison to other corundum localities in the world (Lit Tan14, 15, 24, 26, 28, 29, 30 and 35), the formation of the Winza rubies shows similarities to ruby-bearing mafic granulites (Lit Tan35). The original rock at Winza may have been transformed by hydration into a pargasite-garnet-corundum rock. Rubies formed during metamorphism of these rocks at high-grade metamorphic conditions of the amphibolite to granulite facies, in the presence of Cl-bearing fluids of complex chemical compositions. The chemistry of the Winza rubies (Ni-concentrations) supports the hypothesis that the protolith rock may be a rock of the upper mantle to lower crust origin. This theory is supported by the study on Ni concentrations found in rubies from diamond deposits (Lit. Tan21) and positive Eu-anomalies in mantle rocks (Lit.Tan30 and Tan33). Further fieldwork and fluid inclusion analysis are necessary to reveal the exact conditions and depth of formation of the Winza rubies.

GEMMOLOGICAL CONCLUSIONS

Rubies from Winza Tanzania are offering a new source for high valuable gems with completely different gemological characteristics than other natural and synthetic counterparts.

The new ruby material may contain a completely new type of inclusions (curved and circled long needles) that have never been found in any other ruby material to our knowledge. These inclusion features can easily be utilized to differentiate between all types of synthetic rubies known so far. In the absence of long needles, microscopic analysis may reveal the presence of fluid inclusion feathers, blue growth zones, and series of solid crystal inclusions, very fine whitish zones of submicroscopic particles or clouds of whitish pin points.

Regarding the identification of the origin of these rubies from Tanzania, the set of inclusion features, in combination with special tests (ED-XRF, UV-VIS-NIR and FTIR), enables a clear separation from rubies of other origins.

Unusual large rubies of excellent clarity with a lack of inclusions can be found as well. Their identification needs special analytical methods, such as a combination of FTIR and ED-XRF chemical analysis.
The chemical compositions of the “Winza” Tanzanian rubies are characterized by equal composition of chromium and iron. The iron concentrations are slightly lower than those of Thai rubies, but much higher than rubies from marble deposits (Burma, Vietnam, Afghanistan and Tajikistan). Vanadium and gallium concentrations are lower than in rubies from marble deposits (e.g. Burmese rubies).

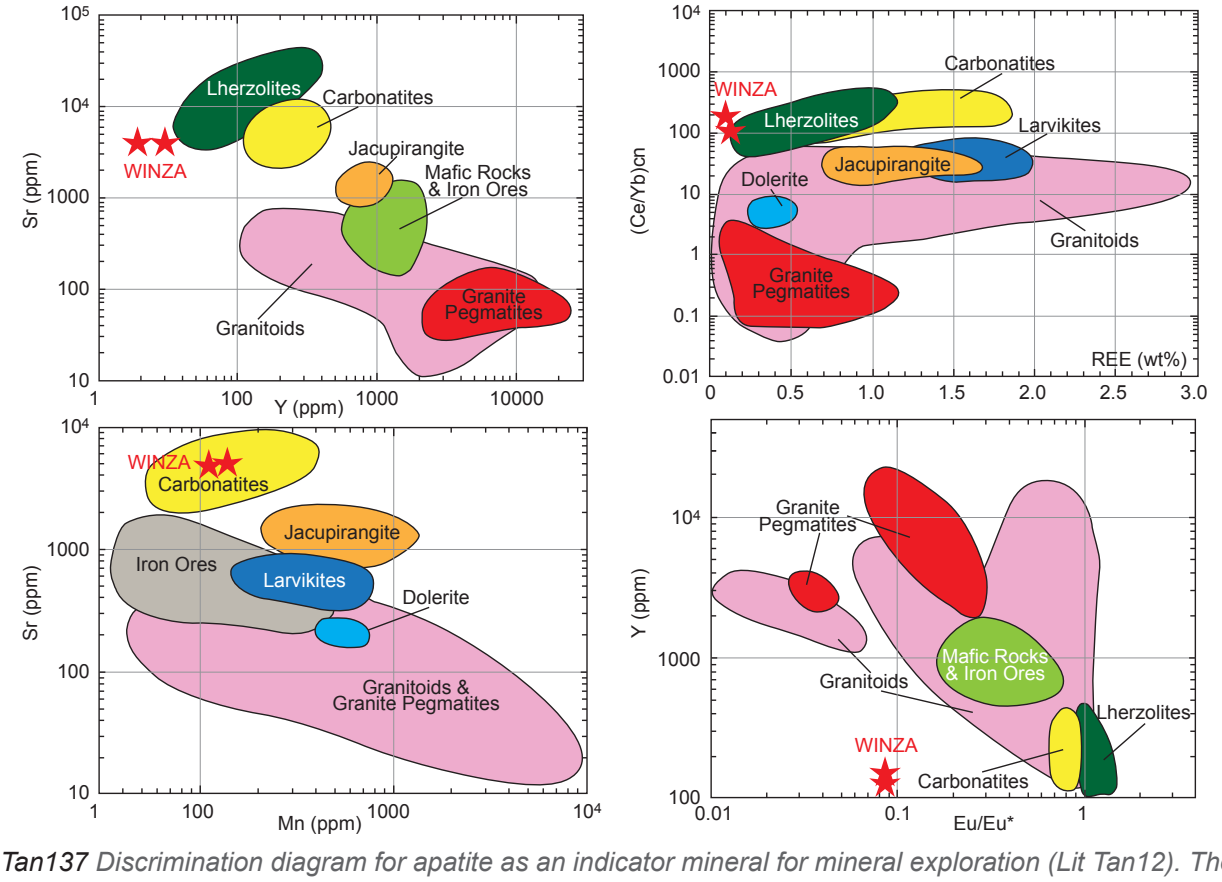

Fig. Tan137 Discrimination diagram for apatite as an indicator mineral for mineral exploration (Lit Tan12). The data points for apatite found as inclusions in a Winza ruby has been added (data see Tab. Tan01). Note that Winza apatite plots near the field of Cabonatites or Lherzonlites.

Tab. Tan01

LA-ICP-MS analysis of pargasite, garnet and apatite (apatite normalized to 39.36 wt.-% Ca). *Note: the presence of REE elements (Eu to Lu).*

				Pargasite				
				Tan25_13	Tan25_72	Tan25_73	Tan25_74	Tan25_75
		Na_2O	wt%	1.87	1.92	1.94	1.95	2.01
		MgO	„	11.54	10.75	10.40	10.62	9.80
		Al_2O_3	„	19.86	16.89	17.19	17.34	17.97
		SiO_2	„	41.68	44.62	44.44	44.22	42.92
		CaO	„	11.70	11.55	11.42	11.58	11.79
		Cr_2O_3	„	0.10	0.04	0.03	0.03	0.03
		MnO	„	0.10	0.14	0.14	0.13	0.13
		FeO	„	11.15	12.09	12.44	12.13	13.35
		Apatite		Normalized to 98wt.-%				
Na	ppm	262	333	13816	13890	14000	14050	14490
Cr	„	88	64	699	282	197	201	224
Li	„	<0.23	0.37	15.9	15.8	14.9	14.9	14.3
Be	„	1.52	<1.68	<1.02	<0.99	<0.95	<1.64	<1.82
B	„	2.01	1.74	2.76	4.57	5.55	4.85	3.40
K	„	201	302	4192	4060	4472	4009	4894
Sc	„	0.39	0.59	2.30	2.91	2.32	2.32	2.51
Ti	„	32.7	32.7	87.1	57.3	51.0	47.3	45.6
V	„	2.78	4.67	11.5	10.4	8.97	8.77	8.67
Co	„	0.45	0.69	109	98.8	95.1	97.3	106
Ni	„	22.9	39.0	918	761	707	713	698
Cu	„	4.37	7.61	3.04	0.42	1.93	4.19	4.47
Zn	„	0.74	1.20	25.9	4.27	5.10	4.62	4.46
Ga	„	7.4	5.15	8.24	3.57	3.52	3.26	3.05
Ge	„	-	-	2.36	2.48	2.45	2.88	3.23
Rb	„	0.66	0.85	11.7	11.8	12.7	11.4	14.9
Sr	„	4220	4200	711	955	890	850	1236
Zr	„	0.08	0.13	0.90	1.50	0.89	0.96	0.97
Nb	„	<0.01	0.02	0.04	0.02	<0.02	0.03	0.01
Sn	„	0.09	0.07	0.37	0.10	0.06	0.17	0.09
Ba	„	19.1	21.3	297	413	395	365	604
La	„	120	184	0.34	0.35	0.35	0.42	0.32
Ce	„	73.8	85.3	0.94	0.95	0.88	0.86	0.89
Pr	„	18.4	29.6	0.10	0.10	0.09	0.12	0.08
Nd	„	76.2	124	0.38	0.48	0.40	0.45	0.46
Sm	„	10.0	16.7	0.13	0.14	0.11	0.16	0.10
Eu	„	2.23	3.56	0.20	0.19	0.18	0.19	0.20
Gd	„	5.11	8.15	0.13	0.19	0.19	0.20	0.13
Tb	„	0.42	0.69	0.01	0.03	0.02	0.02	0.03
Dy	„	2.24	3.39	0.14	0.16	0.17	0.23	0.17
Ho	„	0.24	0.4	0.03	0.03	0.04	0.04	0.04
Tm	„	0.06	0.09	0.01	0.03	0.03	0.02	0.03
Yb	„	0.41	0.57	0.10	0.14	0.09	0.10	0.12
Lu	„	0.04	0.05	0.01	0.02	0.02	0.42	0.02
Pb	„	6.5	6.5	1.92	2.46	2.56	2.35	4.08
Bi	„	0.04	0.05	0.05	0.03	0.03	0.05	0.03
Th	„	0.07	0.07	<0.01	<0.01	0.00	<0.01	0.00
U	„	0.27	0.26	0.10	0.11	0.15	0.14	0.28

Grossular-Almandite-Pyrope-Garnet									
Tan25_65	Tan25_66	Tan25_67	Tan25_68	Tan25_69	Tan25_80	Tan25_81	Tan25_82	Tan25_83	Tan25_84
0.01	0.00	0.01	0.00	0.01	0.00	0.01	0.00	0.00	0.00
8.16	8.19	8.19	8.19	8.23	8.35	8.42	8.42	8.29	8.42
20.7	20.3	20.5	20.5	20.4	20.9	21.1	21.30	21.37	21.64
44.4	44.3	44.1	44.1	44.1	43.1	43.2	42.94	42.66	42.52
11.1	11.3	11.1	11.4	11.3	11.0	11.1	11.28	11.15	11.46
0.04	0.04	0.04	0.04	0.04	0.05	0.05	0.04	0.04	0.05
0.83	0.84	0.84	0.84	0.85	0.86	0.87	0.87	0.86	0.85
14.8	14.9	15.2	14.9	15.1	15.8	15.3	15.15	15.63	15.06
Normalized to 100wt.-%									
36.2	12.2	88.4	9.41	48.7	30.3	49.2	26.0	16.0	19.4
261	271	274	275	271	305	302	291	295	303
<0.23	<0.14	0.57	<0.13	<0.15	<0.17	<0.13	0.36	0.11	0.07
0.99	<1.21	1.63	<1.78	<0.93	<2.24	<1.84	<1.30	<1.68	<0.80
<2.16	7.29	4.07	<2.38	4.94	<1.88	4.37	2.96	1.76	<1.73
<1.52	<1.12	2.98	1.66	2.40	7.93	10.67	14.5	2.92	3.88
2.32	2.14	2.20	2.27	2.23	2.46	2.43	2.43	2.56	2.51
43.9	47.4	47.5	44.7	48.9	42.8	47.0	40.5	39.6	42.8
8.41	8.35	8.35	8.60	8.47	7.39	7.78	7.74	7.46	7.51
51.8	51.8	52.6	51.0	51.3	51.7	51.5	50.9	50.6	52.4
8.82	9.32	7.55	7.97	8.39	9.01	7.52	8.38	8.35	7.58
0.60	0.43	0.43	0.68	0.23	<0.23	<0.31	<0.22	0.62	<0.19
1.82	1.93	1.63	1.46	1.86	1.59	1.68	1.41	1.28	1.26
4.61	3.49	3.59	3.37	3.56	3.46	2.99	3.33	4.68	3.18
3.44	2.89	3.60	2.77	3.22	2.74	2.48	2.75	3.03	2.66
<0.04	0.17	0.26	<0.04	<0.06	<0.04	<0.03	0.11	0.03	<0.02
0.05	0.02	0.02	0.03	0.18	1.25	0.48	0.41	0.41	0.41
1.08	0.93	1.01	0.85	1.03	0.90	0.97	1.02	0.96	0.94
<0.03	<0.02	<0.02	<0.01	0.02	<0.01	<0.01	0.01	<0.01	<0.01
0.03	0.04	0.16	<0.04	<0.05	0.05	<0.06	0.05	<0.04	<0.03
0.10	0.17	<0.13	<0.08	0.29	0.91	0.43	0.31	0.33	0.11
<0.02	0.03	<0.02	<0.02	<0.02	0.02	<0.01	<0.01	<0.01	0.01
0.08	<0.02	0.03	0.03	0.06	0.03	0.01	0.02	0.08	<0.02
0.02	0.02	<0.02	0.01	0.01	0.01	0.01	<0.01	<0.01	<0.01
0.15	0.04	<0.06	<0.07	0.06	0.05	0.05	0.06	<0.07	<0.05
0.08	0.06	0.07	0.09	0.10	0.11	0.09	0.09	0.07	0.15
0.16	0.18	0.15	0.17	0.20	0.16	0.15	0.18	0.17	0.14
0.11	0.14	0.13	<0.08	0.08	0.11	0.11	0.09	0.15	0.09
0.02	0.02	0.03	0.02	0.03	0.02	0.03	<0.02	0.03	0.03
0.11	0.12	0.14	0.10	0.13	0.14	0.14	0.12	0.12	0.14
0.02	0.03	0.03	0.03	0.03	0.02	0.04	0.04	0.01	0.03
<0.01	0.01	<0.01	<0.01	0.02	0.01	0.01	<0.01	0.01	0.01
0.06	0.08	0.06	<0.06	<0.06	<0.08	0.07	0.04	0.06	0.06
0.01	0.01	0.02	0.01	<0.02	<0.01	0.01	<0.01	0.01	0.01
0.32	0.04	0.57	0.23	0.26	0.11	0.03	<0.02	0.02	<0.03
0.15	<0.01	0.04	0.02	0.03	<0.01	0.01	0.01	0.01	<0.01
<0.01	<0.01	<0.01	<0.01	0.01	<0.01	<0.01	<0.01	0.01	<0.01
0.04	0.05	0.18	0.04	0.55	0.04	0.04	0.11	0.03	0.03

	Sapphire			Ruby						Padparadscha			
	Tan24_45	Tan 21_6	Tan 23_19	Tan25_7	Tan 22_20	Tan 23_33	Tan 6_55	Tan 21_41	Tan24_8	Tan 3_16	Tan 3_18	Tan 23_46	Tan24_30
Mg	69.8	52.6	46.4	90.6	121	160	94.8	186	109	223	187	256	304
Si	2880*	429	846	<322	649	814	<375	493	<516	536	<329	544	<430
Ti	986	1120	692	23.8	54.5	37.9	40.4	231	31.2	146	166	225	426
V	5.04	4.59	5.27	2.6	7.1	5.92	4.92	8.43	5.64	6.25	6.79	7.82	11.7
Cr	926	807	822	1140	1770	1620	1460	1890	1900	594	578	723	887
Fe	2980	3130	3180	3810	4150	3430	3680	4560	3040	3420	3260	5010	4740
Co	0.18	<0.08	<0.14	1.22	0.62	0.27	<0.19	0.36	<0.14	<0.13	0.18	0.17	<0.12
Ni	3.79	3.08	1.92	4	8.59	8.3	7.75	10.5	8.01	12.9	12.9	14.2	21.3
Ga	43.3	34.3	38	40.1	36.4	38.3	48.4	41.8	40.7	39.2	39.3	50.2	64.6

Tab. Tan02

LA-ICP-MS chemical analysis of sapphires, rubies and “Padparadscha” from Winza (Tanzania) in ppm. Note the presence of Ni in the rubies. Na, Si, K, Pb, Bi, Th and U concentrations are due to contamination by inclusions. Chemical analysis are normalized to 529300ppm Al. Detection limits: Mg, Si, Ti, V, Cr, Fe, Co, Ni, Ga = 0.8, 450, 0.8, 0.9, 2.1, 3.0, 0.15, 0.8, 0.3 ppm
* Concentration of Si may be partially contaminated by micro inclusions.

The chemical analysis can also be used to distinguish between most synthetic rubies, including flame-fusion type. With minor exceptions this is also true for Flux and iron-rich synthetic hydrothermal rubies (compare Lit Tan23, 31 and 36). Additionally FTIR spectroscopy may be necessary to separate the “Winza“-rubies from synthetic counterparts (Lit Tan32 and 36). FTIR spectra revealed a series of OH-absorption lines near 3158 wave numbers. These Infrared absorptions are in general not present in other unheated or heated rubies of other origin (FTIR spectra of heated rubies from Mong Hsu origin see Lit. Tan07 and 30).

In conclusion, “Winza“-(Dodoma province) rubies can be clearly identified and separated from all synthetic and natural unheated and heated counterparts. The identification can be largely based on inclusion analysis. In special cases, a combination of inclusion analysis with special analytical methods (LA-ICP-MS, UV-VIS-NIR, ED-XRF and FTIR) is needed. Heat-treatment can be identified by a combination of inclusion and FTIR-analyses.

Acknowledgments

We thank the Government of the Republic of Tanzania and Mr. Dr. Kafumu, Commissioner for Minerals from the Ministry of Energy and Minerals, Dar es Salaam for the permission to enter the Winza mine (Permission No. DL19/2008/1) and the Geological Survey of Tanzania (Dodoma) for providing us with the necessary geological maps.

Without the logistical support (transportation, accommodation at the mine and other supports to reach the mine) by Gramack (T) LTD, Dar es Salaam (Tanzania), this expedition would not have been possible.

Other companies and dealers in the local town of Mpwapwa (such as Omar Attas Gems, Try Once Gems&Jewelry and others) provided additional logistical support. Geological assistance (GPS and geological field instructions) was provided by Mr. Rogers Sezinga from Tan Discovery Mineral Consultancy Co. LTD. We thank the anonymous locals from Tanzania for sharing their mining experience with us. The local policemen at the Winza mine were guiding us and provided security. Many thanks also to the Sri Lankan and Thai Gem community (such as Gem Paradise, Colombo and C.H. Lapidaries in Bangkok and others) for support and sponsoring us with further samples. Lewis Allen (Crown Color, Geneva) and Thomas Buckingham provided assistance in English review.

Scientific support of the following persons and Institutions is greatly appreciated: Glenn Lambrecht and Prof. Mercolli (Research Group Rock Water Interaction, Institute of Geological Sciences, University of Berne) for Raman spectroscopy and thin section analyses, Prof. Armbruster from the Institute of Geological Sciences (Mineralogical Crystallography) for structural analyses of minerals. The Institute of Geological Sciences (University of Bern) for providing us access to the SEM laboratory and Dr. Herwegh for assistance (the Institute acknowledges SNF grant nr. 200021-109369) and the Department of Geosciences from the University of Fribourg (Prof. Grobéty) for thin section preparation.

Mr.Tanthadilok for graphic and artwork and Mr. Michael for preparing this report for the Internet online version (www.gemresearch.ch).

About the Authors

Dr. Peretti is Director of the GRS Gemresearch Swisslab Ltd., Lucerne, Switzerland
adolf@peretti.ch

F. Peretti (GG) is Research Scientist of the GRS Gemresearch Swisslab Ltd., Lucerne, Switzerland
francesca@peretti.ch

W. P. Bieri (Bsc, FGA) is Research Gemologist at GRS in Switzerland and Thailand
wbieri@gemresearch.ch

A. Kanpraphai is Photographer at Anong Imaging, Bangkok, Thailand

K. Hametner is Research Assistant for Trace Elements and Microanalysis at the Laboratory for Inorganic Chemistry, ETH Zurich, Switzerland
hametner@inorg.chem.ethz.ch

Dr. Günther is Full Professor for Trace Elements and Microanalysis at the Laboratory for Inorganic Chemistry, ETH Zurich, Switzerland
guenther@inorg.chem.ethz.ch

Publications Winza Ruby mine:

Lit Tan01 Abduriyim A. and Kitawaki H. (2008). New Geological Origin: Ruby from Winza of Tanzania GAAJ-ZENHOKYO Laboratory, On-line Report http://www.gaajzenhokyo.co.jp/researchroom/kanbetu/2008/2008_08en-01.h

Lit Tan02 Gubelin Gem Lab (2008): Field trip to new ruby mines in Tanzania. Newsletter, 22, May 6. On-line: www.gubelinlab.com

Lit Tan03 Hänni H.A , (2008). New Rubies from central Tanzania. Gems & Gemology, 44(2): p.177-178.

Lit Tan04 Krzemnicki M.S. and Hänni H.A. (2008): New Tanzania mine uncovers source of exceptional rubies. InColor magazine, International Colored Gemstone Association. p. 46-47.

Lit Tan05 Laurs B.M. and Pardieu V. (2008): Ruby and Sapphire mining at Winza (Tanzania), Gems & Gemology, 44(2): p. 178-179.

Lit Tan06 Pardieu V. and Schwarz D. (2008): FIELD REPORT FROM WINZA, Gübelin GemLab experts travel to the Winza mines to investigate a new ruby find. Rapaport News (www.diamonds.net/News/)

Lit Tan07 Peretti A. (2008a): New Important Gem Discovery in Tanzania: The Tanzanian “Winza“-(Dodoma) Rubies. Contrib. Gemol. No. 7, 1st edition. April 2008. VCD-Issue. ISBN 978-3-9523359-6-3. On-line issue at www.gemresearch.ch/news/Tanzania/Tanzania.htm

Lit Tan08 Peretti A. (2008b): Youtube - GRS New Winza Tanzania ruby mines visit. May 20.

Lit Tan09 Peretti A. (2008c): Youtube - GRS Magnificent Winza Tanzania rubies. May 20.

Lit Tan10 Senoble J.B. (2008): An expedition to Tanzania’s new ruby deposit in Winza. InColor magazine, International Colored Gemstone Association. p. 44-45.

Lit Tan11 SSEF Newsletter (2008) New Rubies from Tanzania, SSEF Swiss Gemmological Institute Newsletter, May 2008.

Literature:

Lit Tan12 Belousova E.A., Griffin W. L., O'Reilly S. Y., Fisher N. I. (2002): Apatite as an indicator mineral for mineral exploration: trace-element compositions and their relationship to host rock type. J. Geochem. Explor., 76(1): p. 45-69.

Lit Tan13 Bühn B., Wall F. and Le Bas M.J. (2001): Rare-earth element systematics of carbonatitic fluorapatites, and their significance for carbonatite magma evolution. Contributions to Mineralogy and Petrology. 141(5): p. 572-591.

Lit Tan14 Delee-Dubois M.L., Fournier J. and Peretti A. (1993): Rubies du Vietnam. Etude comparative avec les rubies de Birmanie et d'autres provenences. Revue de gemmologie, Association Francais de Gemmologie, 114: p. 7-10.

Lit Tan15 Gübelin E. and Peretti A. (1997): Sapphires from Adranondambo mine in SE Madagascar: Evidence for metasomatic skarn formation. J. Gemm., 25(7): p. 453 - 470.

Lit Tan16 Guillong M. and Günther D. (2001): Quasi 'non-destructive' laser ablation-inductively coupled plasma-mass spectrometry fingerprinting of sapphires. Spectrochimica Acta Part B-Atomic Spectroscopy, 56: p. 1219-1231.

Lit Tan17 Günther D. and Hattendorf B. (2005): Solid sample analysis using laser ablation inductively coupled plasma mass spectrometry. Trac-Trend. Anal.Chem. 24(3): p. 255-265

Lit Tan18 Günther D., Frischknecht R. and Heinrich, C. A. (1997): Capabilities of a 193nm ArF Excimer Laser for LA-ICP-MS Micro Analysis of Geological Materials. J. Anal. At. Spectrom., 12: p. 939-944.

Lit Tan19 Hattendorf B., Latkoczy C. and Günther D. (2003): Laser ablation-ICPMS. Anal. Chem., 75(15): p. 341A-347A.

Lit Tan20 Hermann J. Müntener O. and Günther D. (2001). Differentiation of Mafic Magma in a Continental Crust-to-Mantle Transition Zone. J. Petrology, 42(1): p.189-206.

Lit Tan21 Hutchison M.T., Nixon P.H. and Harley S.L. (2004): Corundum inclusions in diamonds - discriminatory criteria and a corundum compositional dataset. Lithos. 77(1–4): p. 273-286. (Selected Papers from the Eighth International Kimberlite Conference. Vol. 2: The J. Barry Hawthorne Volume).

Lit Tan22 Jiang S.Y., Yu J.M., and Lu J.J., (2004): Trace and rare-earth element geochemistry in tourmaline and cassiterite from the Yunlong tin deposit, Yunnan, China: implication for migmatitic-hydrothermal fluid evolution and ore genesis. Chemical Geology, 209(3-4): p. 193-213.

Lit Tan23 Muhlmeister S., Fritsch E., Shigley J.E., Devouard B. and Laurs B.M., 1998. Separating natural and synthetic rubies on the basis of trace-element chemistry. Gems & Gemology, 34: p. 80-101.

Lit Tan24 Peretti A. (2003): Namya Rubies. Contrib. Gemol., 2: p. 9-14. Online-version at: www.gemresearch.ch/journal/pioneer.htm

Lit Tan25 Peretti A., Armbruster T., Günther D., Grobéty B., Hawthorne F.C., Cooper M.A., Simmons W.B., Falster A.U., Rossman G.R., and Laurs B.M. (2004): The challenge of the identification of a new mineral species: Example “pezzottaite”. Contrib. Gemol., 3: p. 1-12.

Lit Tan26 Peretti A. and Günther D. (2005): The Beryllium-Treatment of Natural Fancy Sapphires with a new Heat-Treatment Technique Part A. Contrib. Gemol., 4: p. 16.

Lit Tan27 Peretti A., Peretti F., Tun N.L., Günther D., Hametner K., Bieri W., Reusser E., Kadiyski M. and Armbruster Th. (2007): Gem Quality Jochachidolite: Occurrence, chemical composition and crystal structure. Contrib Gemol., 5: p. 1-53

Lit Tan28 Peretti A. Mullis J. and Kündig R. (1990): Die Kashmir Sapphire und ihr gelogisches Erinnerungsvermögen. Neue Zürcher Zeitung, 187: p. 59.

Lit Tan29 Peretti A., Mullis J. and Mouawad F. (1996): The role of fluorine in the formation of color zoning in rubies from Mong Hsu (Myanmar, Burma). J. Gemmol. 25: p. 3-19.

Lit Tan30 Peretti A., Schmetzer K., Bernhardt H.H. and Mouawad F. (1995): Rubies from Mong Hsu. Gems & Gemology, 31(1): p. 2-26.

Lit Tan31 Peretti A. and Smith C.P. (1993): A new type of synthetic ruby on the market, offered as hydrothermal rubies form Novosibirsk, Australian Gemmol., 18: p. 149-156.

Lit Tan32 Peretti A. and Smith C.P. (1994): Letter to the Editor. J. Gemm., 24(1): p. 61-63.

Lit Tan33 Promptrated P., Taylor L.A. and Neal C.R. (2003): Petrochemistry of Mafic Granulite Xenoliths from the Chantaburi Basaltic Field: Implications for the Nature of the Lower Crust beneath Thailand. International Geology Review, 45: p. 383-406.

Lit Tan34 Schmetzer K. and Peretti A. (1999): Some Diagnostic Features of Russian Hydrothermal Synthetic Rubies and Sapphires, Gems & Gemology, 35(1), Sp. Iss.: p. 17-28.

Lit Tan35 Simonet C., Fritsch E. and Lasnier B. (2008): A classification of gem corundum deposits aimed towards gem exploration. Ore Geology Reviews. 34(1-2): p. 127-133.

Lit Tan36 Thomas V.G., Mashkovtsev R.I., Smirnov S. Z., Maltsev V.S. (1997): Tairus Hydrothermal Synthetic Sapphires Doped with Nickel and Chromium. Gems & Gemology. 33(3),Fall Iss., p.188-202

Lit Tan37 United Republic of Tanzania (2005): Opportunities for Mineral Resource Development, Ministry of Energy and Minerals, Minerals Department, 4, p.1-130

Lit Tan38 Whittingham, J.K. (1959): The Geology of the Nyanzwa Area, Quarter Degree Sheet 63 NW. Geological Survey of Tanganyika, Printed by the Government Printer Dar es Salaam.

A new source of rubies has been discovered in 2008 from Tanzania. This exciting appearance of a completely new ruby type has electrified the gemological world. Many large rubies with excellent clarity and vibrant color surprised the gem trade.

This 7th Issue of Contributions to Gemology takes us on an adventurous expedition into the source of these interesting gems.

Combining the field experience of GRS Gemresearch Swisslab together with the analytical expertise of the research group for Trace Element and Micro Analysis at the Department of Chemistry and Applied Biosciences at ETH Zurich, Switzerland, we are proud to offer you an in-depth research into the formation and identification of these "Winza" (Tanzania)- rubies.

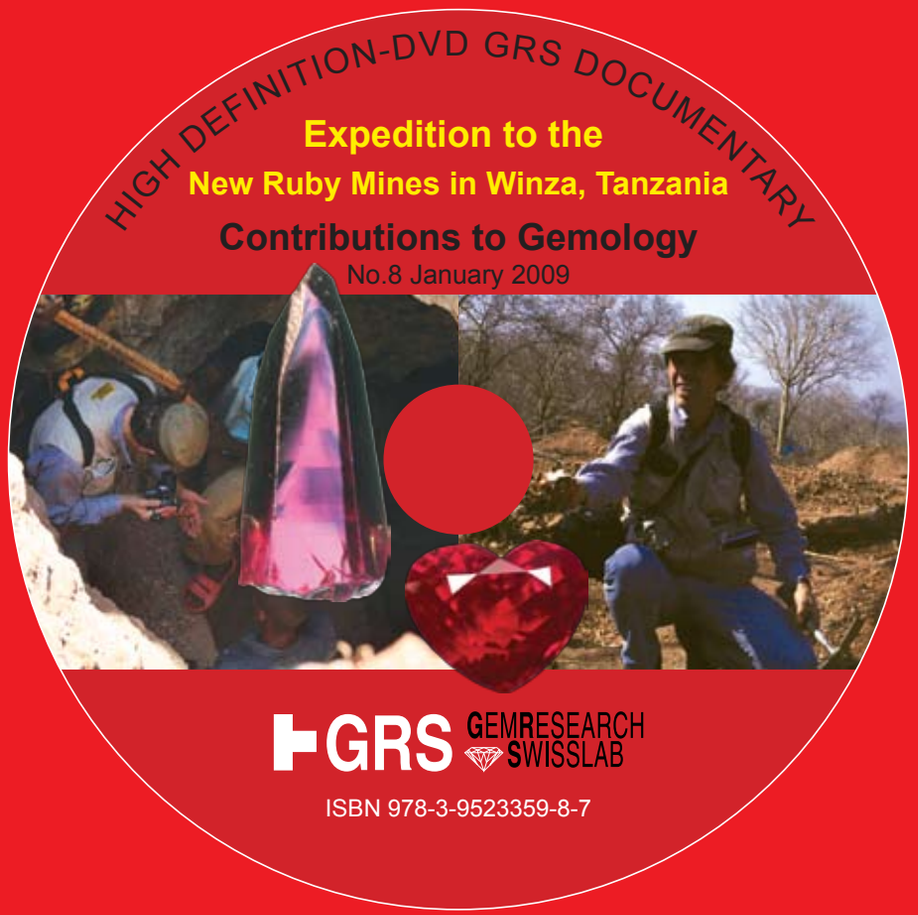

ISBN 978-3-9523359-8-7

Copyright by GRS Gemresearch Swisslab AG
6002 Lucerne, Switzerland.
www.gemresearch.ch

ISBN 978-3-9523359-7-0
9 783952 335970